UNIVERSIDAD DE CHILE
FACULTAD DE CIENCIAS FÍSICAS Y MATEMÁTICAS
DEPARTAMENTO DE INGENIERÍA ELÉCTRICA

VALIDITY RANGE OF STABILITY ASSESSMENTS BASED ON QUASI-STATIC PHASOR CALCULUS IN POWER SYSTEMS WITH HIGH LEVELS OF CONVERTER INTERFACED GENERATION

TESIS PARA OPTAR AL GRADO DE DOCTOR EN
INGENIERÍA ELÉCTRICA

JORGE LUIS VEGA HERRERA

PROFESORA GUÍA:
CLAUDIA RAHMANN ZUÑIGA

MIEMBROS DE LA COMISIÓN
PATRICIO MENDOZA ARAYA
RICARDO ÁLVAREZ MALEBRÁN
HÉCTOR CHÁVEZ ORÓSTICA

SANTIAGO DE CHILE
2022

RESUMEN DE LA TESIS PARA OPTAR AL GRADO DE: Doctor en Ingeniería Eléctrica
POR: Jorge Luis Vega Herrera
FECHA: 2022
PROFESORA GUÍA: Claudia Rahmann Zuñiga

RANGO DE VALIDEZ DE LOS ESTUDIOS DE ESTABILIDAD BASADOS EN CÁLCULO FASORIAL CUASI-ESTÁTICO EN SISTEMAS DE POTENCIA CON ALTOS NIVELES DE GENERACIÓN INTERCONECTADA A LA RED A TRAVÉS DE CONVERTIDORES

La estabilidad de sistemas eléctricos de potencia (SEP) se estudia representando la red con ecuaciones algebraicas, lo que implica el uso del cálculo fasorial cuasi-estático (QPC). QPC desprecia los transitorios rápidos. Sin embargo, debido al aumento de generación interconectada a la red por convertidores (CIG), la respuesta dinámica de los SEP está cambiando. Como resultado, el uso de QPC está siendo cuestionado. Esta tesis identifica, verifica e investiga el rango de validez de estudios de estabilidad basados en QPC. El cálculo fasorial dinámico (DPC) se considera como alternativa. Se propone una metodología para comparar QPC y DPC de manera sistemática. Incluye respuesta en frecuencia, análisis modal y de sensibilidad. Además, se comparan con DPC los modelos de CIG comunes basados en QPC para investigar e identificar el nivel de detalle apropiado para los estudios de estabilidad. Las comparaciones se centran en análisis modal y se realizan en una red de prueba IEEE considerando hasta un 100% de CIG. Los resultados muestran que QPC es adecuado para estudios de estabilidad cuando se consideran anchos de banda bajos en los controles de CIG. Por otro lado, DPC es adecuado a estudios genéricos de estabilidad en SEP con altos niveles de CIG.

RESUMEN DE LA TESIS PARA OPTAR AL
GRADO DE: Doctor en Ingeniería Eléctrica
POR: Jorge Luis Vega Herrera
FECHA: 2022
PROFESORA GUÍA: Claudia Rahmann Zuñiga

VALIDITY RANGE OF STABILITY ASSESSMENTS BASED ON QUASI-STATIC PHASOR CALCULUS IN POWER SYSTEMS WITH HIGH LEVELS OF CONVERTER INTERFACED GENERATION

Power system stability is widely assessed by tools that model the network and the connected machine stators through algebraic equations and synchronous generators through differential equations, meaning that quasi-static phasor calculus (QPC) is used. In QPC, fast transients are neglected. However, the nature of the dynamic response of power systems is changing due to the increase in converter-interfaced generation (CIG). Therefore, the reliance on QPC must be questioned. In this thesis, the validity range of stability assessments based on QPC models is identified, verified, and investigated. Dynamic phasor calculus (DPC) is considered as an alternative. A systematic methodology is proposed to compare QPC and DPC. It includes frequency response, modal, and sensitivity analyses. Furthermore, common CIG models based on QPC are compared with DPC to investigate and identify the appropriate level of detail required for stability studies. In these comparisons, modal analysis is performed. The studies are performed in an IEEE test network considering up to 100% CIG levels. The results show that the QPC is suitable for stability assessments when low bandwidths of the converter controls are given. On the contrary, DPC is suitable and applicable to generic power system stability studies of networks with high penetration of CIG

Dedicated to God, my lovely wife, and my family

Acknowledgments

En primer lugar, agradezco a Dios por haberme dado la oportunidad de entrar a la Universidad de Chile y realizar mis estudios de doctorado. En segundo lugar, por permitirme conocer personas maravillosas durante este periodo.

A mi esposa, mi Mari. Agradezco su paciencia, compañía, apoyo incondicional y ayuda en esta etapa. Sin ella, no podría haber terminado. Agradezco su amor en todos los momentos en los que me sentía muy desanimado o no veía la luz fuera del túnel jeje... Fue y es mi gran bendición.

A mis viejitos, Jorge Vega Palma y Renata Herrera, que siempre han estado ahí cuando lo he necesitado, su apoyo incondicional ha bendecido mi vida. En especial en la recta final del doctorado.

A mi profesora guía, Claudia Rahmann, por invitarme a trabajar duro para lograr la excelencia en todos los desafíos que emprendimos. Gracias por el apoyo y esfuerzo continuo en que creciera como profesional a través de estadías de investigación. Gracias porque cuando aparecieron los grandes desafíos en mi vida, fue comprensiva y paciente. Gracias por corregirme, por compartir su experiencia y conocimientos. En retrospectiva puedo entender mejor y valorar más sus enseñanzas.

Agradezco al profesor Kai Strunz por su guía, buena disposición, enseñanzas y por darse el tiempo de atenderme a pesar de su agenda tan ocupada. Aprendí a ser más riguroso en la investigación.

A mi profesor amigo y jefe jeje…, Felipe Valencia, por escucharme con paciencia mis inquietudes y ayudarme en incontables ocasiones.

A mis amigos de postgrado, Diego Ortiz, Jacqueline Llanos y Oscar Núñez, gracias por su ayuda y apoyo incondicional. Gracias por estar cuando lo necesité y por brindarme de su amistad. Gracias a mis amigos Angela, Bernardo y Yu, sin ellos las estadías en Berlín no hubieran sido lo mismo.

A la Universidad de Antofagasta por apoyarme en la realización de estudios de postgrado en la Universidad de Chile. Finalmente, agradezco a becas chile de doctorado nacional ANID/21161139, SERC Chile ANID/Fondap/15110019 y programa del ministerio de energía de pasantías en el extranjero ANID/Ministerio de energía.

Contents

List of Tables ix
List of Figures x
1 Introduction 1
1.1 Motivation 1
1.2 Problem Statement 3
1.3 Hypotheses 4
1.4 Objectives 4
1.4.1 General Objective 4
1.4.2 Specific Objectives 5
1.5 Scope 5
1.6 Contributions 5
1.7 Publications 6
1.8 Thesis Outline 6
2 Literature Review 7
2.1 Introduction 7
2.2 Power System Stability 7
2.3 Impact of CIG on Power System Stability 8
2.3.1 Reduction of Short Circuit Levels 9
2.3.2 Reduction of System Inertia 9
2.3.3 Dynamic Response of Power Systems 10
2.4 Modeling Approaches for Simulation of Power System Transients 12
2.4.1 Electromagnetic Transient Approach 13
2.4.2 Phasor Calculus 14
2.5 Modeling of Power System Components 19
2.5.1 Transmission Lines 19
2.5.2 Synchronous Generators 20
2.5.3 Converter Interfaced Generation Technologies in Power System 21
2.6 Modeling of CIG for Power System Stability Studies 29
2.6.1 Models Based on a Current Source Representation 31
2.6.2 Models Based on a Voltage Source Representation 32
2.6.3 Comparison of CIG Models Used for Stability Studies 35
2.7 Summary and main findings from the literature review 37
3 Methodology 39

3.1 Introduction 39
3.2 Methodology for the Comparison of QPC and DPC-Based Models 39
3.2.1 Stage 1: Dynamic Modeling 40
3.2.2 Stage 2: Frequency Response 42
3.2.3 Stage 3: Modal Analysis 42
3.2.4 Stage 4: Sensitivity Analysis 43
3.2.5 Stage 5: Validation Through Time Domain Simulation 43
3.3 Methodology for Comparisons of CIG Models Based on QPC 43
3.3.1 Stage 1: Dynamic Modeling 44
3.3.2 Stage 2: Sensitivity Analysis 45
3.3.3 Stage 3: Comparative analysis 46
3.3.4 Stage 4: Validation Through Time Domain Simulation 46
4 Comparative Analysis Between DPC- and QPC-Based Models 47
4.1 Description of Power System Under Study 47
4.2 Implemented Models and Software Used 49
4.3 Results of Comparative Analysis of DPC and QPC-Based Models 49
4.3.1 Frequency Response Analysis 49
4.3.2 Modal Analysis 50
4.3.3 Sensitivity Analysis 53
4.3.4 Validation Through Time Domain Simulation 56
4.4 Summary of Main Findings 62
5 Comparative Analysis of CIG Models Based on QPC 63
5.1 Description of Power System Under Study 63
5.2 Implemented Models and Software Used 64
5.3 Results of Comparative Analysis of CIG Models Based on QPC 65
5.3.1 Case Study 1: Impacts of PLL and CIG Levels 65
5.3.2 Case Study 2: Impacts of SCR Levels 66
5.3.3 Case Study 3: Impacts of Inner Control Loops 67
5.4 Summary of Main Findings 69
6 Conclusions 71
6.1 Future Work 72
Bibliography 73
ANNEXES 88
Annex A: Power System Models Used in Chapter 4 89
A.1 CIG-GFL Model 89

A.2 CIG-GFM Model with Virtual Synchronous Generator 92
A.3 Synchronous Generator Model 95
A.4 Transmission lines, transformers, and loads 99
Annex B: Power System Models Used in Chapter 5 101
B.1 CIG-GFL Model Based on DPC 101
B.2 CIG-GFL Models Based on QPC 104
B.3 CIG-GFM Model 107
B.4 Parameter of CIG Models 107
Annex C: Acronyms and Abreviations 110
Annex D: Detailed Analyses Related to Chapter 5 111
D.1 Sensitivity Analysis 111
D.1.1 Case Study 1: Impacts PLL and CIG Levels 111
D.1.2 Case Study 2: Impacts of SCR Levels 114
D.1.3 Case Study 3: Impacts of Current Control Loops 117
D.2 Validation Through Dynamic Simulation 122
Annex E: Extended Abstract 129

List of Tables

Table 2.1. Comparison of RLC representation 18
Table 2.2. Description of CIG – GFL parameters 27
Table 2.3. Description of CIG – GFM parameters 30
Table 2.4. Summary of CIG models 37
Table 3.1. Summary of power system models 41
Table 3.2. Summary of Case Studies 46
Table 4.1. Main characteristics of synchronous generators 47
Table 4.2. Dispatch and system inertia H_{sys} for different generator portfolios 48
Table 4.3. Control system parameters of CIG units 49
Table 4.4. Summary of main findings 62
Table 5.1. Main characteristics of synchronous generators 63
Table 5.2. Dispatch and system inertia H_{sys} for different generator portfolios 64
Table 5.3. Control system parameters of CIG-GFL units 65
Table A.1. Control system parameters of CIG – GFM 95
Table A.2. Description of synchronous generator parameters. 99
Table B.1. Control system parameters of CIG – GFM with droop control for DPC and QPC based models 108
Table B.2. Control system parameters of CIG-GFL units considering QPC-based approach 109
Table D.1. Participation factors related to M1DPC for 70% of CIG and PLL bandwidth of 20 Hz 113
Table D.2. Participation factors related to M1QPC for the model VS-Type 2 for 70% of CIG and PLL bandwidth of 20 Hz 114
Table D. 3. Participation factors related to M1DPC for 50% of CIG and SCR of 20 Hz 116
Table D.4. Participation factors related to M1QPC for the QPC VS-Type 2, 50% of CIG and SCR of 1.15 117

List of Figures

Figure 1.1. Different time-scale of power systems transients [3]. 1
Figure 2.1. Classification of power system stability extended considering CIG [19], [37] 8
Figure 2.2. Classification of modeling approaches for the simulation of power system transients 13
Figure 2.3. Application of Hilbert Transformation 14
Figure 2.4. Shifting by carrier frequency 15
Figure 2.5. Frequency spectrum of DPC and QPC 17
Figure 2.6. Comparison of transient simulation of a three-phase RL circuit; $R = 1\ \Omega, L = 0.01$ [H] 19
Figure 2.7. Illustrative schematic diagram of a control system used in CIG 22
Figure 2.8. Widely used operations modes of CIG 23
Figure 2.9. Diagram of CIG connected to the grid that operates in GFL mode [125] 25
Figure 2.10. Outer control loops for the d-axis; a) Active power control; b) DC-Link voltage control 25
Figure 2.11. Outer control loops for the q-axis; a) Reactive power control; b) Voltage control 25
Figure 2.12. Doop control for CIG operating in GFL 25
Figure 2.13. SRF - PLL 26
Figure 2.14. Current control loops; a) current controller on the d-axis; b) current controller on the q-axis 26
Figure 2.15. Feed-forward terms; a) d-axis; b) q-axis 27
Figure 2.16. Diagram of CIG connected to the grid operating in GFM mode 28
Figure 2.17. Droop-based active power controller 28
Figure 2.18. Droop-based reactive power controller 29
Figure 2.19. Inner control loops on the dq axis; a) voltage control loops; b) current control loops 29
Figure 2.20. Representation of CIG; a) current source; b) voltage source behind an impedance 30
Figure 2.21. Current source model based on a transfer function 31
Figure 2.22. Inner current control loops without decoupling and feedforward terms; a) d-axis; b) q-axis 33
Figure 2.23. The CIG model developed in [35] 35
Figure 3.1. Proposed methodology 40
Figure 3.2. Illustrative Bode plot for comparing DPC- and QPC-based models in the frequency domain 42
Figure 3.3. Methodology for comparing CIG models 44
Figure 4.1. IEEE-9 bus system with switches to adapt the generation portfolio [247] 47
Figure 4.2 Virtual Synchronous Generator Control [156] 48
Figure 4.3. Magnitude of Bode plot; a) 35% of CIG, b) 70% of CIG 50
Figure 4.4. Eigenvalue loci of the control modes for CIG levels between 5% and 100%; a) QPC-based model, b) DPC-based model 52
Figure 4.5. $\boldsymbol{G}\infty$ as a function of CIG level 52
Figure 4.6. Eigenvalue loci of the control modes for PLL bandwidth between 2 Hz and 30 Hz; a) QPC-based model, b) DPC-based model 53
Figure 4.7. $\boldsymbol{G}\infty$ as a function of CIG penetration level and different PLL bandwidth frequencies; a) QPC-based model, b) DPC-based model 54
Figure 4.8. IEEE 9-bus system for a diverse range of CIG penetration levels and system inertia

$Hsys$ 55
Figure 4.9. Eigenvalue loci of the control modes for power system inertia constant between 3.5 s and 1.16 s; a) QPC-based model, b) DPC-based model 56
Figure 4.10. $\boldsymbol{G}\infty$ as a function of inertia constant for 70% of the CIG penetration level 56
Figure 4.11. Voltage at bus B1 for a 0% of CIG level 57
Figure 4.12. Terminal voltage at bus B1 for 35% of CIG; a) 2 Hz, b) 5 Hz, c) 20 Hz, d) 25 Hz . 58
Figure 4.13. Terminal voltage at bus B1 for 70% of CIG; a) 2 Hz, b) 5 Hz, c) 20 Hz, d) 25 Hz . 58
Figure 4.14. Terminal voltage at bus B1 for 100% of CIG; a) 2 Hz, b) 5 Hz, c) 20 Hz, d) 25 Hz 59
Figure 4.15. Terminal voltage at bus B1 for 70% of CIG and 25 Hz of PLL bandwidth; a) 3.5 s, b) 1.16 s, c) 1.13 s 60
Figure 4.16. Terminal voltage at bus B1 for 100% of CIG and PLL bandwidth of 25 Hz 60
Figure 4.17. Terminal voltage at bus B1 for 100% of CIG and PLL bandwidth of 25 Hz 61
Figure 4.18. Active power injected at bus B1 for 100% of CIG; a) 2 Hz, b) 5 Hz, c) 20 Hz, d) 25 Hz 61
Figure 5.1. IEEE-9 bus system with switches to adapt the generation portfolio [247] 63
Figure 5.2. Comparative of CIG models for CIG levels ranging from 0% to 100% and PLL bandwidths of 2 Hz, 20 Hz, and 50 Hz; a) 2 Hz, b) 20 Hz, c) 50 Hz 66
Figure 5.3. Comparative of CIG models for SCR ranging from 0.4 to 1.2, CIG level of 50%, and PLL bandwidths of 2 Hz, 20 Hz, and 50 Hz; a) 2 Hz, b) 20 Hz, c) 50 Hz 67
Figure 5.4. Comparative of CIG models for CIG level of 50%, integral gain ki ranging 70 to 200, PLL bandwidth of 2 Hz, and VFF terms τvtdq of 0.0001, 0.001, and 0.01; a) $\tau v\text{tdq} = 0.0001$, b) $\tau v\text{tdq} = 0.001$, c) $\tau v\text{tdq} = 0.01$ 68
Figure 5.5. Comparative of CIG models for CIG level of 50%, integral gain ki ranging 70 to 200, PLL bandwidth of 20 Hz, and VFF terms τvtdq of 0.0001, 0.001, and 0.01; a) $\tau v\text{tdq} = 0.0001$, b) $\tau v\text{tdq} = 0.001$, c) $\tau v\text{tdq} = 0.01$ 68
Figure 5.6. Comparative of CIG models for CIG level of 50%, integral gain ki ranging 70 to 200, PLL bandwidth of 50 Hz, and VFF terms τvtdq of 0.0001, 0.001, and 0.01; a) $\tau v\text{tdq} = 0.0001$, b) $\tau v\text{tdq} = 0.001$, c) $\tau v\text{tdq} = 0.01$ 69
Figure 5.7. Summary of key findings 70
Figure A.1. Schematic diagram of a CIG connected to the grid [125] 89
Figure A.2. CIG outer voltage control with the inner current control of q axis 89
Figure A.3. CIG active power control with the inner current control system of d axis 90
Figure A.4. PLL control loop 90
Figure A.5. Diagram of CIG – GFM 92
Figure A.6. Virtual Synchronous Generator Control [156] 92
Figure A.7. Droop-based reactive power controller 93
Figure A.8. Inner control loops on the dq axis; a) voltage control loops; b) current control loops 93
Figure B.1. Diagram of CIG connected to the grid that operates in GFL mode [125] 101
Figure B.2. Active power control 101
Figure B.3. Voltage control 102
Figure B.4. SRF - PLL 102
Figure B.5. Current control loops; a) current controller on the d-axis; b) current controller on the q-axis 103
Figure B.6. Feed-forward terms; a) d-axis; b) q-axis 103
Figure B.7. Current source model based on a transfer function 104
Figure B.8. Inner current control loops without decoupling and feedforward terms; a) d-axis; b) q-

axis 105
Figure B.9. The CIG model developed in [35] 105
Figure B.10. Current control loops; a) current controller on the d-axis; b) current controller on the q-axis 107
Figure B.11. Droop-based active power controller 107
Figure D.1. $\boldsymbol{G}\infty$ as a function of CIG penetration level and different PLL bandwidth frequencies in the DPC-based model 111
Figure D.2. $\boldsymbol{G}\infty$ as a function of CIG penetration level and different PLL bandwidths; a) 2 Hz; b) 20 Hz 112
Figure D.3. Eigenvalue loci for PLL bandwidth between 2 Hz and 80 Hz for 70% of CIG levels; a) DPC – based model, b) VS-Type II model 113
Figure D.4. $\boldsymbol{G}\infty$ as a function of SCR; a) CIG Level 35%; b) CIG Level 50%; c) CIG Level 70% 115
Figure D.5. Eigenvalue loci for SCR between 1.19 and 0.41 for 50% of CIG levels; a) DPC-based model, b) VS-Type II model 116
Figure D.6. $\boldsymbol{G}\infty$ as a function of with the integral gain of the current controller ki ranging from 5 to 200 for a CIG level of 35% and PLL bandwidth of 2 Hz; a) $\tau v\text{tdq} = 0.0001$; b) $\tau v\text{tdq} = 0.001$; c) $\tau v\text{tdq} = 0.01$ 118
Figure D.7. $\boldsymbol{G}\infty$ as a function of with the integral gain of the current controller ki ranging from 5 to 200 for a CIG level of 35% and PLL bandwidth of 20 Hz; a) $\tau v\text{tdq} = 0.0001$; b) $\tau v\text{tdq} = 0.001$; c) $\tau v\text{tdq} = 0.01$ 119
Figure D.8. $\boldsymbol{G}\infty$ as a function of with the integral gain of the current controller ki ranging from 5 to 200 for a CIG level of 35% and PLL bandwidth of 50 Hz; a) $\tau v\text{tdq} = 0.0001$; b) $\tau v\text{tdq} = 0.001$; c) $\tau v\text{tdq} = 0.01$ 119
Figure D.9. $\boldsymbol{G}\infty$ as a function of with the integral gain of the current controller ki ranging from 5 to 200 for a CIG level of 50% and PLL bandwidth of 2 Hz; a) $\tau v\text{tdq} = 0.0001$; b) $\tau v\text{tdq} = 0.001$; c) $\tau v\text{tdq} = 0.01$ 119
Figure D.10. $\boldsymbol{G}\infty$ as a function of with the integral gain of the current controller ki ranging from 5 to 200 for a CIG level of 50% and PLL bandwidth of 20 Hz; a) $\tau v\text{tdq} = 0.0001$; b) $\tau v\text{tdq} = 0.001$; c) $\tau v\text{tdq} = 0.01$ 120
Figure D.11. $\boldsymbol{G}\infty$ as a function of with the integral gain of the current controller ki ranging from 5 to 200 for a CIG level of 50% and PLL bandwidth of 50 Hz; a) $\tau v\text{tdq} = 0.0001$; b) $\tau v\text{tdq} = 0.001$; c) $\tau v\text{tdq} = 0.01$ 120
Figure D.12. $\boldsymbol{G}\infty$ as a function of with the integral gain of the current controller ki ranging from 5 to 200 for a CIG level of 70% and PLL bandwidth of 2 Hz; a) $\tau v\text{tdq} = 0.0001$; b) $\tau v\text{tdq} = 0.001$; c) $\tau v\text{tdq} = 0.01$ 120
Figure D.13. $\boldsymbol{G}\infty$ as a function of with the integral gain of the current controller ki ranging from 5 to 200 for a CIG level of 70% and PLL bandwidth of 20 Hz; a) $\tau v\text{tdq} = 0.0001$; b) $\tau v\text{tdq} = 0.001$; c) $\tau v\text{tdq} = 0.01$ 121
Figure D.14. $\boldsymbol{G}\infty$ as a function of with the integral gain of the current controller ki ranging from 5 to 200 for a CIG level of 70% and PLL bandwidth of 50 Hz; a) $\tau v\text{tdq} = 0.0001$; b) $\tau v\text{tdq} = 0.001$; c) $\tau v\text{tdq} = 0.01$ 121
Figure D.15. Eigenvalue loci for ki between 5 and 100 for 50% of CIG level and the system represented using DPC; a) $\tau v\text{tdq} = 0.0007$, b) $\tau v\text{tdq} = 0.001$; c) $\tau v\text{tdq} = 0.01$ 122
Figure D.16. Angular frequency ωe of CIG1 for 70% of CIG; a) 2 Hz; b) 20 Hz; c) zoom 2 Hz; d) zoom 20 Hz 123
Figure D.17. Active power injected at bus B1 for 70% of CIG; a) 2 Hz; b) 20 Hz;c) zoom 2 Hz; d)

zoom 20 Hz..... 123
Figure D.18. Active power injected at bus B1 for 70% of CIG; a) 2 Hz; b) 20 Hz 124
Figure D.19. Angular frequency ωe of CIG1 for 50% CIG; a) SCR =1.2; b) SCR = 1.15; c) zoom out SCR = 1.2; d) SCR = 1.15..... 125
Figure D.20. Active power injected at bus B1 for 50% CIG; a) SCR =1.2; b) SCR = 1.15; c) zoom out SCR=1.2; d) SCR = 1.15..... 125
Figure D.21. Active power injected at bus B1 for 50% CIG; a) $SCR = 1.2$; b)$SCR = 1.15$ 126
Figure D.22. Active power injected by CIG1 to B1 for 50% CIG and τvtdq $= 0.0001$; a) ki $= 50$; b) ki $= 90$; c) ki $= 100$..... 127
Figure D.23. Active power injected by CIG1 to B1 for 50% CIG and τvtdq $= 0.001$; a) ki $= 50$; b) ki $= 90$; c) ki $= 100$..... 127
Figure D.24. Active power injected by CIG1 to B1 for 50% CIG and τvtdq $= 0.01$; a) ki $= 50$; b) ki $= 90$; c) ki $= 100$..... 127
Figure D.25. Active power injected by CIG1 to B1 for 50% CIG and τvtdq $= 0.0001$; a) ki $= 50$; b) ki $= 90$; c) ki $= 100$..... 128
Figure D.26. Active power injected by CIG1 to B1 for 50% CIG and τvtdq $= 0.001$; a) ki $= 50$; b) ki $= 90$; c) ki $= 100$..... 128
Figure D.27. Active power injected by CIG1 to B1 for 50% CIG and τvtdq $= 0.001$; a) ki $= 50$; b) ki $= 90$; c) ki $= 100$..... 128

1 Introduction

1.1 Motivation

For almost a century, stability has been recognized as one of the key issues to be addressed in order to achieve a secure power system operation [1]. Accordingly, energy regulators and system operators regularly perform stability studies to detect hazardous situations and develop corrective measures. These corrective measures are designed to maintain system stability for various contingencies and thus avoid cascading power interruptions [1]. For assessing stability problems, the study of power system transients is of interest. Figure 1.1 shows the time scales of transient phenomena relevant to power system analysis. These transients range from wave, electromagnetic, and electromechanical to thermodynamic phenomena [2]. Depending on the nature of the transients considered and the specific study, dedicated assumptions on component modeling are to be made. Thus, the system is represented at a respective and appropriate degree of detail for the limited bandwidth of transients under study.

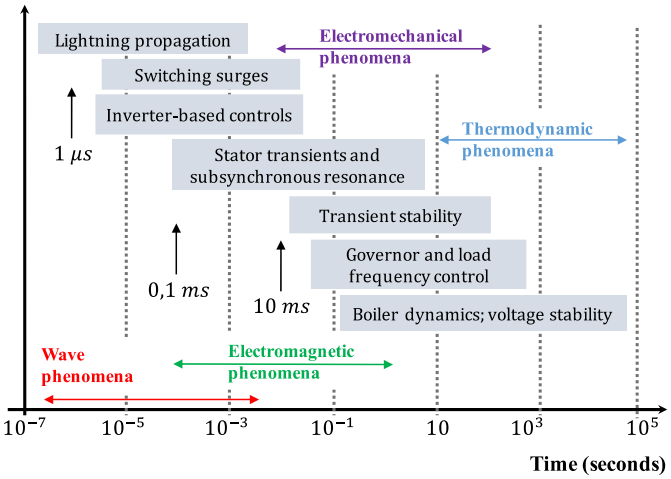

Di

Figure 1.1. Different time-scale of power systems transients [3].

Traditionally, the transients of main interest in stability studies are the electromechanical or slower phenomena related to synchronous machines and their control systems [4]–[6]. The time scale of electromechanical phenomena ranges from several milliseconds to seconds. The oscillation frequencies of the associated transients are typically between 0.1 Hz and 5 Hz [4], [5], [7]. This frequency bandwidth has allowed several modeling simplifications, which has led to the well-known stability assessments based on quasi-static phasor calculus (QPC) [5]. When using QPC, on the one hand, the behavior of the electric network is described by a set of algebraic equations, where electromagnetic transients are neglected. On the other hand, differential equations represent transients in the time scale of electromechanical phenomena. In this sense, it is assumed that voltage and current signals remain more or less at the fundamental frequency of the system, which can be 60 Hz or 50 Hz [8],[9]. Other quantities of system components with fast dynamic responses, such as stator flux linkages of synchronous generators in the range of electromagnetic transients, are neglected. Since the decay of electromagnetic transients associated with the network is

relatively fast, there has been little justification to include their effects in stability studies [4]. The simplified assumptions made in QPC models allow us to perform transient simulations to assess the stability of real-size power systems with adequate accuracy and computational time. Furthermore, it is commonly assumed that neglecting electromagnetic transients yields conservative stability analysis results [4].

Nevertheless, during the last years, there has been an increase in the penetration of converter-interfaced generation (CIG), such as wind and solar power, to meet renewable portfolios. In fact, in regions such as Germany, Ireland, Texas, and Denmark, transmission system operators (TSOs) and independent system operators (ISO) are already facing operational conditions with more than 50% CIG penetration of the instantaneous load demand [10]–[12]. With the increase of CIGs, the nature of transients in power systems is subject to changes because CIGs have fast responses [13], [14]. The dynamic of their control systems has small time constants, leading to dynamic couplings with the electromagnetic transients of the network. This can be seen in Figure 1.1, where the time scale related to the inverter-based controls varies from a few microseconds to several milliseconds, thus being much faster than the electromechanical transients associated with synchronous generators.

Consequently, the transients of power systems dominated by CIG become faster and more complex, leading to new control interactions and stability issues [15]–[19]. Among the key instability drivers in CIG are their control loops with fast response times, such as the phase-lock-loop (PLL) controllers [15], [16], and the inner current loop controllers [15], [20]. Although recent studies have shown that these control loop instabilities are more likely to occur in weak networks with low levels of inertia, they may also appear in the cases of robust power systems with low levels of CIG, depending on the operating conditions of the system [21].

In cases of high penetration of CIG levels, the fast dynamic response of the converters starts to dominate the transient behavior of power systems. The transients of interest for stability studies may thus move outside the validity range of QPC assumptions, extending to the time scale of electromagnetic phenomena. In these cases, the assumption that fast transients do not affect system stability may be incorrect, meaning that they should not be further neglected in case of high penetration levels of CIG. Indeed, according to [11],[22], the fast transients of power electronics converters may invalidate the typical time-scale separation approach used in stability assessments. Therefore, the conclusions drawn based on time-domain simulations using QPC could be erroneous in critical situations. While some recent studies have addressed different stability issues in the presence of CIG [15]–[18], what is still missing is a scientific foundation for the modeling, analysis, and control of power systems dominated by CIG [11], [22].

Given the fact that the fast phenomena of CIG may extend the bandwidth of relevant transients for stability studies, the question of how this affects the validity of using QPC-based models for the evaluation of stability remains unanswered [11], [12], [22]–[24]. With the increasing share of CIG, users of simulation tools and power system planners urgently need to answer these questions. This thesis is concerned with the pertinence of using QPC models for stability assessments of power systems with high CIG levels. This thesis investigates the validity of using these models for stability studies. Furthermore, it is investigated at which point the fast dynamic response of CIG extends the bandwidth of relevant transient for stability assessments. The effects of neglecting fast electromagnetic transients related to the network, machine stator, and fast dynamic response of CIG on the accuracy of stability studies based on QPC models are investigated. The proper degree of detail required in the CIG models and controls for stability assessments and the conditions under

which these models are accurate are also investigated.

To address the above goals, a set of comprehensive comparative analyses is systematically performed to verify the validity of QPC-based models. Dynamic phasor calculus (DPC) is considered as an alternative to QPC. In DPC, the electric network is described through a set of differential equations rather than algebraic ones, which is more accurate than the QPC models [9], [25]–[30]. DPC-based models have been applied to simulate a broad range of transients in different systems, including unbalanced distribution systems [31], microgrids [29], transients of electric machines [25], and power electronic systems [30]. The use of DPC appears to be a suitable solution for stability analysis due to its computational efficiency for simulations where both electromagnetic and slow electromechanical transients are of main interest [26]. To verify the results obtained by using DPC models, Electromagnetic Transient (EMT) simulations are performed in PSCAD [32], [33]. The EMT simulations include high-frequency transients due to the switching of power electronic devices.

1.2 Problem Statement

Assessing power system stability is key to ensuring a secure power system operation. Power system stability studies are performed mainly through time domain simulations [4], [6]. Traditionally, the focus of stability studies has been on slow electromechanical transients, which are typical of synchronous generators. To simulate such transients, the state of the art is to use QPC-based models. This means that EMT associated with the electric network, transients of machine stator, and other fast transients associated with CIG are neglected. The validity of the results obtained from the stability studies based on QPC models relies on the assumption that slow electromechanical transients are relevant and EMT with other fast transients are negligible from a power system stability perspective.

In power systems dominated by synchronous generators, time domain simulations based on QPC models have been shown to provide results with adequate accuracy for stability purposes [4], [6]. This is because the slow electromechanical transients associated with synchronous generators and their control systems dominate the dynamic response of such power systems. However, synchronous generators are being replaced due to the increased penetration of CIG. CIGs have control systems with a fast dynamic response. This may lead to dynamic interactions among electromagnetic transients of the electric network, machine stator, and CIG control systems. For power systems with high levels of CIG penetration, the fast dynamic response of the converters may no longer be negligible and may even dominate the transient behavior. Thus, the bandwidth of relevant transients might be extended toward the electromagnetic time-scale. Under this assumption, fast phenomena related to the network and fast response devices should not be further neglected. Consequently, assumptions made in QPC models may lead to erroneous conclusions about the stability of the power system. These modeling inadequacies can lead to over or underestimating the stability limits. Consequently, power systems may operate under higher risk or less efficient conditions because stricter restrictions may be imposed on the grid code than the system.

Significant efforts have been made to develop CIG models for stability studies based on QPC-based models in the literature during the last years [34]–[36]. However, the validity of the most widely used CIG models for stability studies based on QPC is still not thoroughly investigated. Indeed, what is still missing, is a scientific foundation for the modeling and control of power systems dominated by CIG. The proposed models have different degrees of detail, mainly to

represent the inner control loops and the AC filter. The impacts of the assumptions and simplifications made in the CIG models on the results obtained from stability studies are still neither fully understood nor comprehensively investigated.

In the context above, this thesis is concerned with stability assessments based on QPC models in power systems with high levels of CIG. Specifically, this thesis addresses the following problems:

1. The validity range of stability assessments based on QPC models in power systems with high levels of CIG.
2. The bandwidth of relevant transients for power system stability in the case of power systems dominated by CIG.
3. The proper degree of detail required in CIG models for the assessment of power system stability and the conditions under which these models are accurate.
4. The effects of the fast dynamic responses of CIG on system stability assessments based on QPC models.

1.3 Hypotheses

The central hypothesis of this thesis can be summarized as follows: *As the penetration level of CIG increases and synchronous generators are replaced, there is a point upon which using models based on QPC becomes unsuitable for stability assessments*.

Given the above, the specific hypotheses are as follows:

H1. As CIG levels increase and synchronous generators are replaced, the frequency bandwidth of the relevant transients for stability assessments moves outside the valid range of models based on QPC. Therefore, electromagnetic phenomena related to the network and components with a fast dynamic response cannot be neglected.

H2. The models related to both fast and slow dynamics of CIG control systems significantly influence the accuracy of stability assessments based on QPC in power systems with high levels of CIG.

H3. The appropriate level of detail required to model CIG power plants is dependent on the CIG control systems implemented, their parameters, and the robustness of the power system under study.

H4. As the penetration level of CIG increases and synchronous generators are replaced, there is a point upon which using models based on DPC are more suitable than models based on QPC for stability assessments of power systems.

1.4 Objectives

1.4.1 General Objective

The main objective of this thesis is to investigate the validity range of stability assessments based on QPC models as well as to investigate the appropriate level of detail required for modeling CIG for stability assessments of power systems with an increased share of converters.

1.4.2 Specific Objectives

The specific objectives of this research are:

O1. To identify the advantages and disadvantages of different modeling techniques for simulating power system transients.
O2. To conduct a comprehensive review of the different existing CIG models proposed in the literature to assess system stability.
O3. To develop and implement different CIG models based on DPC and QPC to assess power system stability considering high CIG penetration levels.
O4. To propose a systematic methodology to determine the validity range of QPC-based models for assessing system stability.
O5. To implement and validate the proposed methodology on a test network.
O6. To identify the validity range of QPC- and DPC- based models for power systems with CIG as well as the critical CIG control system parameters that have a significant influence on the accuracy of models based on QPC.
O7. To determine if the frequency bandwidth of relevant transients for stability assessments extends towards the electromagnetic time scale as CIG increases.
O8. To investigate, identify, and conclude on the appropriate level of detail required to model CIG for stability assessments.

1.5 Scope

This thesis investigates the validity range of stability assessments and the appropriate level of detail required to model CIG in stability assessments of power systems with an increased share of converters. To achieve the objective, some general assumptions and considerations are made to delimit the scope of this thesis. The CIG models used are aggregated. As a consequence, internal network topologies of particular plants are not considered. The model used for CIG assumes operation in the grid following mode (GFL) with active and voltage control implemented. The effect of control strategies to support the frequency of the system in CIG operating in GFL is beyond the scope of this document.

The control systems used in all CIG models are generic, where the measurement delays and FRT from particular grid codes are neglected in modeling. Generic switching strategies of electronic devices in converters are considered for validation purposes. Finally, a balanced three-phase power system is considered for all the analyses shown in this work.

1.6 Contributions

The main contributions of this research are as follows:

C1. A systematic methodology to identify the validity range of QPC models for stability assessments. The methodology defines a set of criteria to determine quantitatively and systematically the conditions for which the use of QPC models is suitable. The sequence of stages enables the identification of critical parameters of the CIG control system that significantly influence the accuracy of models based on QPC.

C2. A comprehensive stability analysis using the proposed methodology in a modified IEEE test

network. The study is carried out for a broad range of CIG penetration levels, including 100 %. The results obtained are validated through detailed EMT simulations.

C3. Identification of the validity range of stability assessments based on QPC models in power systems with high CIG levels. Through applying the methodology proposed in **C1**, a clear understanding of the limitations of QPC models for stability studies in power systems dominated by CIG is obtained. The CIG control system parameters that considerably affect the accuracy of QPC are identified. It is also validated that the fast dynamic response of CIG extends the bandwidth of relevant transients to the electromagnetic phenomena (Hypothesis **H1**).

C4. A comprehensive survey and comparative study of the most common CIG models used for stability assessments based on QPC. The models are put into context and related to each other. The DPC models are used as reference models in the comparative study. Assessment is performed using modal analyses to clearly understand the impact of the degree of detail used in CIG models.

1.7 Publications

During the development of this thesis, the following journal paper was published:

1. J. Vega-Herrera, C. Rahmann, F. Valencia, and K. Strunz, "Analysis and application of quasi-static and dynamic phasor calculus for stability assessment of integrated power electric and electronic systems," *IEEE Trans. Power Syst.*, pp. 1–10, 2020

Additionally, the following conference papers were published:

1. C. Rahmann, J. Vega, and F. Valencia, "Validity range of fundamental frequency simulations under high levels of variable generation technologies," in *X Bulk Power Systems Dynamics and Control Symposium, IREP*, 2017, pp. 1–6.
2. J. Vega, C. Rahmann, and F. Valencia, "Stability assessments in systems with high levels of photovoltaic generation," in *ENERSOL*, 2017, pp. 1–5

1.8 Thesis Outline

This thesis is organized as follows. In Chapter 2, the literature review of the main topics related to this thesis is presented. It includes power system stability, the impact of CIG on power system stability, modeling approaches for the simulation of power system transients, CIG technologies, and CIG modeling in power system stability studies. Special attention is dedicated to the last two topics because those are highly related to the thesis's objectives and contributions. Chapter 3 presents the methodologies followed to achieve the objectives and validate the hypotheses of this thesis. First, the proposed methodology to identify the validity range of QPC models is described in the context of stability assessments. Second, another methodology is described, which is followed to understand the impacts of the degree of detail used in CIG models. In Chapter 4, the results obtained by applying the first proposed methodology are presented. Comparative analyzes between DPC and QPC-based models are performed to validate and verify the main hypotheses of this research. Chapter 5 shows the results obtained by applying the second methodology. A set of comparative analyzes among the main CIG models proposed in the literature is carried out. Modal analysis is the primary tool for this purpose. The impacts of different assumptions and simplifications usually made in CIG models for stability assessments are shown. Finally, Chapter 6 shows the main conclusions of this thesis. Furthermore, it describes future work.

2 Literature Review

2.1 Introduction

This chapter describes and summarizes the main topics related to this thesis. Section 2.1 presents fundamental concepts of power system stability. The impacts of CIG on power system stability are summarized in Section 2.2. In Section 2.3, different modeling techniques used for dynamic simulations of power systems are described and analyzed. Section 2.4 summarizes the most typical dynamic models to represent transmission lines and synchronous generators in time-domain simulations for stability assessments. Sections 2.5 and 2.6 present a detailed review of CIG in power systems and modeling approaches used to represent CIG and their controls in power system stability studies. Compared to previous sections, the review is conducted in more depth because it is considered a contribution to this research - specifically, the contribution **C4**. Finally, Section 2.7 summarizes the main finding of the literature review.

2.2 Power System Stability

The IEEE/CIGRE Joint Task Force on Stability Terms and Definition proposed the most common definition of power system stability. It states [1]:

"Power system stability is the ability of an electric power system, for a given initial operating condition, to regain a state of operating equilibrium after being subjected to a physical disturbance, with most system variables bounded so that practically the entire system remains intact."

The above definition considers a power system as a whole. For example, the power system is considered stable if one generator loses synchronism during small or large disturbances without cascading effects. Electric power systems are nonlinear in nature, with a multi-time scale transient response, as shown in Figure 1.1. In addition, power systems constantly change their operating conditions and are subjected to small or large disturbances. The stability of these systems depends on the initial conditions and the nature of the disturbance [4]. In general, a power system can be stable for a specific operating condition and physical disturbance but unstable for another.

Stability may be considered a condition of equilibrium between opposing forces, which is maintained during a wide range of disturbances [1]. The power system is stable if, after a physical disturbance, the system states reach a new equilibrium, and the integrity of the system is maintained. If the system is unstable after a physical disturbance, it will result in cascading interruptions. Under such conditions, a significant portion of an electric power system is not preserved.

Power systems can undergo various forms of instabilities that may be appropriately understood and effectively dealt with when addressed separately. Because of the high dimensionality and complexity of stability problems, it helps to make simplifying assumptions to analyze specific types of problems using an appropriate degree of detail of system representation and appropriate analytical techniques [1], [4].

To facilitate stability analysis, the power system stability problem has traditionally been classified as rotor angle, frequency, and voltage stability. However, recently, in 2020, due to the increasing

share of CIG, the definitions and classification of power system stability were revisited and extended by the IEEE Task Force "Stability definitions and characterization of dynamic behavior in systems with high penetration of power electronic interfaced" [19], [37]. The current classification of power system stability is shown in Figure 2.1. Two new types of stabilities were added, resonance stability and converter-driven stability. These types are shown in Figure 2.1 in red. The works [19], [37] recognize that the dynamic behavior of power systems is changing due to the complex and fast response of CIG. This fact leads to new stability issues in power systems with time constants associated with EMT and electromechanical transients. Detailed models are needed for resonance stability and fast interaction of converter-driven stability. However, the details required for CIG models to assess the other types of stability are unclear [37].

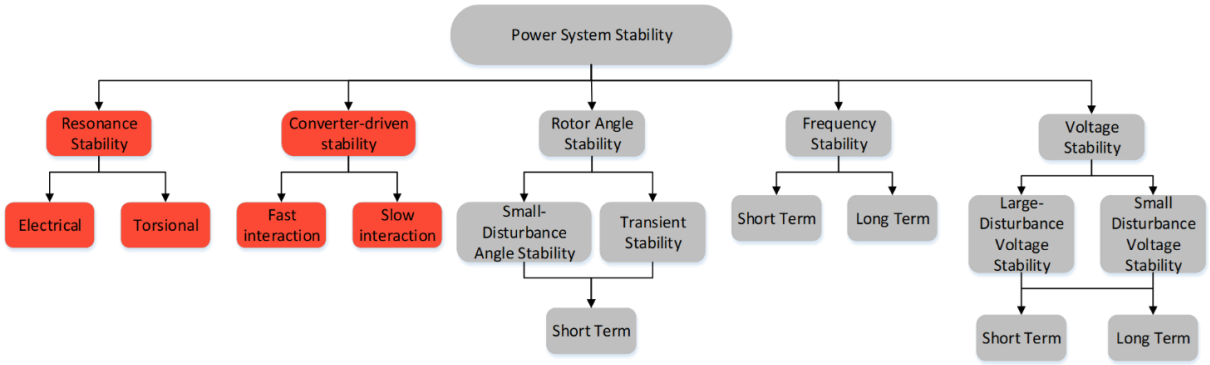

Figure 2.1. Classification of power system stability extended considering CIG [19], [37]

Despite the proposed classifications, it should be noted that power system stability is essentially a single problem [1], [4]. For instance, rotor angle and voltage instabilities often occur simultaneously, or one may lead to another without any clear distinction [4]. This is particularly present in high-stress systems.

Due to the complexity of power system dynamics, time domain simulations based on QPC models have been the main tool to assess the stability of real-size power systems so far [8]. This does not include resonance and converter-driven stability due to fast interaction because they need simulation tools based on EMT models. The simulation based on QPC focuses on the slow electromechanical transients of synchronous generators with typical oscillation frequencies ranging between 0.1 Hz and 5 Hz [4], [5], [7]. The focus on these transients relies on the dynamic responses of synchronous machines and their control systems have traditionally dominated the transient response of power systems. The time frame of interest for short-term phenomena ranges approximately from 0 to 5 s [1]. For long-term phenomena, the time frame of interest typically ranges from several seconds to several minutes [1].

The stability analysis based on time domain simulations verifies if, for a given operating condition and contingency, the trajectories followed by the state variables settle down to an acceptable steady-state [38]. The accuracy of such analysis depends mainly on the validity of the models used in describing the transients of interest. Therefore, appropriate dynamic models are essential to assess power system stability through time-domain simulations.

2.3 Impact of CIG on Power System Stability

This section describes the impacts of CIG on power system stability. The CIGs considered are type

4 wind turbines and photovoltaic power plants because the primary generation source is completely isolated from the grid through the converters. Thus, the effects that CIG has on system stability are mainly due to the dynamic response of the control systems implemented in the CIG units. For this reason, this section focuses on those types of CIG.

2.3.1 Reduction of Short Circuit Levels

In power systems dominated by synchronous generators, the short circuit level (SCL) is an indicator that traditionally represents the voltage stiffness of a network [24], [39], [40]. When the SCL level at a specific busbar is high, the network strength is also high [41]. Thus, the voltages do not deviate significantly from their initial values when the system is subjected to small disturbances. This in turn means that the Thevenin equivalent impedance seen from the pertinent bus is relatively low, meaning that the voltages are less sensitive to changes in power flows (dV/dP and dV/dQ) [42].

Many synchronous generators are connected to the network in power systems with high SCL. During fault conditions, these generators support the stability of the grid. Short circuit currents flowing into the network during a fault condition can be considered as the response of the synchronous generators to voltage drops, which attempt to restore the system to normal operation. Therefore, the SCL is considered a good measure of the dynamic performance of the system during contingencies [43].

In power systems with high penetration levels of CIG, the SCL decreases. CIG can provide low short circuit currents, with values between 1.1 and 1.5 times the rated current [44]. These values are significantly lower than the fault current that a synchronous generator can provide [45]. The exact fault current contribution of CIG varies depending on the fault, its duration, and the pre-fault operating condition. The contribution of the fault current is also influenced by the control strategies implemented in the converters. In fact, this is the main difference of CIG from synchronous machines, where the short circuit current depends only on its natural characteristics in the case of the latter [11].

Since synchronous generators are the main sources of short-circuit current contributions [39], the displacement of synchronous generators by CIG leads to a reduction in the system strength [24], [39], [40]. Reduction of system strength leads to higher values of dV/dP and dV/dQ. Thus, small disturbances in power flows can significantly change the voltages of the network [42]. Weak power systems may experience high voltage drops during contingencies. After the fault clearance, such systems have difficulties in recovering the voltages, and this could cause the nearby synchronous generators to lose their synchronism. As a result, reducing the strength of the system by increasing the CIG can lead to poor dynamic performance of the system during contingencies. This in turn makes the power system more prone to facing stability problems [39], [42], [43].

2.3.2 Reduction of System Inertia

An increase of CIG in power systems implies a reduction of the total system inertia due to the displacement of synchronous generators. The secure operation and stability analysis of low-inertia power systems is a challenge that many researchers have highlighted during recent years [46]–[50]. System inertia is a measure of how well the system can deal with power imbalances and still maintain a stable frequency [47].

The inertial response is naturally provided by rotating machines connected to power systems, e.g., synchronous and induction machines. System inertia significantly affects both: the activation of under-frequency load shedding schemes (UFLSS) during contingencies and the performance of the system frequency control in steady state [51]. During the first seconds after a power imbalance, the system frequency decreases at a rate determined mainly by the system inertia. For power systems with low system inertia, the system frequency decreases faster. Since synchronous generators are electromechanically coupled to the system, rotating masses will inject or absorb kinetic energy into or from the grid for several seconds to counteract the frequency deviation according to their inertia [47], [52], [53]. This natural response from synchronous generators is provided whenever the mismatch between generation and consumption remains. This response makes the system frequency dynamics slower and then easier to regulate [53]. In case of a sudden disconnection of a synchronous generator, the imbalance is initially compensated by extracting kinetic energy from the remaining rotating machines. This natural action is essential to arrest the decline in frequency to prevent the activation of automatic UFLSS. Beyond this natural response, the primary frequency controls of synchronous generators react by changing the generated power in order to recover the power balance.

The CIG behaves differently from a frequency perspective than synchronous generators [11], [52]. The main differences are that most of these sources usually do not contribute either to the system frequency regulation or inertial system response [52]. As synchronous generators do, CIG cannot naturally provide an inertial response to the system. Furthermore, CIGs are usually controlled to inject their maximum available active power into the grid, meaning that these power plants do not maintain power reserves to help maintain the balance between the generated power and demand. Photovoltaic power plants, for example, do not have moving elements, and therefore there is no stored kinetic energy available as in the case of synchronous generators [52]. Although these power plants can store energy in their DC link, it is negligible compared to the energy stored in rotating machines [11]. In the case of wind power plants based on type 3 or type 4, the power converter fully or partly electrically decouples the generator from the grid. This implies that the kinetic energy stored in their moving parts is not used to support the frequency unless a particular control is designed for that purpose [52]. The frequency support depends on the energy storage available, i.e., DC-Link or external energy storage system, and outer control loops such as synthetic inercia and droop control.

Several investigations have shown that replacing synchronous machines with inertia-less CIG can degrade the primary frequency and the inertial system response [40]. This can be especially critical in islanded and small isolated systems, where the inertia without CIG is already low [52], [54]. Reduced system inertia decreases the frequency nadir after a generation loss and leads to a higher rate of change of frequency (RoCoF) at the beginning of a contingency [52]. Thus, leading to faster frequency dynamics of power systems [11], [53]. This may result in more frequent and larger frequency excursions after a generation loss, leading to more frequent and deeper activations of UFLSS. Accordingly, it jeopardizes the frequency stability of the system [52], [55].

2.3.3 Dynamic Response of Power Systems

The power system dynamics are changing due to the increasing share of power electronics in photovoltaic and wind power plants, HVDC transmission, FACTS, and loads. Some examples of the increasing share of CIG are South Australia, Texas, Ireland, and Tasmania, where the maximum instantaneous penetration levels of CIG have reached 150%, 66%, 92%, and 95%, respectively [10]–[12], [56]. CIG control systems are modular and flexible, with dynamic responses on the time

scale of electromechanics and electromagnetic phenomena. This presents challenges and opportunities [57]. On the one hand, the complete modularity in the control systems makes it possible to support the voltage and frequency of the power systems on a time scale much lower than in control systems typically used in synchronous generators [11]. On the other hand, due to the fast dynamic responses of CIG, power systems may experience poor dynamic performance, which can jeopardize power system stability [15]–[19].

Several countries have observed and reported new stability phenomena as CIG connects to the grid. This can occur with a high or low level of CIG. The poor dynamic performance is commonly manifested by the undamped oscillation of variables, e.g., voltage, current, active and reactive power [16], [58]–[60]. The frequencies of these oscillations vary significantly from 4 Hz to 100 Hz approximately, although according to [19], the frequencies might take values in the order of hundred Hz to kilo Hz. Some real-world CIG problems are presented as follows.

In the north of China, from December 2012 to 2013, 58 events were detected [61] [62]. These events are due to poor dynamic performance where the poorly damped oscillation with 6-9 Hz frequencies. The cause is mainly related to the interaction between the control system of wind power plants and the compensated transmission network. Furthermore, in 2015, the west of China experienced another event in wind power plants with an oscillation frequency of 30 Hz [63]. This is considered exceptional because the permanent magnet synchronous generator (PMSG)-based dispatch of the wind power plant was very slow, near to 5% of its rated capacity. This event was spread throughout the grid. The cause was the interaction of PLL and the grid. The PCC of the generator becomes weak for the operating conditions associated with the event.

Other events have been seen worldwide. For example, Hydro One Canada has experienced poorly damped oscillations in solar power plants with frequencies of 80 Hz in 2015 [64] and wind power plants based on PMSG with frequencies of 3.5 Hz [65]. Australia in 2015-2019 [66], [67], Australia in 2020 [68], Great Britain in 2019 [69], and Eastern U.S in 2021 [70] have detected poorly damped oscillations with frequencies of 7 Hz, 17-19 Hz, 9 Hz, and 38 Hz, respectively. These new stability issues are called subsynchronous control interactions in the literature [58], [61]. However, [19] classifies these new stability phenomena as converter-driven stability (see Figure 2.1).

In the previously mentioned events, all CIG operated in the GFL mode. In GFL, the connection of CIG to weak systems may cause the poor dynamic performance of PLL and adverse dynamic interactions between CIG control systems and other CIG or power systems components [16], [58], [71]–[75]. The PLL can interact with the inner current control, voltage control, network, or synchronous generator. The outer controller of CIG, such as voltage control, may interact with the transmission network and becomes unstable when the network is weak. The frequencies related to undamped oscillations vary significantly considering implemented control, operating conditions (dispatch), operating mode, and control system parameters [16], [58], [71]–[75]. This dynamic phenomenon may jeopardize power system stability. Therefore, it is essential to understand these new dynamic phenomena and develop proper models and methods for analyzing and designing power systems with CIG.

The protection systems also are impacted by the fast and complex dynamic responses of CIG power plants. Compared to synchronous generators, the short circuit characteristics of CIG are significantly different [76], [77]. In synchronous generators, the short circuit current characteristics are well known. The fault current is high amplitude, uncontrolled, and mainly determined by the circuit parameters. These characteristics allow the development of well-known and accepted

methods for calculating short circuit currents [4]. Thus, protection systems can be set, and misoperation may be avoided.

On the other hand, in CIG, the fault current has low amplitude and depends on the power electronic devices' control system. The control system is manufacturer-specific, making the detailed implementation of the control structure unknown [78]. Low short circuit currents may impact the performance of various protection functions. These may include line distance protection, memory-polarized zero sequences directional protective relay element, negative sequence quantities-based protection, line current differential protection, phase comparison protection, RoCoF, and power swing detection [39], [76]. Some examples of these issues are described below.

The sequence components of the fault currents of CIG do not have a zero-sequence, and the negative sequence is close to zero. As a result, misoperation of the protection systems might occur because the relay cannot assert the fault condition [77], [79]. Some grid codes have included requirements for injection of negative sequence during unbalanced faults, e.g., Germany [80]. Additionally, the fault current can be of inductive or capacitive nature, causing the protection function of negative sequence-based directional ground fault protection to take incorrect directionally decisions [81].

The transient behavior of short circuit currents of CIG is causing the standard methods based on QPC for calculating fault current to become inappropriate for setting protection systems. Therefore, the method and models used to calculate fault currents need to be improved. In this sense, EMT models can be used to simulate short circuit transients accurately, allowing better tuning of protection systems [79].

As CIG increases, a decrease in system inertia is expected. This may lead to a larger RoCoF, sufficient for an undesired trigger of the RoCoF protection system in synchronous generators [76]. For a fast dynamic response, fast measurements are required, which can lead to higher errors in the frequency and RoCoF [82]. Particularly in the transient period immediately after a fault. This increases the risk of load loss due to the activation of under-frequency load-shedding schemes and the risk of instabilities. Higher RoCoF values can also trigger local protection relays, which can cause cascading disconnection events [82]–[84].

Additionally, the spatial inertia distribution is becoming relevant. Recent research has shown that for a given contingency, the post-fault frequency behavior is no longer a function of the total system inertia but also of its spatial distribution in the grid [11], [85], [86]. In this way, an uneven inertia distribution -owing to not uniformly distributed CIGs- may lead to nonuniform frequency variations across the network busbars characterized by different initial RoCoF rates, which could threaten the stability of the system [86].

2.4 Modeling Approaches for Simulation of Power System Transients

Figure 1.1 shows that the time scales of power system transients span from microseconds to several hours. In general, the complete dynamic response of power systems can be seen as a combination of electromechanical and electromagnetic dynamic systems [2]. The electromagnetic transients are fast dynamics due to the interaction between the magnetic fields of inductances and electrical fields of capacitances in power systems. On the other hand, electromechanical transients are due to the interaction between the mechanical energy storage in electric machines and the electrical energy stored in the network. Due to the characteristics and time scales of transients in power systems, it

is complex to simulate both electromagnetic and electromechanical transients [6], [8]. Accordingly, dedicated assumptions and mathematical transformations can be used to develop component models depending on the transient nature to be studied. Thus, the system can be represented at an appropriate degree of detail for the bandwidth of the transient under study.

In Figure 2.2, a general diagram of the main existing modeling approaches for simulation power system transients. The classification is based on the representation of electrical quantities of power systems, e.g., voltage and current signals. The modeling approaches considered include phasor calculus and the EMT approach. On the one hand, in the EMT approach, real and instantaneous signals represent each power system component in the abc phase domain. Simulators of the EMT programs (EMTP) type are the most commonly used to process such signals [26].

On the other hand, phasor calculus has been used in power systems to efficiently simulate EMT and electromechanical transients [5], [9], [25]–[30]. Complex signals represent the electrical quantities of the power system. QPC is focused on the transient simulation of slow electromechanical transients, whereas DPC is mainly used when electromechanical and EMT are of interest [5]. The main concepts related to modeling techniques are briefly described below. DPC concepts are discussed in more detail than those related to the EMT approach because DPC is key for this thesis.

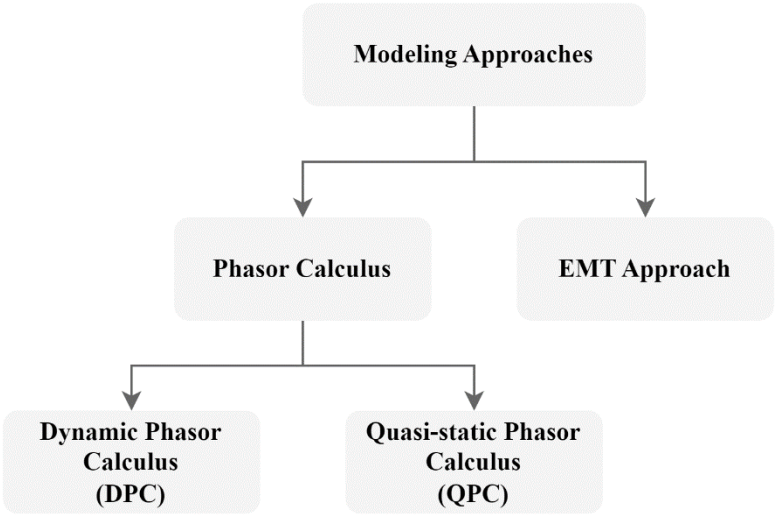

Figure 2.2. Classification of modeling approaches for the simulation of power system transients

2.4.1 Electromagnetic Transient Approach

In power systems, the waveforms of voltages and currents are real and instantaneous signals. These signals are generally represented in abc phase variables in the EMT approach. Component models within a power system based on instantaneous signals are the basis for other modeling techniques. In a representation based on abc phase variables, any component can be modeled directly, e.g., electric machines, transmission networks, and power electronic devices such as FACT, HVDC, and CIG [87], [88]. The representation based on abc phase variables is commonly used in simulators of the EMTP type. EMTP-type simulators are the most widely used for accurately simulating transients in the power system. For instance, studies of subsynchronous oscillations, short circuits, HVDC systems, power electronics, insulation coordination, harmonics, among others, can be performed using simulators of EMTP type [89] [90], [91]. In these simulators, the

accuracy of the numerical integration method depends on the time step size used for the simulation of the transient under study. The time-step size is chosen according to the frequency of transients considered relevant in the studies. As the frequency of the transient increases, a smaller time step is needed for accurate simulation of such transients [92].

Although it is theoretically possible to perform power system stability analyzes using the representation of real and instantaneous signals [93], the computational burden and simulation time in the EMTP tools increase drastically. The reason is that to simulate power system transients accurately using models based on abc phase variables, small time-step sizes in EMTP tools are to be used. For the simulation of transients associated with AC power systems, an upper limit of the time-step size is given because of the system frequency. This means that EMTP tools need to use very small time-step sizes to obtain adequate numerical accuracy in simulations, e.g., 50 μs or even lower. Considering the size of large power systems and small time-step sizes, stability assessments based on EMTP tools require a significant computational burden and simulation time. This in turn makes EMTP unsuitable for stability studies of large power systems [94] [8], [95].

For the above reasons, real and instantaneous signal representations are used mainly for transient simulations of lighting, overvoltage, power converter considering switching devices, and subsynchronous resonances, among others [88], [89], [96]. In these applications, it is usually required to model only a small part of a power system. Therefore, these transient simulations can be performed with reasonable computational times. Moreover, small-signal analysis cannot be performed using this representation of the component model because the equilibrium point cannot be well defined and depends on time [97], [98].

2.4.2 Phasor Calculus

2.4.2.1 Dynamic Phasor Calculus

In normal operation, voltages and currents of power systems are balanced three-phase sinusoidal signals with a system frequency of $f_c = 50$ Hz or $f_c = 60$ Hz [5]. During low-frequency perturbations, power systems experience low-frequency transients. In the frequency domain, these transients are characterized by a bandpass characteristic centered on f_c. This frequency can be considered as the carrier frequency. This band-pass characteristic is displayed in Figure 2.3, where the signal $x(t)$ can be a voltage or a current signal [26], [28]. The bandwidth is usually smaller than the system frequency. From the figure, it can be seen that the Fourier spectrum $|\mathcal{F}[x(t)]|$ is symmetric to the axis $f = 0$ Hz. Accordingly, the negative frequency components of the spectrum do not provide further information about the real signal $x(t)$.

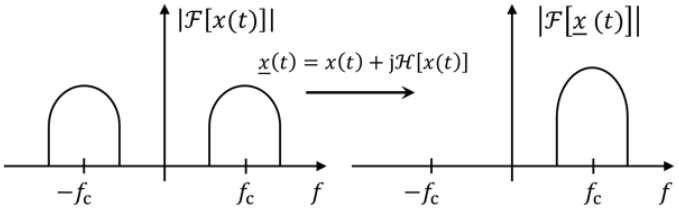

Figure 2.3. Application of Hilbert Transformation

The real signal $x(t)$ can be represented by its analytic signal. An analytic signal is a complex signal with no negative components on its Fourier spectrum. The analytic signal $\underline{x}(t)$ of the real signal

$x(t)$ is defined as follows [99]:

$$\underline{x}(t) = x(t) + \mathrm{j}\mathcal{H}[x(t)] \tag{2.1}$$

where the underscore indicates that $\underline{x}(t)$ is complex, and $\mathcal{H}[\,.\,]$ is the Hilbert transform, which is formally defined as:

$$\mathcal{H}[x(t)] = \frac{1}{\pi}\int_{-\infty}^{\infty} \frac{x(\tau)}{t-\tau}\,\mathrm{d}\tau \tag{2.2}$$

The resulting Fourier spectrum $\left|\mathcal{F}\left[\underline{x}(t)\right]\right|$ only extends to positive frequencies, as shown in Figure 2.3 on the right. An analytic signal can be shifted by the shift frequency f_s as follows:

$$\underline{x}_\mathrm{s}(t) = \mathcal{P}\left[\underline{x}(t)\right] = \underline{x}(t)\mathrm{e}^{-\mathrm{j}2\pi f_\mathrm{s} t} \tag{2.3}$$

In power systems, it is of major interest to set the shift frequency $f_\mathrm{s} = f_\mathrm{c}$ of 50 Hz or 60 Hz. The new signal $\underline{x}_\mathrm{s}(t)$ then appears as a dynamic phasor, and its frequency spectrum changes, as shown in Figure 2.4. The shifted signal behaves as a low-pass signal, whose maximum frequency is reduced due to the shifting. As a result, a lower sampling rate can be used to simulate the transients using dynamic phasor signals compared with the natural bandpass signals $x(t)$. The original signal can be reconstructed through the reverse process:

$$x(t) = \mathrm{Re}\left[\underline{x}_\mathrm{s}(t)\mathrm{e}^{\mathrm{j}2\pi f_\mathrm{s} t}\right] \tag{2.4}$$

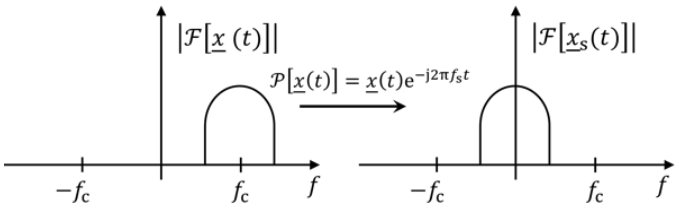

Figure 2.4. Shifting by carrier frequency

The simulation of power system transients involves the numerical solution of a set of differential and algebraic equations (DAEs). To obtain the DAEs using DPC, the derivative of $\underline{x}_\mathrm{s}(t)$ is to be known. Deriving the analytical signal $\underline{x}(t)$ described in (2.3) and defining $\omega_\mathrm{s} = 2\pi f_\mathrm{s}$ yields:

$$\mathrm{e}^{-\mathrm{j}\omega_\mathrm{s} t}\frac{\mathrm{d}\underline{x}(t)}{\mathrm{d}t} = \frac{\mathrm{d}\underline{x}_\mathrm{s}(t)}{\mathrm{d}t} + \mathrm{j}\omega_\mathrm{s}\underline{x}_\mathrm{s}(t) \tag{2.5}$$

In DPC, the EMT related to the electric network can be modeled through differential equations. DPC was developed to simulate efficiently electromagnetic and electromechanical transients [26], [28], [100]. Thus, fast variations of voltage and current signals can be accurately represented [9], [25]–[28]. DPC models have been successfully applied to simulate a broad range of transients in balanced and unbalanced three-phase power systems. DPC-based models have been demonstrated to be accurate and computationally efficient for simulating the transients under study in all the applications.

Furthermore, in steady-state, the dynamic phasor $\underline{x}_\mathrm{s}(t)$ is a constant signal, then it is possible to

obtain a well-defined equilibrium point. Accordingly, small-signal analysis can be performed in a system modeled using DPC [97]. Even though DPC has many advantages, the stability assessment based on DPC has not been thoroughly investigated yet [10].

2.4.2.2 Dynamic Phasor Calculus for Modeling Balanced Three-Phase Power Systems

This section presents the modeling of balanced three-phase power systems using DPC. This system is of particular interest because it is closely related to the Park Transform [9], [101]. For this reason, the modeling of power systems using the Park transform is not considered a modeling approach in Figure 2.2. This section verifies that using the Park transform on a three-phase balanced signal is equivalent to use a mono-phase equivalent model based on DPC.

A three-phase balanced signal $\boldsymbol{x}_{\mathrm{abc}}(t)$ composed of $x_{\mathrm{a}}(t)$, $x_{\mathrm{b}}(t)$, and $x_{\mathrm{c}}(t)$ can be described as follows:

$$\boldsymbol{x}_{\mathrm{abc}}(t) = \begin{bmatrix} x_{\mathrm{a}}(t) \\ x_{\mathrm{b}}(t) \\ x_{\mathrm{c}}(t) \end{bmatrix} = \begin{bmatrix} A(t)\cos(\omega_{\mathrm{c}}t + \theta(t)) \\ A(t)\cos\left(\omega_{\mathrm{c}}t + \theta(t) - \frac{2\pi}{3}\right) \\ A(t)\cos\left(\omega_{\mathrm{c}}t + \theta(t) - \frac{4\pi}{3}\right) \end{bmatrix} \tag{2.6}$$

A mono-phase equivalent model can describe this system. To represent the system by DPC, the analytic signal of phase a is obtained and then shifted by $\omega_{\mathrm{s}} = \omega_{\mathrm{c}}$ as follows:

$$\underline{x}_{\mathrm{a}}(t) = x_{\mathrm{a}}(t) + \mathrm{j}\,\mathcal{H}[x_{\mathrm{a}}(t)] = A(t)\mathrm{e}^{\mathrm{j}\theta(t)}\mathrm{e}^{\mathrm{j}\omega_{\mathrm{c}}t} \tag{2.7}$$

$$\underline{x}_{\mathrm{sa}}(t) = \underline{x}_{\mathrm{a}}(t)\mathrm{e}^{-\mathrm{j}\omega_{\mathrm{s}}t} = A(t)\mathrm{e}^{\mathrm{j}\theta(t)} \tag{2.8}$$

with $\underline{x}_{\mathrm{sa}}(t)$ being a complex signal with eliminated carrier f_{c}. In this way, the information related to the other phases can be obtained by shifting $\underline{x}_{\mathrm{sa}}(t)$ in $\frac{2\pi}{3}$. The real and imaginary part of $\underline{x}_{\mathrm{sa}}(t)$ can be seen as the direct and quadrature components resulting from the Park transform applied to (2.6) [9], [101]. This yields to:

$$\underline{x}_{\mathrm{sa}}(t) = \underline{x}_{\mathrm{dq}}(t) = x_{\mathrm{d}}(t) + \mathrm{j}x_{\mathrm{q}}(t) \tag{2.9}$$

Given this equivalence, it can be seen that applying the Park transform to a three-phase balanced signal is a particular case of applying DPC to obtain a monophase model from a three-phase balanced system. Therefore, the benefits of using dq or DPC-based models to represent three-phase balanced systems are identical. For this reason, further comments related to the modeling approach based on the Park transform are not given hereafter.

2.4.2.3 Quasi-static Phasor Calculus

Quasi-static phasor can be obtained from a dynamic phasor representation. To do this, a differential equation that describes the relationship between the two analytic signals $\underline{x}(t)$ and $\underline{y}(t)$ is considered as follows:

$$k\frac{\mathrm{d}\underline{x}(t)}{\mathrm{d}t} = \underline{y}(t) \tag{2.10}$$

Both quantities are supposed to have a Fourier spectrum similar to the one shown in Figure 2.3 on the right. Using (2.5) to calculate the derivative of an analytical signal, (2.10) can be expressed by DPC as follows [5]:

$$k\left[\frac{\mathrm{d}\underline{x}_\mathrm{s}(t)}{\mathrm{d}t} + \mathrm{j}\omega_\mathrm{s}\underline{x}_\mathrm{s}(t)\right] = \underline{y}_\mathrm{s}(t) \tag{2.11}$$

The QPC model is then obtained by setting $\frac{\mathrm{d}\underline{x}_\mathrm{s}(t)}{\mathrm{d}t} = 0$ in (2.11). This results in the algebraic equation:

$$\mathrm{j}k\omega_\mathrm{s}\underline{x}_\mathrm{s}(t) = \underline{y}_\mathrm{s}(t) \tag{2.12}$$

By neglecting the derivatives from (2.11), transient responses of $\underline{x}_\mathrm{s}(t)$ are not represented. It is assumed that the transient response of the state variable $\underline{x}_\mathrm{s}(t)$ is fast with respect to the time scale of interest. In the literature, this model reduction process is known as the singular perturbation theory [102]. This theory has been successfully applied within stability studies for neglecting transients in the stator fluxes of synchronous generators and electric networks [103].

A representation of a signal based on QPC can only yield an approximate power system model that can be considered appropriate if the transients of interest only involve small and negligible values of $\frac{\mathrm{d}\underline{x}_\mathrm{s}(t)}{\mathrm{d}t}$. This is the case for very small magnitudes or very small frequency deviations contained in the Fourier spectrum of the dynamic phasor $\underline{x}_\mathrm{s}(t)$. In Figure 2.5, the reduced validity in the frequency range of a QPC representation is qualitatively illustrated [5], [9]. Figure 2.5 shows that the Fourier spectrum of a quasi-static phasor approximates the Fourier spectrum of a dynamic phasor for frequencies close to $f \approx 0$. This is the case where the relevant transients for stability assessments are slow rotor electromechanical oscillations of synchronous generators, which cause small frequency deviations from the system frequency f_c in electric quantities such as voltages and currents. The bandwidth of frequencies of these transients typically ranges from 0.1 Hz to 5 Hz [1], [5], [7]. Focusing on this range of frequencies in stability studies, the accuracy of time-domain simulations using QPC has shown to be appropriate for stability studies in power systems dominated by synchronous generators.

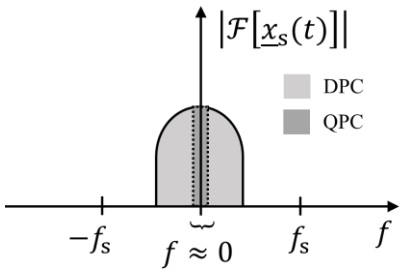

Figure 2.5. Frequency spectrum of DPC and QPC

2.4.2.4 Basic Models of RLC Components

The resistor, inductor, and capacitor models are briefly described using real, dynamic phasor and quasi-static phasor signals. The following equation defines the transients of an inductance:

$$L\frac{\mathrm{d}i_{\mathrm{L}}(t)}{\mathrm{d}t} = v_{\mathrm{L}}(t) \tag{2.13}$$

Considering the analytic signals $\underline{i}_{\mathrm{L}}$ and $\underline{v}_{\mathrm{L}}$, and then applying (2.11) to (2.13), the DPC model of the inductance is:

$$L\frac{\mathrm{d}\underline{i}_{\mathrm{Ls}}(t)}{\mathrm{d}t} + \mathrm{j}\omega_s L\underline{i}_{\mathrm{Ls}}(t) = \underline{v}_{\mathrm{Ls}}(t) \tag{2.14}$$

The QPC model of the inductance is then obtained by neglecting the derivative of the DPC model:

$$\mathrm{j}\omega_{\mathrm{s}} L\underline{i}_{\mathrm{Ls}}(t) = \underline{v}_{\mathrm{Ls}}(t) \tag{2.15}$$

Proceeding similarly, the models of the resistor and capacitor can also be obtained. A summary of the models using different techniques is shown in Table 2.1. The representation of basic circuit elements displayed in Table 2.1 is used to implement power system models when lumped parameters are assumed.

Table 2.1. Comparison of RLC representation

Circuit element	Real and instantaneous signal	DPC	QPC
R	$v_{\mathrm{R}} = Ri_{\mathrm{R}}$	$\underline{v}_{\mathrm{Rs}} = R\underline{i}_{\mathrm{Rs}}$	$\underline{v}_{\mathrm{Rs}} = R\underline{i}_{\mathrm{Rs}}$
L	$v_{\mathrm{L}} = L\frac{\mathrm{d}i_{\mathrm{L}}}{\mathrm{d}t}$	$\underline{v}_{\mathrm{Ls}} = L\frac{\mathrm{d}\underline{i}_{\mathrm{Ls}}}{\mathrm{d}t} + \mathrm{j}\omega_{\mathrm{s}} L\underline{i}_{\mathrm{Ls}}$	$\underline{v}_{\mathrm{Ls}} = \mathrm{j}\omega_{\mathrm{s}} L\underline{i}_{\mathrm{Ls}}$
C	$i_{\mathrm{Cs}} = C\frac{\mathrm{d}v_{\mathrm{C}}}{\mathrm{d}t}$	$\underline{i}_{\mathrm{Cs}} = C\frac{\mathrm{d}\underline{v}_{\mathrm{Cs}}}{\mathrm{d}t} + \mathrm{j}\omega_{\mathrm{s}} C\underline{v}_{\mathrm{Cs}}$	$\underline{i}_{\mathrm{Cs}} = \mathrm{j}\omega_{\mathrm{s}} C\underline{v}_{\mathrm{Cs}}$

Figure 2.6 shows a time domain simulation of a three-phase RL circuit using different modeling approaches. It can be seen that QPC and DPC are equal in the steady-state while the model based on instantaneous signal oscillates with the system frequency, which in this case is 50 [Hz]. Both DPC and QPC track the envelope of the instantaneous signals. However, only the DPC model can accurately represent the transient of the RL circuit, tracking the envelope of the real signal.

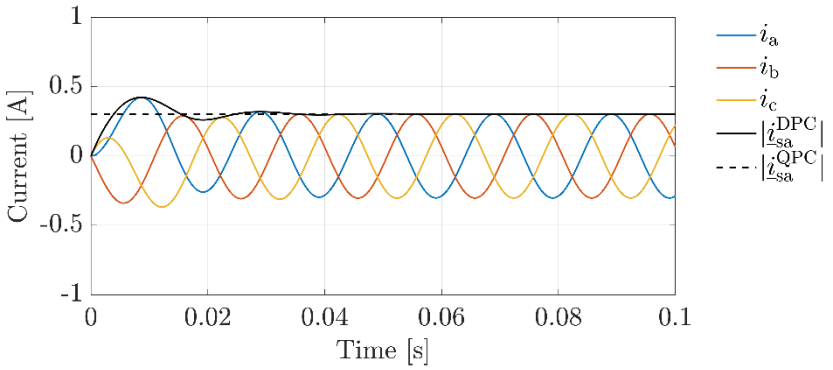

Figure 2.6. Comparison of transient simulation of a three-phase RL circuit; $R = 1\ [\Omega], L = 0.01$ [H]

2.5 Modeling of Power System Components

This section describes the modeling of transmission lines and synchronous generators. This section aims to summarize the models used for simulating power system transients. This includes models used for both the simulation of EMT, which are typically neglected in stability assessments and the simulation of slow electromechanical transients, which are the focus of traditional stability assessments.

2.5.1 Transmission Lines

There are two main transmission line models in power systems: based on lumped and distributed parameters [104], [105]. Transmission line models using lumped parameters are based on the π circuit, where the parameters are calculated for a specific frequency. The transmission line models with distributed parameters are categorized into two types. These are transmission line models with constant parameters and transmission line models with frequency-dependent parameters [87]. If wave propagation phenomena are of interest, the transmission line model with distributed and frequency-dependent parameters can give accurate results in transient simulations. The Universal Line model is widely known and is usually used as a reference for developing new models [106], [107].

In stability studies where the focus is on slow electromechanical transients, QPC is used to model transmission lines [7], [98]. The EMTs related to the network are neglected. Thus, its behavior is modeled through a set of algebraic equations, which are obtained from the π circuit model with lumped parameters. In the case of long lines, the electrical parameters of the equivalent π circuit are adjusted to take into account the traveling wave equations associated with the line [108], [109].

When electromagnetic and electromechanical transients are of interest, transmission lines based on lumped or distributed parameters can be used. Differential equations describe the dynamic instead of just algebraic equations, as used in DPC. The degree of detail depends on the frequency of the transients of interest. In general, for studies where the focus is on the stability of CIG control systems, the π circuit model with lumped parameters has been used to model transmission lines in [14], [98], [110]. This transmission line model has also been used for studies in which the main interest is to analyze whether there are adverse effects due to the dynamic interaction of CIG control systems and other power system components. It includes CIG based on wind turbine type 3, type 4, and photovoltaic power plants [59], [111]. Furthermore, in [9], [27], [112], [113], both models

based on lumped parameters and based on distributed parameters have been developed using DPC.

2.5.2 Synchronous Generators

The classical approach to model synchronous generators is based on the Park transform [114]. The main advantage of the Park transform is that the inductances related to the stator flux linkages are not dependent on the rotor position. Various widely accepted types of approximate models use the dq transform [115]–[117]. The models commonly used for simulating power system transients are [4]:

1) The eight-order model is used for synchronous generators with a round rotor. The model includes a field, stator, damper circuit on the d-axis, and a stator and two damper circuits on the q-axis. The swing equation is included in this model and is represented as two first-order differential equations.
2) The seventh-order model is used for a synchronous generator with a salient pole rotor. The only difference from the eight-order model is that there is one damper circuit on the q-axis instead of two.

The derivations of these models can be found in books such as [118] and [2]. For this reason, in this document, a detailed description of the derivations of the model is not given.

The above models have been used to analyze the interaction between synchronous generators and the electric network [115]–[117]. This means that electromechanical and electromagnetic phenomena are of interest to study. The electromagnetic phenomena are low-frequency electromagnetic transients. Electromechanical transients are faster than slow electromechanical transients, which are the focus of stability studies of power systems dominated by synchronous generators.

Other formulations have also been proposed to improve the accuracy of synchronous generator models based on the dq transformation. However, more accuracy increases the computational burden. Examples of such models are phase-domain (PD) models based on phase representation [119], [120], and the voltage behind reactance (VBR) introduced in [121] for the state space approach and extended to EMTP and DPC in [122], [123]. The above models represent the same physical system. Therefore, these models are equivalent and should give similar results in time-domain simulations [116]. They have been used mainly in small test systems but not for stability assessments of real power systems.

For stability studies where slow electromechanical transients are of main interest, synchronous generator models based on the Park transform are considered standard [2], [4], [6], [124], [125]. The derivatives related to the stator flux linkages of the synchronous generators are neglected. Therefore, the stator voltage behavior is modeled as algebraic equations. It is assumed that the stator transient is faster and well-damped than rotor transients. If the stator voltage behavior is modeled using algebraic equations, then the transmission network has to be modeled using algebraic equations. It means that QPC is used to represent the behavior of the transmission network. Consequently, a consistent set of differential-algebraic equations representing the power system can be obtained [4]. Neglecting the stator flux linkages of the synchronous generators causes the eight-order and seventh-order models to become sixth-order and fifth-order models, respectively [2]. In addition, it is widely accepted that the stability analysis is conservative when stator transients are neglected [4], [125].

2.5.3 Converter Interfaced Generation Technologies in Power System

The overall dynamic performance of CIG and its impacts on power systems are widely governed by the control strategy implemented to control the power electronic converter. This section discusses a general structure extensively used to control CIG, which can be used regardless of the primary energy source behind the converter, solar or wind energy. Additionally, it reviews the CIG operation modes. For each operation mode, representative control systems are described. These are established as a benchmark model to comprehensively discuss the CIG models based on QPC reviewed in Section 2.6 and perform the comparative study in Chapter 5.

2.5.3.1 General Control Structure of CIG

In general, CIG requires four controllers, two for DC-AC conversion itself through pulse width modulation (PWM), one for the energy source, and one for energy storage on the DC side of the converter [95]. However, how these controllers are handled is flexible. Various possibilities have been explored during the last few years, although more in theory than in practice [11]. Figure 2.7 shows the schematic diagram of a typical control system of a CIG, where the dotted arrows represent the variables that can be controlled. The voltage source converter (VSC) is a controllable DC-AC device [95]. The VSC configuration is the mostly used in CIG power plants [11], [15], [126]; for example, wind turbines type 3 [111], [127]–[129] and type 4 [15], [59], [130]–[132] and photovoltaic power plants [133]–[135]. A power plant based on CIG also considers an AC filter, which can be based on an inductance (L), an inductance and a capacitor (LC) or an inductance and a capacitor and inductance (LCL) [95], [136]. The filter improves the quality of the voltage and current wave obtained from the VSC.

The CIG control system is based on a cascade control structure with low- and high-level control loops. The outer control loops (high-level controls) have a slower dynamic response than the inner control loops (low-level control loops). This allows the outer control loops to give reference signals to the inner control loops. The high-level control ensures the synchronization of the converter and can also provide a variety of services to the AC grid [137]–[139], such as active power control, ride-through capability, voltage/reactive control, and frequency response capabilities, among others [10], [11], [140], [141]. The synchronization control is needed to achieve good dynamic performance during the operation of CIG. The control needs to measure signals from the network to synchronize the converter with the grid, e.g., voltage amplitude, frequency, and angle, or it can set the frequency used to synchronize the converter with the grid [142]. Depending on the operation mode, different control strategies can be adopted.

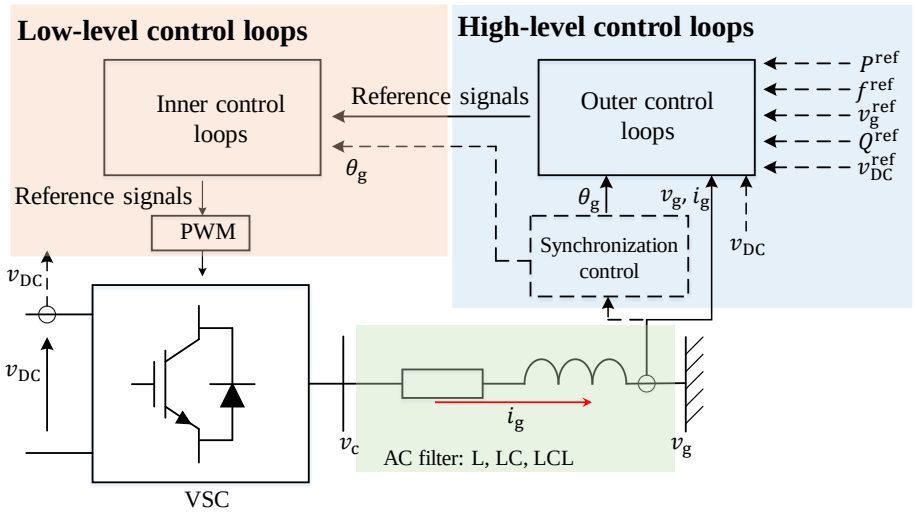

Figure 2.7. Illustrative schematic diagram of a control system used in CIG

The inner control loops generate the reference signals for the VSC. The dynamic response of these control loops is fast, with time scales in the range of EMT, typically with time constants less than 20 ms [143]. The VSC can regulate the magnitude and angle of the voltage through PWM techniques. In high-power applications, the VSC switching frequencies are in the order of a few kHz to limit the losses in the power converter.

As shown in Figure 2.8, the modeling of control systems is a highly complex task. The complexity is due to the various functionalities and control strategies that can be implemented in real CIG power plants. These power plants may have controllers for the DC-link circuit, maximum power point tracker (MPPT), voltage or reactive power, frequency regulation, inertial response, accomplishing requirements of LVRT/HVRT, for DC and AC current protection, among others [135], [10]. Furthermore, various control strategies implemented by the manufacturers of CIG power plants are proprietary and subject to industrial secrets. This significantly increases the stability assessment complexity in future operating conditions of power systems [78]. On the other hand, due to the dynamic behavior and response of the CIG, it may be operating conditions in which new adverse control interactions, with a fast and slow dynamic response, arise in the systems [15], [16], [59], [144]. Traditional simulation tools based on QPC models may not be suitable for such new stability issues.

Given the above reasons, different assumptions are commonly made to model CIG in power system stability studies. These assumptions are generally related to how the low-level controls and the AC filter are represented in the CIG models. A detailed discussion of these assumptions is presented in Section 2.6. In the case of high-level controls, it is common to consider those that comply with specific grid codes. This may include voltage control, LVRT/HVRT requirements, inertial response, and frequency control, among others [10], [135]. Since the high-level model depends on the particular grid code, we describe typical generic control strategies used in stability analysis.

2.5.3.2 Operation Modes of CIG

The converters of power plants based on CIG are modular and almost totally actuated devices that admit several control options with very fast response times. However, so far, there is still no consensus on the terminology and distinction among the different operating modes of the CIG. In

fact, many of them are even contradictory and depend on the researcher's perspective, e.g., power electronics or power systems [11]. Most of the ongoing efforts to classify the different modes of operation of the CIG have been made in the context of microgrids [142], [145]. However, these classifications can also be applied in the context of power systems [11], [12], [146]–[148]. Two of the most commonly used operation modes are referred to as grid forming (GFM) and GFL [142], [145]. The latter is also referred as grid-feeding or PQ control [142], [145], [149]. The term grid-following is used in this work hereafter. A third operation mode named grid-supporting was also described in [142], [145]. However, the concept describing the grid supporting mode in both references differs. In this work, the grid supporting mode is considered a subclassification of the GFL mode. This will be discussed later in this section. The most widely known operating modes for CIG are depicted in Figure 2.8. However, it is important to note that other operating modes are possible from the perspective of the power system [11].

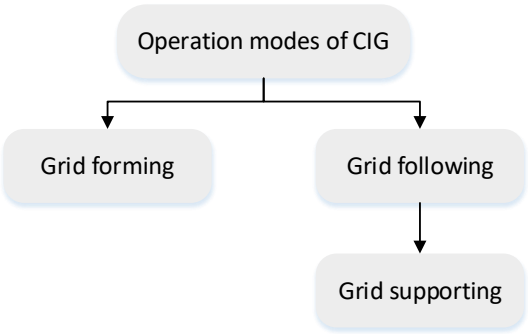

Figure 2.8. Widely used operations modes of CIG

In the GFM operation mode, the CIG regulates the magnitude of the frequency of the voltage and the system frequency at its terminal to specific set points [11], [142], [145], similar to synchronous generators. It can also balance generation and load by properly implementing active power-sharing controllers. CIG operating in GFM mode exhibits black start capability, frequency regulation, voltage regulation, and load sharing [147]. Accordingly, CIG operating in GFM mode should be connected to the system [148], [150].

The CIG provides active and reactive power to the grid according to the power dispatch requirements in the GFL operation mode. This mode operates appropriately when the grid regulates the frequency and voltage at which the CIG is connected. As a result, the GFL mode is only possible if other generators impose the voltage and frequency of the AC grid [12], [142], [145], [146]. The GFL operation mode is currently the dominant method used by vendors to operate CIG connected to the grid. However, as the CIG level increases, it is required that the CIG participate in regulating voltage and frequency.

The third operation mode of CIG is the grid-supporting mode, and it was introduced in [142] and [145] in the context of microgrids. In both works, the grid-supporting mode includes additional high-level controllers to regulate the voltage and frequency of the system. However, both concepts are different in both references. In [145], the grid supporting mode is based on a GFL mode plus high-level controllers. Although it may include voltage or/and frequency regulation, the grid-supporting mode is unsuitable for operating under isolated conditions. Therefore, according to [145], the grid-supporting mode is only possible if other generators impose the voltage and frequency of the AC grid. On the other hand, [142] considers the grid supporting as a grid following (GFL) or grid-forming (GFM) with high-level controllers implemented to regulate the voltage and

frequency of the AC grid. Under this description, the grid supporting mode based on a GFM mode plus high-level controllers is suitable for operating in isolated grids.

As mentioned previously, in GFM mode, the CIG can operate during isolated conditions; thus, controllers to regulate voltage, frequency of the AC grid, and power-sharing are to be implemented to operate under such conditions. Therefore, the grid supporting mode described and discussed in [142] is redundant.

Given the above reasons, the definition of the grid supporting mode presented in [145] is used here. In the context of power systems, any CIG with fault ride through, voltage control, and/or frequency control can be considered operating in grid supporting mode [146]. Furthermore, assuming the definition in [145], the CIG model used to represent the inner control loops associated with the GFL and grid supporting operation mode is identical. The term GFL is mainly used in the power system community, independently of whether the CIG supports the system's frequency and/or voltage. Accordingly, the term GFL is used in this work rather than grid supporting when the CIG models with voltage support are presented. This does not include CIG operating in GFM.

2.5.3.3 Representative Control Systems used in CIG

This section describes models of representative control systems used in power plants based on CIG operating in GFL and GFM mode. The control system models presented in this section are generic and commonly used for the simulation of transients [35], [125], [151]–[153]. For a CIG operating in GFL and GFM mode, an average VSC model where switching transients are neglected is considered representative and appropriate for stability studies [136], [147], [148], [154]–[156]. The switching of power electronic devices is not modeled when system stability is of interest. This is because the time scale of the switching is considered fast compared with the transients of interest at the system level [59], [111]. Therefore, in this model, the dynamic response of the CIG is determined by the outer, inner control loops and the AC filter. They are represented in a rotational dq reference frame. This representation has been recommended and used to study control interactions between CIG and power systems [15], [35], [58], [59], [125], [148], [151], [157], [158]. The above assumptions are considered to describe the representative CIG model below. It includes GFL and GFM operation modes.

- **Grid Following Operation Mode**

Figure 2.9 shows a diagram of a CIG connected to the grid. It comprises a DC side, a VSC, and an AC side. A capacitor is connected to the DC side. This is referred as DC-link circuit. Further, a DC source or another VSC that transforms AC to DC can be used on the DC side. The latter is used, for instance, in a type-4 wind turbine. In the AC side, an AC filter is connected, which is represented as a coupling inductance L_f. The AC filter can be an L, LC, or LCL. However, the capacitor is commonly neglected at the system level because its effect is negligible [159]. Thus, the AC filter is represented by an RL circuit modeled by differential equations. This simplification has been employed in [15], [16], [158], [160]–[167] to model type 3 and type 4 wind turbines, photovoltaic power plants, and HVDC links based on VSC. The variables shown in Figure 2.9 to Figure 2.15 are defined in Table 2.2.

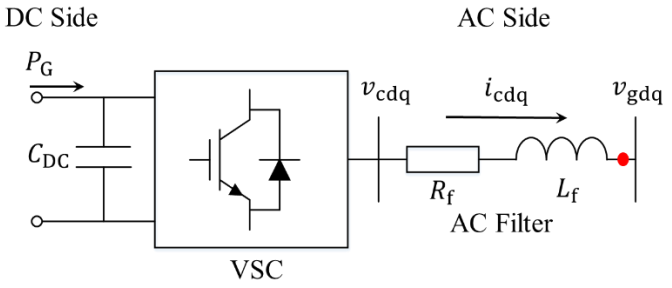

Figure 2.9. Diagram of CIG connected to the grid that operates in GFL mode [125]

For the high-level control loops, the outer control loops regulate the voltage or the reactive power through the current on the q-axis and the active power or voltage at the DC -link through the current on the d-axis. These outer control loops are shown in Figure 2.10 and Figure 2.11, respectively. The outer control loops are based on PI controllers, as is usual in stability assessments [15], [35], [58], [158]. Other control loops can be added to support the system frequency. This is done by changing the P_{ref} in Figure 2.10, i.e., droop control shown in Figure 2.12 [168].

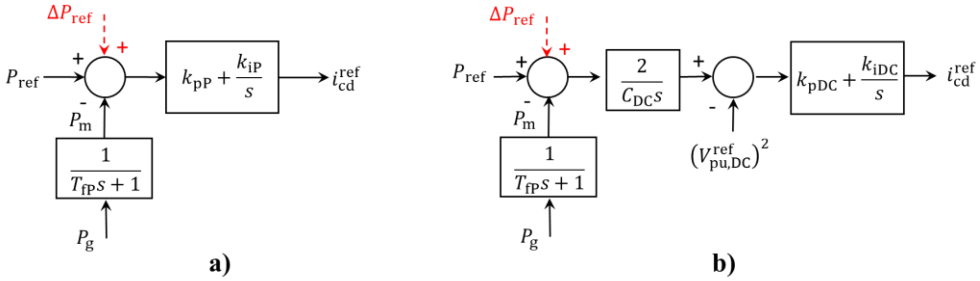

Figure 2.10. Outer control loops for the d-axis; a) Active power control; b) DC-Link voltage control

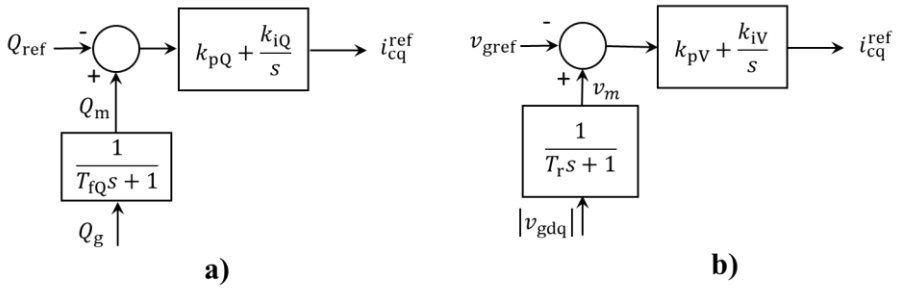

Figure 2.11. Outer control loops for the q-axis; a) Reactive power control; b) Voltage control

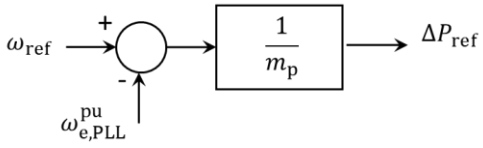

Figure 2.12. Doop control for CIG operating in GFL

Regarding the synchronization method, a phase-locked loop (PLL) in a synchronous reference frame (SRF) is commonly used in current CIG applications in power systems [169] (see Figure 2.13). The PLL is used to estimate the phase angle of the voltage at the point of common coupling (PCC). The phase angle transforms abc to dq signals and then controls the CIG [170].

In addition to the SRF - PLL shown in Figure 2.13, other synchronization methods have been proposed. Relevant alternatives that can be found in the literature include: i) PLL based on decoupled double synchronous reference frames (DDSRF) [58], [171], [172], ii) the Kalman filter-based synchronization method [173], [174], and iii) the recursive discrete Fourier Transform [175], [176]. A few works have modeled the PLL-DDSRF for stability analysis of power systems, and it has been observed that the dynamic performance of the system under study is better than when the SRF - PLL is considered [58], [172]. Although various synchronization methods have been proposed in the literature, the SRF - PLL is mainly considered in stability assessments of power systems [15], [58], [172]. This is because SRF - PLL is still the most widely used synchronization method in existing CIG units, and TSOs have reported problems due to SRF - PLL [177], [178]. Accordingly, this thesis uses the SRF - PLL as a representative synchronization method of a CIG operating in the GFL mode.

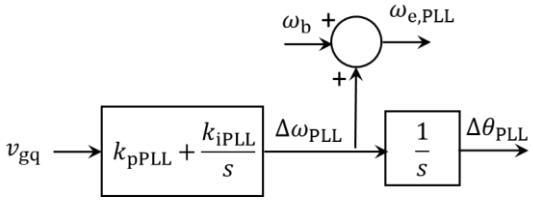

Figure 2.13. SRF - PLL

Regarding the low-level control loops, the current control loops shown in Figure 2.14 based on PI controllers are widely used [10], [11], [15], [35], [58], [78], [131], [158], [179]. Both control loops include cross-decoupling terms to enhance the dynamic performance of current controllers. The cross-decoupling terms allow the decoupled control of the active and reactive power injected by the CIG into the grid. The voltages v_{gdq} are signals which pass through a low-pass filter represented through a first-order transfer function as is shown in Figure 2.15. The terms are referred to as feed-forward terms and may significantly affect the control stability [180], [181]. The output of the current control loops is the voltage to be synthesized by the VSC using a PWM technique [136]. As mentioned, the switching of power electronic devices due to the PWM is neglected.

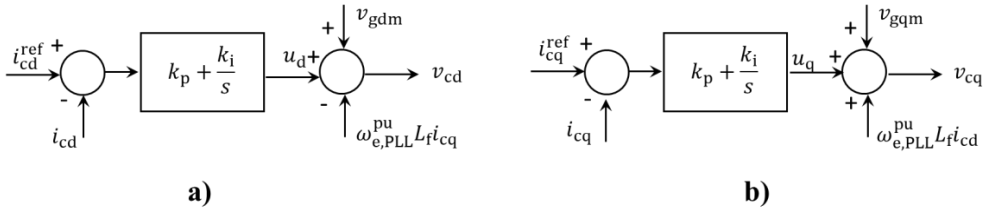

Figure 2.14. Current control loops; a) current controller on the d-axis; b) current controller on the q-axis

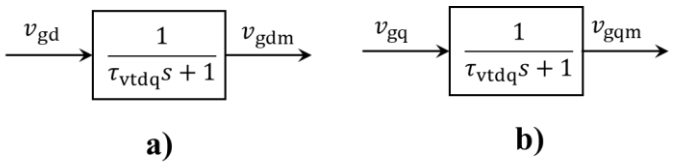

Figure 2.15. Feed-forward terms; a) d-axis; b) q-axis

It should be mentioned that further implementations for the inner current controllers are also conceivable. They can be based on resonant controllers implemented on a stationary frame, using signals on αβ or abc [142]. Furthermore, nonlinear control structures have also been proposed. They include hysteresis, sliding, or predictive controllers [142]. Both resonant controllers and nonlinear controllers can track sinusoidal reference currents in a fast and robust way. However, such control structures, different from typical controllers based on a reference frame dq, are used mainly in power electronic engineering and have not been widely considered in the context of power systems [19]. Accordingly, they are not discussed further here.

Table 2.2. Description of CIG – GFL parameters

Parameter	Description
P_G	Active power injected by the primary energy source
C_{DC}	Capacitance of the DC-Link circuit
v_{cdq}, i_{cdq}	Voltage and current injected by the VSC on a dq reference frame, respectively
v_{gdq}	Voltage at the PCC on a dq reference frame
L_f, R_f	Inductance and resistance of the AC filter of type L, respectively
$P_{ref}, P_m, P_g, \Delta P_{ref}$	Active power reference, measured active power, active power injected at PCC, and incremental reference active power, respectively
Q_{ref}, Q_m, Q_g	Reactive power reference, measured reactive power, reactive power injected at PCC, respectively
$v_{gref}, v_m, \lvert v_{gdq} \rvert$	Voltage reference, measured voltage, and voltage at PCC, respectively
$i_{cd}^{ref}, i_{cq}^{ref}$	Current reference on d- and q-axis, respectively
$\omega_{ref}, \omega_{e,PLL}, \omega_b$	Angular velocity reference, angular velocity estimated by the PLL, and angular velocity base, respectively
$\Delta\omega_{PLL}, \Delta\theta_{PLL}$	Incremental angular velocity and incremental angular angle estimated by PLL, respectively
k_{pP}, k_{iP}, T_{fP}	Proportional gain and integral gain of the active power controller and time constant of the measured active power, respectively
$k_{pDC}, k_{iDC}, \left(V_{pu,DC}^{ref}\right)^2$	Proportional gain and integral gain of the DC-Link control system, and voltage at capacitor of DC-Link circuit reference to the square, respectively
k_{pV}, k_{iV}, T_r	Proportional gain and integral gain of the active power controller, and time constant of the measured active power, respectively
m_p	Droop coefficient
k_{pPLL}, k_{iPLL}	Proportional gain and integral gain of PLL controller, respectively
k_p, k_i, τ_{vtdq}	Proportional gain and integral gain of the current controller and time constant of VFF, respectively
v_{gdm}, v_{gqm}	VFF term on d- and q- axis respectively

- **Grid Forming Operation Mode**

Figure 2.16 shows a diagram of a CIG operating in GFM mode connected to the grid. This diagram is commonly used when the control structure of this operation mode is based on multiple control

loops, similar to the GFL mode. This is the most common structure considered in stability assessments [148], [150], [182]. Thus, it is described in this section.

The CIG comprises a DC side, a VSC, and an AC side. A capacitor is connected on the DC side. Further, a DC source can be connected to the DC side. The LCL filter is considered in the CIG model. The LCL filter is represented as an RLC circuit modeled by differential equations [148], [156]. The inductance L_c can be part of the AC filter or can represent a couling inductance related to a transformer used to connect the CIG to the grid. Contrary to the GFL mode, the dynamic related to the capacitor C_f has to be considered because it is the control plant used to design and implement the inner control loops that set the voltage $v_{C_{fdq}}$ of the CIG unit shown in Figure 2.16.

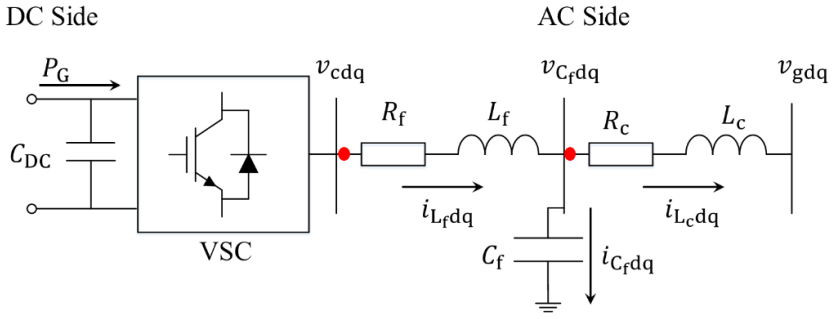

Figure 2.16. Diagram of CIG connected to the grid operating in GFM mode

High-level control loops typically use droop controllers to share active and reactive power. The controller models are depicted in Figure 2.17 and Figure 2.18, respectively. The droop-based active power controller sets the frequency in the VSC and synchronizes the CIG with the AC grid [142], [148]. The droop-based reactive power controller sets the reference voltage $v_{C_fdq}^{ref}$ for the inner control loops. Both droop controllers allow the CIG to participate in the voltage and frequency regulation and hence in the power-sharing among generators. Other control strategies for regulating the system frequency and synchronizing CIG have been proposed in the literature, such as virtual synchronous machines [156], [183], matching control [184], and virtual oscillators [185]. Virtual synchronous machines and matching control attempt to mimic the dynamic response of traditional synchronous machines. These control strategies perform the same tasks as droop-based active power controllers and are also mathematically equivalent [137], [139], [186], [187]. Accordingly, droop-based controllers can be considered representative outer control loops for general-purpose stability analysis.

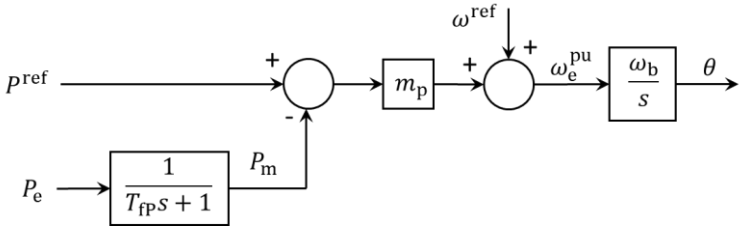

Figure 2.17. Droop-based active power controller

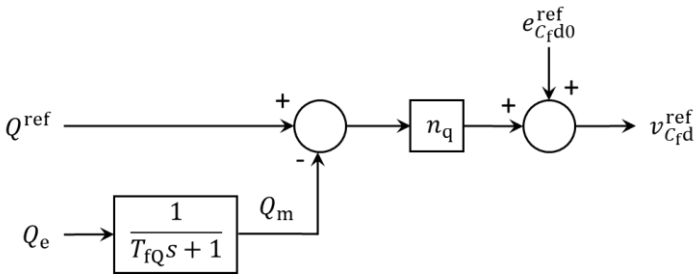

Figure 2.18. Droop-based reactive power controller

In CIG, voltage and current control loops in a cascade structure are used in low-level control loops. Both the voltage and current control loops use PI controllers, as shown in Figure 2.19 [148], [156], [188]. The voltage controllers set the reference current for the current controllers. The latter sets the reference voltage to be synthesized by the VSC. Inner control loops consider cross-decoupling terms for better dynamic performance [136]. The feedforward term related to the current control may also be included with or without a filter. Similar to the CIG operating in grid-following mode, the inner control loops can also be implemented in a stationary reference frame using αβ signals and resonant controllers [142], [149]. However, to the best of the author's knowledge, such controllers have not been used so far in power system stability studies. For this reason, they are not discussed here.

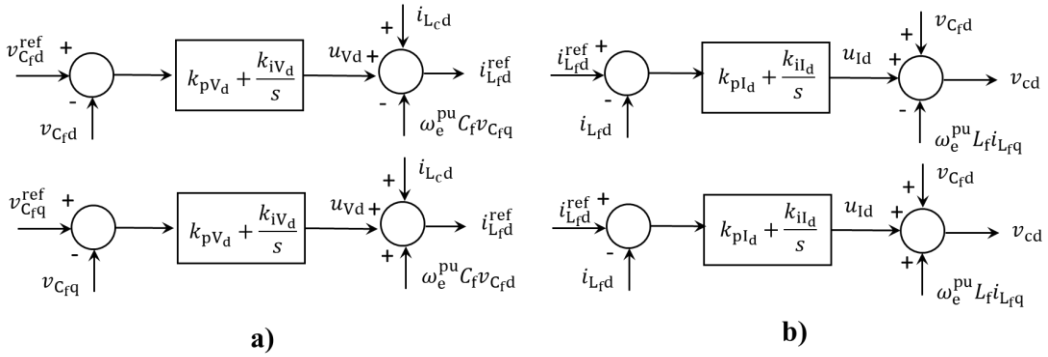

Figure 2.19. Inner control loops on the dq axis; a) voltage control loops; b) current control loops

2.6 Modeling of CIG for Power System Stability Studies

Different representations for the inner control loops and AC filters used in CIG have been proposed in the literature. They have the fastest dynamic response in CIG units [35], [78], [162]. Since stability studies traditionally focus on slow electromechanical phenomena, the representations of the fast dynamic response of CIG vary considerably depending on the assumptions and simplifications considered in the pertinent study. Depending on the representation used for the inner control loops and the AC filter in stability studies, the CIG has been represented as a controlled current source or as a controlled voltage source behind an impedance. These representations can be seen in Figure 2.20a and Figure 2.20.b, respectively. Both representations consider a VSC configuration where an average VSC model is used. The switching transients are neglected in this model, and the CIG control systems are represented in a rotational dq reference frame.

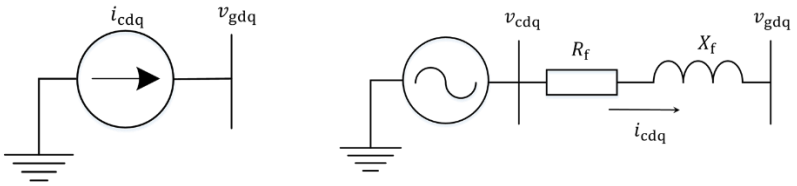

Figure 2.20. Representation of CIG; a) current source; b) voltage source behind an impedance

Table 2.3. Description of CIG – GFM parameters

Parameter	Description
P_G	Active power injected by the primary energy source
C_{DC}	Capacitor of the DC-Link circuit
v_{cdq}, v_{gdq}	Voltage at VSC and voltage at the PCC on a dq reference frame, respectively
L_f, L_c, R_f, R_c, C_f	Inductances, resistances, and capacitance of the AC filter of type LCL, respectively
$v_{C_{fdq}}, i_{C_{fdq}}$, $i_{L_{fdq}}, i_{L_{cdq}}$,	Voltage and currents in the capacitor C_f, currents through inductor L_f and L_c on a dq reference frame, respectively
P_{ref}, P_m, P_e	Active power reference, measured active power, and active power injected at PCC, respectively
Q_{ref}, Q_m, Q_e	Reactive power reference, measured reactive power, reactive power injected at PCC, respectively
$\omega^{ref}, \omega_e^{pu}, \omega_b, \theta$	Angular velocity reference, measured angular velocity, base angular velocity and angle reference for voltage synthetized in VSC, respectively
$e_{C_{fdo}}^{ref}, v_{C_{fd}}^{ref}, v_{C_{fq}}^{ref}$	Voltage reference in the droop-based reactive control on d-axis, voltage in the capacitor C_f reference on d- and q-axis, respectively
$i_{L_{fd}}^{ref}, i_{L_{fq}}^{ref}$	Current reference on d- and q-axis, respectively
T_{fP}, T_{fQ}	Proportional gain and integral gain of the active power controller and time constant of the measured active power, respectively
k_{pV_d}, k_{iV_d}	Proportional gain and integral gain of the voltage controllers, respectively
m_p, n_p	Droop coefficiets of active and reactive control, respectivaly
$k_{pI_d}, k_{iId}, \tau_{v_{tdq}}$	Proportional gain and integral gain of the current controllers, and time constant of VFF, respectively

This section reviews and discusses both representations with their respective variations and assumptions typical in stability studies based on QPC. The focus is on how the fastest dynamic responses in CIG are modeled in such studies. It must be mentioned that in most studies reported in the literature, the CIG is considered to operate in GFL mode [35], [78], [179], [189]. Both representations have been used for modeling CIG in GFL mode. Accordingly, the CIG models reviewed and discussed in this section consider this operation mode.

Furthermore, it must be noted that there has recently been an increased interest in the academy and industry in studying the dynamic performance and stability of power systems with CIG operating in GFM mode. The model described in Section 2.5.3.2 is mainly used when GFM is considered for power system stability studies [148], [182], [190]. Compared to CIG models operating in the GFL, fewer works have been proposed for stability analyses based on QPC [146]. In addition, the works considering CIG in GFM are more theoretical than based on actual CIG power plants. These are other reasons why this section focuses on CIG models operating in the GFL mode rather than the

CIG models operating in GFM. However, according to [150], the study, modeling, and simulation of power systems are considered relevant to understanding dynamic behavior and achieving secure operation of future power systems dominated by CIG operating in GFM. Accordingly, it will be part of future work.

2.6.1 Models Based on a Current Source Representation

The CIG model based on a current source representation is shown in Figure 2.21. In this model, the dynamics of the current controllers, the L filter, and the PLL are simplified as a first-order transfer function. The CIG model assumes that the inner control loops can track the reference values. In Figure 2.21, the time constants T_{d} and T_{q} represent the time upon which the control achieves its reference values. Typically, values ranging from 10 to 20 ms have been used in stability studies [35], [131], [191], [192]. This model also assumes that the voltage through the capacitor in the DC-link circuit remains constant. Thus, the dynamic related to the capacitor in the DC-link circuit is not modeled. This representation has been used for modeling CIG with different energy sources such as wind power plants type 3 [193], type 4 [15], [192], and photovoltaic power plants [78], [191].

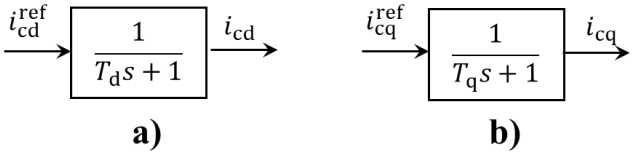

Figure 2.21. Current source model based on a transfer function

The controlled current source for CIG modeling has been proposed mainly by CIGRE [10], [151], General Electric (GE) [191], [192], Western Electricity Coordinating Council (WECC) [194], [78], [191], [192], and the standard IEC 61400-27-1 [189], [195]. Comparative studies have been performed to validate the accuracy and pertinence of these models. The comparisons are between simulations based on QPC models and simulations based on EMT models. Furthermore, it has been possible to validate the CIG models using existing measurements of wind or photovoltaic power plants in some cases. The use of measurements has been applied mainly for the validation of the generic models developed by WECC or IEC [189], [196], [197].

In general, the results obtained from the validation process show that this model represents the dynamic response of test systems with a proper degree of accuracy. However, the test systems are usually very small. The test systems consist of a CIG unit connected to an infinite bus through a transmission line when validation is performed by EMT simulations [197]–[199]. It also includes systems where CIG penetration levels are not too high or not specified [198]. Thus, despite the accuracy shown in some works, the validity and applicability of this CIG model for stability studies in existing power systems with high penetration levels of CIG cannot be ensured [12], [24], [200].

Since the CIG model was developed for stability analyses based on QPC, the focus is on the time scale of the slow electromechanical transients related to synchronous generators. Therefore, this CIG model has limitations, which are described below. This CIG model, represented as a current source, can experience numerical instability [78], [201]. The numerical instability may appear in scenarios of weak systems [78] or when faults close to the CIG are considered [201]. Moreover, real CIG can experience loss of synchronism during very low-voltage conditions, causing the PLL

to become unstable. Since the PLL is not represented in this model, loss of synchronism may cause convergence problems in time domain simulations [202]. This is because the solver cannot reach a new quasi-steady state operating point at the end of each iteration.

According to the report developed by CIGRE [151], this CIG model can capture transients with oscillation frequencies of up to 2 Hz. Another report developed by CIGRE [10] indicates that the applicability of this model is for transients with oscillation frequencies between 0.1 and 5 Hz. In the WECC model (where a current source represents the converter), the range is between 0.1 and 3 Hz [10], [24], [78]. [203] states that time-domain simulations are unreliable if stability issues occur because some variables become poorly damped and oscillation frequencies above 5 Hz. Therefore, the results should be questioned. The cited references suggest different frequency bandwidths for the applicability of CIG models based on the current representation, but they do not describe how those ranges can be obtained.

Furthermore, the CIG models developed by CIGRE and WECC are not recommended when CIG are connected in buses with low Short Circuit Ratios (SCR). According to [10], [24], [203], these models are not recommended for SCR less than 3. This is because, for SCR lower than 3, the system can be considered weak. However, this value may vary depending on factors such as technology used in CIG and power system characteristics. In fact, [24] indicates that each system should define the minimum SCR that makes these CIG models suitable for stability assessments. The minimum SCR might be obtained through EMT simulations. Although the minimum SCR can be obtained, some cases can still require EMT simulations for stability studies, at least under special conditions where the CIG are connected to a very weak part of the power system [10], [200],[73]. It should be noted that the requirement for EMT simulations in [24] does not consider the existence of other modeling techniques which can properly represent electromagnetic and electromechanical phenomena with an adequate degree of accuracy.

As the CIG level increases, some researchers have proposed integrating the PLL into the CIG model represented by a controlled current source [15] [170]. This has been proposed to study stability issues that arise when CIG are connected at buses with low SCR. In [15], stability analyses compare an average CIG model, a CIG modeled as a controlled current source with PLL, and the last without PLL. These three CIG models consider the same outer control loops. Active and voltage controllers are considered for the studies. The test system consists of a CIG unit connected to an infinite bus through a transmission line. The results show that including the PLL improves the accuracy of the CIG model based on a current source representation. This model can predict the small signal stability of the test system due to modes poorly damped with low oscillation frequencies. This is because the modes are mainly related to the state space variables associated with the PLL. However, the results obtained in [15] are based on a small test system; therefore, they cannot be generalized to power systems with multiple synchronous machines and multiple CIG units.

2.6.2 Models Based on a Voltage Source Representation

Various CIG models based on a voltage source representation behind an impedance have been proposed in the literature. These CIG models have been commonly validated, comparing their dynamic response with more detailed CIG models using EMT simulations [35], [164], [204]. In general, the results show that these models represent the dynamic response of test systems with appropriate accuracy. However, the test systems used for validation vary significantly among investigations. Since the test systems and the scenarios under study are considerably different, a

comparison of accuracy cannot be made from the result presented in the reviewed works.

Additionally, there is less information regarding the limitation and applicability of these CIG models for stability studies of power systems with significant penetration of CIG. Consequently, this section focuses mainly on the assumptions and simplifications considered in developing these models. Five types of CIG models based on a voltage source representation have been identified in the reviewed works. Each of them is now described below.

First, the CIG model used in [166] is described. It models the inner current control loops, the PLL, and the L filter represented by an RL circuit, as shown in Figure 2.14, Figure 2.13, and Figure 2.9, respectively. Differential equations model the L filter expressed on a dq-reference frame. This model has been used for the modeling of wind turbine type 3, wind turbine type 4, PV, and HVDC based on VSC [75], [165], [166], [205]–[210]. The control systems related to the CIG are represented in detail, but the power system is modeled based on QPC. This model has been used to study power system stability in multi-machine and multi-converter power systems, including weak systems. However, [166] states that further studies are needed to determine the effects of neglecting the EMT related to transmission lines on the accuracy of this model. It has to be noted that the inner controller and the L filter have a fast dynamic response. Therefore, the computational burden related to transient simulations increases when they are included in stability studies. This is because smaller time-step sizes have to be used in transient simulations to observe the dynamic response of the inner control loops and the AC filter.

Second, the CIG model proposed and used in [127], [211]–[213] is described. This model is obtained from the previous one. The only difference is how the L filter is modeled, represented by algebraic equations. This model has been used in a few works to study the dynamic performance and stability of HVDC based on VSC [127], [211]–[213]. It can be inferred that this model can be used for CIG, such as wind turbine type 4 and photovoltaic power plants. In [212], it is shown that the model decreases its accuracy when the system becomes weak. The analyzes were performed on a system consisting of a VSC connected to an infinite bus through a transmission line. Therefore, the accuracy of the model on a multi-machine and multi-converter power system is unknown.

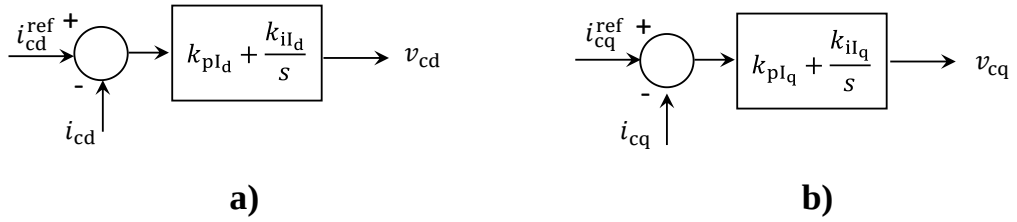

Figure 2.22. Inner current control loops without decoupling and feedforward terms; a) d-axis; b) q-axis

Third, the CIG model proposed in [125], [162], [164] is described. The inner current control loops are modeled in this model, but the decoupling and feedforward terms are ignored, as Figure 2.22 shows. The PLL is considered, and a set of algebraic equations models the L filter. The authors in [201] indicate that using a voltage source representation avoids the numerical stabilities that may appear when the current source representation is used. This model has been proposed to represent wind turbines type 3, type 4, and HVDC based on VSC [125], [162]–[164], [201], [214]–[224]. In

the reviewed works, the behavior and accuracy of this model under scenarios of high penetration of CIG or when the CIG are connected at buses with low levels of SCR have not been thoroughly investigated.

Fourth, the CIG model recently proposed in [134] is described. The authors proposed this model to represent the dynamic response related to photovoltaic power plants. The motivation for developing a new model is because models based on a current source representation [191], [192], [131] were unable to predict the actual transient behavior of photovoltaic power plants. In fact, the simulations did not predict the transmission faults induced by photovoltaic power plants. The Southern California electric grid experienced 1200 MW and 900 MW of photovoltaic generation disconnections in 2016 and 2017, respectively. The reports developed by the TSO indicate that the photovoltaic generation tripped due to i) off-nominal PLL frequency, ii) overcurrent in the DC-Link circuit, and iii) AC overcurrent. These issues were not predicted by the CIG models because the PLL, the DC link circuit, and the filter are not explicitly modeled in the current source representation [191], [192], [131]. Given the above, the CIG model proposed in [134] consists of current control loops, the PLL, an LCL filter, the DC link, and the photovoltaic array. The current control loops and the PLL are the same as those shown in Figure 2.14 and Figure 2.13, respectively. The LCL is modeled in two parts. First, the LC is modeled by differential equations in a dq-reference frame. Second, the L used to connect the CIG to the grid is modeled by algebraic equations. The authors indicate that the assumptions made on the LCL filter allow for the use of a voltage source presentation behind an impedance. Thus, it is possible to explicitly include the solution of the transmission network, which is modeled based on QPC. The author considers the CIG model to be suitable for transient stability studies. This is because some dynamic phenomena obtained from transient simulations are similar to those reported by the TSO.

The work shown in [134] concludes that stability studies can be performed using the proposed model without performing EMT simulations. However, this work does not perform EMT simulations to validate the proposed model. Also, the CIG level is low, so the conclusions may not apply to any system. It has to be mentioned that the details used in this model include the fast dynamic responses of the inner control systems of a CIG and the AC filter. Then, the computational burden increases because small time-step sizes should be used to simulate these dynamic responses.

Fifth, the CIG model proposed in [35], [225] is described. This model is proposed to improve the CIG model based on a current source representation [191], [192], [131]. This model is shown in Figure 2.23 and differs from the CIG models described in this section. The current control loops are presented as a transfer function of the first order. The PLL is not modeled. It is assumed that the current controllers can track the reference current, and the PLL works appropriately. The time constants T_{d} and T_{q} represent the time response of the current controller and the PLL. These constants take values in order of 10 ms. An L filter is considered and represented by a set of algebraic equations. The voltage to be synthesized by the VSC is calculated using the equations shown in Figure 2.23 in the center. A transfer function of first order, with time constants T_{ed} and T_{eq}, is used to model the delay related to the PWM in the VSC.

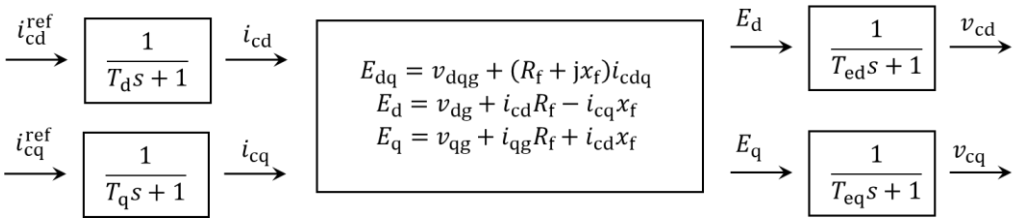

Figure 2.23. The CIG model developed in [35]

This CIG model is compared to the CIG model based on a current source representation. The results of transient simulations using these models are compared with a benchmark model. The latter includes the current controller and a set of differential equations model the L filter. The PLL is not modeled. The IEEE 9-bus system is implemented for validation purposes. The results show that the proposed model in [35] is more accurate than the CIG model based on a current source representation, mainly in the transient, once a perturbation occurs on the test system. The Electric Power Research Institute (EPRI) indicates that this model can be used in an additional step before performing EMT simulations [226]. It should be noted that the CIG model is validated considering scenarios where the penetration of converters is not significant, and the SCR is not low. Accordingly, whether the proposed model is suitable or gives accurate results for stability studies in weak or low-inertia systems is unclear. As the PLL is not modeled, its effects cannot be studied. However, the modularity of the proposed model makes it possible to include the PLL, even if it was not modeled in [35], [225].

2.6.3 Comparison of CIG Models Used for Stability Studies

Table 2.4 summarizes the CIG models most widely used in the literature to perform stability studies. All these models consider a grid-following operation mode for the converter. The DPC-based model is considered a representative model for stability assessments. This means that the EMT related to the transmission network is modeled using differential equations. In the column "Model" of Table 2.4, the term VS means that the CIG is represented as a controlled voltage source behind an impedance and the term CS means that the CIG is represented as the controlled current source. In the VS- and CS-type models, the EMT related to the transmission network is represented using QPC, meaning that a set of algebraic equations models its dynamic behavior.

It can be seen in Table 2.4 that these models only indicate how the low-level control loops, the AC filter, and the PLL are represented in stability studies. The high-level control loops are neither mentioned nor shown in Table 2.4 because all models can consider different control strategies in the high-level control system. Accordingly, the number of CIG models proposed in the literature consists of a combination of high-level control loops, low-level control loops, AC filter, and synchronization methods.

According to [10], [24], [78], [151], [203], the CIG models based on a current source representation capture transients with oscillation frequencies ranging between 0.1 Hz and 5 Hz. The frequency range varies in the cited references. The frequencies in which these CIG models may be used for stability assessments are mentioned in some reports. However, there is a lack of how the frequency range may be obtained for a particular power system. On the other hand, the frequency range in which these models may be used for stability assessments is unknown in the CIG models based on a voltage source representation. Nonetheless, it can be inferred that they cannot capture transients with oscillation frequencies much further away from 5 Hz. This is because fast EMT related to the

transmission lines is neglected in these models.

As a final remark, it should be pointed out that some works, for example [10], [200],[73], mention that CIG models based on current and voltage source representation decrease their accuracy when the CIG are connected at buses with a low level of SCR. This occurs when synchronous machines are displaced by increasing the CIG levels. In [10], [24], [203], it is suggested that for SCR lower than 3, the CIG models based on the current representation should not be used. This value is not mentioned for the CIG models based on a voltage source representation. However, the value of SCR may change depending on the power system characteristics where the CIG are connected. How to calculate the minimum SCR for which CIG models give accurate results in a power system is still not fully understood nor investigated. Indeed, some TSOs have recognized that CIG models decrease their accuracy when CIG are connected at buses with low levels of SCR. Consequently, they have mentioned that EMTP simulations may be required for power system stability studies [12], [24], [73], [200]. For example, ERCOT conducted detailed analyses on the Panhandle region using EMTP simulations in PSCAD to validate the CIG models implemented in PSS / E [24]. PSS/E is commercial software used by ERCOT for performing power system stability studies based on QPC models. Furthermore, the Australian Electricity Market Operator, the Electric Reliability Council of Texas, and the National Grid of Great Britain developed EMT models for regions with high CIG levels in their respective networks [12]. However, the conditions in which the CIG models should include more details considering electromagnetic transients are still unknown.

Table 2.4. Summary of CIG models

Model	Type of Technology	Current Control	VFF	Type of PLL	Type of AC Filter	AC filter model	References
Representative model DPC	WTG type 3 WTG type 4 PV HVDC-VSC Generic CIG	PI controller	Transfer function of first order	SRF	L	Differential equations	[15], [16], [74], [158], [161]–[166], [180], [181]
CS-Type I	WTG type 4 PV	Transfer function of first order	-	-	-	-	[10], [78], [131], [151], [179], [189], [193], [194], [196]–[199], [227]–[233][234][73], [200]
CS-Type II	WTG type 4 WTG type 3	Transfer function of first order	-	SRF	-	-	[15], [170]
VS-Type I	HVDC-VSC WTG type 4 WTG type 3	PI controller	-	SRF	L	Algebraic equations	[127], [211]–[213]
VS-Type II	WTG type 4 WTG type 3 Generic CIG VSC-HVDC	PI controller without cross-decoupling terms	-	SRF	L	Algebraic equations	[125], [162]–[164], [201], [214]–[224]
VS-Type III	Generic CIG	Transfer function of first order	-	-	L	Algebraic equations	[35], [225]
VS-Type IV	VSC-HVDC	PI controller	-	SRF	L	Differential equations	[75], [165], [166], [205]–[210]
VS-Type V	PV	PI controller	-	SRF	LCL	Differential equations of LC and algebraic equations for L	[134]
VS-Type VI	Generic CIG	Transfer function of first order	-	SRF	L	Algebraic equations	[35], [225] (including PLL)

2.7 Summary and main findings from the literature review

This chapter reviews the main research topics addressed in this thesis. It includes fundamental concepts of power system stability, impacts of CIG on power systems, and different modeling techniques used in simulation tools suitable for generic stability assessment. Finally, a detailed review of the most common CIG models used in the literature for stability assessment based on QPC. The operation mode and the generic and typical control strategies used in real CIG were discussed to understand the CIG models.

The literature review shows that CIG models have limitations in representing fast converter dynamics, hence their impact on the stability of power systems. Low SCR values can cause conditions in which QPC-based CIG models are less accurate for stability studies. However, the

SCR does not show whether a CIG model will give erroneous results in simulator tools based on QPC. Although there are limitations, QPC-based models are still widely used in industry and academia to analyze the stability of power systems with high levels of CIG. With the increasing penetration of CIG, the dynamic response of power systems is starting to be dominated by fast transients due to the control systems associated with CIG. In this context, the reliance on the QPC-based stability assessment results should be questioned, at least under operating conditions with high CIG levels. This fact has led to a lack of consensus on the pertinence of using these models in stability assessments based on QPC. Due to the computational burden, DPC simulation tools appear as an alternative to QPC models.

On the other hand, different CIG models have been proposed in the literature to represent fast-response CIG in stability assessments based on QPC. Table 2.4 summarizes the CIG models most widely used in the literature to perform stability studies. Despite the considerable efforts made by academia and industry in developing CIG models and simulation tools, there is no consensus on the appropriate level of detail needed in stability studies. The main findings mentioned above motivate the research carried out in this thesis, as stated in the problem statement.

3 Methodology

3.1 Introduction

As mentioned in Chapter 1, this thesis investigates the validity range of stability assessments based on QPC. It also investigates the appropriate level of detail required to model CIG in power system stability studies. It is assumed that the increasing penetration of CIG by replacing synchronous generators may lead to an extension of relevant transients for stability assessment towards the electromagnetic time scales.

To verify the hypotheses and achieve the objectives presented in Sections 1.3 and 1.4, respectively, this thesis is carried out in two stages. In the first stage, a methodology is proposed to verify the main hypothesis of this work. The hypothesis states, "As the penetration level of CIG increases and synchronous generators are replaced, there is a point upon which using models based on QPC becomes unsuitable for stability assessments." The methodology is based on systematic comparisons between DPC- and QPC-based models. Applying the methodology will allow us to verify the specific hypotheses **H1**, **H2** (partially), **H3**, and **H4**. These hypotheses are achieved by verifying specific objectives **O1**, **O3**, **O4**, **O5**, and **O7**. Specific objectives **O2**, **O3**, and **O8,** are partially achieved. The results obtained by applying the first methodology are the main contribution of this thesis and were published in the article [235] (see Section 1.6).

In the second stage, a comprehensive survey and comparative study of the most common CIG models used for QPC-based stability assessments are carried out. The CIG models for the comparisons are presented in Table 2.4. The DPC models are used as the reference model, and modal analyses are used to clearly understand the impact of the degree of detail used in CIG models based on QPC. In this manner, hypothesis **H2** is thoroughly verified, and the specific objectives **O2**, **O3**, and **O8** are fully accomplished. These studies consider the knowledge obtained from the paper [235]. For this reason, it will consider specific scenarios and some modeling modifications compared to the models used in the application of the first methodology.

Chapter 3 is organized as follows. Section 3.2 describes the first and main methodology of this thesis. Then in Section 3.3, the second methodology to compare CIG models is described.

3.2 Methodology for the Comparison of QPC and DPC-Based Models

The proposed methodology is depicted in Figure 3.1. In the methodology, DPC-based models are considered an alternative to QPC-based models. It establishes procedures and evaluation criteria to compare both modeling techniques systematically. The objective is to determine how high penetration of CIG levels extends the relevant bandwidth for stability assessment from slow electromechanical time scales where QPC models are used to electromagnetic time scales where DPC models are used. Through these comparisons, the validity range of the QPC is established. The application of the proposed methodology results in the contributions **C1**, **C2**, and **C3** of this thesis.

The methodology makes use of a simulation-based approach. This approach focuses on evaluating the performance of the power system for particular scenarios. Compared to a system-theoretic analytical approach, the main advantage of simulation-based approaches is that they are less restricted by modeling limitations, allowing them to obtain more accurate results [11]. However, it

is difficult to draw general conclusions. In order to enhance confidence in the results, a wide range of penetration levels of CIG is considered. The methodology comprises five stages: dynamic modeling, frequency response, modal analysis, sensitivity analysis, and validation through time domain simulations. An essential contribution lies in the proposed sequence of steps. It is of significant practical value that the stages use recognized and well-accepted simulation and analysis techniques in this context. As such, power system planners, TSOs, and power system engineers. The stages related to the proposed methodology are described in the following sections.

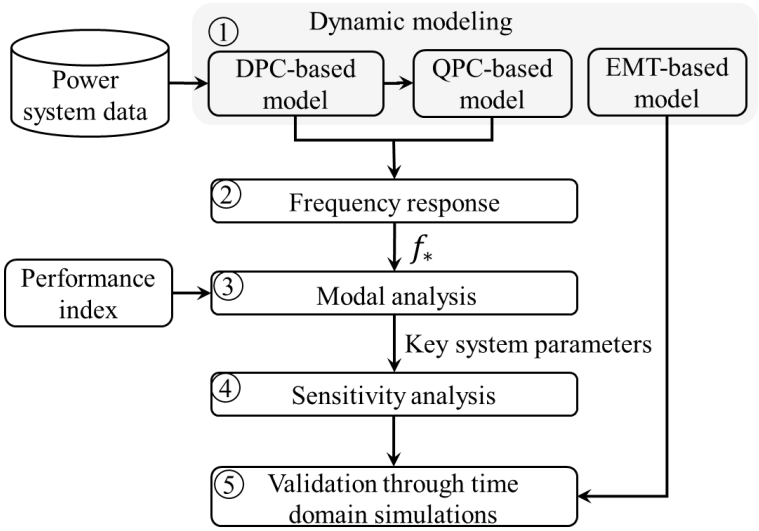

Figure 3.1. Proposed methodology

3.2.1 Stage 1: Dynamic Modeling

In the first stage of the methodology, models for the power system under study considering DPC, QPC, and EMT techniques are to be obtained. When DPC is used, synchronous generators with steam turbines are represented with an eighth-order model, whereas a seventh-order model is used for synchronous generators with hydraulic turbines [4], [118]. In both cases, standard models for governors and automatic voltage regulators are included [236], [237]. The synchronous generator models are based on the dq transform. For CIG, an average voltage source converter model in which the switching transients of the converters are neglected is considered [152], [153]. In this model, the transient behavior of the CIG is determined mainly by its control systems. There are various control structures for CIG; however, vector control is the most commonly applied. Accordingly, it is used in comparative analyses. The control loops are represented in a rotational dq reference frame [136]. The considered loops comprise an outer voltage control loop, an inner current control loop, and a PLL. It is important to point out that the PLL is used to estimate the phase angle of the voltage at the point of common coupling. The phase angle is used to transform abc to dq signals and then to control the CIG [170]. The above CIG control systems are generic and commonly used for transient simulations [35], [125], [151].

The transmission lines are modeled using π equivalent circuits with lumped parameters. Transformers are represented through series RL circuits. Loads are modeled as constant impedances, which are series RL circuits. In several previous studies, these models above have been recommended for examining electromechanical oscillations and control interactions between CIG and the rest of the power system [59], [97], [111].

A DPC model of the form shown in (3.1) is obtained by combining the models of all power system components. In (3.1), $\boldsymbol{x}$, $\boldsymbol{z}$, $\boldsymbol{u}$, and $\boldsymbol{y}$ represent the vectors of the state variables, variables related to the algebraic equations, inputs, and outputs, respectively [124].

$$\begin{aligned} \dot{\boldsymbol{x}} &= \boldsymbol{f}(\boldsymbol{x}, \boldsymbol{z}, \boldsymbol{u}) \\ \boldsymbol{0} &= \boldsymbol{g}(\boldsymbol{x}, \boldsymbol{z}, \boldsymbol{u}) \\ \boldsymbol{y} &= \boldsymbol{h}(\boldsymbol{x}, \boldsymbol{z}, \boldsymbol{u}) \end{aligned} \tag{3.1}$$

When the DPC-based model is derived, the QPC-based model is mainly derived by neglecting some derivatives of (3.1). The derivatives to be neglected can be selected mainly by two approaches: based on physical system understanding and manual reduction [15], [35], [78] or based on singular perturbation theory [102]. By neglecting the derivatives, it is assumed that the transients of the related state variables decay rapidly, and therefore there would be little justification to include their effects in stability studies [4]. This has been the case for the stator flux linkages of synchronous generators, the voltages in capacitances, and the currents in inductances of transmission networks of power systems dominated by synchronous machines. Hence, their derivatives have been set to zero in stability assessments based on QPC [4], [5]. By neglecting the derivatives of the selected state variables, some differential equations in (3.1) become algebraic. It should be mentioned that the CIG models CS-Type I, CS-Type II, and VS-Type III shown in Table 2.4 are not entirely derived by neglecting the derivatives of some selected state variables. As described in Sections 2.6.1 and 2.6.1, these models assume a dynamic behavior of the inner control loops and then propose a dynamic model to represent such behaviors.

Table 3.1 shows the references where the component models considered in this step are described in detail. Additionally, the quantities neglected for each component are indicated. A detailed description of each component model is presented in Appendix A.

Table 3.1. Summary of power system models

Component	**References**		**Quantities neglected in QPC-based models**
	DPC	**QPC**	
Synchronous generator	[4]	[2]	Derivatives of the stator flux linkages
Transmission networks, Transformers, and loads	[238]	[2]	Derivatives of the voltages in capacitors and derivatives of the currents in inductors.
CIG current control and coupling inductance	[125]	[125]	Derivatives of the current in the coupling inductance.
CIG PLL	[169]	[169]	-
CIG outer voltage control	[151]	[151]	-

For EMT models, transformers, loads, SGs with their control systems, and CIG control systems are identical to those used in DPC-based models. The distributed-parameter transmission lines models are used. The VSC considered in the CIG is the two-level three-phase VSC. The high-frequency switching transients due to PWM control are represented as the switching function model described in [136].

3.2.2 Stage 2: Frequency Response

Once the DPC- and QPC-based models of the power system are obtained, the steady-state frequency responses of both models are compared in the second stage. To see changes in frequency responses as CIG penetration increases, this assessment is performed for different levels of CIG. The objective is to identify the lowest frequency f_* at which the magnitudes of both frequency responses differ by a given threshold ϵ. This allows for determining the frequency bandwidth in which QPC-based models are still suitable for representing the system transients as a function of the CIG level. The frequency f_* is obtained from a Bode diagram, as illustrated in Figure 3.2.

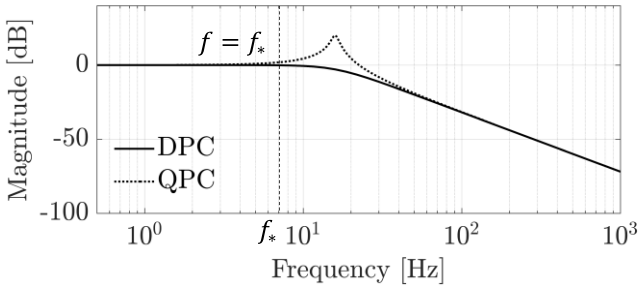

Figure 3.2. Illustrative Bode plot for comparing DPC- and QPC-based models in the frequency domain

3.2.3 Stage 3: Modal Analysis

The third stage of the methodology includes a modal analysis using small-signal linearization around the steady-state operating point for both models. The objective is to analyze the modes that involve oscillations with frequencies higher than f_* and to determine the relevant state variables for different levels of CIG. The focus is on the modes with frequencies higher than f_* because those are in the region where differences between both modeling techniques become pronounced (see Figure 3.2). The state variables related to these modes are identified by analyzing participation factors [124].

In this stage, the dynamic performance for both linearized models is also quantitatively analyzed, and the H-infinity norm $\mathcal{H}_\infty$ is used for this purpose. For a MIMO (multiple inputs, multiple outputs) system described by: $\dot{\boldsymbol{x}}(t) = \boldsymbol{A}\boldsymbol{x}(t) + \boldsymbol{B}\boldsymbol{u}(t)$, $\boldsymbol{y}(t) = \boldsymbol{C}\boldsymbol{x}(t) + \boldsymbol{D}\boldsymbol{u}(t)$, and with a transfer matrix $\boldsymbol{G}(s) = \boldsymbol{C}(s\boldsymbol{I} - \boldsymbol{A})^{-1}\boldsymbol{B} + \boldsymbol{D}$, the H-infinity norm can be defined as follows [124], [239]:

$$\|\boldsymbol{G}(s)\|_\infty \triangleq \max_{\boldsymbol{u}(t)\neq 0} \frac{\|\boldsymbol{y}(t)\|_2}{\|\boldsymbol{u}(t)\|_2} \tag{3.1}$$

with:

$$\|\boldsymbol{y}(t)\|_2 = \left(\int_0^\infty \boldsymbol{y}^{\mathrm{T}}(t)\boldsymbol{y}(t)\,\mathrm{d}t\right)^{\frac{1}{2}} \tag{3.2}$$

$$\|\boldsymbol{u}(t)\|_2 = \left(\int_0^{\infty} \boldsymbol{u}^{\mathrm{T}}(t)\boldsymbol{u}(t)\,\mathrm{d}t \right)^{\frac{1}{2}} \tag{3.3}$$

The value of $\|\boldsymbol{G}\|_\infty$ represents the maximum root-mean-square gain of the system for any direction of the input vector. If the system has all eigenvalues in the left half of the complex plane, the small-signal model is stable and $\|\boldsymbol{G}\|_\infty$ is bounded [240]. On the other hand, if $\|\boldsymbol{G}\|_\infty$ is not bounded, the small-signal model is unstable or has poles on the imaginary axis. Therefore, as the $\|\boldsymbol{G}\|_\infty$ increases, the system becomes less damped. Accordingly, if the QPC-based model has a significantly different value of $\|\boldsymbol{G}\|_\infty$ compared with its counterpart based on DPC, then the results obtained with the QPC-based model are less accurate because the dynamic performance becomes significantly different due to the simplifications made. Using this performance index allows us to compare both modeling techniques straightforwardly despite the number of state variables, which are considerably different.

3.2.4 Stage 4: Sensitivity Analysis

The next stage consists of performing a sensitivity analysis of key system parameters. This allows verifying if the observations of Stage 3 are plausible even when relevant parameters of the system change. The parameters are selected according to the relevant state variables, which are defined from the analysis of the participation factors in Stage 3. Once the key parameters have been identified, a range of variations of these parameters is defined based on typical values used in transient studies. The analysis specified in Stage 3 is then repeated.

3.2.5 Stage 5: Validation Through Time Domain Simulation

In this stage, time domain simulations are performed to verify and validate all relevant observations of the previous stages and draw main conclusions. For this purpose, simulations of a system disturbance are carried out using DPC, QPC, and EMT modeling techniques. EMT simulations in abc phase variables are performed in PSCAD [32], [33] to verify the accuracy of DPC models. Finally, the time series of selected system variables are compared.

3.3 Methodology for Comparisons of CIG Models Based on QPC

The methodology used to compare common CIG models based on QPC is shown in Figure 3.3. It comprises four stages: dynamic modeling, sensitivity analysis, comparative analyses, and validation through time domain simulation. The DPC model is used as the reference model for comparative studies. The methodology is based on modal analysis, which is based on small-signal models that are not used for transient stability studies but help to understand dynamic interactions. Stability issues due to the CIG are mostly related to control dynamics between the components of the power system [15], [58], [241]–[243]. Therefore, modal analysis can be used to understand and identify the increased dynamic interactions due to CIG.

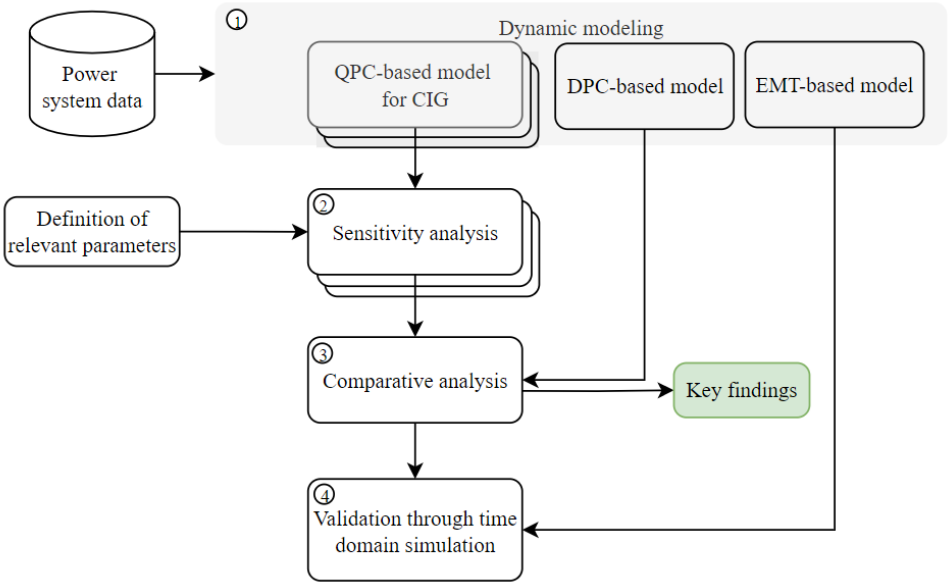

Figure 3.3. Methodology for comparing CIG models

The analyses carried out in the comparisons focus on the impact of fast dynamics on the accuracy of stability assessment using CIG models based on QPC. Also, it is studied whether fast dynamic responses related to CIG can affect the slow dynamics. The DPC model is used as the reference model in all studies. The results are validated using EMT simulations in PSCAD. The results obtained by applying the methodology allow us to clearly understand the impacts of the degree of detail used in the most common CIG models based on QPC. The CIG models shown in Table 2.4 are considered and implemented. The results obtained by applying this methodology and the comprehensive review described in Sections 2.5.3 and 2.6 are considered contribution **C4** of this thesis (see Section 1.5). The stages of the methodology are described in detail in the following sections.

3.3.1 Stage 1: Dynamic Modeling

In the first stage of the methodology, the power system under study is modeled using DPC, QPC, and EMT-based approaches. This power system is a multi-machine and multi-converter network. Some components are represented using the same models described in Section 3.2. For this reason, this section presents in more detail the differences between the models used in Section 3.2.1. When DPC and QPC approaches are used, synchronous generators with steam turbines, synchronous generators with hydraulic turbines, governors, automatic voltage regulators, transmission lines, transformers, and load are represented according to the models shown in Table 3.1.

When using a DPC-based approach, the average voltage converter model, in which the switching transients of the converter are neglected, is considered to represent CIG units [152], [153]. Dynamic responses are mainly determined by the control systems implemented. Vector control is used for comparative analyzes because it is widely applied in actual CIG power plants. The control loops are presented in a rotational dq reference frame [136]. The CIG units have implemented high- and low-level control loops. In the case of high-level control loops, active power and voltage control are considered with PI controllers. The block diagrams are shown in Figure 2.10.a and Figure 2.11.b, respectively.

It should be noted that active power and voltage control structures are slightly different from those used in Stage 1 of Section 3.2.1. Here, a PI controller is used for both control loops, and Section 3.2.1 is only used for voltage control. The differences can be seen in Appendices A and B.

A PLL in SRF, as is shown in Figure 2.13, is considered. The PLL estimates the phase angle of the voltage at PCC. The phase angle transforms abc to dq signals and then controls the CIG [170]. Finally, the inner current control loops with VFF terms shown in Figure 2.14 and Figure 2.15 are implemented in low-level loops. The above control systems are generic and commonly used for transient simulations and modal analysis of power systems with CIG [35], [74], [125], [151], [241], [244].

In the power system under study, all the CIG models shown in Table 2.2 are implemented when QPC is used. The same CIG models are used in all the CIG units of the test system. The modular structure of the CIG models allows us to preserve the same outer control loops used in DPC. Therefore, active and voltage controls are the same as DPC models for each CIG model. The PLL and the inner control loops are represented as indicated in Table 2.4. A detailed description of the set of differential equations is given in Appendix B.

In the case of EMT simulations, transformers, loads, synchronous generators with their control systems, and CIG control systems are identical to those used in DPC-based. The distributed-parameter transmission lines models are used. The VSC considered in the CIG is the two-level three-phase VSC. The high-frequency switching transients due to PWM control are represented as the switching function model described in [136].

3.3.2 Stage 2: Sensitivity Analysis

This stage performs sensitivity analysis on key control system parameters and operating conditions of the system under study. The control system parameters are varied according to the generic values used in various research works [59], [74], [75], [170], [180], [181], [244]–[246]. The modal analysis is used for this purpose. The analyses use linearized models around a steady-state operating point for the system represented by applying DPC and QPC-based models. The main objective is to determine the impacts of commonly employed simplifications regarding fast dynamic phenomena on the scale of electromagnetic and slow electromechanical phenomena on CIG models used in stability studies based on QPC. Stability issues due to the CIG are mostly related to control dynamics between the components of the power system [15], [58], [241]–[243]. Consequently, participation factor analysis is used to understand and identify the dynamic interactions that have increased due to CIG and its impacts on the suitability of QPC.

The differences and assumptions of each CIG model based on QPC are presented in Table 2.4. This table shows differences in how the current loops with VFF terms, the PLL, and the AC filter are represented. For this reason, sensitivity analyses on control system parameters are carried out during this stage. Especially when there are differences among CIG models. Furthermore, sensitivity in parameters such as SCR is considered because, in the literature, several studies show possible stability problems when CIG plants are connected to busbars with low levels of SCR [15], [16], [74], [242], [244].

Three case studies are carried out in this stage. Table 3.2 summarizes the impacts on the CIG models based on QPC to be analyzed. Case Study 1 analyses the effects of CIG levels and PLL bandwidths. The effects of SCR levels are analyzed in Case Study 2. Case study 3 analyzes the

impact of the dynamic response of the inner current loops.

Table 3.2. Summary of Case Studies

Case Studies	Impacts Under Study on CIG Models Based on QPC
Case study 1	PLL and CIG levels
Case study 2	SCR levels
Case study 3	Inner Control Loops

In order to summarize the results obtained and highlight the conditions where there are significant differences among the CIG models, the H-infinity norm $\|\boldsymbol{G}\|_\infty$ is used as a performance index. This norm is defined in equations (3.1), (3.2), and (3.3). The value of $\|\boldsymbol{G}\|_\infty$ represents the maximum root-mean-square gain of the system for any direction of the input vector. If the system has all eigenvalues in the left half of the complex plane, the small-signal model is stable and $\|\boldsymbol{G}\|_\infty$ is bounded [240]. On the other hand, if $\|\boldsymbol{G}\|_\infty$ is not bounded, the small-signal model is unstable or has poles on the imaginary axis. Therefore, as the $\|\boldsymbol{G}\|_\infty$ increases, the system becomes less damped. Consequently, if a CIG model based on QPC has a significantly different value of $\|\boldsymbol{G}\|_\infty$ with its counterpart based on DPC, the results obtained with that CIG model are less accurate because the dynamic performance becomes significantly different due to the simplifications. In these cases, modal analysis is performed to understand the causes of the differences between the DPC model and the particular CIG model based on QPC. Through the analysis of the participation factors, the main dynamic interactions with the respective state variables that cause the difference between models are identified.

3.3.3 Stage 3: Comparative analysis

The results obtained from the previous stage (sensitivity analyses) are summarized and systematically compared. For all the case studies in Table 3.2, key findings regarding the limitation and suitability of CIG models based on QPC for stability studies are identified.

3.3.4 Stage 4: Validation Through Time Domain Simulation

In Stage 4, time domain simulations are carried out to verify and validate the key findings of Stage 3 and the results obtained in Stage 2. For this purpose, transient simulations of the test system are performed using the DPC, and QPC approaches. Sensitivity analysis is based on small-signal models. Consequently, to validate the finding of the previous stage, a small system disturbance is considered. The time series of selected system variables are compared and associated with the results obtained from the modal analysis. Finally, EMT simulations are performed to validate the results of DPC models.

4 Comparative Analysis Between DPC- and QPC-Based Models

This chapter shows and discusses the main results obtained by applying the methodology proposed in Section 3.2 (see Figure 3.1). Section 4.1 describes the power system used to perform the study. In Section 4.2, the models used for each component are presented, as well as some details of the software used. Finally, in Section 4.3, the proposed methodology is applied to the selected system, and then a comprehensive comparison is performed considering DPC and QPC-based models.

4.1 Description of Power System Under Study

The selected system is the IEEE 9-bus network, shown in Figure 4.1 [247]. A set of configuration switches extends the system to allow the study of various generation portfolios. The system has three synchronous generators at 60 Hz, two with steam turbines, G2 and G3, and one with a hydraulic turbine, G1. The main characteristics of these generators are summarized in Table 4.1. The total system load is 315 MW and 115 MVAR, with a 0.94 power factor lagging. System parameters are given in [247]. The load is equivalent to 56 % of the total rated generation capacity of the system.

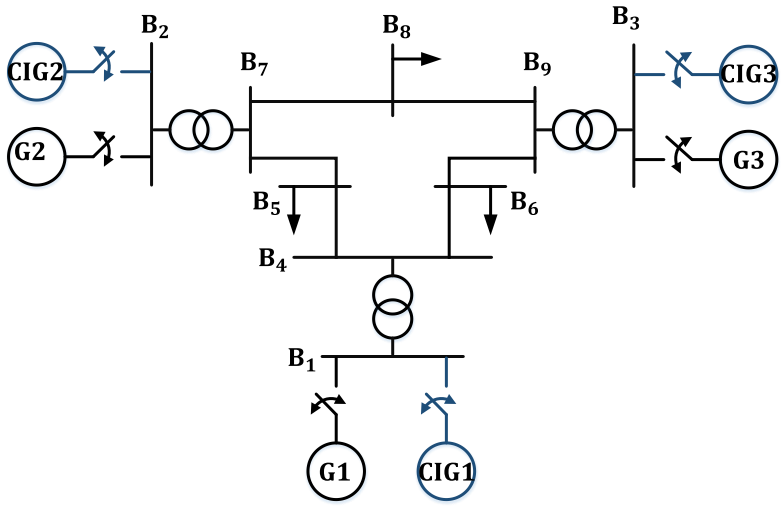

Figure 4.1. IEEE-9 bus system with switches to adapt the generation portfolio [247]

Table 4.1. Main characteristics of synchronous generators

Properties	G1	G2	G3
Type	Hydro	Steam	Steam
Rated power [MVA]	247.5	192	128
Inertia constant [s]	11.82	3.2	1.505
Rated voltage [kV]	16.5	18	13.8

To compare DPC- and QPC-based models, two CIG units are added at buses B1 and B3. The capacities of CIG1 and CIG3 are the same as the synchronous generators G1 and G3, respectively. To reach 100% CIG level, the generator G2 is replaced by the CIG2 unit operating in GFM mode as a virtual synchronous generator [156]. In this operation mode, the frequency is controlled by

implementing the two-order swing equations of synchronous generators into the outer control loops associated with CIG2. The swing equations allow for mimicking the electromechanical dynamic response of synchronous machines and, thus, the role of frequency as an indicator of power balance. Figure 4.2. show outer control loops implemented. The CIG-GFM model and parameters are detailed in Appendix A.2. The control frameworks for frequency support are decentralized. Accordingly, there is no inter-generator communication latency.

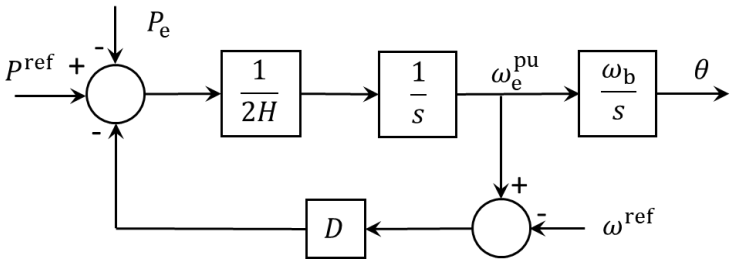

Figure 4.2 Virtual Synchronous Generator Control [156]

The capacity of CIG2 is equal to generator G2, and the synthetic inertia of CIG2 is equivalent to the inertia of generator G2. The CIG penetration levels considered are summarized in Table 4.2. The penetration levels are calculated as a function of the total active power demand of the test system. When the power of a generator is zero in Table 4.2, the connection switch related to the generator is open. For all CIG penetration levels, the generator connected to bus 2 is considered as slack bus. Table 4.2 also includes the system inertia H_{sys}, which is defined as [4]:

$$H_{\text{sys}} = \frac{\sum_{i=1}^{n} H_i S_i}{\sum_{i=1}^{n} S_i} \tag{4.1}$$

where H_i, S_i, and n respectively denote the inertia constant, the rated power of the generator, and the number of generators connected to the system contributing finite inertia. Since the CIG2 operates as a virtual synchronous generator, its synthetic inertia (see Figure 4.2) is also included for calculating the system inertia H_{sys}. This explains the unchanged values of H_{sys} in rows three and four of Table 4.2.

Table 4.2. Dispatch and system inertia H_{sys} for different generator portfolios

CIG Levels [%]	**G1 [MW]**	**G2 [MW]**	**G3 [MW]**	**CIG1 [MW]**	**CIG2 [MW]**	**CIG3 [MW]**	$\boldsymbol{H_{\text{sys}}}$ **[s]**
0	163	77	80	0	0	0	5.82
35	0	91	120	55	0	55	1.66
70	0	98	0	110	0	110	1.13
100	0	0	0	189	4	126	1.13*[1]

[1] Synthetic inertia related to CIG2 operating in GFM

4.2 Implemented Models and Software Used

For the model of the system using DPC, the synchronous generators are modeled as given in Table 3.1 [118]. All synchronous generators are equipped with a voltage regulator of type DC1A IEEE [236]. The governor of the steam turbines is of type IEEE TGOV1, while the hydraulic turbine is of type IEEE HYGOV [237]. The models of the CIG1 and CIG3 units include the control systems described in Table 3.1. The current control loop parameters are chosen to obtain a settling time of 20 ms, a typical value used in simulations with power converters [35], [248]. The PLL control system has a bandwidth of 20 Hz [170]. The control parameters of the CIG1 and CIG3 units are summarized in Table 4.3. These parameters are also expressed in pu. In the case of QPC-based models, G2 and G3 models are of sixth-order, and G1 is a fifth-order model because the stator flux linkage transients are neglected [2]. CIG1 and CIG3 units are represented using VS-Type II, shown in Table 2.4. The control systems of the synchronous generators are kept identical to those used for the DPC-based models.

The accuracy of DPC models is verified by performing EMT simulations in PSCAD. For these simulations, distributed-parameter transmission line models are used. The VSC configuration considered in CIG is the two-level three-phase VSC. To represent high-frequency switching transients due to PWM control, the switching function model of the VSC converter described in [136] is used. The PWM compares a high-frequency triangular carrier signal with a modulating signal with a lower frequency. The transformer, load, and synchronous generator models with their control systems and the control systems of CIG are identical to those used in DPC models.

Table 4.3. Control system parameters of CIG units

Properties	Value
Proportional gain of current controller k_{p}	0.40
Integral gain of current controller k_{i}	90.00
Proportional gain of PLL controller k_{pPLL}	101
Integral gain of PLL controller k_{iPLL}	2562
Time constant of voltage measure T_{r} $[s]$	0.05
Proportional gain of reactive power controller k_{pq}	5.00
Integral gain of reactive power controller k_{iq}	0.50

The test system using DPC and QPC was implemented in MATLAB/Simulink. To perform frequency response and modal analysis, the system was linearized using the MATLAB / Simulink Linear Analysis Tool [249]. The "bode" function of MATLAB was used for the frequency response analysis. The input and output signals considered are the reference power and the angular electrical frequencies of the generators, respectively. These relations are chosen because in power systems with low inertia, frequency control is one of the main control challenges [250].

4.3 Results of Comparative Analysis of DPC and QPC-Based Models

In the following, the main results obtained by applying the proposed methodology for comparing the DPC and QPC modeling techniques are presented. The results are presented starting from Stage 2 of the methodology shown in Figure 3.1.

4.3.1 Frequency Response Analysis

The Bode diagrams of the system, when considering 35 % and 70% of CIG penetration levels, are

depicted in Figure 4.3. The considered input signal is the reference power of the generator connected at B3, $P_{\mathrm{B3}}^{\mathrm{ref}}$. The output signal is the angular electrical frequency at bus B1, $\omega_{\mathrm{B1}}^{\mathrm{elec}}$. The frequency f_* upon which the simulation based on DPC differs from the QPC was determined considering a tolerance of $\epsilon = 5\%$.

Figure 4.3 shows that the maximum frequency up to which both models give a similar frequency response is $f_* \approx 5$ Hz. For CIG levels higher than 35%, G3 is disconnected. In such configurations, the system modeled by QPC shows a resonance close to 12 Hz, whereas the DPC-based model does not show such behavior. This suggests that QPC-based models become less accurate if the frequency of the transients of interest adopts values higher than 5 Hz. The frequency range in which both models give a similar frequency response coincides with the frequency range related to slow rotor oscillations of electric machines, which typically vary between 0.1 Hz and 5 Hz. In the DPC-based models, the rapid changes of magnitudes observed for frequencies higher than 500 Hz are mainly because the network is modeled by differential equations rather than just algebraic ones (as shown in Table 3.1). In these frequency ranges, the outputs are well attenuated because the gain of the transfer function is lower than -40 dB. Therefore, their relative impact on the transfer function compared to those of other frequency ranges is low. Qualitatively, similar observations are made at other levels of penetration of the CIG. The frequency f_* is also retained for different selections of input-output combinations. For these reasons, the frequency response for 35% and 70% of the CIG level is shown here.

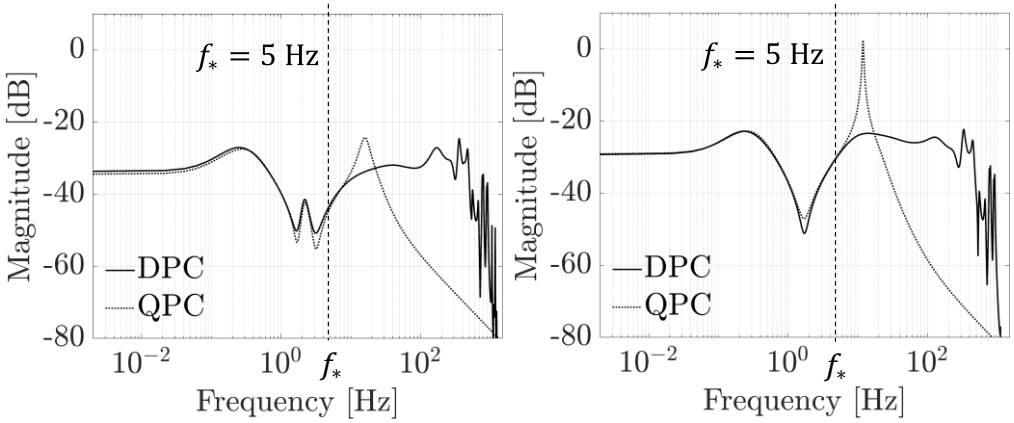

Figure 4.3. Magnitude of Bode plot; a) 35% of CIG, b) 70% of CIG

4.3.2 Modal Analysis

As described in Stage 3 of the methodology, the modal analysis is focused on modes with frequencies higher than f_* since the modes are expected to have a detrimental effect on the accuracy of QPC. In this frequency range, the system modeled using QPC has two modes of oscillation, hereafter identified by $\mathrm{M1}_{\mathrm{QPC}}$ and $\mathrm{M2}_{\mathrm{QPC}}$, respectively. Figure 4.4 shows the effect of penetration levels of CIG on the eigenvalues corresponding to the modes $\mathrm{M1}_{\mathrm{QPC}}$ and $\mathrm{M2}_{\mathrm{QPC}}$. The analysis of participation factors reveals that the modes $\mathrm{M1}_{\mathrm{QPC}}$ and $\mathrm{M2}_{\mathrm{QPC}}$ are pertaining to the control systems of the CIG1 and CIG3 units. These modes are mainly related to the state variables of the current control loops and the PLL of those CIG units.

In Figure 4.4, the root loci reveal a reduction in damping as CIG penetration levels increase.

However, the mode $M1_{QPC}$ still remains well damped for all the penetration levels, with its oscillation frequency moving from 18 Hz to 16 Hz. Its lowest damping ratio is 49% for the case of a CIG level of 100%. On the other hand, the mode $M2_{QPC}$ becomes poorly damped as CIG penetration levels grow. The damping ratio changes from 16% to 1.3%, and the oscillation frequency moves from 16 Hz to 11 Hz. The decrease in the damping ratio is accentuated when the CIG levels exceed 35%. This is because generator G3 is then disconnected from the system, leading to a reduced system inertia H_{sys} as Table 4.2 shows.

Given the above observations, the modal analysis performed when the system is modeled by QPC suggests poor dynamic performance for high levels of CIG and a reduced presence of synchronous machines connected to the system. Moreover, QPC analysis suggests that the system is close to losing small-signal stability.

The system modeled using DPC has high, medium, and low frequency oscillation modes. These modes can be categorized into the following frequency ranges: 400 Hz to 1500 Hz, 60 Hz to 400 Hz, and 0 Hz to 60 Hz, respectively. For high frequency modes, the analysis based on the participation factors shows that these modes are mainly related to electromagnetic transients pertaining to the transmission network, the stator fluxes of the synchronous generators, and the CIG control systems. Dominant state variables are not observed in the high frequency modes. Some of these modes have low damping ratios. However, as shown in the frequency response analysis, the outputs are very well attenuated for frequencies higher than 500 Hz. Therefore, the high frequency modes are not critical for the small-signal stability of the system. This observation was also reported in [111]. The participation factor analysis for medium frequency modes (60 Hz to 400 Hz) shows they are related to the electrical network modes and are well damped. Both high- and medium-frequency modes are not significantly affected by the penetration levels of CIG. As a result, further analysis of these modes is not very relevant to this thesis.

The critical difference between QPC and DPC modeling techniques appears for the low frequency modes, particularly in the modes associated with the control system of the CIG1 and CIG3 units. In the system modeled using DPC, there are four control modes related to the CIG, $M1_{DPC}$, $M2_{DPC}$, $M3_{DPC}$, and $M4_{DPC}$, respectively. The participation factor analysis reveals that the mode $M1_{DPC}$ is mainly related to the state variables of the current control loops and the PLL of both CIGs. The mode $M1_{DPC}$ is the only control mode for which its corresponding eigenvalue appears in the same complex plane area as the eigenvalues of the modes $M1_{QPC}$ and $M2_{QPC}$. This can be recognized in Figure 4.4. For all penetration levels of CIG, the mode $M1_{DPC}$ is well damped, taking a minimum damping value of 60%. In the cases of the modes $M2_{DPC}$, $M3_{DPC}$, and $M4_{DPC}$, the state variables that have high participation are related to the current control loop and the filter of both CIGs. The penetration levels of CIG do not significantly affect these control modes. In fact, they are always well damped with damping ratios higher than 70%.

Given the above observations, the modal analysis performed on the system modeled by DPC suggests that the linearized system is stable regardless of the penetration levels of CIG. In addition, it has better dynamic performance compared to its QPC-based counterpart.

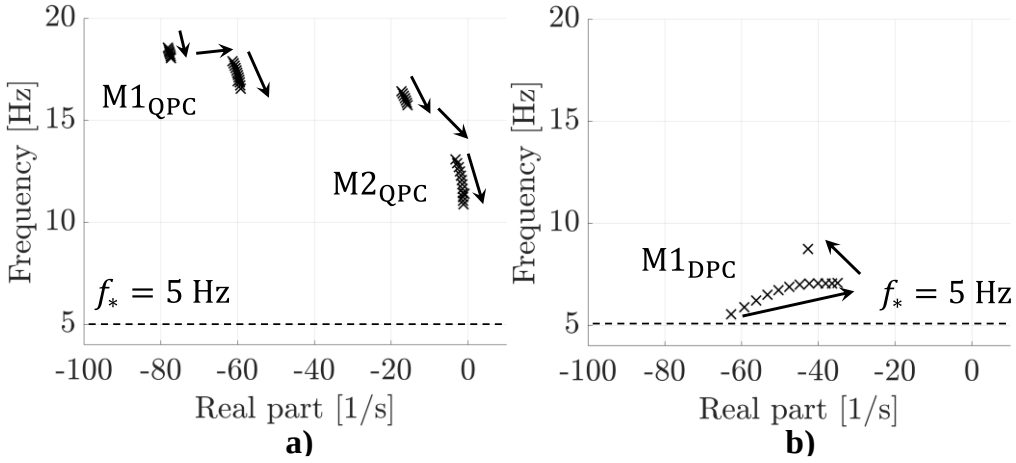

Figure 4.4. Eigenvalue loci of the control modes for CIG levels between 5% and 100%; a) QPC-based model, b) DPC-based model

Figure 4.5 shows the H-infinity norm $\|\boldsymbol{G}\|_\infty$ for different levels of CIG. The value of $\|\boldsymbol{G}\|_\infty$ represents the maximum root-mean-square gain of the system for any direction of the input vector. If the system has all eigenvalues in the left half of the complex plane, the small-signal model is stable and $\|\boldsymbol{G}\|_\infty$ is bounded [240]. On the other hand, if $\|\boldsymbol{G}\|_\infty$ is not bounded, the small-signal model is unstable or has poles on the imaginary axis. Therefore, as the $\|\boldsymbol{G}\|_\infty$ increases, the system becomes less damped.

Figure 4.5 shows that as the CIG increases, there are no significant variations in the $\|\boldsymbol{G}\|_\infty$ when the system is modeled using DPC. However, in the case of the QPC-based model, the $\|\boldsymbol{G}\|_\infty$ tends to increase. The difference between the infinity norms of both models is accentuated as the level of CIG exceeds 35%. For CIG levels higher than 35%, the generator G3 is disconnected from the power system, leading to a reduction of the system inertia H_{sys}. This causes that for such CIG levels the transients of the system simulated through the QPC-based model are considerably different from those obtained through its counterpart based on DPC.

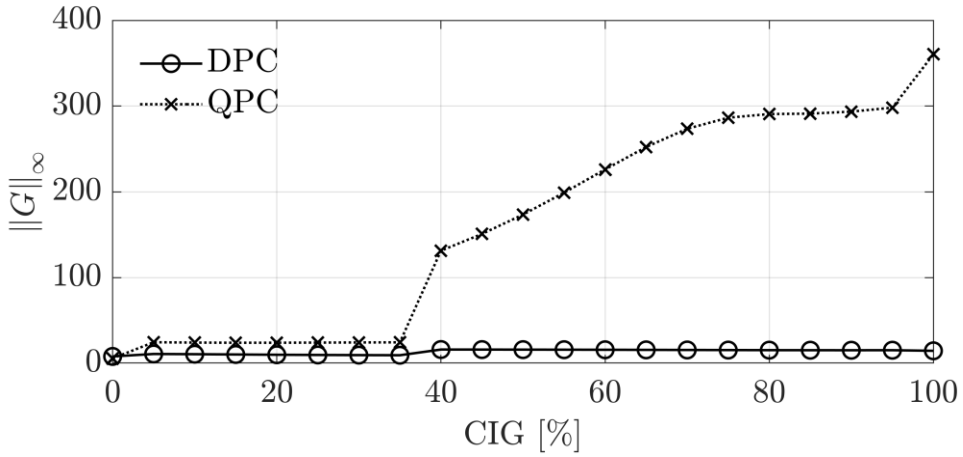

Figure 4.5. $\|\boldsymbol{G}\|_\infty$ as a function of CIG level

4.3.3 Sensitivity Analysis

The modal analysis has shown that the critical modes of the system based on QPC-models are the modes $M1_{QPC}$ and $M2_{QPC}$. In the case of DPC-based models, there are no critical modes. However, for this analysis, the control mode $M1_{DPC}$ is considered because it is the mode for which its corresponding eigenvalue is relatively close to the eigenvalues pertaining to the modes $M1_{QPC}$ and $M2_{QPC}$. The first sensitivity analysis is carried out for different parameters of the control systems of the CIG. The effects of changing the PLL control parameters are presented because it significantly impacts this analysis. To do this, the frequency bandwidth of the PLL is modified between 2 Hz and 30 Hz, which are typical values found in the literature [59], [170].

The impact of the different PLL bandwidths on the eigenvalues related to the modes of interest at 35%, 70%, and 100% of the CIG penetration levels is shown in Figure 4.6. The system modeled using the QPC approach becomes less damped or unstable as the PLL bandwidth and the CIG level increase. Figure 4.6a shows that the eigenvalue associated with the mode $M2_{QPC}$ is close to the right half-complex plane. More precisely, the instability appears for PLL bandwidths above 25 Hz and penetration levels over 70%. The unstable modes are highlighted in red in Figure 4.6a. In the case of DPC-based models, the effect on the eigenvalue of $M1_{DPC}$ is shown in Figure 4.6b. As the PLL bandwidth increases, the mode $M1_{DPC}$ always remains well damped, taking minimum damping of 51%. For this case, the small-signal model is always stable when using a DPC regardless of the PLL bandwidth and the CIG penetration level. It should be highlighted that this result does not mean that the system modeled by DPC will always be small-signal stable for any values that take the PLL bandwidths or for any operating conditions. In this case, the QPC-based models overestimate the small-signal stability of the power system because it indicates that the system is unstable when it is small signal stable according to DPC-based models.

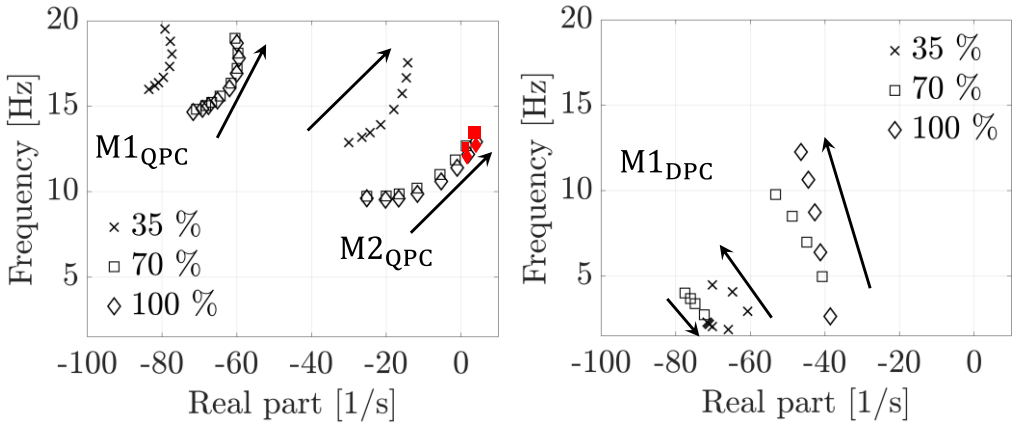

Figure 4.6. Eigenvalue loci of the control modes for PLL bandwidth between 2 Hz and 30 Hz; a) QPC-based model, b) DPC-based model

Figure 4.7 shows the H-infinity norm $\|\boldsymbol{G}\|_\infty$ for different CIG levels and PLL bandwidths. According to Figure 4.7a for QPC-based models, as the PLL bandwidth increases, resulting in a faster PLL response, the $\|\boldsymbol{G}\|_\infty$ also increases with the penetration level of CIG. For PLL bandwidths higher than 20 Hz, the models based on QPC suggest instability even at low levels of CIG. On the other hand, for the DPC-based models, Figure 4.7b reveals no significant variations

in the $\|\boldsymbol{G}\|_\infty$ for different levels of CIG and PLL designs. When CIG levels takes values higher than 35 %, there is a step in the $\|\boldsymbol{G}\|_\infty$. For such levels, the synchronous generator G3 is disconnected, decreasing the system inertia, as is shown in Table 4.2. The change is due to the number of synchronous generators and not due to the CIG level itself. These results are consistent with Figure 4.6b, showing that the system is always stable in small signal when a DPC-based model is used. The visible differences in the $\|\boldsymbol{G}\|_\infty$ of both models point to inaccurate transient simulations using QPC. Therefore, erroneous conclusions regarding power system stability may be drawn.

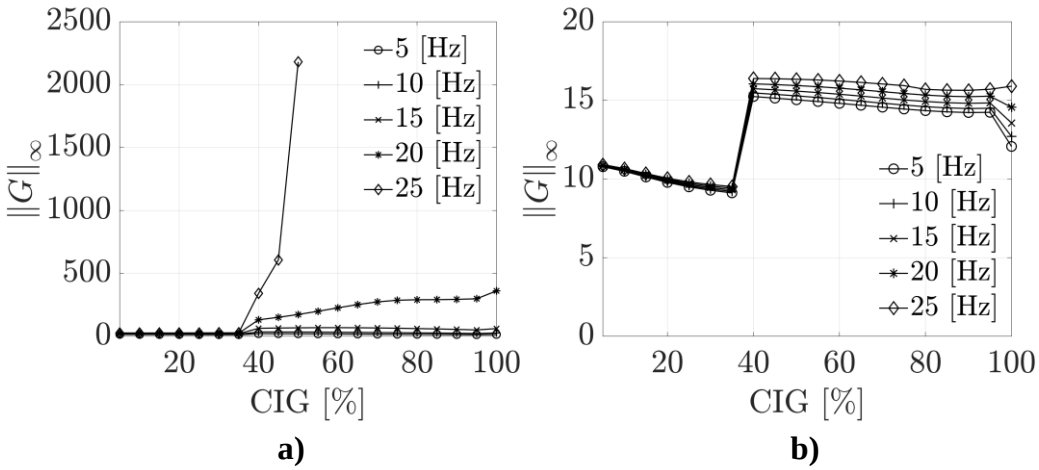

Figure 4.7. $\|\boldsymbol{G}\|_\infty$ as a function of CIG penetration level and different PLL bandwidth frequencies; a) QPC-based model, b) DPC-based model

A second sensitivity analysis is performed in terms of system inertia H_{sys}. This is because it was observed in the first sensitivity analysis that the QPC-based models significantly decrease their accuracy when the CIG levels take values greater than 35%. G3 is disconnected from the power system for such ranges of CIG levels. This reduces the system inertia H_{sys} from 1.66 s to 1.13 s. The change in the operating conditions due to the disconnection of G3 makes the QPC-based models unstable when the PLL has a fast dynamic response. For this reason, the second sensitivity analysis is performed to study the effects of changing the inertia of the power system on the accuracy of QPC-based models. The change of the system inertia H_{sys} is an emulation of the increasing replacement of synchronous machines by CIG.

In order to perform the second sensitivity analysis in terms of system inertia H_{sys}, the synchronous generators G1 and G3 are connected to the system, as shown in Figure 4.8. It is assumed that the transformer connecting G1 and CIG1 have the same reactance and rated voltage. Similarly, it is done for G3 and CIG1. To reduce the system inertia H_{sys}, the rated power of the synchronous generators G1 and G3 are reduced. The inertia constant H of these generators, which is shown in Table 4.1, is kept constant. This means that the energy stored at the rated speed of the synchronous generators G1 and G3 decreases with their rated capacities. By decreasing the rated capacity of G1 and G3, the displacement of synchronous generators is emulated due to the increase of CIG in power systems. Accordingly, the system inertia H_{sys} ranges from 3.5 s to 1.16 s.

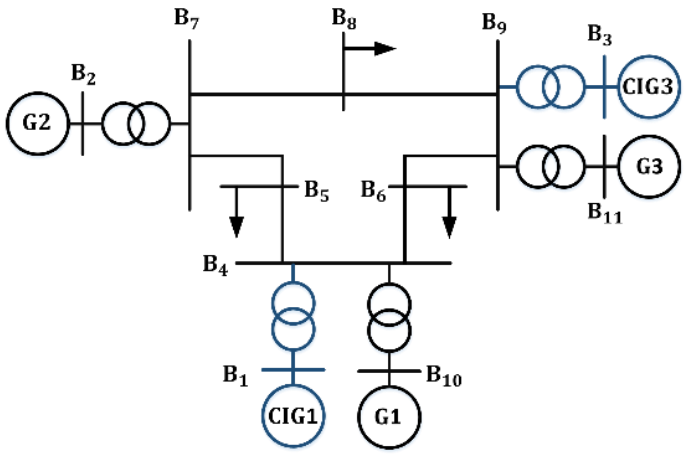

Figure 4.8. IEEE 9-bus system for a diverse range of CIG penetration levels and system inertia H_{sys}

The results related to the PLL bandwidth of 25 Hz with 70% of CIG penetration level are described in the following. These results are representative, and qualitatively the same observations are kept for other GIG levels and PLL bandwidths.

In Figure 4.9a, the effect of changing the inertia constant of the power system on the eigenvalues associated with the modes M1_{QPC} and M2_{QPC} is depicted. The root loci reveal a reduction in damping as the system inertia H_{sys} decrease. The mode M1_{QPC} remains well-damped for all the system inertia H_{sys} and its lowest damping ratio is 47% in the case of the system inertia H_{sys} of 1.16 s. For the mode M2_{QPC}, the damping ratio changes between 36% and 0.4%. The oscillation frequencies move from 18 Hz to 13 Hz. The decreasing of the system inertia H_{sys} makes the mode M2_{QPC} poorly damped and makes the system close to losing the small-signal stability. Consequently, the modal analysis of the system using QPC models suggests a poor dynamic performance for PLL bandwidth of 25 Hz as the CIG increasingly replaces the synchronous generators associated with the power system.

In the case of DPC-based models, the effect on the eigenvalues related to M1_{DPC} is depicted in Figure 4.9b. For the range of the system inertia H_{sys}, the mode M1_{DPC} always remains well damped, taking a minimum damping ratio of 71%. Thus, the modal analysis of the system modeled by DPC reveals that the small-signal stability is retained regardless of the PLL bandwidths and system inertia H_{sys}.

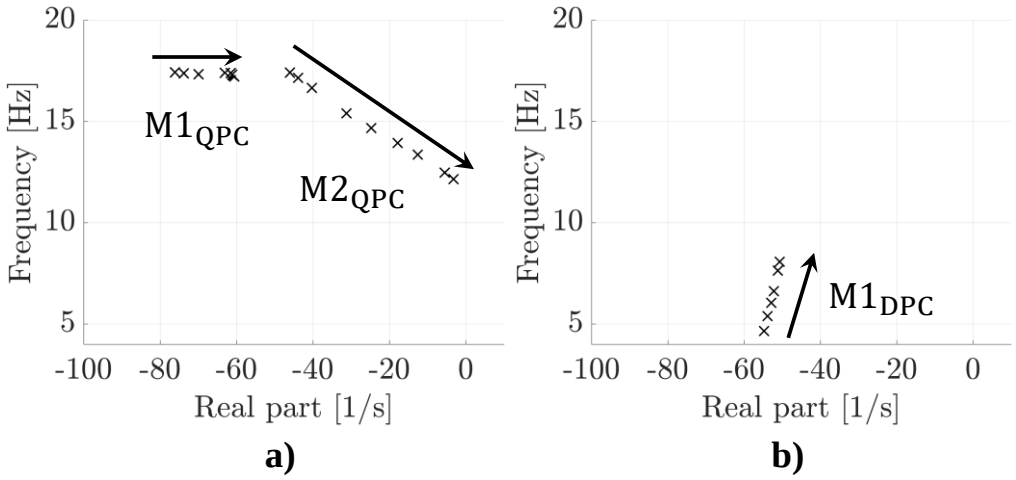

Figure 4.9. Eigenvalue loci of the control modes for power system inertia constant between 3.5 s and 1.16 s; a) QPC-based model, b) DPC-based model

In Figure 4.10, the H-infinity norm $\|\boldsymbol{G}\|_\infty$ for various system inertias are displayed. It can be seen that for 70% of CIG penetration levels and the inertia constants ranging from 3.5 s to 1.52 s, the QPC-based model is small signal stable, even if the PLL bandwidth is 25 Hz. In such range, the $\|\boldsymbol{G}\|_\infty$ of both models is similar. Therefore, transient simulations using QPC should give acceptable results. On the other hand, Figure 4.10 reveals a significant variation in the $\|\boldsymbol{G}\|_\infty$ between both models when the system has system inertia H_{sys} lower than 1.16 s. This is consistent with the first sensitivity analysis, where the QPC-based models become significantly inaccurate when the generator G3 is disconnected, leading to a reduction of system inertia from 1.66 s to 1.33 s, as shown in Table 4.2. This fact can be seen in Figure 4.7.

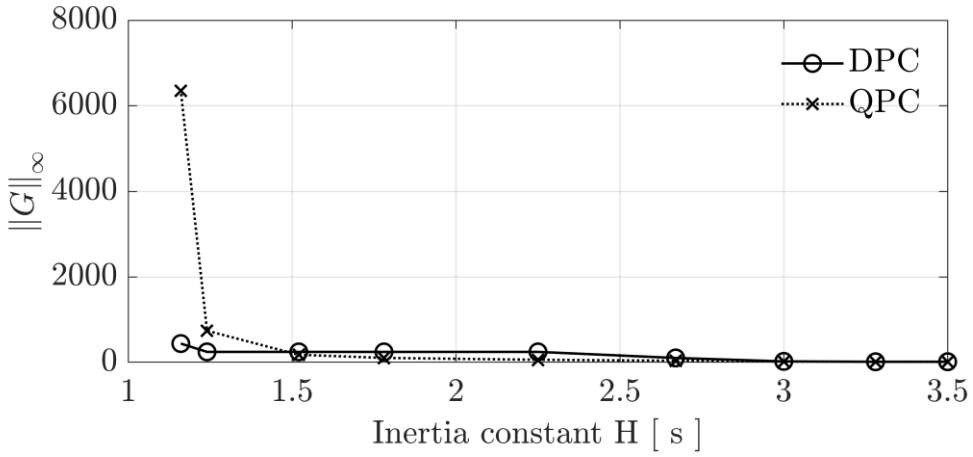

Figure 4.10. $\|\boldsymbol{G}\|_\infty$ as a function of inertia constant for 70% of the CIG penetration level

4.3.4 Validation Through Time Domain Simulation

The results are now verified by time-domain simulations using DPC, QPC, and EMT models. For EMT simulations, PSCAD is used as a well-known software for these analyses. At a time instant of 1 s, a step decrease of 5% of the active power reference for the generator connected at bus B1 is

considered. Firstly, the CIG penetration levels considered are 0%, 35%, 70%, and 100%. In the cases of 35%, 70%, and 100% of CIG levels, the simulations are performed for PLL bandwidths of 2 Hz, 5 Hz, 20 Hz, and 25 Hz. Secondly, for 70% of CIG level, the simulations are carried out for system inertia H_{sys} of 3.5 s, 1.16 s, and 1.13 s with a PLL bandwidth of 25 Hz.

Figure 4.11 shows the simulated voltage at bus B1 considering 0% of CIG level. From this figure, it can be seen that both modeling techniques give similar results. Therefore, the assumptions made in QPC are suitable for stability analysis when synchronous generators dominate the power system.

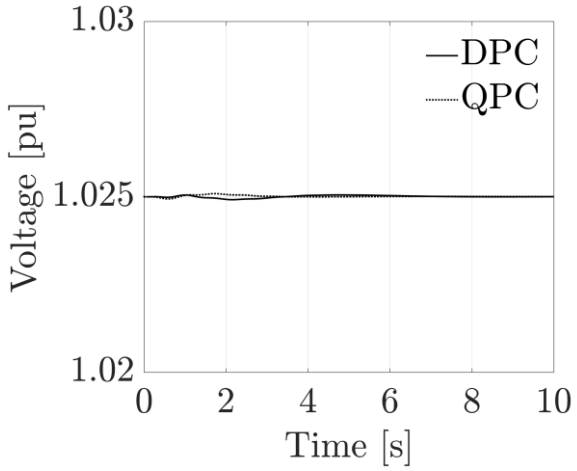

Figure 4.11. Voltage at bus B1 for a 0% of CIG level

Figure 4.12, Figure 4.13, and Figure 4.14 show the evolution of the voltage at bus B1 for 35%, 70%, and 100% of CIG level, respectively. Based on these figures, when the PLL has a slow response at 2 Hz or 5 Hz bandwidths, both the QPC and the DPC models lead to similar dynamic behavior regardless of the CIG levels. This was expected since the $\|\boldsymbol{G}\|_\infty$ of both models does not differ significantly in these cases, as shown in Figure 4.7. However, as the PLL bandwidth increases to values above 20 Hz and the CIG levels increase to values above 35%, the error obtained by the QPC-based model becomes significant. This can be seen in Figure 4.13c and Figure 4.14c. In these figures, when a PLL bandwidth of 20 Hz is used, the oscillations of the voltage are considerably less damped. These oscillations become more pronounced as the CIG levels increase.

Furthermore, as shown in Figure 4.13d and Figure 4.14d, the system based on QPC becomes unstable for a PLL bandwidth of 25 Hz. Both modeling approaches show similar dynamic behavior for CIG levels below 35% and PLL bandwidths of 20 Hz and 25 Hz, as shown in Figure 4.12c and Figure 4.12d. These observations are consistent with the eigenvalue loci depicted in Figure 4.6a.

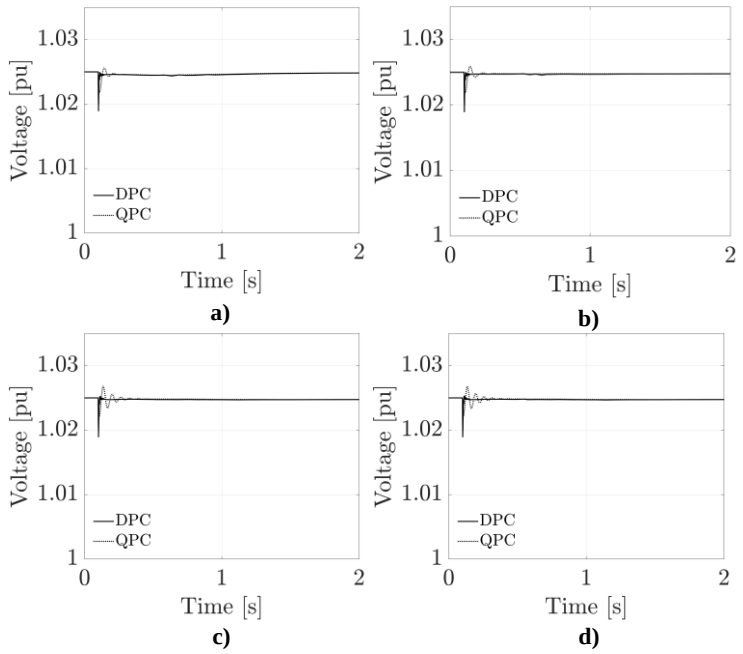

Figure 4.12. Terminal voltage at bus B1 for 35% of CIG; a) 2 Hz, b) 5 Hz, c) 20 Hz, d) 25 Hz

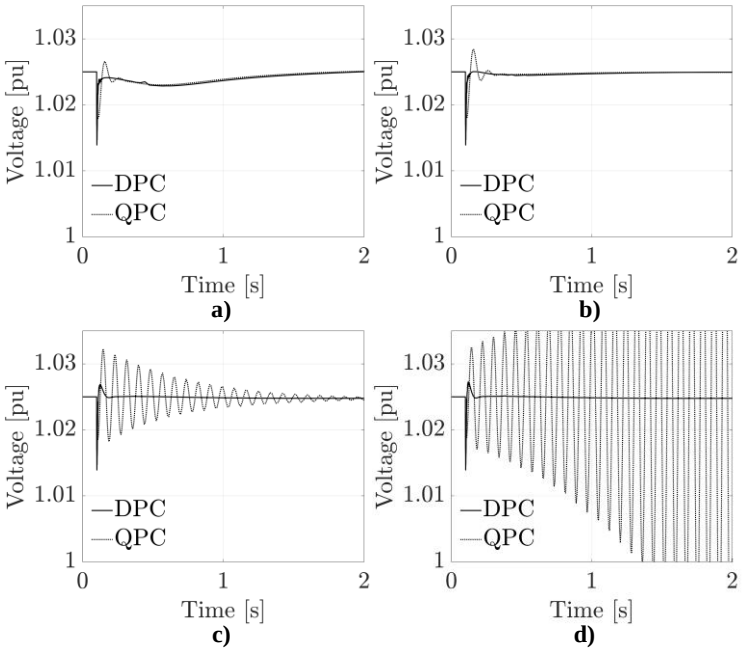

Figure 4.13. Terminal voltage at bus B1 for 70% of CIG; a) 2 Hz, b) 5 Hz, c) 20 Hz, d) 25 Hz

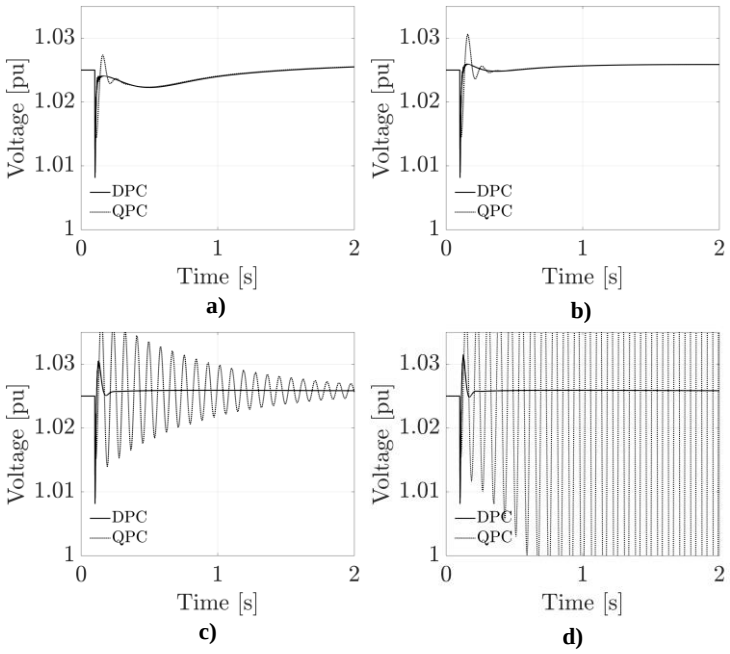

Figure 4.14. Terminal voltage at bus B1 for 100% of CIG; a) 2 Hz, b) 5 Hz, c) 20 Hz, d) 25 Hz

In the case of simulations for different system inertia H_{sys}, Figure 4.15 shows the evolution of the voltage at bus B1 considering both DPC- and QPC-based models. A CIG level of 70% and a PLL bandwidth of 25 Hz are considered. According to Figure 4.15a, when the system inertia H_{sys} is 3.5 s, both modeling approaches lead to similar dynamic behavior. This was expected since the $\|\boldsymbol{G}\|_{\infty}$ of both models does not differ significantly in these cases, as shown in Figure 4.10. Figure 4.8 indicates that, in this case, generators G1 and G3 are connected to the power systems. Therefore, the dynamics of the synchronous generators determine the dynamic response of the system. This means that QPC-based models give similar dynamic behavior than DPC-based models. On the other hand, this operating condition implies a high spinning reserve, causing an increase in the operating costs related to the power system. This operating condition is helpful to study the effect on the validity range of QPC-based models when the system inertia H_{sys} is reduced, but it does not appear as a condition expected in power systems as CIG levels grow. In these cases, it is expected that the system inertia H_{sys} decreases because the generation based on CIG replaces the generation based on synchronous generators.

According to Figure 4.15b and Figure 4.15c, as the system inertia H_{sys} decreases and takes values below 1.16 s, the error obtained by the QPC-based model becomes significant. In Figure 4.15b, when the system inertia H_{sys} Taking a value of 1.16 s, the oscillation of the voltage is considerably less damped. Figure 4.15c shows that the system becomes unstable for the system inertia of $H_{\text{sys}} = 1.13$ s. This result is consistent with the $\|\boldsymbol{G}\|_{\infty}$differing considerably for such range of system inertia H_{sys} as can be seen in Figure 4.10.

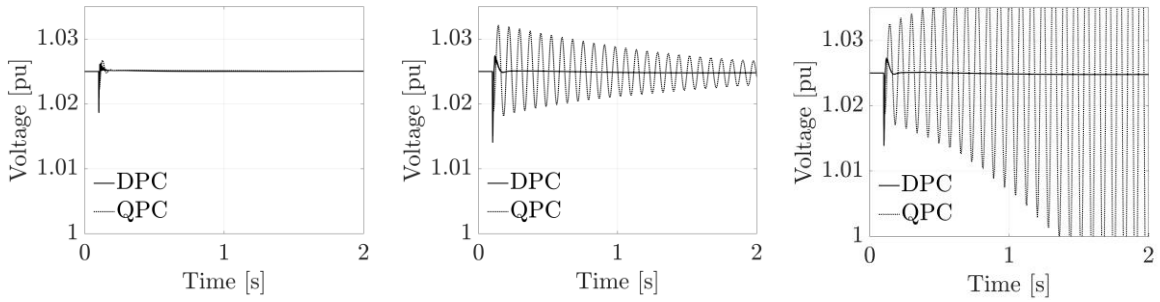

Figure 4.15. Terminal voltage at bus B1 for 70% of CIG and 25 Hz of PLL bandwidth; a) 3.5 s, b) 1.16 s, c) 1.13 s

Furthermore, Figure 4.16 shows the voltage simulated at B1 using DPC and EMT approaches for a PLL bandwidth of 25 Hz and a CIG level of 100%. At this PLL bandwidth, the simulations of DPC and QPC differ significantly (see Figure 4.13.d). If DPC- and EMT simulations give similar results, then DPC appropriately represents the transient behavior and stability of the power system under study. It is seen that DPC-based simulation gives a precise envelope of the three-phase voltages obtained using EMT models in PSCAD. For better visualization, the three-phase signal obtained from EMT is transformed into a dynamic phasor, and its magnitude is calculated based on equation (2.9). This magnitude is compared with DPC, and the results are shown in Figure 4.17. It is verified that the DPC model can track the envelope of the real three-phase signals with the difference related to the high frequency transients.

Figure 4.18 depicts the active power injected into bus B1 for PLL bandwidths of 2 Hz, 5 Hz, 20 Hz, and 25 Hz. The high-frequency transients in the active power can be seen as a result of the PWM control. The results obtained from DPC-based models match very closely those obtained from EMT simulations using PSCAD. There are no significant differences, regardless of the PLL bandwidth used in these cases. This was expected since the H-infinity norms $\|\boldsymbol{G}\|_\infty$ of DPC models shown in Fig.10b are similar to those PLL bandwidths.

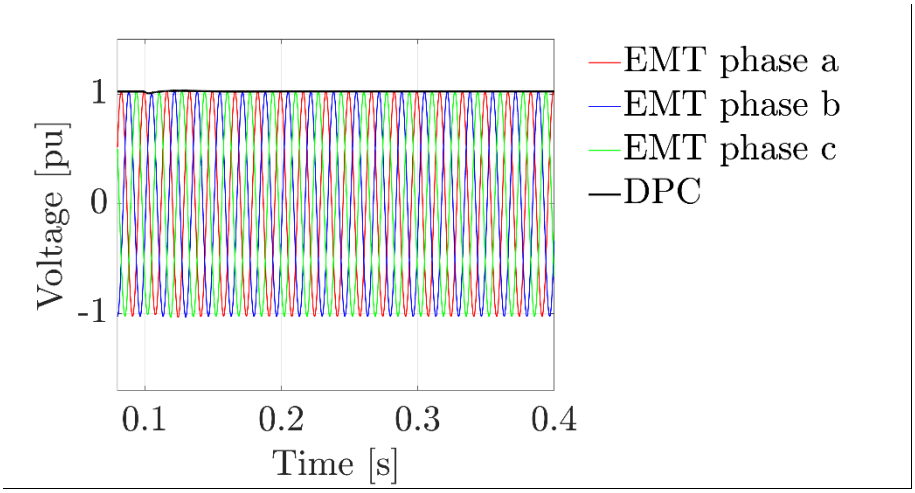

Figure 4.16. Terminal voltage at bus B1 for 100% of CIG and PLL bandwidth of 25 Hz

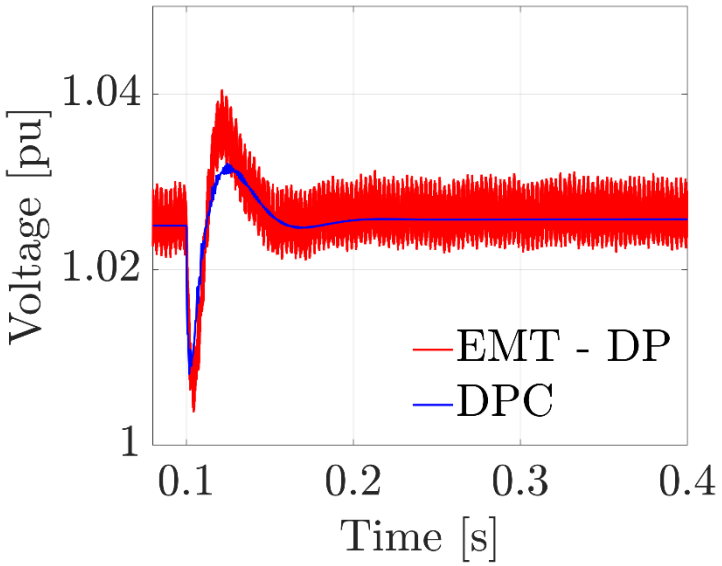

Figure 4.17. Terminal voltage at bus B1 for 100% of CIG and PLL bandwidth of 25 Hz

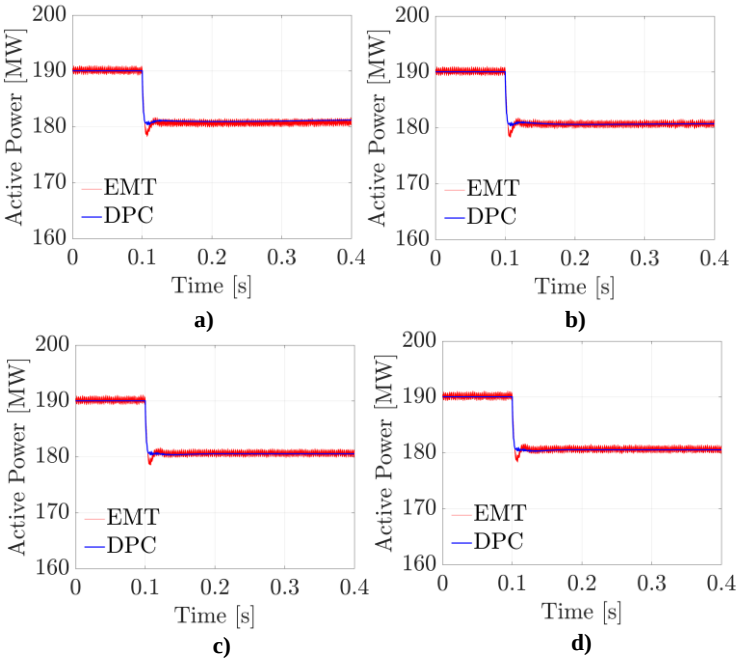

Figure 4.18. Active power injected at bus B1 for 100% of CIG; a) 2 Hz, b) 5 Hz, c) 20 Hz, d) 25 Hz

The time domain simulations confirm and validate the assessments of Stages 2, 3 and 4 of Figure 3.1. The fast response of the CIG control systems leads to a decrease in the accuracy of QPC models in time domain simulation. This in turn makes the use of QPC unsuitable for generic stability

assessment of power systems with increasing and significant CIG levels.

4.4 Summary of Main Findings

Table 4.4 summarizes some of the main findings obtained from this analysis so far. In general, it was observed that QPC models should not be used for transients with a frequency range above 5 Hz. DPC models in turn have been shown to be practical for simulating higher frequencies, even in power systems with very high CIG penetration levels.

Table 4.4. Summary of main findings

Findings	QPC	DPC
Frequency bandwidth of transients wherein the modeling technique is suitable to simulate AC grids	≤ 5 Hz	> 0 Hz
Capability for modeling slow electromechanical transients	High	High
Capability for modeling both electromagnetic and electromechanical transients	-	High
Accuracy in the representation of fast control systems of CIG	Low	High
Accuracy in transient simulations of systems with high CIG penetration levels	Low	High

5 Comparative Analysis of CIG Models Based on QPC

This chapter compares CIG models based on QPC shown in Table 2.4, with the reference model based on DPC. Section 5.1 and Section 5.2 describe the power system used to perform the studies and the model details of the software used. In Section 5.3, the results and analysis are presented. For better readability, some details shown in chapter 4 are repeated here.

5.1 Description of Power System Under Study

In this section, the system selected for the comparison is described. CIG models are compared in the IEEE 9-bus network shown in Figure 5.1 [247]. The system is modified to consider a diverse set of penetration levels of CIG. This is included in Figure 5.1 as a set of switches. The main characteristics of these generators are summarized in Table 5.1. The system has three synchronous generators at 60 Hz, two with steam turbines, G2 and G3, and one with a hydraulic turbine, G1. The total system load is 315 MW with 0.94 lagging power factor and system parameters as given in [247]. The load is equivalent to 56% of the total rated generation capacity of the system.

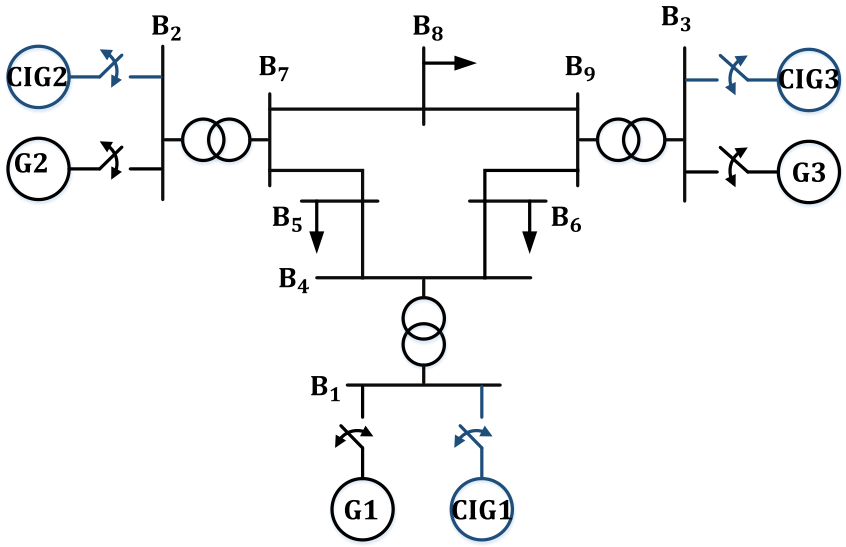

Figure 5.1. IEEE-9 bus system with switches to adapt the generation portfolio [247]

Table 5.1. Main characteristics of synchronous generators

Properties	G1	G2	G3
Type	Hydro	Steam	Steam
Rated power [MVA]	247.5	192	128
Inertia constant [s]	11.82	3.2	1.505
Rated voltage [kV]	16.5	18	13.8

In order to compare the DPC models and the CIG models based on the QPC approach, two CIG units are added at buses B1 and B3. The capacities of CIG1 and CIG3 are the same as those of the synchronous generators G1 and G3, respectively. A case of 100% CIG is also performed. The generator G2 is replaced by the CIG2 operating in GFM mode with the droop control described in

Section 2.6.3, Figure 2.7. According to [137], [139], [186], [187], the droop control is mathematically equivalent to the synchronous virtual machine. With a proper selection of parameters, the dynamic behavior is similar. The parameters of the droop control of the CIG-GFM are selected as the equivalent inertia constant H is similar to G2. For this reason, for 100% of CIG in Table 4.2 the system inertia H_{sys} is different from zero. The capacity of CIG2 is equal to the generator G2.

The dispatch considering the main penetration levels of CIG is summarized in Table 4.2. When Table 4.2 indicates that the dispatch is zero, the generator is not connected to the system. This table also includes the system inertia H_{sys}, defined in equation (4.1). The generator connected at bus B2 is considered the slack bus for all the operating conditions. Penetration levels are calculated as a function of the total active power demand of the test system. It should be noted that the above assumptions are similar to those shown in Chapter 4.

Table 5.2. Dispatch and system inertia H_{sys} for different generator portfolios

CIG Levels [%]	**G1 [MW]**	**G2 [MW]**	**G3 [MW]**	**CIG1 [MW]**	**CIG2 [MW]**	**CIG3 [MW]**	H_{sys} **[s]**
0	163	77	80	0	0	0	5.82
35	0	91	120	55	0	55	1.66
50	0	162	0	79	0	79	1.13
70	0	98	0	110	0	110	1.13
100	0	0	0	189	4	126	1.13*[2]

5.2 Implemented Models and Software Used

For the synchronous generators with steam turbines, the synchronous generators with hydraulic and voltage regulators are the same as those used in the DPC and QPC-based models of Chapter 4. These models are shown in Table 3.1. Synchronous generators are equipped with a DC1A IEEE-type voltage regulator [236]. The steam turbine governor is of type IEEE TGOV1, while the hydraulic turbine is IEEE HYGOV [237].

In the case of the system represented using DPC, the CIG1 and CIG3 units operate in GFL mode. The control structures used are those described in the methodology in Section 3.3.1. These are active power control, voltage control, inner current control with VFF terms, and PLL. The parameters of the current control loop are chosen to obtain a settling time of 20 ms, which is a typical value used in simulations with power converters [35], [248]. The PLL control system has a bandwidth of 20 Hz [170]. All implemented controllers are based on a PI controller because it is the most common control structure used for stability assessment [15], [35], [58], [158].

It should be noted that the above controllers are slightly different from those applied in the previous chapter, as is described in 3.3.1. In this case, a PI controller is used for active power, and the VFF is considered in the inner control loops of CIG-GFL for DPC models. The main parameters of the CIG operating in GFL are shown in Table 5.3. These parameters are chosen according to various research works and actual CIG units [15], [16], [74], [158], [244], [251]. In the case of CIG

[2] Equivalent synthetic inertia related to CIG2 operating in GFM

operating in GFM, their model and parameters are shown in Appendix B because this thesis does not focus on this operating mode.

In the case of the system modeled using QPC, the outer control loops are equal to those used in DPC models. The representation of each CIG model varies according to the assumption made in the model. The parameter used for each CIG model and the set of differential equations related to the DPC models and the CIG models using QPC is shown in Appendix B.

Table 5.3. Control system parameters of CIG-GFL units

Properties	Value
Proportional gain of the current controller k_{p}	0.40
Integral gain of the current controller k_{i}	90
The time constant $\tau_{v_{\mathrm{tdq}}}$ of VFF term	0.001
Proportional gain of PLL controller k_{pPLL}	101
Integral gain of PLL controller k_{iPLL}	2562
Time constant of voltage measure T_{r} $[s]$	0.05
Proportional gain of voltage controller k_{pV}	5.00
Integral gain of voltage controller k_{iV}	25
Proportional gain of the active power controller k_{pP}	0.4
Integral gain of the active power controller k_{iP}	40
Time constant of active power measure T_{rP}	0.05

The test system using DPC and QPC with all the CIG models of Table 2.4 was implemented in MATLAB/Simulink. The system was linearized using the MATLAB/Simulink linear analysis tool [249]. This tool makes use of numerical linearization.

5.3 Results of Comparative Analysis of CIG Models Based on QPC

This section presents the main results obtained by applying the methodology described in Section 3.2. Only the main results and key findings are presented for better readability. A detailed description of the modal analysis, the participation factor analysis, the plots of the H-infinity norm $\|\boldsymbol{G}\|_{\infty}$ related to Stage 2, and the validation by time-domain simulations related to Stage 4 can be found in Appendix D. Given the above, this section starts from stage 3 of the methodology shown in Figure 3.3. The results are described from Case Study 1 to Case Study 3.

5.3.1 Case Study 1: Impacts of PLL and CIG Levels

In order to perform the sensitivity analysis of this case study, the PLL bandwidths and the CIG levels are varied. The PLL bandwidth changes in CIG1 and CIG3 from 2 Hz to 80 Hz. These bandwidths are typical values used in the literature to study the impact of PLL on the stability and dynamic performance of CIG power plants [15], [16], [75], [251]. The PLL estimated the angle used to transform abc signals to *dq* signals, and a fast response is desired for better dynamic performance. Unbalance and harmonics can create errors in estimating the angle and frequency at the PCC, deteriorating the performance [252]. These facts impose practical limitations on selecting the PLL bandwidth. Therefore, it is unlikely that PLL bandwidths higher than 100 Hz would be implemented in real CIG plants [15], [16], [252]. However, any values that belong to the reported range of PLL bandwidths could be implemented in actual CIG power plants. The CIG levels increase to 100%.

Illustrative plots are developed to show and summarize the results and identify the main findings. Figure 5.2 compares the CIG models based on QPC and the DPC-based model. The PLL bandwidths of 2 Hz, 20 Hz, and 50 Hz are sufficient to identify the key findings of this case study because similar observations can be made for other PLL bandwidths. In this figure, green boxes indicate that the system is small signal stable when that specific model is used. On the other hand, boxes in orange mean that the system is unstable when that specific model is used.

Figure 5.2 shows that the CIG models based on QPC represent the dynamic response with sufficient accuracy for low PLL bandwidths independently of the CIG levels. The QPC models give similar results for PLL bandwidths of 20 Hz and 50 Hz but CIG levels lower than 35%. As the PLL bandwidths increase (faster dynamic response), only the VS-Type II and DPC models show that the system is unstable for CIG levels higher than 35%. However, this result does not mean that VS-Type II is a suitable model for CIG. VS-Type II predicts the stability of the system, but not the root cause (See Appendix D.1.1 for a detailed analysis). Therefore, as the PLL bandwidths and CIG levels increase, all the CIG models based on QPC do not represent the system's dynamic response with sufficient accuracy, and then wrong conclusions may be drawn regarding system stability.

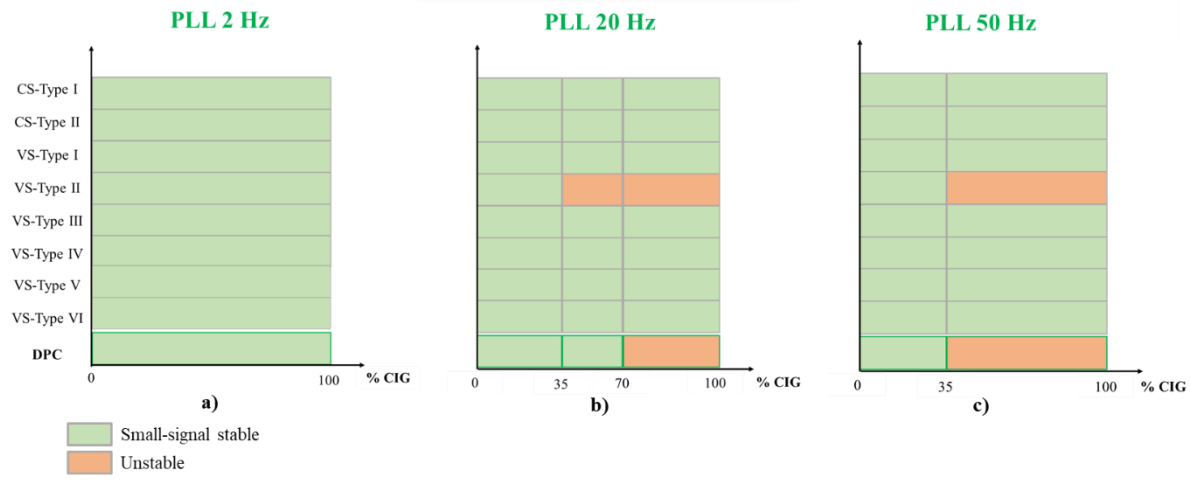

Figure 5.2. Comparative of CIG models for CIG levels ranging from 0% to 100% and PLL bandwidths of 2 Hz, 20 Hz, and 50 Hz; a) 2 Hz, b) 20 Hz, c) 50 Hz

5.3.2 Case Study 2: Impacts of SCR Levels

This study analyses the effects of SCR levels on the suitability of CIG models based on QPC by considering a CIG level of 50% and PLL bandwidths of 2 Hz, 20 Hz, and 50 Hz. SCR is defined by [39]:

$$\mathrm{SCR} = \frac{S_{\mathrm{SCMVA}}}{P_{\mathrm{RMW}}} \tag{5.1}$$

Where S_{SCMVA} is the short–circuit MVA capacity at the bus in the existing network before connecting a CIG unit and P_{RMW} is the rated active power in MW of the new CIG unit. The value of the SCR levels depends on the synchronous generators connected to the systems. In the test system, the SCR is modified by changing the inductive reactance x_{14} from 0.05 to 1 in [pu] on a base of 100 [MVA]. This reactance is related to the transformer between bus B1 and B4 (see Figure 5.1). For a CIG level of 50%, the SCR at bus B1 ranges from 1.2-0.4 [pu] because only the

synchronous generator G2 is connected. Other CIG levels are also studied, but those results are not shown here because the key findings are the same for 50% of the CIG level.

Figure 5.3 shows the comparison among the CIG models. A decrease in the PLL bandwidth extends the accuracy of the CIG based on QPC, as shown in Figure 5.3.a. There is an area where all the QPC models are small-signal stable. However, there is a point where all the models cannot predict system stability. As in the previous case, the model VS-Type II is unsuitable because system instability differs from DPC. When the PLL bandwidths become faster, the area where all QPC models are suitable decreases significantly, as Figure 5.3.b and Figure 5.3.c depict.

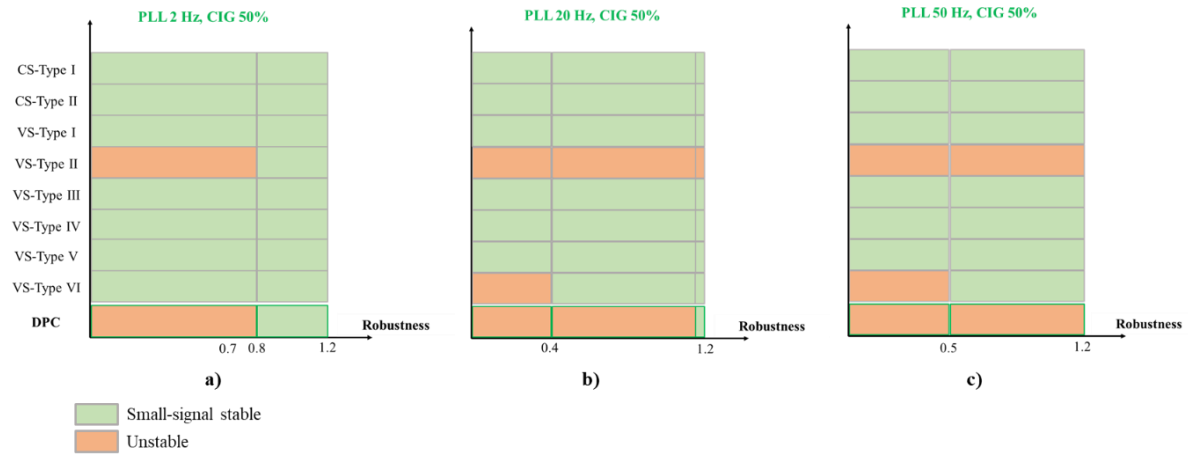

Figure 5.3. Comparative of CIG models for SCR ranging from 0.4 to 1.2, CIG level of 50%, and PLL bandwidths of 2 Hz, 20 Hz, and 50 Hz; a) 2 Hz, b) 20 Hz, c) 50 Hz

Furthermore, VS-Type VI reveals that the system is unstable in these cases. However, as VS-Type II, the cause of instability differs from DPC. Consequently, for low SCR values and fast dynamic response of PLL, all CIG models based on QPC are unsuitable for system stability.

5.3.3 Case Study 3: Impacts of Inner Control Loops

To analyze the impacts of inner control loops, a sensitivity analysis is performed by varying the integral gain k_{i} associated with the current controller and the time constant $\tau_{v\mathrm{dq}}$ associated with the VFF terms for a PLL of 2 Hz, 20 Hz, 50 Hz, and CIG 50%. The control parameters are changed in CIG1 and CIG3. The integral gain k_i of the current controller range from 70 to 200, and the time constant $\tau_{v\mathrm{dq}}$ associated with the VFF take values of 0.01, 0.001, and 0.0001. According to Table 5.3, in previous cases $\tau_{v\mathrm{dq}} = 0.001$ and $k_i = 90$. The selected values are generic and typical [74], [75], [180], [181], [244]–[246]. These parameters are selected to perform sensitivity analysis because the study of participation factors reveals a considerable impact on the accuracy of QPC-based models. This fact is described in detail in Appendix D.1. Additionally, the representation of the inner current control differs from the CIG models in Table 2.4. Thus, the analyses presented in this section allow identifying the effect of fast dynamic response related to inner control loops on the accuracy of CIG models based on QPC.

In Figure 5.4, Figure 5.5, and Figure 5.6, the comparison among the CIG models is shown for PLL bandwidths of 2 Hz, 20 Hz, and 50 Hz, respectively. For a PLL bandwidth of 2 Hz, it can be seen in Figure 5.4.a that all the QPC models work adequately as the time constant $\tau_{v_{\mathrm{tdq}}}$ decreases. This

is independent of the values taken by the integral constant k_{i}. When the time constant $\tau_{v_{\mathrm{tdq}}}$ becomes higher, which means a slower response, there is a region where all QPC models become unsuitable because is non-representative of DPC, as shown in Figure 5.4.b and Figure 5.4.c. As the PLL bandwidths increase, the region extends to all the selected values of integral gain k_{i}. VS-Type II is still not suitable as in previous cases.

Given the above, it is observed that for high levels of CIG, the dynamic response of the inner current control has a significant impact on the suitability of using QPC to represent CIG units. In this sense, the fast dynamic response of the CIG and the network becomes relevant for stability studies. Therefore, the inner current control and PLL should be modeled when high levels of CIG are considered. These cannot be adequately represented by QPC models.

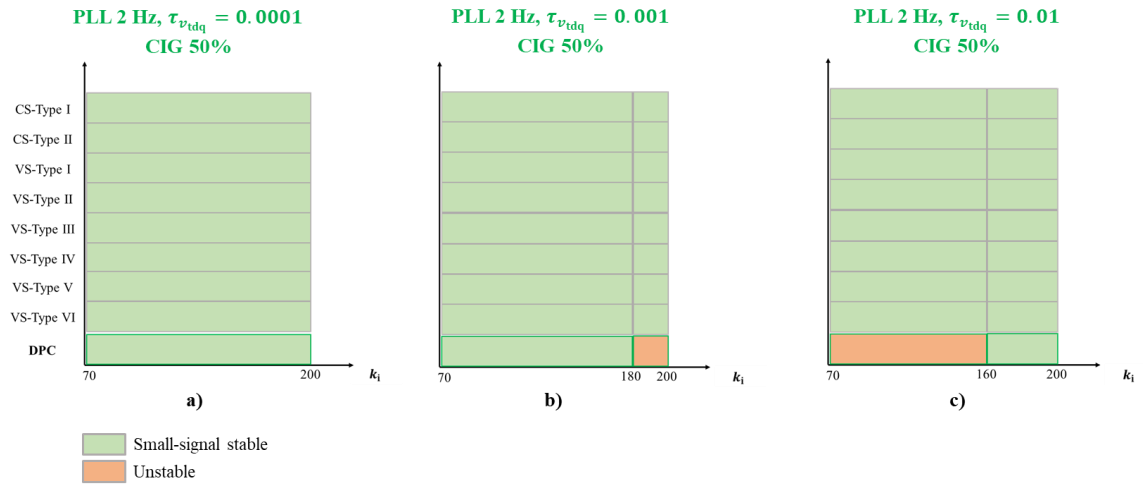

Figure 5.4. Comparative of CIG models for CIG level of 50%, integral gain k_{i} ranging 70 to 200, PLL bandwidth of 2 Hz, and VFF terms $\tau_{v_{\mathrm{tdq}}}$ of 0.0001, 0.001, and 0.01; a) $\tau_{v_{\mathrm{tdq}}} = 0.0001$, b) $\tau_{v_{\mathrm{tdq}}} = 0.001$, c) $\tau_{v_{\mathrm{tdq}}} = 0.01$

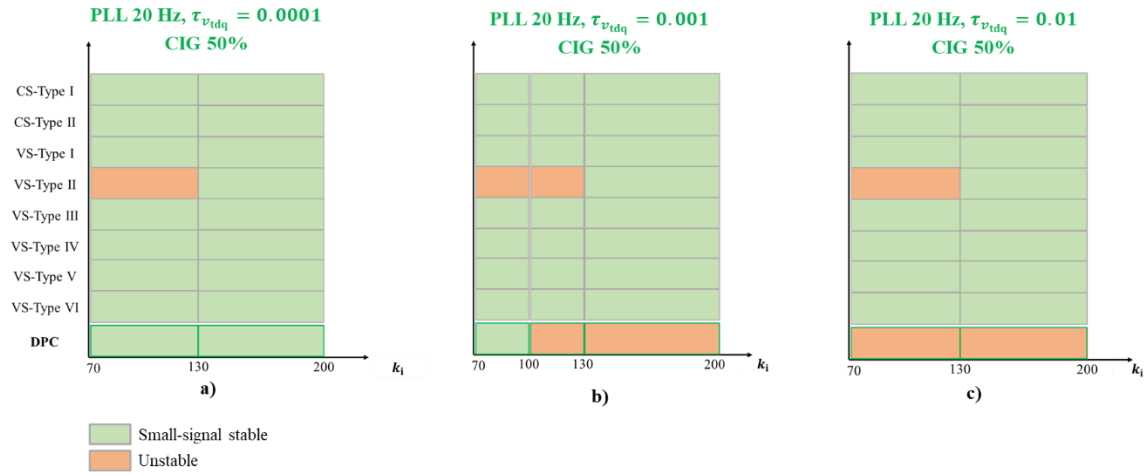

Figure 5.5. Comparative of CIG models for CIG level of 50%, integral gain k_{i} ranging 70 to 200, PLL bandwidth of 20 Hz, and VFF terms $\tau_{v_{\mathrm{tdq}}}$ of 0.0001, 0.001, and 0.01; a) $\tau_{v_{\mathrm{tdq}}} = 0.0001$, b) $\tau_{v_{\mathrm{tdq}}} = 0.001$, c) $\tau_{v_{\mathrm{tdq}}} = 0.01$

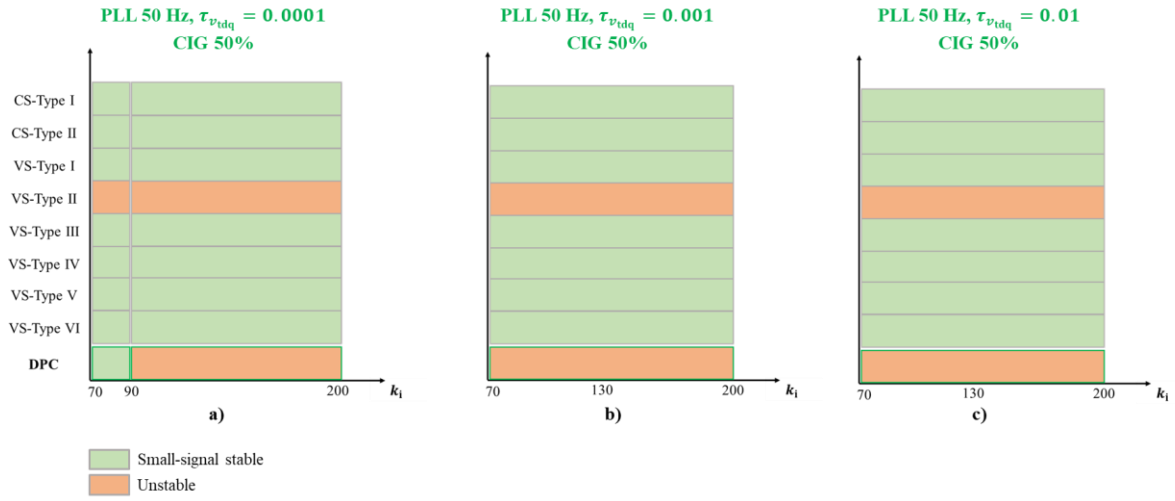

Figure 5.6. Comparative of CIG models for CIG level of 50%, integral gain k_i ranging 70 to 200, PLL bandwidth of 50 Hz, and VFF terms $\tau_{v_{tdq}}$ of 0.0001, 0.001, and 0.01; a) $\tau_{v_{tdq}} = 0.0001$, b) $\tau_{v_{tdq}} = 0.001$, c) $\tau_{v_{tdq}} = 0.01$

5.4 Summary of Main Findings

This chapter compared CIG models based on QPC typically used for power system stability studies. The objective is to identify and investigate the impact of the fast dynamic of CIG on the accuracy of QPC-based models for high penetration levels of CIG. In particular, the impacts of current control, PLL, and AC filter were thoroughly studied. Thus, the appropriate level of detail required to model CIG is found. This section summarizes the main observations obtained from the results.

The results obtained in this chapter show that two types of errors can be made when CIG models based on QPC are used. The system is small-signal stable when it is unstable and vice versa. Both cases are undesirable in the context of stability assessments. In the first case, the system could be at risk due to undetected hazardous operating conditions. On the other hand, a power system could operate inefficiently in the second case, as more restrictive than necessary conditions may prevent the system from exploiting the full flexibility of its infrastructure.

Figure 5.7 summarizes the key findings of the comparative analysis related to Case Studies 1 and 2. These studies are considered sufficient to summarize the main findings of this chapter. In Figure 5.7, letters A, B, and C mean that the CIG models based on QPC are suitable (small-signal stable), only the VS-Type II is unsuitable (the rest of the models are small signal-stable), and all the CIG models based on QPC are unsuitable, respectively. The color boxes indicate the range of k_i and $\tau_{v_{tdq}}$ where A, B, and C occur.

The CIG models based on QPC give a similar dynamic behavior to DPC models when DPC models are small-signal stable. The fast dynamics are irrelevant for those cases, and there is no significant difference among the models used. The outer control loops dominate the dynamic behavior of the power system. On the other hand, when the DPC model is unstable, all CIG models based on QPC give erroneous results. VS-Type II predicts the instability of the system due to the high penetration of CIG and PLL with high bandwidths (see Figure 5.2). However, the dynamic interactions differ from the DPC model. The oscillation frequency and participation factors vary significantly

compared to DPC. Therefore, VS-Type II also gives erroneous results, making it unsuitable. A detailed description of this fact is given in Appendix D.1.2 and D.1.3.

Furthermore, despite the PLL, under low values of SCR, the current control with decoupling terms and VFF also affects the suitability of QPC models. Figure 5.7 shows that the validity range of QPC-based models is highly dependent on CIG levels, PLL bandwidths, and tuning of the current controller. The dynamic interactions between these control systems and the electric network must be adequately represented to assess system stability.

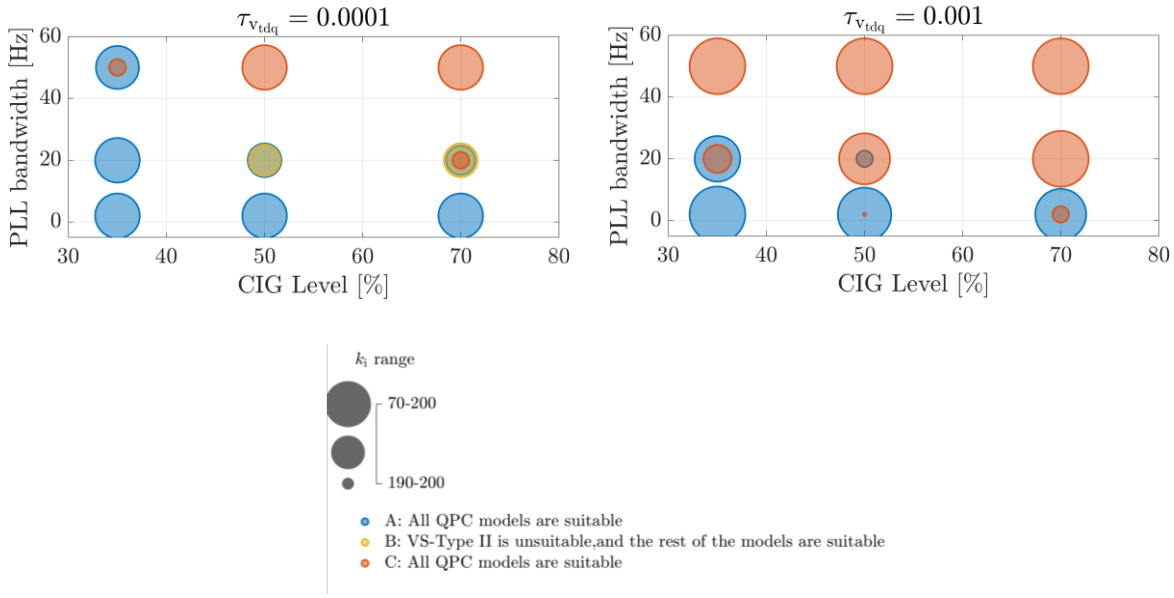

Figure 5.7. Summary of key findings

In the results described in this chapter, the models based on the current-controlled representation seem suitable for simulating slow transients. However, according to the literature review, it is not an appropriate model because numerical stability issues can impede simulating a power system's transient response. Consequently, CIG models based on a voltage-controlled source representation are preferable when using QPC.

As final remarks, the DPC-based models seem to be a suitable option to represent power systems with high levels of CIG. These models are suitable for generic stability studies and more efficient simulations using EMT models.

6 Conclusions

This thesis thoroughly investigates the validity range of traditional stability assessments based on QPC and the proper level of detail required to model CIG in power systems with high penetration levels of renewables connected by power electronics. Comparative analyses between QPC and DPC were performed considering a wide range of CIG levels (including 100%) and various operating conditions. Furthermore, a review of the most common CIG models used in stability studies based on QPC was carried out to investigate the impact of the fast dynamics associated with the control systems of CIG on the stability of power systems. These models are implemented and compared to a benchmark model based on DPC. The analyses performed offer new information and foster the understanding of power system modeling for stability assessments in case of high shares of CIG.

In Chapter 3.2, a novel methodology for a systematic analysis of the underlying modeling framework was developed to achieve the objectives of this thesis. Based on the results obtained in Chapter 4, the accuracy of QPC decreases in cases of high levels of CIG. In these cases, the bandwidth of the relevant transients for stability is extended to cover both slow electromagnetic and electromechanical transients, with oscillation frequencies higher than $f_* \approx 5$ Hz. Therefore, the relevant oscillation frequencies for stability studies move outside the range of 0.1 Hz to 5 Hz, which has traditionally been a relevant bandwidth for stability analysis of systems dominated by synchronous generators. The electromagnetic phenomena related to the network and fast response devices cannot be neglected because fast transients with oscillation frequencies higher than 5 Hz become relevant for stability analysis. Furthermore, control loops such as those for the PLL impact the system so that electromagnetic transients on the grid side cannot be ignored. Models based on DPC can accurately represent such transients and are suitable for assessing stability in the presence of CIG.

Considering the results of the comparative study between CIG models based on QPC presented in Chapter 5, the CIG may cause stability issues due to undamped modes with oscillation frequencies higher than 5 Hz. CIG models based on QPC decrease their accuracy for high levels of CIG and low levels of SCR. The fast dynamic response of PLL, inner control loops, and the electric network also considerably impact the accuracy of QPC. For conditions where DPC models were small-signal stable, models based on voltage source representation are recommended because these models have better numerical stability characteristics than those based on current source representation. Under these conditions, it is observed that the dynamic response is similar to that of DPC. On the other hand, depending on the dynamic response of PLL and inner control loops, all the representations of CIG using QPC differ from DPC in the behavior of power system transients. Therefore, the fast and slow control systems of CIG-GFL and the transmission network should be adequately represented for power system stability studies to determine stability boundaries. Otherwise, erroneous conclusions may be drawn, making power systems prone to loss of stability, or operating in inefficient conditions.

Finally, DPC models accurately represent the relevant transients for stability assessments of power systems dominated by CIG. This technique can simulate both electromechanical and electromagnetic transients of AC systems using less computational burden than transient simulations based on EMT models. In addition, it is more accurate than QPC. These features of DPC models make it a promising technique for studying power system dynamics. Given the strong interest in advancing wind and solar energy worldwide, modeling power systems based on DPC is

recommended.

6.1 Future Work

Some interesting topics to extend and add to the work of this thesis are described as follows:

- To apply DPC to study the stability of large power systems. DPC has some applications in modeling distribution systems [31], [253]. However, despite the advantages of DPC, there is a lack of its application in large and real power systems. According to [10], one of the main reasons is that no commercial software can perform transient simulations using DPC, which hinders its application. With small power systems, it is possible to study the accuracy of DPC simulations, the computational burden, and the applicability of DPC for stability studies, as has been shown throughout this thesis. However, to demonstrate how promising this technique is for stability studies, its application in actual and large grid networks is necessary. Power system planners, TSOs, and power system engineers need to rely on the results obtained from DPC simulations for use in their stability studies. DPC models could bridge the compromise between EMT and QPC in terms of accuracy and computational burden, at least in the context of power system stability.
- To propose a methodology to study the stability of the power system using DPC and heterogenous control parameters of CIG-GFL. The analysis performed in this thesis considers the same control parameters in all CIG-GFL. This is not the case in current power systems. This future work assumes that QPC models can not be used.
- To analyze the effects of fast dynamics on power systems stability with 100% of CIG-GFM, i.e., transmission network transients, inner voltage, and current control loops. This also includes the effects from a modeling perspective.
- To investigate the limitation of QPC-based models where the frequency control is implemented in CIG-GFL and CIG-GFM. In this work, frequency control was not considered in CIG-GFL, and the effects of frequency control in CIG-GFM were not analyzed because it is out of scope. New control dynamic interactions related to CIG, including frequency control, may add more limitations to QPC-based stability assessment models.
- To investigate if the limitation of QPC-based models shown in this work is affected by modeling the primary energy source used in CIG units, i.e., solar and wind energy.
- To investigate if proper tuning of CIG-GFL with frequency control may decrease the amount of CIG units with GFM capabilities needed for a secure operation. A few works [232], [233] are currently investigating this through transient simulations using mainly EMT models. The results show that operating a system with a high level of CIG-GFL with a proper control system implemented for supporting voltage and frequency is possible. This is especially relevant to define interconnection requirements [254]. Instead of requiring GFM capabilities with specific control structures, system operators might require FRT capabilities based on time response.

Bibliography

[1] P. Kundur *et al.*, "Definition and classification of power system stability," *IEEE Trans. Power Syst.*, vol. 19, no. 3, pp. 1387–1401, May 2004, doi: 10.1109/TPWRS.2004.825981.

[2] P. W. Sauer and M. A. Pai, *Power system dynamics and stability*. New Jersey, NJ, USA: Prentice-Hall, 1998.

[3] "Analytic research foundations for the next-generation electric grid." The National Academies Press, Washington DC, USA, 2016.

[4] P. Kundur, *Power system stability and control*. New York, NY, USA: McGraw-Hill, 1994. doi: 10.1016/S0022-3115(02)01404-6.

[5] M. Ilic and J. Zaborszky, *Dynamics and control of large electric power systems*. New York, NY: Wiley-IEEE Press, 2000.

[6] F. Milano, *Power system modelling and scripting*. London, UK: Springer, 2010.

[7] G. Gross, C. F. Imparato, and P. M. Look, "A tool for the comprehensive analysis of power system dynamic stability," *IEEE Trans. Power Appar. Syst.*, no. I, pp. 147–157, 1982, doi: 10.1080/00431672.1982.9932019.

[8] V. Jalili-Marandi, V. Dinavahi, K. Strunz, J. A. Martinez, and A. Ramirez, "Interfacing techniques for transient stability and electromagnetic transient programs," *IEEE Trans. Power Deliv.*, vol. 24, no. 4, pp. 2385–2395, 2009, doi: 10.1109/TPWRD.2008.2002889.

[9] V. Venkatasubramanian, "Tools for dynamic analysis of the general large power system using time-varying phasors," *Int. J. Electr. Power Energy Syst.*, vol. 16, no. 6, pp. 365–376, 1994, doi: 10.1016/0142-0615(94)90023-X.

[10] J. working group C4/C6.35/CIRED, "Modelling of inverter-based generation for power system dynamic studies." 2018.

[11] F. Milano, F. Dörfler, G. Hug, D. J. Hill, and G. Verbic, "Foundations and challenges of low-inertia systems," in *20th Power Systems Computation Conference (PSCC)*, 2018, pp. 1–25.

[12] J. Matevosyan *et al.*, "Grid-forming inverters: Are they the key for high renewable penetration?," *IEEE Power Energy Mag.*, vol. 17, no. 6, pp. 89–98, 2019, doi: 10.1109/MPE.2019.2933072.

[13] I. Erlich, A. Korai, and F. Shewarega, "Control challenges in power systems dominated by converter interfaced generation and transmission technologies," in *IEEE PES General Meeting*, 2017.

[14] Y. Levron and J. Belikov, "Modeling power networks using dynamic phasors in the dq0 reference frame," *Electr. Power Syst. Res.*, vol. 144, pp. 233–242, 2017, doi: 10.1016/j.epsr.2016.11.024.

[15] L. Fan, "Modeling type-4 wind in weak grids," *IEEE Trans. Sustain. Energy*, vol. 10, no. 2, pp. 853–863, 2019, doi: 10.1109/TSTE.2018.2849849.

[16] L. Fan and Z. Miao, "Wind in weak grids : 4 Hz or 30 Hz oscillations?," *IEEE Trans. Power Syst.*, vol. 33, no. 5, pp. 5803–5804, 2018, doi: 10.1109/TPWRS.2018.2852947.

[17] H. Liu, X. Xie, and W. Liu, "An oscillatory stability criterion based on the unified dq - frame impedance network model for power systems with high-penetration renewables," *IEEE Trans. Power Syst.*, vol. 33, no. 3, pp. 3472–3485, 2018, doi: 10.1109/TPWRS.2018.2794067.

[18] H. Liu and X. Xie, "Impedance network modeling and quantitative stability analysis of Sub - / Super-synchronous oscillations for large-scale wind power systems," *IEEE Access*, vol. 6, pp. 34431–34438, 2018, doi: 10.1109/ACCESS.2018.2849830.

[19] P. Kundur *et al.*, "Definition and classification of power system stability - Revisited & extended," *IEEE Trans. Power Syst.*, vol. 36, no. 4, pp. 3271–3281, 2021, doi: 10.1109/TPWRS.2004.825981.
[20] M. Zhao, X. Yuan, J. Hu, and Y. Yan, "Voltage dynamics of current control time-scale in a VSC-connected weak grid," *IEEE Trans. Power Syst.*, vol. 31, no. 4, pp. 2925–2937, 2016, doi: 10.1109/TPWRS.2015.2482605.
[21] W. Du, X. Chen, and H. Wang, "PLL-induced modal resonance of grid-connected PMSGs with the power system electromechanical oscillation modes," *IEEE Trans. Sustain. Energy*, vol. 8, no. 4, pp. 1581–1591, 2017.
[22] M. Paolone *et al.*, "Fundamentals of power systems modelling in the presence of converter-interfaced generation," *Electr. Power Syst. Res.*, vol. 189, no. June, pp. 1–33, 2020, doi: 10.1016/j.epsr.2020.106811.
[23] M. Paolone *et al.*, "Fundamentals of power systems modelling in the presence of converter-interfaced generation," in *21st Power Systems Computation Conference - PSCC2020*, 2020, pp. 1–35.
[24] NERC, "Integrating inverter - based resources into low short circuit strength systems - Reliability guideline," 2017.
[25] A. M. Stankovic, B. C. Lesieutre, and T. Aydin, "Modeling and analysis of single-phase induction machines with dynamic phasors," *IEEE Trans. Power Syst.*, vol. 14, no. 1, pp. 9–14, 1999.
[26] K. Strunz, R. Shintaku, and F. Gao, "Frequency-adaptive network modeling for integrative simulation of natural and envelope waveforms in power systems and circuits," *IEEE Trans. Circuits Syst. I Regul. Pap.*, vol. 53, no. 12, pp. 2788–2803, 2006, doi: 10.1109/TCSI.2006.883864.
[27] F. Gao and K. Strunz, "Frequency-adaptive power system modeling for multiscale simulation of transients," *IEEE Trans. Power Syst.*, vol. 24, no. 2, pp. 561–571, 2009, doi: 10.1109/TPWRS.2009.2016587.
[28] P. Zhang, J. R. Martí, and H. W. Dommel, "Shifted-frequency analysis for EMTP simulation of power-system dynamics," *IEEE Trans. Circuits Syst. I Regul. Pap.*, vol. 57, no. 9, pp. 2564–2574, 2010.
[29] Z. Shuai, Y. Peng, J. M. Guerrero, Y. Li, and Z. J. Shen, "Transient response analysis of inverter-based microgrids under unbalanced conditions using a dynamic phasor model," *IEEE Trans. Ind. Electron.*, vol. 66, no. 4, pp. 2868–2879, 2019, doi: 10.1109/TIE.2018.2844828.
[30] T. Yang, S. Bozhko, G. Asher, and C. I. Hill, "Dynamic phasor modeling of multi-generator variable frequency electrical power systems," *IEEE Trans. Power Syst.*, vol. 31, no. 1, pp. 563–571, 2016.
[31] Z. Miao, L. Piyasinghe, J. Khazaei, and L. Fan, "Dynamic phasor-based modeling of unbalanced radial distribution systems," *IEEE Trans. Power Syst.*, vol. 30, no. 6, pp. 3102–3109, 2015.
[32] Y. Xia and K. Strunz, "Multi-scale induction machine model in the phase domain with constant inner impedance," *IEEE Trans. Power Syst.*, pp. 1–13, 2019, doi: 10.1109/TPWRS.2019.2947535.
[33] A. M. Gole, R. W. Menzies, H. M. Turanli, and D. A. Woodford, "Improved interfacing of electrical machine models to electromagnetic transients programs," *IEEE Trans. Power Appar. Syst.*, vol. PAS-103, no. 9, pp. 2446–2451, 1984.
[34] D. Ramasubramanian, W. Wang, P. Pourbeik, E. Farantatos, S. Soni, and V. Chadliev, "Positive sequence voltage source converter mathematical model for use in low short circuit

systems," *IET Gener. Transm. Distrib.*, vol. 14, no. 1, pp. 87–97, 2020.
[35] D. Ramasubramanian, Z. Yu, R. Ayyanar, V. Vittal, and J. Undrill, "Converter model for representing converter interfaced generation in large scale grid simulations," *IEEE Trans. Power Syst.*, vol. 32, no. 1, pp. 765–773, 2017.
[36] P. Pourbeik, N. Etzel, and S. Wang, "Model Validation of Large Wind Power Plants Through Field Testing," *IEEE Trans. Sustain. Energy*, pp. 1–8, 2017, doi: 10.1109/TSTE.2017.2776751.
[37] N. Hatziargyriou *et al.*, "Stability definitions and characterization of dynamic behavior in systems with high penetration of power electronic interfaced technologies," *IEEE Power and Energy Society*. Technical Report, PES-TR77, pp. 1–42, 2020.
[38] H.-D. Chiang, *Direct methods for electric power systems*. Hoboken, New Jersey: John Wiley & Sons, 2011.
[39] NERC, "Short-circuit modeling and system strength," 2018.
[40] K. Jones *et al.*, "Impact of inverter based generation on bulk power system dynamics and short-circuit performance," *IEEE Power Energy Soc. Tech. Rep. PES -TR68*, no. Jul, 2018.
[41] A. Gavrilovic, "AC/DC system strength as indicated by short circuit ratios," in *International Conference on AC and DC Power Transmission*, 1968, pp. 27–32.
[42] NERC, "Integrating inverter based resources into weak power system reliability guideline," 2017.
[43] S. H. Huang, J. Schmall, J. Conto, J. Adams, Y. Zhang, and C. Carter, "Voltage control challenges on weak grids with high penetration of wind generation: ERCOT experience," *IEEE Power Energy Soc. Gen. Meet.*, pp. 1–7, 2012, doi: 10.1109/PESGM.2012.6344713.
[44] R. A. Walling, E. Gursoy, and B. English, "Current contributions from yype 3 and type 4 wind turbine generators during faults," *2011 IEEE Power Energy Soc. Gen. Meet.*, pp. 1–6, 2011, doi: 10.1109/PES.2011.6039740.
[45] N. Tleis, *Power systems modelling and fault analysis*, 1 st ed. Oxford, Eng.: Newnes Power Engineering, 2008.
[46] P. Tielens and D. Van Hertem, "The relevance of inertia in power systems," *Renew. Sustain. Energy Rev.*, vol. 55, pp. 999–1009, 2016, doi: 10.1016/j.rser.2015.11.016.
[47] B. Benjamin, B. Johnson, P. Denholm, and B. Hodge, "Achieving a 100% renewable grid: operating electric power systems with extremely high levels of variable renewable energy," *IEEE Power Energy Mag.*, vol. 15, no. 2, pp. 61–73, 2017, doi: 10.1109/MPE.2016.2637122.
[48] B. W. Winter, K. Elkington, and G. Bareux, "Pushing the limits: Europe's new grid: innovative tools to combat transmission bottlenecks and reduced inertia," *IEEE Power Energy Mag.*, vol. 13, no. february, pp. 60–74, 2015, doi: 10.1109/MPE.2014.2363534.
[49] A. B. Attya, J. L. Dominguez-Garcia, and O. Anaya-Lara, "A review on frequency support provision by wind power plants: Current and future challenges," *Renew. Sustain. Energy Rev.*, vol. 81, no. June 2017, pp. 2071–2087, 2018, doi: 10.1016/j.rser.2017.06.016.
[50] H. Bevrani, A. Ghosh, and G. Ledwich, "Renewable energy sources and frequency regulation: survey and new perspectives," *IET Renew. Power Gener.*, vol. 4, no. 5, pp. 438–457, 2010, doi: 10.1049/iet-rpg.2009.0049.
[51] C. Rahmann and A. Castillo, "Fast frequency response capability of photovoltaic power plants: The necessity of new grid requirements and definitions," *Energies*, vol. 7, no. 10, pp. 6306–6322, 2014, doi: 10.3390/en7106306.
[52] P. Tielens and D. Van Hertem, "The relevance of inertia in power systems," *Renew. Sustain. Energy Rev.*, vol. 55, pp. 999–1009, 2016, doi: 10.1016/j.rser.2015.11.016.
[53] A. Ulbig, T. S. Borsche, and G. Andersson, "Impact of low rotational inertia on power

system stability and operation," *IFAC Proc. Vol.*, vol. 47, no. 3, pp. 7290–7297, 2014, doi: 10.3182/20140824-6-ZA-1003.02615.

[54] A. Etxegarai, P. Eguia, E. Torres, A. Iturregi, and V. Valverde, "Review of grid connection requirements for generation assets in weak power grids," *Renew. Sustain. Energy Rev.*, vol. 41, pp. 1501–1504, 2015, doi: 10.1016/j.rser.2014.09.030.

[55] D. Groß and F. Dörfler, "On the steady-state behavior of low-inertia power systems," *IFAC-PapersOnLine*, vol. 50, no. 1, pp. 10735–10741, 2017, doi: 10.1016/j.ifacol.2017.08.2264.

[56] J. Matevosyan, "Survey of grid-forming inverter applications," *PST/ESIG webinar*, 2021, [Online]. Available: https://globalpst.org/wp-content/uploads/Survey-of-Grid-Forming-Inverter-Applications-Julia-Matevosyan.pdf

[57] B. J. Matevosyan, J. Macdowell, N. Miller, A. Isaacs, and R. Quint, "A future with inverter-based resources: Finding strength from traditional weakness," *IEEE Power Energy Mag.*, vol. 19, no. 6, pp. 18–28, 2021.

[58] Y. Li, L. Fan, and Z. Miao, "Wind in weak grids : Low-frequency oscillations, subsynchronous oscillations , and torsional interactions," *IEEE Trans. Power Syst.*, vol. 35, no. 1, pp. 109–117, 2020, doi: 10.1109/TPWRS.2019.2924412.

[59] L. P. Kunjumuhammed, B. C. Pal, R. Gupta, and K. J. Dyke, "Stability analysis of a PMSG-based large offshore wind farm connected to a VSC-HVDC," *IEEE Trans. Energy Convers.*, vol. 32, no. 3, pp. 1166–1176, 2017, doi: 10.1109/TEC.2017.2705801.

[60] L. Kong, Y. Xue, L. Qiao, and F. Wang, "Review of small-signal converter-driven stability issues in power system," *IEEE Open Access J. Power Energy*, vol. 9, no. September 2021, pp. 29–41, 2022, doi: 10.1109/OAJPE.2021.3137468.

[61] T. F. on W. SSO, "Wind energy systems sub-synchronous oscillations: Events and modeling," *IEEE Power Energy Soc.*, vol. PES-TR80, pp. 1–163, 2020.

[62] X. Xie, X. Zhang, H. Liu, H. Liu, Y. Li, and C. Zhang, "Characteristic analysis of subsynchronous resonance in practical wind farms connected to series-compensated transmissions," *IEEE Trans. Energy Convers.*, vol. 32, no. 3, pp. 1117–1126, 2017, doi: 10.1109/TEC.2017.2676024.

[63] H. Liu *et al.*, "Subsynchronous interaction between direct-drive PMSG based wind farms and weak AC networks," *IEEE Trans. Power Syst.*, vol. 32, no. 6, pp. 4708–4720, 2017, doi: 10.1109/TPWRS.2017.2682197.

[64] C. Li, "Unstable operation of photovoltaic inverter from field experiences," *IEEE Trans. Power Deliv.*, vol. 33, no. 2, pp. 2018–2020, 2018.

[65] C. Li and R. Reinmuller, "Asset condition anomaly detections by using power quality data analytics," in *2019 IEEE Power Energy Society General Meeting (PESGM)*, 2019, pp. 1–5. doi: 10.1109/PESGM40551.2019.8973741.

[66] B. Badrzadeh, N. Modi, N. Crooks, and A. Jalali, "Power system operation with reduced system strength for inverter-connected generation during prior outage conditions," *Cigre Sci. Eng.*, vol. 17, pp. 141–149, 2020.

[67] A. Jalali, B. Badrzadeh, J. Lu, N. Modi, and M. Gordon, "System strength challenges and solutions developed for a remote area of australian power system with high penetration of inverter-based resources," *Cigre Sci. Eng.*, vol. 20, pp. 27–37, 2021.

[68] AEMO, "System strength workshop," 2021, [Online]. Available: https://aemo.com.au/en/learn/energy-explained/%0Asystem-strength-workshop.

[69] NGESO, "GB power system disruption on 9 august 2019," no. April, pp. 1–20, 2021, [Online]. Available: https://assets.publishing.service.gov.uk/government/%0Auploads/system/uploads/attachment data/file/836626/20191003 E3C%0AInterim Report into GB Power Disruption.pdf

[70] C. Wang, L. Vanfretti, C. Mishra, K. D. Jones, and R. M. Gardner, “Identifying ooscillations injected by inverter-based solar energy sources in Dominion Energy’s Service Territory using synchrophasor data and point on wave data,” in *IEEE PES General Meeting*, 2022, pp. 1–5.

[71] L. Fan, “Interarea oscillations revisited,” *IEEE Trans. Power Syst.*, vol. 32, no. 2, pp. 1585–1586, 2017.

[72] Y. Li, L. Fan, and Z. Miao, “Replicating real-world wind farm SSR events,” *IEEE Trans. Power Deliv.*, pp. 1–10, 2019, doi: 10.1109/TPWRD.2019.2931838.

[73] S. Wang, E. Farantatos, and K. Tomsovic, “Wind turbine generator modeling considerations for stability studies of weak Systems,” in *IEEE North American Power Symposium (NAPS)*, 2017, pp. 1–6.

[74] L. Huang *et al.*, “Grid-synchronization stability analysis and loop shaping for PLL-based power converters with different reactive power control,” *IEEE Trans. Smart Grid*, vol. 11, no. 1, pp. 501–516, 2020.

[75] J. Z. Zhou, H. Ding, S. Fan, Y. Zhang, and A. M. Gole, “Impact of short circuit ratio and phase locked loop parameters on the small signal behavior of a VSC HVDC converter,” *IEEE Trans. Power Deliv.*, vol. 29, no. 5, pp. 2287–2296, 2014, doi: 10.1109/TPWRD.2014.2330518.

[76] A. Haddadi, E. Farantatos, I. Kocar, and U. Karaagac, “Impact of Inverter Based Resources on System Protection,” *Energies*, vol. 14, no. 4, p. 1050, 2021, doi: 10.3390/en14041050.

[77] G. Kou, L. Chen, P. Vansant, F. Velez-Cedeno, and Y. Liu, “Fault characteristics of distributed solar generation,” *IEEE Trans. Power Deliv.*, vol. 35, no. 2, pp. 1062–1064, 2020, doi: 10.1109/TPWRD.2019.2907462.

[78] P. Pourbeik *et al.*, “Generic dynamic models for modeling wind power plants and other renewable technologies in large scale power system studies,” *IEEE Trans. Energy Convers.*, vol. 32, no. 3, pp. 1108–1116, 2017, [Online]. Available: http://ieeexplore.ieee.org/abstract/document/7782402/

[79] T. Kauffmann *et al.*, “Short-circuit model for Type-IV wind turbine generators with decoupled sequence control,” *IEEE Trans. Power Deliv.*, vol. 34, no. 5, pp. 1998–2007, 2019, doi: 10.1109/TPWRD.2019.2908686.

[80] VDE-ARN, “Technische Regeln für den Anschluss von Kundenanlagen an das Hochspannungsnetz und deren Betrieb (TAR Hochspan-nung).” Berlin, Germany, p. 11, 2018.

[81] “Modification of commercial fault calculation programs for wind turbine generators, IEEE Power System Relaying Committee WG-24,” 2020.

[82] Q. Hong, M. A. U. Khan, C. Henderson, A. Egea-Àlvarez, D. Tzelepis, and C. Booth, “Addressing Frequency Control Challenges in Future Low-Inertia Power Systems: A Great Britain Perspective,” *Engineering*, vol. 7, no. 8, pp. 1057–1063, 2021, doi: 10.1016/j.eng.2021.06.005.

[83] K. S. Ratnam, K. Palanisamy, and G. Yang, “Future low-inertia power systems: Requirements, issues, and solutions - A review,” *Renew. Sustain. Energy Rev.*, vol. 124, no. February, p. 109773, 2020, doi: 10.1016/j.rser.2020.109773.

[84] M. Garmroodi, G. Verbiˇ, and D. J. Hill, “Frequency Support From Wind Turbine Generators With a Time-Variable Droop Characteristic,” *IEEE Trans. Sustain. Energy*, vol. 9, no. 2, pp. 676–684, 2018, doi: 10.1109/TSTE.2017.2754522.

[85] F. Milano, F. Dorfler, G. Hug, D. J. Hill, and G. Verbič, “Foundations and challenges of low-inertia systems (Invited Paper),” *20th Power Syst. Comput. Conf. PSCC 2018*, 2018, doi: 10.23919/PSCC.2018.8450880.

[86] A. S. Ahmadyar, S. Riaz, G. Verbic, A. Chapman, and D. J. Hill, "A Framework for Assessing Renewable Integration Limits with Respect to Frequency Performance," *IEEE Trans. Power Syst.*, vol. 33, no. 4, pp. 4444–4453, 2018, doi: 10.1109/TPWRS.2017.2773091.
[87] N. Watson and J. Arrillaga, "Power Systems Electromagnetic Transients Simulation," *IEE Power Energy Ser.*, vol. 39, p. 449, 2003, doi: 10.1049/PBPO039E.
[88] J. A. Martinez-Velasco, Ed., *Transient analysis of power Systems solution techniques, tools and applications*. Wiley-IEEE Press, 2015. doi: 10.1002/9781118694190.
[89] J. Mahseredjian, V. Dinavahi, and J. a. Martinez, "Simulation Tools for Electromagnetic Transients in Power Systems: Overview and Challenges," *IEEE Trans. Power Deliv.*, vol. 24, no. 3, pp. 1657–1669, 2009, doi: 10.1109/TPWRD.2008.2008480.
[90] IEEE, "Modeling and analysis of system transients using digital programs part 1," 1998.
[91] IEEE, "Modeling and analysis of system transients using digital programs part 2," 1998. doi: 99TP133-0.
[92] K. Strunz, "Position-dependent control of numerical integration in circuit simulation," *IEEE Trans. Circuits Syst. II Express Briefs*, vol. 51, no. 10, pp. 561–565, 2004, doi: 10.1109/TCSII.2004.834542.
[93] L. Gérin-lajoie and J. Mahseredjian, "Simulation of an extra large network in EMTP : from electromagnetic to electromechanical transients," in *IPST International Conference on Power Systems Transients*, 2009, pp. 1–8.
[94] Q. Huang and V. Vittal, "Advanced EMT and phasor-domain hybrid simulation with simulation mode switching capability for transmission and distribution systems," *IEEE Trans. Power Syst.*, vol. 33, no. 6, pp. 6298–6308, 2018, doi: 10.1109/TPWRS.2018.2834561.
[95] F. Milano and Á. O. Manjavacas, *Converter-interfaced energy storage systems: Context, modelling and dynamic analysis*. Cambridge: Cambridge University Press, 2019.
[96] E. Hinomori, T. Koshiduka, J. Arai, and H. Ikeda, *Power system transient analysis theory and practice using simulation program (ATP-EMTP)*. Wiley, 2016.
[97] D. Baimel, J. Belikov, J. M. Guerrero, and Y. Levron, "Dynamic modeling of networks, microgrids, and renewable sources in the dq0 reference frame: A survey," *IEEE Access*, vol. 5, pp. 21323–21335, 2017, doi: 10.1109/ACCESS.2017.2758523.
[98] J. Belikov and Y. Levron, "Comparison of time-varying phasor and dq 0 dynamic models for large transmission networks," *Int. J. Electr. Power Energy Syst.*, vol. 93, pp. 65–74, 2017, doi: 10.1016/j.ijepes.2017.05.017.
[99] H. D. Lüke, *Signalübertragung*, 4th Ed. Berlin, Germany: Springer-Verlag, 1990.
[100] S. R. Sanders, T. Aydin, and A. M. Stankovic, "Dynamic phasors in modeling and analysis of unbalanced polyphase AC machines," *IEEE Trans. Energy Convers.*, vol. 17, no. 1, pp. 107–113, 2002.
[101] V. Venkatasubramanian, H. Schättler, and J. Zaborszky, "Fast time-varying phasor analysis in the balanced three-phase large electric power system," *IEEE Trans. Automat. Contr.*, vol. 40, no. 11, pp. 1975–1982, 1995.
[102] J. R. Winkelman, J. H. Chow, and J. J. Allemong, "Multi-time-scale analysis of a power system," *Automatica*, vol. 16, pp. 35–43, 1980.
[103] S. Ahmed-Zaid, P. W. Sauer, M. A. Pai, and M. K. Sarioglu, "Reduced order modeling of synchronous machines using singular perturbation," *Trans. Circuits Syst.*, vol. 29, no. 11, pp. 782–786, 1982.
[104] J. A. Martínez-velasco, *Coordinación de aislamiento en redes eléctricas de alta tensión*. McGraw-Hill, 2008.

[105] J. Arrillaga and B. Smith, *AC-DC Power System Analysis*. London, UK: The Institution of Engineering and Technology, 1998.
[106] A. Morched, B. Gustavsen, and M. Tartibi, "A universal model for accurate calculation of electromagnetic transients on overhead lines and underground cables," *IEEE Trans. Power Deliv.*, vol. 14, no. 3, pp. 1032–1038, 1999.
[107] J. R. Marti, "Accurate Modeling of Frequency-Dependent Transmission Lines in Electromagnetic Transient Simulations," *IEEE Trans. Power Appar. Syst.*, vol. PAS-101, no. 1, pp. 147–157, 1982, doi: 10.14288/1.0095571.
[108] T. Report, "Modeling and Analysis of System Transients Using Digital Programs Part 1," 1998.
[109] R. R., *Power System Dynamics Analysis and Simulation*. PHI Learning, 2010.
[110] J. Belikov and Y. Levron, "Integration of long transmission lines in large-scale dq0 dynamic models," *Electr. Eng.*, vol. 100, no. 2, pp. 1219–1218, 2017, doi: 10.1007/s00202-017-0582-7.
[111] L. P. Kunjumuhammed, B. C. Pal, C. Oates, and K. J. Dyke, "Electrical oscillations in wind farm systems: analysis and insight based on detailed modeling," *IEEE Trans. Sustain. Energy*, vol. 7, no. 1, pp. 51–62, 2016, doi: 10.1109/TSTE.2015.2472476.
[112] F. Gao and K. Strunz, "Modeling of constant distributed parameter transmission line for simulation of natural and envelope waveforms in power electric networks," *Proc. 37th Annu. North Am. Power Symp. 2005*, vol. 2005, no. 3, pp. 247–252, 2005, doi: 10.1109/NAPS.2005.1560533.
[113] H. Ye and K. Strunz, "Multi-scale and frequency-dependent modeling of electric power transmission lines," *IEEE Trans. Power Deliv.*, vol. 33, no. 1, pp. 32–41, 2018.
[114] R. H. PARK, "Two-Reaction theory of synchronous machines: generalized method of analysis-part I," *Trans. Am. Inst. Electr. Eng.*, vol. 48, no. 3, pp. 716–727, 1929, doi: 10.1109/T-AIEE.1929.5055275.
[115] H. K. Lauw and W. S. Meyer, "Universal machine modeling for the representation of rotating electric machinery in an electromagnetic transients program," *IEEE Trans. Power Appar. Syst.*, vol. PAS-101, no. 6, pp. 1342–1351, 1982, doi: 10.1109/TPAS.1982.317181.
[116] L. Wang, J. Jatskevich, and H. W. Dommel, "Re-examination of synchronous machine modeling techniques for electromagnetic transient simulations," *IEEE Trans. Power Syst.*, vol. 22, no. 3, pp. 1221–1230, 2007, doi: 10.1109/TPWRS.2007.901308.
[117] U. Karaagac, J. Mahseredjian, and O. Saad, "Synchronous machine modeling precision and efficiency in electromagnetic transients," *IEEE Trans. Power Deliv.*, vol. 26, no. 2, pp. 1072–1082, 2011.
[118] P. Krause, O. Wasynczuk, S. Sudhoff, and Steven Pekarek, *Analysis of electric machinery and drive systems*, Third edit. Hoboken, NJ, USA: Wiley-IEEE Press, 2013. doi: 10.1002/9781118524336.
[119] P. Subramaniam and O. P. Malik, "Digital simulation of a synchronous generator in direct-phase quantities," *Proc. Inst. Electr. Eng.*, vol. 118, no. 1, p. 153, 1971, doi: 10.1049/piee.1971.0024.
[120] J. Marti and K. Louie, "A Phase-Domain synchronous Generator Model Including Saturation Effects," *IEEE Trans. Power Syst.*, vol. 12, no. 1, pp. 222–229, 1997, [Online]. Available: http://ieeexplore.ieee.org/xpls/abs_all.jsp?arnumber=574943
[121] S. D. Pekarek, O. Wasynczuk, and H. J. Hegner, "An Efficient and Accurate Model for the Simulation and Analysis of Synchronous Machine/Converter Systems," *IEEE Trans. Energy Convers.*, vol. 13, no. 1, pp. 42–48, 1998.
[122] P. Zhang, S. Member, J. R. Martí, H. W. Dommel, and L. Fellow, "Synchronous machine

modeling based on shifted frequency analysis," *IEEE Trans. Power Syst.*, vol. 22, no. 3, pp. 1139–1147, 2007.
[123] L. Wang and J. Jatskevich, "A voltage behind reactance synchronous machine model for the EMTP-type solution," *IEEE Trans. Power Syst.*, vol. 21, no. 4, pp. 1539–1549, 2006.
[124] B. Pal and B. Chaudhuri, *Robust control in power systems*. New York, NY: Springer, 2005. doi: 10.1007/b136490.
[125] M. Eremia and M. Shahidehpour, *Handbook of electrical power system dynamics*. Hoboken, NJ,USA: John Wiley & Sons, 2013.
[126] A. Ortega and F. Milano, "Generalized model of VSC-based energy storage systems for transient stability analysis," *IEEE Trans. Power Syst.*, vol. 31, no. 5, pp. 1–12, 2016, doi: 10.1109/TPWRS.2015.2496217.
[127] H. Geng, G. Yang, and X. Xi, "Enhanced model of the doubly fed induction generator-based wind farm for small-signal stability studies of weak power system," *IET Renew. Power Gener.*, vol. 8, no. 7, pp. 765–774, 2014, doi: 10.1049/iet-rpg.2013.0394.
[128] J. Ma, Y. Qiu, Y. Li, W. Zhang, Z. Song, and J. S. Thorp, "Research on the impact of DFIG virtual inertia control on power system small-signal stability considering the phase-locked loop," *IEEE Trans. Power Syst.*, vol. 32, no. 3, pp. 2094–2105, 2017, doi: 10.1109/TPWRS.2016.2594781.
[129] F. Mei and B. Pal, "Modal analysis of grid-connected doubly fed induction generators," *IEEE Trans. Energy Convers.*, vol. 22, no. 3, pp. 728–736, 2007.
[130] S. Ma, H. Geng, L. Liu, G. Yang, and B. C. Pal, "Grid-synchronization stability improvement of large scale wind farm during severe grid fault," *IEEE Trans. Power Syst.*, vol. 33, no. 1, pp. 1–1, 2018, doi: 10.1109/TPWRS.2017.2700050.
[131] A. M. Khalil and R. Iravani, "Enhanced generic nonlinear and linearized models of wind power plants," *IEEE Trans. Power Syst.*, vol. 32, no. 5, pp. 3968–3980, 2017.
[132] W. Du, J. Bi, H. Wang, and J. Yi, "Inter-area low-frequency power system oscillations caused by open-loop modal resonance," *IET Gener. Transm. Distrib.*, vol. 12, no. 19, pp. 4249–4259, 2018, doi: 10.1049/iet-gtd.2018.5187.
[133] D. Remon, C. A. Cañizares, and P. Rodriguez, "Impact of 100-MW-scale PV plants with synchronous power controllers on power system stability in northern Chile," *IET Gener. Transm. Distrib.*, vol. 11, no. 11, pp. 2958–2964, 2017, doi: 10.1049/iet-gtd.2017.0203.
[134] H. N. V. Pico and B. B. Johnson, "Transient stability assessment of multi-machine multi-converter power systems," *IEEE Trans. Power Syst.*, vol. 34, no. 5, pp. 3504–3514, 2019, doi: 10.1109/TPWRS.2019.2898182.
[135] K. Y. Member, H. R. Member, and T. V. A. N. C. Fellow, "Industrial recommendation of modeling of inverter-based generators for power system dynamic studies with focus on photovoltaic," *IEEE Power Energy Technol. Syst. J.*, vol. 5, no. 1, pp. 1–10, 2018.
[136] A. Yazdani and R. Iravani, *Voltage-sourced converters in power systems*. Hoboken, NJ, USA: John Wiley & Sons, 2010. doi: 10.1002/9780470551578.index.
[137] T. Qoria, F. Gruson, F. Colas, G. Denis, T. Prevost, and X. Guillau, "Inertia effect and load sharing capability of grid forming converters connected to a transmission grid," in *15th IET International Conference on AC and DC Power Transmission (ACDC 2019)*, 2019, pp. 1–6.
[138] J. Hu, Q. Hu, B. Wang, H. Tang, and Y. Chi, "Small signal instability of PLL-synchronized type-4 wind turbines connected to high-impedance AC grid during LVRT," *IEEE Trans. Energy Convers.*, vol. 31, no. 4, pp. 1676–1687, 2016, doi: 10.1109/TEC.2016.2577606.
[139] B. Johnson, M. Rodriguez, M. Sinha, and S. Dhople, "Comparison of virtual oscillator and droop control," *2017 IEEE 18th Work. Control Model. Power Electron. COMPEL 2017*,

2017, doi: 10.1109/COMPEL.2017.8013298.
[140] A. Etxegarai, P. Eguia, E. Torres, A. Iturregi, and V. Valverde, "Review of grid connection requirements for generation assets in weak power grids," *Renew. Sustain. Energy Rev.*, vol. 41, pp. 1501–1504, 2015, doi: 10.1016/j.rser.2014.09.030.
[141] M. T. S. Papathanassiou, "A review of grid code technical requirements for wind farms," *IET Renew. Power Gener.*, vol. 3, no. July 2008, pp. 308–332, 2009, doi: 10.1049/iet-rpg.2008.0070.
[142] J. Rocabert, A. Luna, F. Blaabjerg, and P. Rodríguez, "Control of power converters in AC microgrids," *IEEE Trans. Power Electron.*, vol. 27, no. 11, pp. 4734–4749, 2012, doi: 10.1109/TPEL.2012.2199334.
[143] Y. Yan, X. Yuan, and J. Hu, "Stationary-frame modeling of VSC based on current-balancing driven internal voltage motion for current control timescale dynamic analysis," *Energies*, vol. 11, no. 2, p. 374, 2018, doi: 10.3390/en11020374.
[144] H. Liu, X. Xie, X. Gao, H. Liu, and Y. Li, "Stability analysis of SSR in multiple wind farms connected to series-compensated systems using impedance network model," *IEEE Trans. Power Syst.*, vol. 33, no. 3, pp. 3118–3128, 2018, doi: 10.1109/TPWRS.2017.2764159.
[145] X. Wang, J. M. Guerrero, F. Blaabjerg, and Z. Chen, "A review of power electronics based microgrids," *J. Power Electron.*, vol. 12, no. 1, pp. 181–192, 2012, doi: 10.6113/JPE.2012.12.1.181.
[146] D. Ramasubramanian, E. Farantatos, S. Ziaeinejad, and A. Mehrizi-Sani, "Operation paradigm of an all converter interfaced generation bulk power system," *IET Gener. Transm. Distrib.*, vol. 12, no. 19, pp. 4240–4248, 2018, doi: 10.1049/iet-gtd.2018.5179.
[147] A. Tayyebi, F. Dorfler, F. Kupzog, Z. Miletic, and W. Hribernik, "Grid-forming converters-inevitability, control strategies and challenges in future grids application," in *CIRED Workshop*, 2018, pp. 1–5.
[148] A. T. Qoria, Q. Cossart, C. Li, and X. Guillaud, "MIGRATE- WP3: Control and operation of a grid with 100 % converter-based devices. Deliverable 3.2: Local control and simulation tools for large transmission systems," 2018.
[149] F. Katiraei, R. Iravani, N. Hatziargyriou, and A. Dimeas, "Microgrids management: controls and operation aspects of microgrids," *IEEE Power Energy Mag.*, vol. 6, no. 3, pp. 54–65, 2008.
[150] Y. Lin *et al.*, "Research roadmap on grid-forming inverters," *Natl. Renwable Energy Lab. NREL/TP-5D00-73476*, pp. 1–60, 2020.
[151] CIGRE, "Modeling and dynamic behavior of wind generation as it relates to power system control and dynamic performance," CIGRE Working group C4.601, 2007.
[152] S. Chiniforoosh *et al.*, "Definitions and applications of dynamic average models for analysis of power systems," *IEEE Trans. Power Deliv.*, vol. 25, no. 4, pp. 2655–2669, 2010, doi: 10.1109/TPWRD.2010.2043859.
[153] A. Yazdani *et al.*, "Modeling guidelines and a benchmark for power system simulation studies of three-phase single-stage photovoltaic systems," *IEEE Transactions on Power Delivery*, vol. 26, no. 2, pp. 1247–1264, 2011. doi: 10.1109/TPWRD.2010.2084599.
[154] J. Watson, Y. Ojo, and I. Lestas, "Stability of power networks with grid-forming converters," *2019 IEEE Milan PowerTech*, pp. 0–5, 2019.
[155] M. A. Hannan, M. S. H. Lipu, P. J. Ker, R. A. Begum, V. G. Agelidis, and F. Blaabjerg, "Power electronics contribution to renewable energy conversion addressing emission reduction: Applications, issues, and recommendations," *Appl. Energy*, vol. 251, no. December 2018, p. 113404, 2019, doi: 10.1016/j.apenergy.2019.113404.
[156] S. D'Arco, J. A. Suul, and O. B. Fosso, "A virtual synchronous machine implementation for

distributed control of power converters in SmartGrids," *Electr. Power Syst. Res.*, vol. 122, pp. 180–197, 2015, doi: 10.1016/j.epsr.2015.01.001.
[157] F. Mei and B. C. Pal, "Modelling of doubly-fed induction generator for power system stability study," *IEEE Power Energy Soc. Gen. Meet. - Convers. Deliv. Electr. Energy 21st Century*, no. 2, pp. 1–8, 2008, doi: 10.1109/PES.2008.4596214.
[158] Y. Li, L. Fan, and Z. Miao, "Stability control for wind in weak grids," *IEEE Trans. Sustain. Energy*, vol. 10, no. 4, pp. 2094–2103, 2019, doi: 10.1109/TSTE.2018.2878745.
[159] S. Cole, "Steady-state and dynamic modelling of VSC HVDC systems for power system simulation," Katholieke Universiteit, 2010.
[160] N. Hamrouni, M. Jraidi, A. Dhouib, and A. Cherif, "Design of a command scheme for grid connected PV systems using classical controllers," *Electr. Power Syst. Res.*, vol. 143, pp. 503–512, 2017, doi: 10.1016/j.epsr.2016.10.064.
[161] L. Fan and Z. Miao, "An explanation of oscillations due to wind power plants weak grid interconnection," *IEEE Trans. Sustain. Energy*, vol. 9, no. 1, pp. 488–489, 2018.
[162] J. Conroy and R. Watson, "Aggregate modelling of wind farms containing full-converter wind turbine generators with permanent magnet synchronous machines: transient stability studies," *IET Renew. Power Gener.*, vol. 3, no. 1, pp. 39–52, 2009, doi: 10.1049/iet-rpg.
[163] A. D. Hansen and G. Michalke, "Modelling and control of variable-speed multi-pole permanent magnet synchronous generator wind turbine," *Wind Energy*, vol. 11, no. 5, pp. 537–554, 2008, doi: 10.1002/we.278.
[164] A. D. Hansen, F. Lov, P. E. Sorensen, N. A. Cutululis, J. Clemens, and F. Blaabjerg, "Dynamic wind turbine models in power system simulation tool DIgSILENT," Roskilde, Denmark, 2007.
[165] N. R. Chaudhuri, B. Chaudhuri, R. Majumder, and A. Yazdani, *Multi-terminal direct-current grids: modeling, analysis, and control*. Wiley-IEEE Press, 2014.
[166] L. Papangelis, M.-S. Debry, T. Prevost, and T. Van Cutsem, "Stability of a voltage source converter subject to decrease of short-circuit capacity : a case study," in *20th Power System Computation Conference (PSCC)*, 2018, pp. 1–7.
[167] Y. Zhou, Y. Li, and J. Liu, "Complete models of transmission-connected photovoltaic plant using modularity principle for power system small signal stability study," *IEEJ J. Ind. Appl.*, vol. 6, no. 6, pp. 435–442, 2017, doi: 10.1541/ieejjia.6.435.
[168] C. Collados-Rodriguez, M. Cheah-Mane, E. Prieto-Araujo, and O. Gomis-Bellmunt, "Stability analysis of systems with high VSC penetration: Where is the limit?," *IEEE Trans. Power Deliv.*, pp. 1–11, 2019, doi: 10.1109/TPWRD.2019.2959541.
[169] L. Fan, *Control and dynamics in power systems and microgrids*. CRC Press, 2017.
[170] D. Zhang, Y. Wang, J. Hu, S. Ma, Q. He, and Q. Guo, "Impacts of PLL on the DFIG-based WTG's electromechanical response under transient conditions: analysis and modeling," *CSEE J. Power Energy Syst.*, vol. 2, no. 2, pp. 30–39, 2016, doi: 10.17775/CSEEJPES.2016.00019.
[171] P. Rodríguez, J. Pou, J. Bergas, J. I. Candela, R. P. Burgos, and D. Boroyevich, "Decoupled double synchronous reference frame PLL for power converters control," *IEEE Trans. Power Electron.*, vol. 22, no. 2, pp. 584–592, 2007.
[172] Á. Ortega and F. Milano, "Comparison of different PLL implementations for frequency estimation and control," in *18th International Conference on Harmonics and Quality of Power (ICHQP)*, 2018, pp. 1–6.
[173] A. Bagheri, M. Mardaneh, A. Rajaei, and A. Rahideh, "Detection of grid voltage fundamental and harmonic components using Kalman filter and generalized averaging method," *IEEE Trans. Power Electron.*, vol. 31, no. 2, pp. 1064–1073, 2016, doi:

10.1109/TPEL.2015.2418271.
[174] R. Cardoso, R. F. Camargo, H. Pinheiro, and H. A. Gründling, “Kalman filter based synchronisation methods,” *IET Gener. Transm. Distrib.*, vol. 2, no. 4, pp. 542–555, 2008, doi: 10.1049/iet-gtd.
[175] M. S. Pádua, S. M. Deckmann, G. S. Sperandio, F. P. Marafão, and D. Colón, “Comparative analysis of synchronization algorithms based on PLL, RDFT and Kalman filter,” in *IEEE International Symposium on Industrial Electronics*, 2007, pp. 964–970. doi: 10.1109/ISIE.2007.4374728.
[176] B. P. McGrath, D. G. Holmes, and J. J. H. Galloway, “Power converter line synchronization using a discrete Fourier transform (DFT) based on a variable sample rate,” *IEEE Trans. Power Electron.*, vol. 20, no. 4, pp. 877–884, 2005, doi: 10.1109/TPEL.2005.850944.
[177] NERC/WECC, “900 MW fault induced solar photovoltaic resource interruption disturbance report,” *Tech. Rep.*, pp. 1–30, 2018.
[178] NERC, “1200 MW fault induced solar photovoltaic resource interruption disturbance report,” *Tech. Rep.*, pp. 1–38, 2017.
[179] A. M. Khalil and R. Iravani, “Impact of high-depth penetration of wind power on low-frequency oscillatory modes of interconnected power systems,” *Int. J. Electr. Power Energy Syst.*, vol. 104, no. March 2018, pp. 827–839, 2019, doi: 10.1016/j.ijepes.2018.07.062.
[180] S. B. Subramanian, R. K. Varma, and T. Vanderheide, “Impact of grid voltage feed-forward filters on coupling between DC-link voltage and AC voltage controllers in smart PV solar systems,” *IEEE Trans. Sustain. Energy*, vol. 11, no. 1, pp. 381–390, 2020, doi: 10.1109/TSTE.2019.2891571.
[181] M. Zhao, X. Yuan, J. Hu, and Y. Yan, “Voltage dynamics of current control time-scale in a VSC-connected weak grid,” *IEEE Trans. Power Syst.*, vol. 31, no. 4, pp. 2925–2937, 2016, doi: 10.1109/TPWRS.2015.2482605.
[182] A. Tayyebi, D. Groß, A. Anta, F. Kupzog, and F. Dörfler, “Frequency stability of synchronous machines of grid-forming power converters,” *IEEE J. Emerg. Sel. Top. Power Electron.*, pp. 1–15, 2020, doi: 10.1109/JESTPE.2020.2966524.
[183] H. P. Beck and R. Hesse, “Virtual synchronous machine,” in *9th International Conference on Electrical Power Quality and Utilisation*, 2007, pp. 1–6. doi: 10.1109/EPQU.2007.4424220.
[184] C. Arghir, T. Jouini, and F. Dörfler, “Grid-forming control for power converters based on matching of synchronous machines,” *Automatica*, vol. 95, no. September, pp. 273–282, 2018, doi: 10.1016/j.automatica.2018.05.037.
[185] B. B. Johnson, M. Sinha, N. G. Ainsworth, F. Dorfler, and S. V. Dhople, “Synthesizing Virtual Oscillators to Control Islanded Inverters,” *IEEE Trans. Power Electron.*, vol. 31, no. 8, pp. 6002–6015, 2016, doi: 10.1109/TPEL.2015.2497217.
[186] A. T. Jouini, U. Markovic, and D. Groß, “MIGRATE - WP3 - Control and operation of a grid with 100 % converter-based devices Deliverable 3.3 : New options for existing system services and needs for new system services,” 2018.
[187] S. D’Arco and J. A. Suul, “Equivalence of virtual synchronous machines and frequency-droops for converter-based microgrids,” *IEEE Trans. Smart Grid*, vol. 5, no. 1, pp. 394–395, 2014, doi: 10.1109/TSG.2013.2288000.
[188] Q. Cossart, F. Colas, and X. Kestelyn, “Simplified converters models for the analysis and simulation of large transmission systems using 100% power electronics,” in *20th European Conference on Power Electronics and Applications, EPE 2018 ECCE Europe*, 2018, pp. 1–10.
[189] A. Lorenzo-bonache, A. Honrubia-escribano, and J. Fortmann, “Generic type 3 WT models :

comparison between IEC and WECC approaches," *IET Renew. Power Gener.*, pp. 1–11, 2019, doi: 10.1049/iet-rpg.2018.6098.
[190] U. Markovic, O. Stanojev, P. Aristidou, E. Vretos, D. Callaway, and G. Hug, "Understanding small-signal stability of low-inertia systems," *IEEE Trans. Power Syst.*, pp. 1–19, 2021, doi: 10.1109/TPWRS.2021.3061434.
[191] K. Clark, N. W. Miller, and R. Walling, "Modeling of GE solar photovoltaic plants for grid studies," 2010.
[192] K. Clark, K. Clark, N. W. Miller, and J. J. Sanchez-Gasca, "Modeling of GE wind turbine-generators for grid studies," General Electric International, Schenectady, NY, USA, 2010.
[193] EPRI, "WECC type 3 wind turbine generator model - Phase II," 2014. [Online]. Available: https://www.wecc.org/Reliability/WECC-Type-3-Wind-Turbine-Generator-Model-Phase-II-012314.pdf
[194] Ö. Göksu, P. Sørensen, J. Fortmann, A. Morales, and S. Weigel, "Compatibility of IEC 61400-27-1 Ed 1 and WECC 2 nd generation wind turbine models," in *15th Wind Integration Workshop*, 2016, pp. 1–7.
[195] P. Sorensen, B. Andresen, J. Fortmann, and P. Pourbeik, "Modular structure of wind turbine models in IEC 61400-27-1," in *IEEE Power and Energy Society General Meeting*, 2013, pp. 1–5. doi: 10.1109/PESMG.2013.6672279.
[196] G. Lammert, L. D. Pabón, P. Pourbeik, D. Fetzer, and M. Braun, "Implementation and validation of WECC generic photovoltaic system models in DIgSILENT PowerFactory," in *IEEE Power and Energy Society General Meeting*, 2016, pp. 3–7. doi: 10.1109/PESGM.2016.7741608.
[197] A. Lorenzo-Bonache, A. Honrubia-Escribano, F. Jiménez-Buendía, and E. Gómez-Lázaro, "Field validation of generic type 4 wind turbine models based on IEC and WECC guidelines," *IEEE Trans. Energy Convers.*, vol. 34, no. 2, pp. 933–941, 2019, doi: 10.1109/TEC.2018.2875167.
[198] A. Lorenzo-Bonache, A. Honrubia-Escribano, F. Jiménez-Buendía, and E. Gómez-Lázaro, "Field validation of generic type 4 wind turbine models based on IEC and WECC guidelines," *IEEE Trans. Energy Convers.*, vol. 34, no. 2, pp. 933–941, 2019, doi: 10.1109/TEC.2018.2875167.
[199] E. Muljadi, M. Singh, and V. Gevorgian, "User guide for PV dynamic model simulation written on PSCAD platform," 2014.
[200] W. Wang *et al.*, "Instability of PLL-synchronized converter-based generators in low short-circuit systems and the limitations of positive sequence modeling," in *North American Power Symposium (NAPS)*, 2018, pp. 1–6.
[201] S. Achilles and M. Poller, "Direct drive synchronous machine models for stability assessment of wind farms," in *4th Int. Workshop on Large Scale Integration of Wind Power and Transmission Networks for Offshore Windfarms*, 2003, pp. 1–9.
[202] M. Altin, O. Goksu, P. Sorensen, A. Morales, J. Fortmann, and F. J. Buendia, "Phase angle calculation dynamics of type-4 wind turbines in rms simulations during severe voltage dips," *IET Renew. Power Gener.*, vol. 10, no. 8, pp. 1069–1186, 2016, doi: 10.1049/iet-rpg.2015.0501.
[203] CIGRÉ, "Connection of wind farms to weak AC networks," 2016.
[204] F. Shewarega and I. Erlich, *Simplified modeling of VSC-HVDC in power system stability studies*, vol. 19, no. 3. IFAC, 2014. doi: 10.3182/20140824-6-ZA-1003.01806.
[205] G. Kalcon, G. Adam, O. Anaya-Lara, S. Lo, and K. Uhlen, "Small - signal stability analysis of multi - terminal VSC - based DC transmission systems," *IEEE Trans. Power Syst.*, vol. 27, no. 4, pp. 1818–1830, 2012, doi: 10.1109/TPWRS.2012.2190531.

[206] K. R. Padiyar and N. Prabhu, "Modelling , control design and analysis of VSC based HVDC transmission systems," in *International Conference on Power System Technology*, 2004, pp. 774–779.
[207] S. Cole, J. Beerten, and R. Belmans, "Generalized dynamic VSC MTDC model for power system stability studies," *IEEE Trans. Power Syst.*, vol. 25, no. 3, pp. 1655–1662, 2010, doi: 10.1109/TPWRS.2010.2040846.
[208] L. Yang, G. Y. Yang, Z. Xu, Z. Y. Dong, K. P. Wong, and X. Ma, "Optimal controller design of a doubly-fed induction generator wind turbine system for small signal stability enhancement," *IET Gener. Transm. Distrib.*, vol. 4, no. 5, pp. 579–597, 2010, doi: 10.1049/iet-gtd.2009.0553.
[209] S. Xie, X. Wang, C. Qu, X. Wang, and J. Guo, "Controlling PMSG based wind generation by a locally available signal to damp power system inter-area oscillations," *Int. Trans. Electr. energy Syst.*, vol. 20, pp. 1–6, 2013, doi: 10.1002/etep.
[210] H. Huang, C. Mao, J. Lu, and D. Wang, "Small-signal modelling and analysis of wind turbine with direct drive permanent magnet synchronous generator connected to power grid," *IET Renew. Power Gener.*, vol. 6, no. 1, pp. 48–58, 2012, doi: 10.1049/iet-rpg.2010.0217.
[211] W. Du, X. Chen, and H. Wang, "Parameter tuning of the PLL to consider the effect on power system small-signal angular stability," *IET Renew. Power Gener.*, vol. 12, no. 1, pp. 1–8, 2018, doi: 10.1049/iet-rpg.2016.0835.
[212] O. L. V. Traff, "Modelling of VSC-HVDC for slow dynamic studies," Chalmers University of Technology, 2013.
[213] S. Cole and R. Belmans, "A proposal for standard VSC HVDC dynamic models in power system stability studies," *Electr. Power Syst. Res.*, vol. 81, no. 4, pp. 967–973, 2011, doi: 10.1016/j.epsr.2010.11.032.
[214] A. D. Hansen and G. Michalke, "Fault ride-through capability of DFIG wind turbines," *Renew. Energy*, vol. 32, no. 9, pp. 1594–1610, 2007, doi: 10.1016/j.renene.2006.10.008.
[215] A. D. Hansen, P. Sørensen, F. Iov, and F. Blaabjerg, "Centralised power control of wind farm with doubly fed induction generators," *Renew. Energy*, vol. 31, no. 7, pp. 935–951, 2006, doi: 10.1016/j.renene.2005.05.011.
[216] M. Poller and S. Achilles, "Aggregated wind park models for analyzing power system dynamics," in *Fourth International Workshop on Large-Scale Integration of Wind Power and Transmission Networks2*, 2003, pp. 1–10.
[217] M. Garmroodi, D. J. Hill, G. Verbic, and J. Ma, "Impact of tie-line power on inter-area modes with increased penetration of wind Power," *IEEE Trans. Power Syst.*, vol. 31, no. 4, pp. 3051–3059, 2016.
[218] B. Weise, "Impact of K-factor and active current reduction during fault-ride-through of generating units connected via voltage-sourced converters on power system stability," *IET Renew. Power Gener.*, vol. 9, no. 1, pp. 25–36, 2015, doi: 10.1049/iet-rpg.2014.0116.
[219] Z. Liu, L. Wang, N. Li, and J. Song, "Performance analysis and model comparison of PMSG for power system transient stability studies," in *IEEE International Conference on Power Renewable Energy*, 2016, pp. 294–300. doi: 10.1109/ICPRE.2016.7871219.
[220] S. Silwal, M. Karimi-ghartemani, R. Sharma, and H. Karimi, "Impact of feed-forward and decoupling terms on stability of grid-connected inverters," in *IEEE 28th International Symposium on Industrial Electronics (ISIE)*, 2019, pp. 2641–2646.
[221] K. Ding and D. Song, *Chapter 3 - Simulation Calculations for Wind Power Transmission Capability*. China Electric Power Press. Published by Elsevier Inc. All rights reserved., 2016. doi: 10.1016/B978-0-12-849895-8.00003-8.

[222] J. Huang and X. Yuan, “Impact of the voltage feed-forward and current decoupling on VSC current control stability in weak grid based on complex variables,” in *IEEE Energy Conversion Congress and Exposition (ECCE)*, 2015, pp. 6845–6852. doi: 10.1109/ECCE.2015.7310618.
[223] C. Yu, G. James, Y. Xue, and F. Xue, “Impacts of large scale wind power on power system transient stability,” in *4th International Conference on Electric Utility Deregulation and Restructuring and Power Technologies (DRPT)*, 2011, pp. 277–283. doi: 10.1109/DRPT.2011.5993903.
[224] G. Michalke and A. D. Hansen, “Modelling and control of variable speed wind turbines for power system studies,” *Wind Energy*, vol. 13, no. 4, pp. 307–322, 2010, doi: 10.1002/we.
[225] D. Ramasubramanian and V. Vittal, “Small signal stability analysis of controlled voltage source converter model for positive sequence time domain simulations,” in *North American Power Symposium (NAPS)*, 2016, no. 1, pp. 1–6. doi: 10.1109/NAPS.2016.7747917.
[226] D. Ramasubramanian, E. Farantatos, and A. GAikwad, “Proposal for improved voltage source converter model – an update,” 2018.
[227] K. Bolton *et al.*, “Modeling and dynamic behavior of battery energy storage: A simple model for large-scale time-domain stability studies,” *IEEE Electrif. Mag.*, vol. 3, no. 3, pp. 47–51, 2015, doi: 10.1109/mele.2015.2447974.
[228] K. Clark, N. W. Miller, and J. J. Sanchez-gasca, “Modeling of GE wind turbine - generators for grid studies,” 2010.
[229] WECC, “WECC solar plant dynamic modeling guidelines,” 2014. [Online]. Available: http://www.wecc.biz/committees/StandingCommittees/PCC/TSS/MV
[230] EPRI, “WECC type 4 wind turbine generator model - Phase II,” 2014.
[231] WECC, “WECC wind plant dynamic modeling guidelines,” 2014.
[232] M. Singh and S. Santoso, “Dynamic models for wind turbines and wind power plants,” 2011.
[233] A. Honrubia-Escribano, F. Jiménez-Buendía, E. Gómez-Lázaro, and J. Fortmann, “Field validation of a standard type 3 wind turbine model for power system stability, according to the requirements imposed by IEC 61400-27-1,” *IEEE Trans. Energy Convers.*, vol. 33, no. 1, pp. 137–145, 2018, doi: 10.1109/TEC.2017.2737703.
[234] N. W. Miller, J. J. Sanchez-Gasca, W. W. Price, and R. W. Delmerico, “Dynamic modeling of GE 1.5 and 3.6 MW wind turbine-generators for stability simulations,” in *Power Engineering Society General Meeting*, 2003, pp. 1977–1983.
[235] J. Vega-Herrera, C. Rahmann, F. Valencia, and K. Strunz, “Analysis and application of quasi-static and dynamic phasor calculus for stability assessment of integrated power electric and electronic systems,” *IEEE Trans. Power Syst.*, vol. 36, no. 2, pp. 1750–1760, 2021, doi: 10.1109/TPWRS.2020.3030225.
[236] “IEEE Recommended practice for excitation system models for power system stability studies,” *IEEE Stand. 421.5*, 2016, [Online]. Available: https://scholar.google.com/scholar?q=IEEE+Recommended+Practice+for+Excitation+System+Models+for+Power+System+Stability+Studies%2B2005&btnG=&hl=en&as_sdt=0%2C5#0
[237] P. Pourbeik *et al.*, “Dynamic models for turbine-governors in power system studies,” *IEEE Power Energy Soc. Tech. Rep. PES -TR1*, 2013.
[238] M. Parniani and M. Iravani, “Computer analysis of small-signal stability of power systems including network dynamics,” *IEE Proc. - Gener. Transm. Distrib.*, vol. 142, no. 6, pp. 613–617, 1995.
[239] R. Toscano, *Structured controllers for uncertain systems: A stochastic optimization approach*. London, UK: Springer London, 2013.

[240] M. Green and D. J. N. Limebeer, *Linear robust control*. Courier Corporation, 2012.
[241] C. Collados-Rodriguez, M. Cheah-Mane, E. Prieto-Araujo, and O. Gomis-Bellmunt, "Stability analysis of systems with high VSC penetration: Where is the limit?," *IEEE Trans. Power Deliv.*, vol. 35, no. 4, pp. 2021–2031, 2020, doi: 10.1109/TPWRD.2019.2959541.
[242] L. Fan, "Inter-IBR oscillation modes," *IEEE Trans. Power Syst.*, pp. 1–4, 2021, doi: 10.1109/tpwrs.2021.3124667.
[243] L. Fan and Z. Miao, "Root Cause Analysis of AC Overcurrent in July 2020 San Fernando Disturbance," *IEEE Trans. Power Syst.*, vol. 36, no. 5, pp. 4892–4895, 2021, doi: 10.1109/TPWRS.2021.3094367.
[244] R. Yin *et al.*, "Modeling and stability analysis of grid-tied VSC considering the impact of voltage feed-forward," *Int. J. Electr. Power Energy Syst.*, vol. 135, no. July 2021, pp. 1–12, 2022, doi: 10.1016/j.ijepes.2021.107483.
[245] J. F. Morris, K. H. Ahmed, and A. Egea-Alvarez, "Analysis of controller bandwidth interactions for vector-controlled VSC connected to very weak AC grids," *IEEE J. Emerg. Sel. Top. Power Electron.*, pp. 1–10, 2020, doi: 10.1109/jestpe.2020.3031203.
[246] C. Li, S. Wang, F. Colas, and J. Liang, "Dominant instability mechanism of VSI connecting to a very weak grid," *IEEE Trans. Power Syst.*, pp. 1–4, 2021, doi: 10.1109/TPWRS.2021.3115968.
[247] P. M. Anderson and A. A. Fouad, *Power system control and stability*, Second edi. Wiley, 2003.
[248] S. Nanou, G. Tsourakis, and C. D. Vournas, "Full-converter wind generator modelling for transient stability studies," *2011 IEEE PES Trondheim PowerTech Power Technol. a Sustain. Soc. POWERTECH 2011*, pp. 1–7, 2011, doi: 10.1109/PTC.2011.6019268.
[249] D. Xue and Y. Chen, *System simulation techniques with MATLAB and Simulink*, First edit. John Wiley & Sons, 2014.
[250] M. Dreidy, H. Mokhlis, and S. Mekhilef, "Inertia response and frequency control techniques for renewable energy sources: A review," *Renew. Sustain. Energy Rev.*, vol. 69, no. November 2016, pp. 144–155, 2017, doi: 10.1016/j.rser.2016.11.170.
[251] Y. Xu, M. Zhang, L. Fan, and Z. Miao, "Small-signal stability analysis of type-4 wind in series compensated networks," *IEEE Trans. Energy Convers.*, vol. 35, no. 1, pp. 529–538, 2020.
[252] A. Kulkarni and V. John, "Analysis of bandwidth-unit-vector-distortion tradeoff in PLL during abnormal grid conditions," *IEEE Trans. Ind. Electron.*, vol. 60, no. 12, pp. 5820–5829, 2013, doi: 10.1109/TIE.2012.2236998.
[253] Q. Huang and V. Vittal, "Integrated Transmission and Distribution System Power Flow and Dynamic Simulation Using Mixed Three-Sequence/Three-Phase Modeling," *IEEE Trans. Power Syst.*, vol. 32, no. 5, pp. 3704–3714, 2017, doi: 10.1109/TPWRS.2016.2638910.
[254] D. Ramasubramanian, S. Achilles, W. Baker, J. Matevosyan, and S. Pant, "Asking for fast terminal voltage control in grid following plants could provide benefits of grid forming behavior," *IET Gener. Transm. Distrib.*, pp. 1–16, 2022, doi: 10.1049/gtd2.12421.
[255] X. Wang, K. Qin, S. Member, and X. Ruan, "A Robust Grid-Voltage Feedforward Scheme to Improve Adaptability of Grid-Connected Inverter to Weak Grid Condition," *IEEE Trans. Power Electron.*, vol. 36, no. 2, pp. 2384–2395, 2021.

ANNEXES

Annex A: Power System Models Used in Chapter 4

This appendix shows the state-space model of CIG-GFL, CIG-GFM, the synchronous generator, and the electric network used to obtain the results described in Section 3.3. The purpose of this appendix is to show in more detail the models used, which are cited in Table 3.1. We describe the model based on DPC and its counterpart based on QPC for each component.

A.1 CIG-GFL Model

An average voltage source converter (VSC) model is considered regarding the CIG model based on DPC. In this model, the switching transients are neglected. Thus, the transient behavior of the CIG is determined mainly by its control loops. Figure A.1 shows a schematic diagram of a CIG connected to the grid. It comprises a generator, a VSC, and a coupling inductance. Furthermore, the loops considered in 3.3 are composed of an outer voltage control loop, an inner current control loop, and a PLL. These control loops are represented in a rotational dq reference frame. The control loops are depicted in Figure A.2, Figure A.3, and Figure A.4. In the figures, the subscript dq indicates the synchronous reference frame.

It has to be mentioned that the box related to the generator in Figure A.1 may involve different energy resources, such as wind power, solar power, or other types of generation interfaced by the VSC to the grid. On the other hand, the box related to the VSC in Figure A.1 involves the control loops mentioned and considered in 3.3.

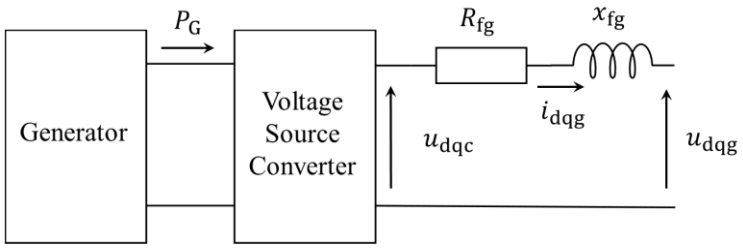

Figure A.1. Schematic diagram of a CIG connected to the grid [125]

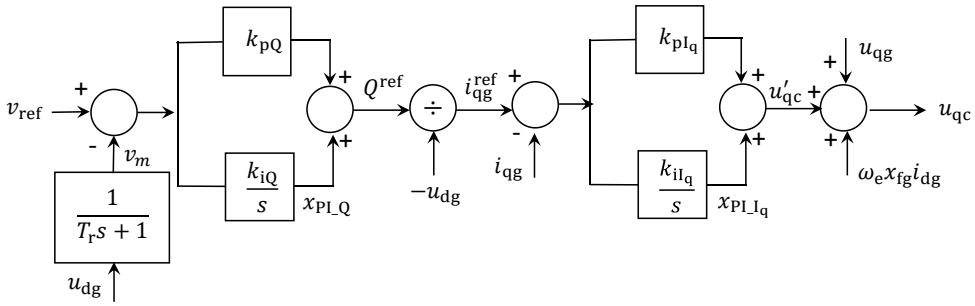

Figure A.2. CIG outer voltage control with the inner current control of q axis

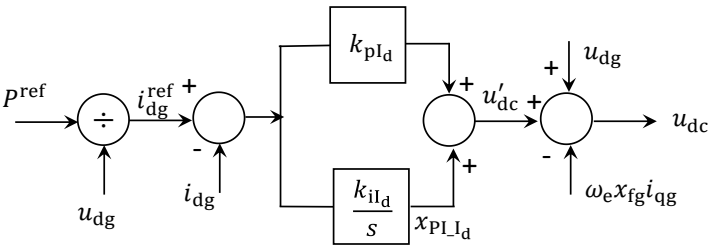

Figure A.3. CIG active power control with the inner current control system of d axis

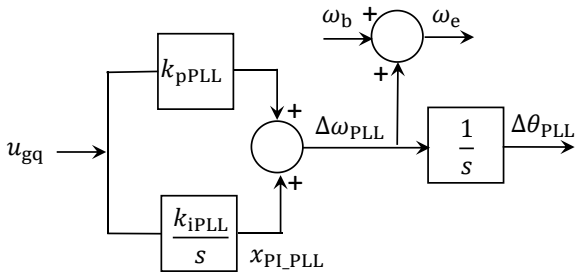

Figure A.4. PLL control loop

The state-space model considering DPC is described below. This model is obtained from the block diagrams shown in Figure A.2 to Figure A.4. It can be seen in these figures that for each output in integration blocks, there is an associated state variable. This is also for the transfer function block related to first-order in Figure A.2. Furthermore, all the quantities are considered in per unit system, and the generator convention is used for the VSC.

The CIG outer voltage control with the inner current control loop of q axis is modeled by the following set of equations:

$$\frac{\mathrm{d}v_{\mathrm{m}}}{\mathrm{d}t} = \frac{1}{T_{\mathrm{r}}}\left(u_{\mathrm{dg}} - v_{\mathrm{m}}\right) \tag{A.1}$$

$$\frac{\mathrm{d}x_{\mathrm{PI\_Q}}}{\mathrm{d}t} = k_{\mathrm{iQ}}(v_{\mathrm{ref}} - v_{\mathrm{m}}) \tag{A.2}$$

$$Q^{\mathrm{ref}} = k_{\mathrm{pQ}}(v_{\mathrm{ref}} - v_{\mathrm{m}}) + x_{\mathrm{PI\_Q}} \tag{A.3}$$

$$i_{\mathrm{qg}}^{\mathrm{ref}} = -\frac{Q^{\mathrm{ref}}}{u_{\mathrm{dg}}} \tag{A.4}$$

$$\frac{\mathrm{d}x_{\mathrm{PI\_I_q}}}{\mathrm{d}t} = k_{\mathrm{iI_q}}\left(i_{\mathrm{qg}}^{\mathrm{ref}} - i_{\mathrm{qg}}\right) \tag{A.5}$$

$$u'_{\mathrm{qc}} = k_{\mathrm{pI_q}}\left(i_{\mathrm{qg}}^{\mathrm{ref}} - i_{\mathrm{qg}}\right) + x_{\mathrm{PI\_I_q}} \tag{A.6}$$

$$u_{\mathrm{qc}} = u'_{\mathrm{qc}} + u_{\mathrm{qg}} + \omega_{\mathrm{e}} x_{\mathrm{fg}} i_{\mathrm{dg}} \tag{A.7}$$

The CIG active power control with the inner current control loop of d axis is modeled by the

following set of equations:

$$i_{\mathrm{dg}}^{\mathrm{ref}} = \frac{P_{\mathrm{ref}}}{u_{\mathrm{dg}}} \tag{A.8}$$

$$\frac{\mathrm{d}x_{\mathrm{PI\_I_d}}}{\mathrm{d}t} = k_{\mathrm{iI_d}}\left(i_{\mathrm{dg}}^{\mathrm{ref}} - i_{\mathrm{dg}}\right) \tag{A.9}$$

$$u'_{\mathrm{dc}} = k_{\mathrm{pI_d}}\left(i_{\mathrm{dg}}^{\mathrm{ref}} - i_{\mathrm{dg}}\right) + x_{\mathrm{PI\_I_d}} \tag{A.10}$$

$$u_{\mathrm{dc}} = u'_{\mathrm{dc}} + u_{\mathrm{dg}} - \omega_{\mathrm{e}} x_{\mathrm{fg}} i_{\mathrm{qg}} \tag{A.11}$$

The PLL is described as follows:

$$\frac{\mathrm{d}x_{\mathrm{PI\_PLL}}}{\mathrm{d}t} = k_{\mathrm{iPLL}} u_{\mathrm{gq}} \tag{A.12}$$

$$\Delta\omega_{\mathrm{PLL}} = k_{\mathrm{pPLL}} u_{\mathrm{gq}} + x_{\mathrm{PI\_PLL}} \tag{A.13}$$

$$\omega_{\mathrm{e}} = \Delta\omega_{\mathrm{PLL}} + \omega_{\mathrm{b}} \tag{A.14}$$

$$\frac{\mathrm{d}\Delta\theta_{\mathrm{PCC}}}{\mathrm{d}t} = \Delta\omega_{\mathrm{PLL}} \tag{A.15}$$

Finally, the coupling inductance is modeled as follows:

$$\frac{x_{\mathrm{fg}}}{\omega_{\mathrm{b}}}\frac{\mathrm{d}i_{\mathrm{dg}}}{\mathrm{d}t} = u_{\mathrm{dc}} - R_{\mathrm{fg}} i_{\mathrm{dg}} + \omega_{\mathrm{PLL}} x_{\mathrm{fg}} i_{\mathrm{qg}} - u_{\mathrm{dg}} \tag{A.16}$$

$$\frac{x_{\mathrm{fg}}}{\omega_{\mathrm{b}}}\frac{\mathrm{d}i_{\mathrm{qg}}}{\mathrm{d}t} = u_{\mathrm{qc}} - R_{\mathrm{fg}} i_{\mathrm{qg}} - \omega_{\mathrm{PLL}} x_{\mathrm{fg}} i_{\mathrm{dg}} - u_{\mathrm{qg}} \tag{A.17}$$

In the case of the CIG model based on QPC, the active power control, the PLL, and the outer voltage control are the same as in the CIG model based on DPC. According to [125], the inner current control of dq axes is modified as follows. Equations(A.6) and (A.10) become equations (A.18) and (A.19), respectively.

$$u_{\mathrm{dc}} = k_{\mathrm{pI_d}}\left(i_{\mathrm{dg}}^{\mathrm{ref}} - i_{\mathrm{dg}}\right) + x_{\mathrm{PI\_I_d}} \tag{A.18}$$

$$u_{\mathrm{qc}} = k_{\mathrm{pI_q}}\left(i_{\mathrm{qg}}^{\mathrm{ref}} - i_{\mathrm{qg}}\right) + x_{\mathrm{PI\_I_q}} \tag{A.19}$$

The set of differential and algebraic equations (A.1)-(A.5), (A.8), and (A.9) is used in the CIG model based on QPC. Furthermore, as Table 3.1 describes, the quantities neglected are the derivatives of the current in the coupling inductor. This makes the differential equations (A.16) and (A.17) become the following algebraic equations:

$$0 = u_{dc} - R_{fg} i_{dg} + \omega_{PLL} x_{fg} i_{qg} - u_{dg} \quad \text{(A.20)}$$

$$0 = u_{qc} - R_{fg} i_{qg} - \omega_{PLL} x_{fg} i_{dg} - u_{qg} \quad \text{(A.21)}$$

The CIG is represented as a controlled voltage source behind an impedance. This model was widely used in the literature [125], [162], [164], [201], [214], [218]. The parameter values used are given in Table 4.3.

A.2 CIG-GFM Model with Virtual Synchronous Generator

The model of CIG-GFM is used only for 100% of the CIG level in Chapter 4. Figure A.5 shows a schematic diagram of the CIG-GFM connected to the power system, which is composed of the VSC, the AC filter of LCL type. The DC-side is considered a constant DC-Voltage.

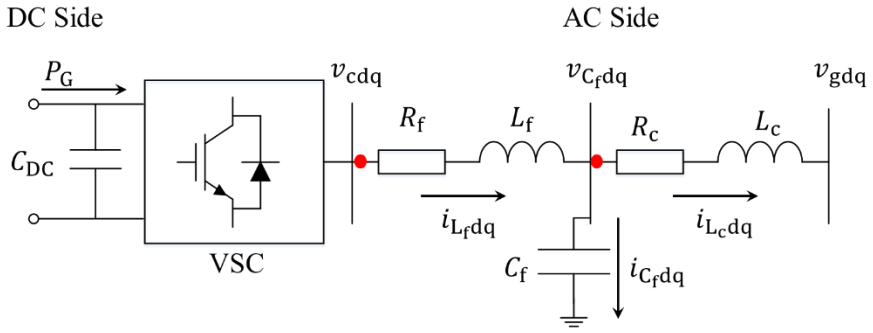

Figure A.5. Diagram of CIG – GFM

The control system consists of outer and inner control loops. The frequency control is implemented by virtual synchronous generator control for outer control loops. There are several control structures with a diverse complexity to implement this control. Here, it is considered a virtual synchronous generator that represents the mechanical behavior of a synchronous generator by a second-order differential equation [156]. Furthermore, droop-based reactive power controllers are implemented for voltage support. In the case of inner loops, voltage and current control based on dq reference frame are considered. The control loops implemented are shown in Figure A.6, Figure A.7, and Figure A.8, respectively. The DPC model is described, and the QPC-based model indicates the neglected derivatives.

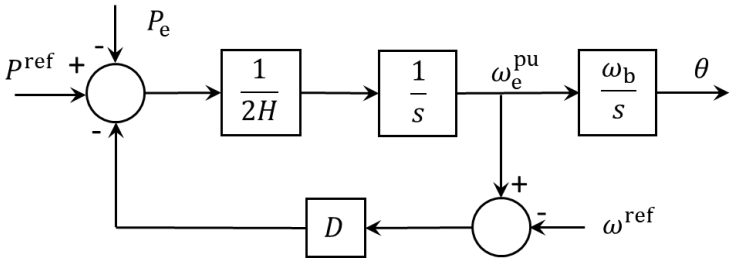

Figure A.6. Virtual Synchronous Generator Control [156]

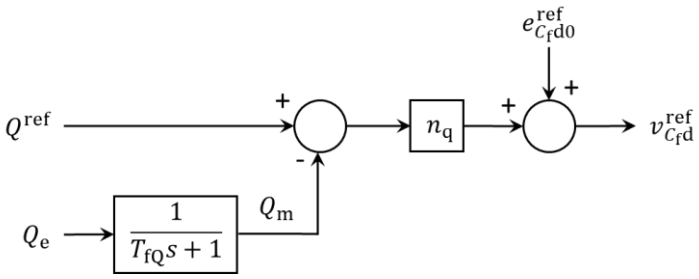

Figure A.7. Droop-based reactive power controller

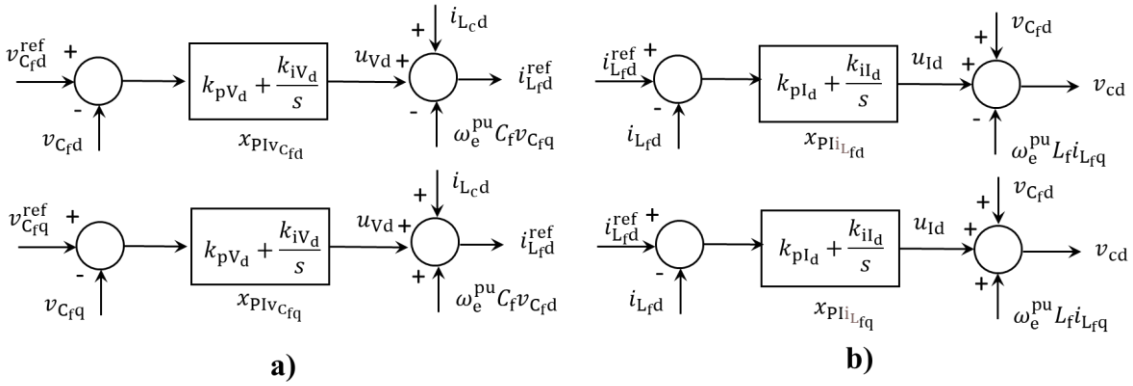

Figure A.8. Inner control loops on the dq axis; a) voltage control loops; b) current control loops

The control loops of the CIG-GFM depicted in Figure A.6, Figure A.7, and Figure A.8 are used to develop the state-space model. Each transfer function is associated with a state variable. As in the case of the CIG-GFL model, all the quantities are considered in per unit system. The virtual synchronous generator control and the droop-based reactive power control are represented by the following set of differential and algebraic equations:

$$2H\frac{\mathrm{d}\omega_{\mathrm{e}}^{\mathrm{pu}}}{\mathrm{d}t} = P^{\mathrm{ref}} - P_{\mathrm{e}} - D\left(\omega_{\mathrm{e}}^{\mathrm{pu}} - \omega^{\mathrm{ref}}\right) \tag{A.22}$$

$$\frac{\mathrm{d}\theta}{\mathrm{d}t} = \omega_{\mathrm{b}}\omega_{\mathrm{e}}^{\mathrm{pu}} \tag{A.23}$$

$$P_{\mathrm{e}} = v_{\mathrm{C_f d}} i_{\mathrm{L_c d}} + v_{\mathrm{C_f q}} i_{\mathrm{L_c q}} \tag{A.24}$$

$$v_{C_{\mathrm{f}}\mathrm{d}}^{\mathrm{ref}} = e_{C_{\mathrm{f}}\mathrm{d}0}^{\mathrm{ref}} + n_{\mathrm{q}}\left(Q^{\mathrm{ref}} - Q_{\mathrm{m}}\right) \tag{A.25}$$

$$\frac{\mathrm{d}Q_{\mathrm{m}}}{\mathrm{d}t} = \frac{1}{T_{\mathrm{fQ}}}\left(Q_{\mathrm{e}} - Q_{\mathrm{m}}\right) \tag{A.26}$$

$$v_{\mathrm{C_f q}}^{\mathrm{ref}} = e_{\mathrm{C_f q}0}^{\mathrm{ref}} = 0 \tag{A.27}$$

The following set of equations model the inner voltage control loop on dq axis shown in Figure A.8.a:

$$\frac{\mathrm{d}x_{\mathrm{PIv}_{\mathrm{C_{fd}}}}}{\mathrm{d}t} = k_{\mathrm{iV_d}}(v_{\mathrm{C_fd}}^{\mathrm{ref}} - v_{\mathrm{C_fd}}) \tag{A.28}$$

$$u_{\mathrm{Vd}} = x_{\mathrm{PIv}_{\mathrm{C_{fd}}}} + k_{\mathrm{pV_d}}(v_{\mathrm{C_fd}}^{\mathrm{ref}} - v_{\mathrm{C_fd}}) \tag{A.29}$$

$$i_{\mathrm{L_{fd}}}^{\mathrm{ref}} = u_{\mathrm{Vd}} + i_{\mathrm{L_cd}} - \omega_{\mathrm{b}}^{\mathrm{pu}} C_{\mathrm{f}} v_{\mathrm{C_fq}} \tag{A.30}$$

$$\frac{\mathrm{d}x_{\mathrm{PIv}_{\mathrm{C_{fq}}}}}{\mathrm{d}t} = k_{\mathrm{iV_q}}(v_{\mathrm{C_fq}}^{\mathrm{ref}} - v_{\mathrm{C_fq}}) \tag{A.31}$$

$$u_{\mathrm{Vd}} = x_{\mathrm{PIv}_{\mathrm{C_{fd}}}} + k_{\mathrm{pV_d}}(v_{\mathrm{C_fd}}^{\mathrm{ref}} - v_{\mathrm{C_fd}}) \tag{A.32}$$

$$i_{\mathrm{L_{fq}}}^{\mathrm{ref}} = u_{\mathrm{Vq}} + i_{\mathrm{L_cq}} + \omega_{\mathrm{s}}^{\mathrm{pu}} C_{\mathrm{f}} v_{\mathrm{C_fd}} \tag{A.33}$$

The voltage control output is the reference current to the current control loops. According to Figure A.8.b, the current control can be represented as follows:

$$\frac{\mathrm{d}x_{\mathrm{PIi}_{\mathrm{L_{fd}}}}}{\mathrm{d}t} = k_{\mathrm{iI_d}}(i_{\mathrm{L_fd}}^{\mathrm{ref}} - i_{\mathrm{L_fd}}) \tag{A.34}$$

$$u_{\mathrm{Id}} = x_{\mathrm{PIi}_{\mathrm{L_{fd}}}} + k_{p\mathrm{I_d}}(i_{\mathrm{L_fd}}^{\mathrm{ref}} - i_{\mathrm{L_fd}}) \tag{A.35}$$

$$v_{\mathrm{cd}} = u_{\mathrm{Id}} - \omega_{\mathrm{e}}^{\mathrm{pu}} L_{\mathrm{f}} i_{\mathrm{L_fq}} + v_{\mathrm{C_fd}} \tag{A.36}$$

$$\frac{\mathrm{d}x_{\mathrm{PIi}_{\mathrm{L_{fq}}}}}{\mathrm{d}t} = k_{\mathrm{iI_q}}(i_{\mathrm{L_fq}}^{\mathrm{ref}} - i_{\mathrm{L_fq}}) \tag{A.37}$$

$$u_{\mathrm{Iq}} = x_{\mathrm{PIi}_{\mathrm{L_{fq}}}} + k_{\mathrm{pI_q}}(i_{\mathrm{L_fq}}^{\mathrm{ref}} - i_{\mathrm{L_fq}}) \tag{A.38}$$

$$v_{\mathrm{cq}} = u_{\mathrm{Iq}} + \omega_{\mathrm{e}}^{\mathrm{pu}} L_{\mathrm{f}} i_{\mathrm{L_fd}} + v_{\mathrm{C_fq}} \tag{A.39}$$

Finally, the model of the AC filter of type LCL is obtained by applying circuit methods based on Kirchhoff laws to the schematic shown in Figure A.8 and the equations of RLC circuit element based on DPC depicted in Table 2.1. This yields to:

$$\frac{L_{\mathrm{f}}}{\omega_{\mathrm{b}}}\frac{\mathrm{d}i_{\mathrm{L_fd}}}{\mathrm{d}t} = v_{\mathrm{cd}} - v_{\mathrm{C_fd}} - R_{\mathrm{f}} i_{\mathrm{L_fd}} + \omega_{\mathrm{b}}^{\mathrm{pu}} L_{\mathrm{f}} i_{\mathrm{L_fq}} \tag{A.40}$$

$$\frac{L_{\mathrm{f}}}{\omega_{\mathrm{b}}}\frac{\mathrm{d}i_{\mathrm{L_fq}}}{\mathrm{d}t} = v_{\mathrm{cq}} - v_{\mathrm{C_fq}} - R_{\mathrm{f}} i_{\mathrm{L_fq}} - \omega_{\mathrm{b}}^{\mathrm{pu}} L_{\mathrm{f}} i_{\mathrm{L_fd}} \tag{A.41}$$

$$\frac{L_{\mathrm{c}}}{\omega_{\mathrm{b}}}\frac{\mathrm{d}i_{\mathrm{L_cd}}}{\mathrm{d}t} = v_{\mathrm{C_fd}} - v_{\mathrm{gd}} - R_{\mathrm{c}} i_{\mathrm{L_cd}} - \omega_{\mathrm{b}}^{\mathrm{pu}} L_{\mathrm{c}} i_{\mathrm{L_cq}} \tag{A.42}$$

$$\frac{L_{\mathrm{c}}}{\omega_{\mathrm{b}}}\frac{\mathrm{d}i_{\mathrm{L_cq}}}{\mathrm{d}t} = v_{\mathrm{C_fq}} - v_{\mathrm{gq}} - R_{\mathrm{c}} i_{\mathrm{L_cq}} + \omega_{\mathrm{b}}^{\mathrm{pu}} L_{\mathrm{c}} i_{\mathrm{L_cd}} \tag{A.43}$$

$$\frac{C_{\mathrm{f}}}{\omega_{\mathrm{b}}}\frac{\mathrm{d}v_{\mathrm{C_{fd}}}}{\mathrm{d}t} = i_{\mathrm{L_{fd}}} - i_{\mathrm{L_{cd}}} - \omega_{\mathrm{b}}^{\mathrm{pu}} C_{\mathrm{f}} v_{\mathrm{C_{fq}}} \tag{A.44}$$

$$\frac{C_{\mathrm{f}}}{\omega_{\mathrm{b}}}\frac{\mathrm{d}v_{\mathrm{C_{fq}}}}{\mathrm{d}t} = i_{\mathrm{L_{fq}}} - i_{\mathrm{L_{cq}}} + \omega_{\mathrm{b}}^{\mathrm{pu}} C_{\mathrm{f}} v_{\mathrm{C_{fd}}} \tag{A.45}$$

When the QPC model is used, the derivatives related to the state variables $i_{\mathrm{L_{cd}}}$ and $i_{\mathrm{L_{cq}}}$ are neglected, while the rest of the differential and algebraic equations are equal to the DPC models. Thus, the differential equations (A.42) and (A.43) become the algebraic equations (A.46) and (A.47), respectively.

$$0 = v_{\mathrm{C_{fd}}} - v_{\mathrm{gd}} - R_{\mathrm{c}} i_{\mathrm{L_{cd}}} - \omega_{\mathrm{b}}^{\mathrm{pu}} L_{\mathrm{c}} i_{\mathrm{L_{cq}}} \tag{A.46}$$

$$0 = v_{\mathrm{C_{fq}}} - v_{\mathrm{gq}} - R_{\mathrm{c}} i_{\mathrm{L_{cq}}} + \omega_{\mathrm{b}}^{\mathrm{pu}} L_{\mathrm{c}} i_{\mathrm{L_{cd}}} \tag{A.47}$$

The control system parameters of CIG-GFM considered in Chapter 4 are presented in Table A.1. The parameters are expressed in per unit system and are obtained from [148].

Table A.1. Control system parameters of CIG – GFM

Properties	Value
Inductance L_{f} of AC filter LCL	0.150
Resistance R_{f} of AC filter LCL	0.005
Inductance L_{c} of AC filter LCL	0.005
Resistance R_{c} of AC filter LCL	0.005
Capacitance C_{f} of AC filter LCL	0.066
Damping coefficient of virtual synchronous generator *D*	20.00
Inertia constant of virtual synchronous generator *H*	3.333
Proportional gain of the voltage controller $k_{\mathrm{pV_d}}, k_{\mathrm{pV_q}}$	0.520
Integral gain of the voltage controller $k_{\mathrm{iV_d}}, k_{\mathrm{iV_q}}$	1.160
Proportional gain of the current controller $k_{\mathrm{pI_d}}, k_{\mathrm{pI_q}}$	0.730
Integral gain of the current controller $k_{\mathrm{iI_d}}, k_{\mathrm{iI_q}}$	1.190
Time constant of reactive power measurement T_{fQ}	0.333

A.3 Synchronous Generator Model

For DPC models, the eighth-order model is used for synchronous generators using a steam turbine, whereas a seventh-order model is used for synchronous generators with hydraulic turbines. The derivations of these models can be found in books such as [118] and [2]. For this reason, in this document, we list the model without a detailed description of the derivations.

The set of differential equations of the eighth-order model for the synchronous generator are described by:

$$\frac{1}{\omega_{\mathrm{b}}}\frac{\mathrm{d}\psi_{\mathrm{ds}}}{\mathrm{d}t} = v_{\mathrm{ds}} + \omega_{\mathrm{r}}\psi_{\mathrm{qs}} + \frac{R_{\mathrm{s}}}{x_{\mathrm{ls}}}(\psi_{\mathrm{md}} - \psi_{\mathrm{ds}}) \tag{A.48}$$

$$\frac{1}{\omega_\mathrm{b}}\frac{\mathrm{d}\psi_\mathrm{qs}}{\mathrm{d}t} = v_\mathrm{qs} - \omega_\mathrm{r}\psi_\mathrm{ds} + \frac{R_\mathrm{s}}{x_\mathrm{ls}}\left(\psi_\mathrm{mq} - \psi_\mathrm{qs}\right) \tag{A.49}$$

$$\frac{1}{\omega_\mathrm{b}}\frac{\mathrm{d}\psi_\mathrm{fd}}{\mathrm{d}t} = \frac{R_\mathrm{fd}}{x_\mathrm{md}}E_\mathrm{fd} + \frac{R_\mathrm{fd}}{x_\mathrm{fd}}(\psi_\mathrm{md} - \psi_\mathrm{fd}) \tag{A.50}$$

$$\frac{1}{\omega_\mathrm{b}}\frac{\mathrm{d}\psi_\mathrm{1d}}{\mathrm{d}t} = v_\mathrm{1d} + \frac{R_\mathrm{1d}}{x_{1d}}(\psi_\mathrm{md} - \psi_\mathrm{1d}) \tag{A.51}$$

$$\frac{1}{\omega_\mathrm{b}}\frac{\mathrm{d}\psi_\mathrm{1q}}{\mathrm{d}t} = v_\mathrm{1q} + \frac{R_\mathrm{1q}}{x_\mathrm{1q}}\left(\psi_\mathrm{mq} - \psi_\mathrm{1q}\right) \tag{A.52}$$

$$\frac{1}{\omega_\mathrm{b}}\frac{\mathrm{d}\psi_\mathrm{2q}}{\mathrm{d}t} = v_\mathrm{2q} + \frac{R_\mathrm{2q}}{x_\mathrm{2q}}\left(\psi_\mathrm{mq} - \psi_\mathrm{2q}\right) \tag{A.53}$$

$$\frac{\mathrm{d}\omega_\mathrm{r}}{\mathrm{d}t} = \frac{1}{2H}\left(T_\mathrm{m} - T_\mathrm{e} - D(\omega_\mathrm{r} - 1)\right) \tag{A.54}$$

$$\frac{\mathrm{d}\delta}{\mathrm{d}t} = \omega_\mathrm{b}(\omega_\mathrm{r} - 1) \tag{A.55}$$

The state variables are the stator and rotor flux linkages, rotor angular velocity, and the angular position of the rotor. The stator currents must be known to interconnect the synchronous generators with the network. These currents can be expressed as functions of the stator and rotor flux linkages as follows:

$$i_\mathrm{ds} = \frac{1}{x_\mathrm{ls}}(\psi_\mathrm{md} - \psi_\mathrm{ds}) \tag{A.56}$$

$$i_\mathrm{qs} = \frac{1}{x_\mathrm{ls}}\left(\psi_\mathrm{mq} - \psi_\mathrm{qs}\right) \tag{A.57}$$

$$i_\mathrm{fd} = \frac{1}{x_\mathrm{fd}}(\psi_\mathrm{fd} - \psi_\mathrm{md}) \tag{A.58}$$

$$i_\mathrm{1d} = \frac{1}{x_\mathrm{1d}}(\psi_\mathrm{1d} - \psi_\mathrm{md}) \tag{A.59}$$

$$i_\mathrm{1q} = \frac{1}{x_\mathrm{1q}}\left(\psi_\mathrm{1q} - \psi_\mathrm{mq}\right) \tag{A.60}$$

$$i_\mathrm{2q} = \frac{1}{x_\mathrm{2q}}\left(\psi_\mathrm{2q} - \psi_\mathrm{mq}\right) \tag{A.61}$$

Furthermore, the set of equations relies on the following definitions:

$$\psi_\mathrm{md} = x_\mathrm{ad}\left(\frac{\psi_\mathrm{ds}}{x_\mathrm{ls}} + \frac{\psi_\mathrm{fd}}{x_\mathrm{fd}} + \frac{\psi_\mathrm{1d}}{x_\mathrm{1d}}\right) \tag{A.62}$$

$$\psi_\mathrm{mq} = x_\mathrm{aq}\left(\frac{\psi_\mathrm{qs}}{x_\mathrm{ls}} + \frac{\psi_\mathrm{1q}}{x_\mathrm{1q}} + \frac{\psi_\mathrm{2q}}{x_\mathrm{2q}}\right) \tag{A.63}$$

$$x_\mathrm{ad} = \left(\frac{1}{x_\mathrm{md}} + \frac{1}{x_\mathrm{ls}} + \frac{1}{x_\mathrm{lfd}} + \frac{1}{x_\mathrm{l1d}}\right)^{-1} \tag{A.64}$$

$$x_\mathrm{aq} = \left(\frac{1}{x_\mathrm{mq}} + \frac{1}{x_\mathrm{ls}} + \frac{1}{x_\mathrm{l1q}} + \frac{1}{x_\mathrm{l2q}}\right)^{-1} \tag{A.65}$$

$$T_{\mathrm{e}} = i_{\mathrm{qs}}\psi_{\mathrm{ds}} - i_{\mathrm{ds}}\psi_{\mathrm{qs}} \tag{A.66}$$

The seventh-order model of the synchronous generator is shown below. For this model, there is only one damper circuit on the q-axis. Therefore, the set of equations is kept with this small difference as follows:

$$\frac{1}{\omega_{\mathrm{b}}}\frac{\mathrm{d}\psi_{\mathrm{ds}}}{\mathrm{d}t} = v_{\mathrm{ds}} + \omega_{\mathrm{r}}\psi_{\mathrm{qs}} + \frac{R_{\mathrm{s}}}{x_{\mathrm{ls}}}(\psi_{\mathrm{md}} - \psi_{\mathrm{ds}}) \tag{A.67}$$

$$\frac{1}{\omega_{\mathrm{b}}}\frac{\mathrm{d}\psi_{\mathrm{qs}}}{\mathrm{d}t} = v_{\mathrm{qs}} - \omega_{\mathrm{r}}\psi_{\mathrm{ds}} + \frac{R_{\mathrm{s}}}{x_{\mathrm{ls}}}\left(\psi_{\mathrm{mq}} - \psi_{\mathrm{qs}}\right) \tag{A.68}$$

$$\frac{1}{\omega_{\mathrm{b}}}\frac{\mathrm{d}\psi_{\mathrm{fd}}}{\mathrm{d}t} = \frac{R_{\mathrm{fd}}}{x_{\mathrm{md}}}E_{\mathrm{fd}} + \frac{R_{\mathrm{fd}}}{x_{\mathrm{fd}}}(\psi_{\mathrm{md}} - \psi_{\mathrm{fd}}) \tag{A.69}$$

$$\frac{1}{\omega_{\mathrm{b}}}\frac{\mathrm{d}\psi_{1\mathrm{d}}}{\mathrm{d}t} = v_{1\mathrm{d}} + \frac{R_{1\mathrm{d}}}{x_{1\mathrm{d}}}(\psi_{\mathrm{md}} - \psi_{1\mathrm{d}}) \tag{A.70}$$

$$\frac{1}{\omega_{\mathrm{b}}}\frac{\mathrm{d}\psi_{1\mathrm{q}}}{\mathrm{d}t} = v_{1\mathrm{q}} + \frac{R_{1\mathrm{q}}}{x_{1\mathrm{q}}}\left(\psi_{\mathrm{mq}} - \psi_{1\mathrm{q}}\right) \tag{A.71}$$

$$\frac{\mathrm{d}\omega_{\mathrm{r}}}{\mathrm{d}t} = \frac{1}{2H}\left(T_{\mathrm{m}} - T_{\mathrm{e}} - D(\omega_{\mathrm{r}} - 1)\right) \tag{A.72}$$

$$\frac{\mathrm{d}\delta}{\mathrm{d}t} = \omega_{\mathrm{b}}(\omega_{\mathrm{r}} - 1) \tag{A.73}$$

The state variables are the stator and rotor flux linkages, rotor angular velocity, and the angular position of the rotor. In order to interconnect the synchronous generators with the transmission network, the stator currents are to be known. These currents can be expressed as functions of the stator and rotor flux linkages as follows:

$$i_{\mathrm{ds}} = \frac{1}{x_{\mathrm{ls}}}(\psi_{\mathrm{md}} - \psi_{\mathrm{ds}}) \tag{A.74}$$

$$i_{\mathrm{qs}} = \frac{1}{x_{\mathrm{ls}}}\left(\psi_{\mathrm{mq}} - \psi_{\mathrm{qs}}\right) \tag{A.75}$$

$$i_{\mathrm{fd}} = \frac{1}{x_{\mathrm{fd}}}(\psi_{\mathrm{fd}} - \psi_{\mathrm{md}}) \tag{A.76}$$

$$i_{1\mathrm{d}} = \frac{1}{x_{1\mathrm{d}}}(\psi_{1\mathrm{d}} - \psi_{\mathrm{md}}) \tag{A.77}$$

$$i_{1\mathrm{q}} = \frac{1}{x_{1\mathrm{q}}}\left(\psi_{1\mathrm{q}} - \psi_{\mathrm{mq}}\right) \tag{A.78}$$

Furthermore, the above set of the equations requires to define the following terms:

$$\psi_{\mathrm{md}} = x_{\mathrm{ad}}\left(\frac{\psi_{\mathrm{ds}}}{x_{\mathrm{ls}}} + \frac{\psi_{\mathrm{fd}}}{x_{\mathrm{fd}}} + \frac{\psi_{1\mathrm{d}}}{x_{1\mathrm{d}}}\right) \tag{A.79}$$

$$\psi_{\mathrm{mq}} = x_{\mathrm{aq}}\left(\frac{\psi_{\mathrm{qs}}}{x_{\mathrm{ls}}} + \frac{\psi_{1\mathrm{q}}}{x_{1\mathrm{q}}}\right) \tag{A.80}$$

$$x_{\mathrm{ad}} = \left(\frac{1}{x_{\mathrm{md}}} + \frac{1}{x_{\mathrm{ls}}} + \frac{1}{x_{\mathrm{lfd}}} + \frac{1}{x_{\mathrm{l1d}}}\right)^{-1} \tag{A.81}$$

$$x_{\mathrm{aq}} = \left(\frac{1}{x_{\mathrm{mq}}} + \frac{1}{x_{\mathrm{ls}}} + \frac{1}{x_{\mathrm{l1q}}}\right)^{-1} \tag{A.82}$$

$$T_{\mathrm{e}} = i_{\mathrm{qs}}\psi_{\mathrm{ds}} - i_{\mathrm{ds}}\psi_{\mathrm{qs}} \tag{A.83}$$

As is explained in Section 3.2.1, when the system is modeled by QPC, the derivatives of the stator flux linkages in the eighth- and seventh-order models are neglected. Therefore, for the eighth-order model, the differential equations (A.48) and (A.49) related to the stator flux linkages become algebraic equations. For the seventh-order model, differential equations (A.67) and (A.68) related to the stator flux linkages become algebraic equations. This, in turn, leads to a reduction in the order of the synchronous generator models. A sixth-order model is used for synchronous generators using a steam turbine, whereas a fifth-order model is used for synchronous generators with hydraulic turbines. The algebraic equations related to the stator flux linkages of the synchronous generator are described as follows:

$$0 = R_{\mathrm{s}} i_{\mathrm{ds}} + \omega_{\mathrm{r}}\psi_{\mathrm{qs}} + v_{\mathrm{ds}} \tag{A.84}$$

$$0 = R_{\mathrm{s}} i_{\mathrm{qs}} - \omega_{\mathrm{r}}\psi_{\mathrm{ds}} + v_{\mathrm{qs}} \tag{A.85}$$

In addition, it is assumed that $\omega_{\mathrm{r}} \approx 1$ in the stator voltage equations. This in turn means that the speed changes are small and do not significantly affect the stator voltages [4]. Finally, the differential equations from (A.48) to (A.55) are retained for the sixth-order model, whereas the differential equations from (A.69) to (A.73) are retained for the fifth-order model.

The synchronous generator model comprises several circuit parameters. Therefore, such parameters must be calculated from the typical operational data of synchronous generators. We used the “classical definitions” presented in chapter 4 of the book [4] to calculate the circuit parameters. It is not presented here because a complete description can be found in the cited reference. The following table shows the parameters associated with the model of the synchronous generators used for both modeling techniques.

Table A.2. Description of synchronous generator parameters.

Parameter	Description
R_s, R_{fd}, R_{1d}, R_{1q}, and R_{2q}	Resistance of the windings related to the stator, excitation, d-axis damper circuit, first q-axis damper circuit, and second q-axis damper circuit
x_d, x_q	Reactance of d- and q axis
x_{ls}	Stator leakage reactance
x_{md} and x_{mq}	Magnetizing reactance of d- and q-axis
x_{l1d} and x_{1d}	Leakage reactance and reactance related to the damper circuit of d-axis
x_{lfd} and x_{fd}	Leakage reactance and reactance related to the field circuit of d-axis
x_{l1q} and x_{1q}	Leakage reactance and reactance of the first damper circuit of q-axis
x_{l2q} and x_{2q}	Leakage reactance and reactance of the second damper circuit of q-axis
i_{ds}, i_{fd}, and i_{1d}	Stator, field, and damper circuit currents of d-axis
i_{qs}, i_{1q}, and i_{2q}	Stator, first, and second damper circuit currents of q-axis
v_{ds}, v_{1d}	Stator and damper circuit voltages of d-axis
v_{qs}, v_{1q} and v_{2q}	Stator and two damper circuit voltages of q-axis
ψ_{ds}, ψ_{fd}, and ψ_{1d}	Stator, field, and damper circuit fluxes of d-axis
ψ_{qs}, ψ_{1q}, and ψ_{2q}	Stator and the two damper circuit fluxes of q-axis
T_m, T_e	Mechanical and electrical torques
D	Damping factor
H	Inertia constant

A.4 Transmission lines, transformers, and loads

The transmission lines are modeled using π equivalent circuits with lumped parameters. Transformers are presented through series RL circuits. Loads are modeled as constant impedances, which are series RL circuits. For the system modeled using DPC, all these components can be represented by the state-space model of the form:

$$\dot{\boldsymbol{x}} = \boldsymbol{A}\boldsymbol{x} + \boldsymbol{B}\boldsymbol{u} \tag{A.86}$$

Using the RLC representation using DPC is shown in Table 2.1. Comparison of RLC representation of the paper, the state model of the electric network, including transmission lines, transformers, and loads, was obtained. The complete model can be obtained by applying circuit methods based on Kirchhoff laws. The voltages related to capacitors and the currents related to inductances are the state variables of the electric network. As the dynamic phasor signal is complex, the differential

equations associated with the electric network are separated by real and imaginary parts. In particular, we follow the method developed in [238] to build the state space matrix $\boldsymbol{A}$, which is also cited in Table II.

The electric network, including transmission lines, transformers, and loads, is represented by the same RLC circuits used in DPC-based models for the system modeled using QPC. However, since the derivatives associated with capacitor voltages and currents in inductors are neglected in QPC, the electric network is represented by algebraic equations. Therefore, the electric network can be represented through an admittance matrix $\underline{\boldsymbol{Y}}$ [4]. This matrix was used to model the power system considering the current injection model [6].

Annex B: Power System Models Used in Chapter 5

This appendix describes the CIG-GFL, CIG-GFM models based on DPC and CIG-GFL, and CIG-GFM models based on QPC used in Chapter 5. The synchronous generators, transformers, and loads models are identical to the model used in Chapter 4. These models are not described in Appendix B because a detailed description can be found in Appendix A, Sections A.3 and A.4. First, we present CIG-GFL models based on DPC and QPC. Finally, the CIG-GFM model with droop control using DPC and QPC.

B.1 CIG-GFL Model Based on DPC

The CIG-GFL models described in the section use the schematic diagram shown in Figure B.1. Regarding the CIG-GFL based on DPC, an average VSC model is considered where the switching transients are neglected. The active power control, voltage control, PLL, inner control loops, and VFF terms are implemented. The control systems implemented are displayed from Figure B.2 to Figure B.6.

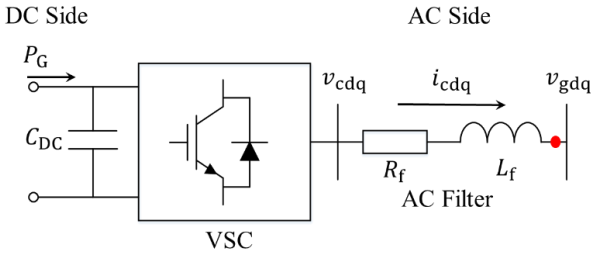

Figure B.1. Diagram of CIG connected to the grid that operates in GFL mode [125]

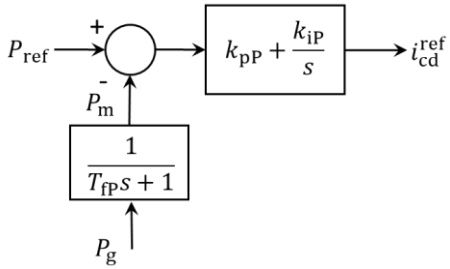

Figure B.2. Active power control

The state-space model of the active power control is obtained from the block diagram shown in Figure B.2. The differential and algebraic equations (B.1) - (B.4) represent the active power control.

$$\frac{dP_m}{dt} = \frac{1}{T_{fP}}\left(P_g - P_m\right) \tag{B.1}$$

$$P_g = v_{gd}i_{cd} + v_{gq}i_{cq} \tag{B.2}$$

$$\frac{\mathrm{d}xPI_{\mathrm{P}}}{\mathrm{d}t} = k_{\mathrm{pP}}(P_{\mathrm{ref}} - P_{\mathrm{m}}) \tag{B.3}$$

$$i_{\mathrm{cd}}^{\mathrm{ref}} = k_{\mathrm{pP}}(P_{\mathrm{ref}} - P_{\mathrm{m}}) + xPI_{\mathrm{P}} \tag{B.4}$$

The voltage control implemented is shown in Figure B.3. The current on the q axis controls the voltage at the PCC.

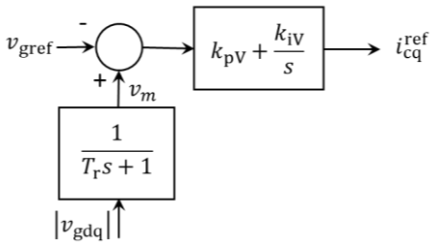

Figure B.3. Voltage control

According to the block diagram in Figure B.3, the voltage control model is described as follows:

$$\frac{\mathrm{d}v_{\mathrm{m}}}{\mathrm{d}t} = \frac{1}{T_{\mathrm{r}}}\left(\left|v_{\mathrm{gdq}}\right| - v_{\mathrm{m}}\right) \tag{B.5}$$

$$\frac{\mathrm{d}xPI_{\mathrm{V}}}{\mathrm{d}t} = k_{\mathrm{iV}}(v_{\mathrm{m}} - v_{\mathrm{ref}}) \tag{B.6}$$

$$i_{\mathrm{cq}}^{\mathrm{ref}} = k_{\mathrm{pV}}(v_{\mathrm{m}} - v_{\mathrm{ref}}) + xPI_{\mathrm{V}} \tag{B.7}$$

The SRF - PLL shown in Figure B.4 is modeled by equations (B.8)-(B.11). Compared to the PLL used in Chapter 4, the PLL of Chapter 5 uses as input the voltage v_{gqm}. This term is the ouput from VFF term. In Chapter 4 this term is not considered.

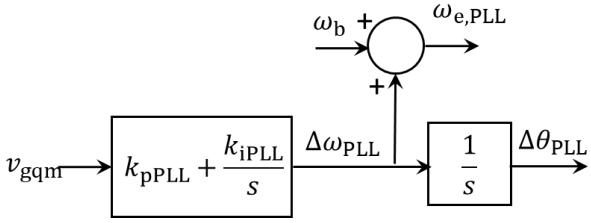

Figure B.4. SRF - PLL

$$\frac{\mathrm{d}xPI_{\mathrm{PLL}}}{\mathrm{d}t} = k_{\mathrm{iPLL}}v_{\mathrm{gqm}} \tag{B.8}$$

$$\Delta\omega_{\mathrm{PLL}} = k_{\mathrm{pPLL}}v_{\mathrm{gq}} + xPI_{\mathrm{PLL}} \tag{B.9}$$

$$\omega_{\mathrm{e,PLL}} = \Delta\omega_{\mathrm{PLL}} + \omega_{\mathrm{b}} \tag{B.10}$$

$$\frac{\mathrm{d}\Delta\theta_{\mathrm{PLL}}}{\mathrm{d}t} = \Delta\omega_{\mathrm{PLL}} \tag{B.11}$$

The inner current control with decoupling and VFF term can be seen in Figure B.5 and Figure B.6, respectively.

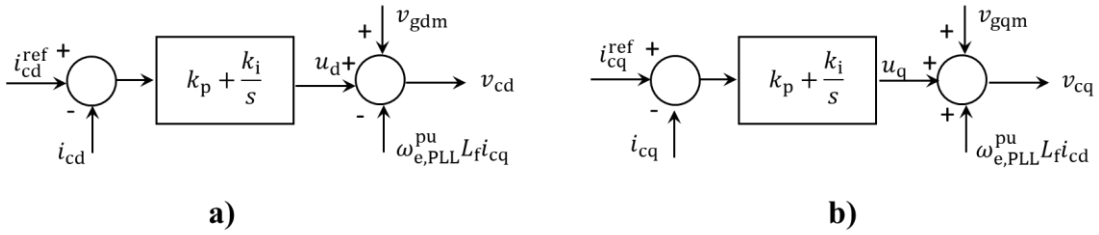

Figure B.5. Current control loops; a) current controller on the d-axis; b) current controller on the q-axis

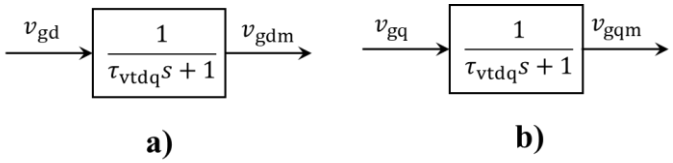

Figure B.6. Feed-forward terms; a) d-axis; b) q-axis

The model of this control loop is described as follows:

$$\frac{\mathrm{d}xPI_{\mathrm{i_{cd}}}}{\mathrm{d}t} = k_{\mathrm{i}}(i_{\mathrm{cd}}^{\mathrm{ref}} - i_{\mathrm{cd}}) \tag{B.12}$$

$$u_{\mathrm{d}} = xPI_{\mathrm{i_{cd}}} + k_{\mathrm{p}}(i_{\mathrm{cd}}^{\mathrm{ref}} - i_{\mathrm{cd}}) \tag{B.13}$$

$$v_{\mathrm{cd}} = u_{\mathrm{d}} - \omega_{\mathrm{e}}^{\mathrm{pu}} L_{\mathrm{f}} i_{\mathrm{cq}} + v_{\mathrm{gdm}} \tag{B.14}$$

$$\frac{\mathrm{d}xPI_{\mathrm{i_{cq}}}}{\mathrm{d}t} = k_{\mathrm{i}}(i_{\mathrm{cq}}^{\mathrm{ref}} - i_{\mathrm{cq}}) \tag{B.15}$$

$$u_{\mathrm{q}} = xPI_{\mathrm{i_{cq}}} + k_{\mathrm{p}}(i_{\mathrm{cq}}^{\mathrm{ref}} - i_{\mathrm{cq}}) \tag{B.16}$$

$$v_{\mathrm{cq}} = u_{\mathrm{q}} + \omega_{\mathrm{e}}^{\mathrm{pu}} L_{\mathrm{f}} i_{\mathrm{cd}} + v_{\mathrm{gqm}} \tag{B.17}$$

$$\frac{\mathrm{d}v_{\mathrm{gdm}}}{\mathrm{d}t} = \frac{1}{\tau_{\mathrm{vtdq}}}\left(v_{\mathrm{gd}} - v_{\mathrm{gdm}}\right) \tag{B.18}$$

$$\frac{\mathrm{d}v_{\mathrm{gqm}}}{\mathrm{d}t} = \frac{1}{\tau_{\mathrm{vtdq}}}\left(v_{\mathrm{gq}} - v_{\mathrm{gqm}}\right) \tag{B.19}$$

Finally, the coupling inductance (AC Filter of type L) is given by:

$$\frac{L_{\mathrm{f}}}{\omega_{\mathrm{b}}}\frac{\mathrm{d}i_{\mathrm{cd}}}{\mathrm{d}t} = v_{\mathrm{cd}} - R_{\mathrm{f}} i_{\mathrm{cd}} + L_{\mathrm{f}} i_{\mathrm{cq}} - v_{\mathrm{gd}} \tag{B.20}$$

$$\frac{L_{\mathrm{f}}}{\omega_{\mathrm{b}}}\frac{\mathrm{d}i_{\mathrm{cq}}}{\mathrm{d}t} = v_{\mathrm{cq}} - R_{\mathrm{f}} i_{\mathrm{cq}} - L_{\mathrm{f}} i_{\mathrm{cd}} - v_{\mathrm{gq}} \tag{B.21}$$

B.2 CIG-GFL Models Based on QPC

This section describes the CIG models based on QPC. Due to the modularity of the control structure typically implemented in CIG, the CIG models considered in Chapter 0 and presented in Table 2.4 can use the same outer control loops and SRF-PLL. Therefore, the model related to the outer control presented in the previous section applies to CIG models based on QPC. Specifically, active power and voltage control are applied. In the case of the SRF-PLL, the model related to Figure B.4 is used when the CIG models based on QPC are considered.

This section focuses on the assumptions made in CIG models based on QPC. The description is done according to similarities present in some CIG models. For instance, the only difference between CS-Type I and CS-Type II is the implementation of PLL. The CS-Type II model considers a PLL, and the CS-Type I model does not.

Firstly, the current source models CS-Type I and CS-Type II are described. Figure B.7 shows the block diagram used to develop the model. Equations (B.22) and (B.23) are used. Additionally, the CS-Type II model implements the SRF-PLL by equations (B.8) and (B.11).

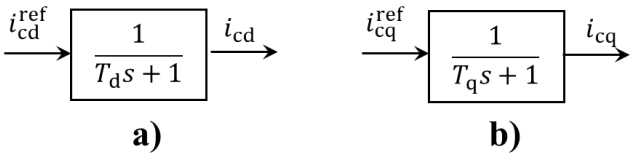

Figure B.7. Current source model based on a transfer function

$$\frac{\mathrm{d}i_{\mathrm{cd}}}{\mathrm{d}t} = \frac{1}{T_{\mathrm{d}}}\left(i_{\mathrm{cd}}^{\mathrm{ref}} - i_{\mathrm{cd}}\right) \tag{B.22}$$

$$\frac{\mathrm{d}i_{\mathrm{cq}}}{\mathrm{d}t} = \frac{1}{T_{\mathrm{q}}}\left(i_{\mathrm{cq}}^{\mathrm{ref}} - i_{\mathrm{cq}}\right) \tag{B.23}$$

Secondly, the VS-Type I and VS-Type IV are described. These models are based on a voltage-controlled representation. There are slight differences. Accordingly, these models are jointly explained. VS-Type I is similar to the CIG model based on DPC, except that VFF terms are neglected, and algebraic equations represent the AC filter. Therefore, the same equations can be used, assuming $v_{\mathrm{gdq}} = v_{\mathrm{gdqm}}$ Furthermore, the AC filter is as follows:

$$0 = v_{\mathrm{cd}} - R_{\mathrm{f}} i_{\mathrm{cd}} + L_{\mathrm{f}} i_{\mathrm{cq}} - v_{\mathrm{gd}} \tag{B.24}$$

$$0 = v_{\mathrm{cq}} - R_{\mathrm{f}} i_{\mathrm{cq}} - L_{\mathrm{f}} i_{\mathrm{cd}} - v_{\mathrm{gq}} \tag{B.25}$$

As these equations are expressed in pu system, $x_{\mathrm{f}} = L_{\mathrm{f}}$. For this reason, the angular frequency ω_{b} is omitted in equations (B.24) and (B.25).

VS-Type IV differs from the latter only by representing the AC filter. In this case, the AC filter is modeled through differential equations (B.20) and (B.21).

Thirdly, the VS-Type II model is developed. This model does not include decoupling and VFF terms, as shown in Figure B.8. Further, the AC filter is represented by algebraic equations using (B.24) and (B.25).

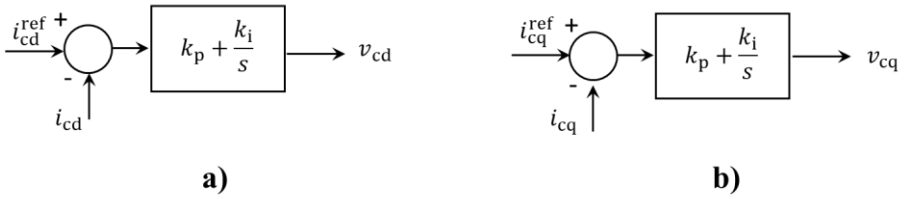

Figure B.8. Inner current control loops without decoupling and feedforward terms; a) d-axis; b) q-axis

The following algebraic equations represent VS-Type II.

$$v_{dc} = k_p\left(i_{dg}^{ref} - i_{dg}\right) + xPI_{i_{cd}} \tag{B.26}$$

$$v_{qc} = k_p\left(i_{qg}^{ref} - i_{qg}\right) + xPI_{i_{cq}} \tag{B.27}$$

Fourthly, VS-Type III and VS-Type VI are described. VS-Type III does not represent the PLL, and VS-Type VI does. Figure B.9 shows a diagram related to this model.

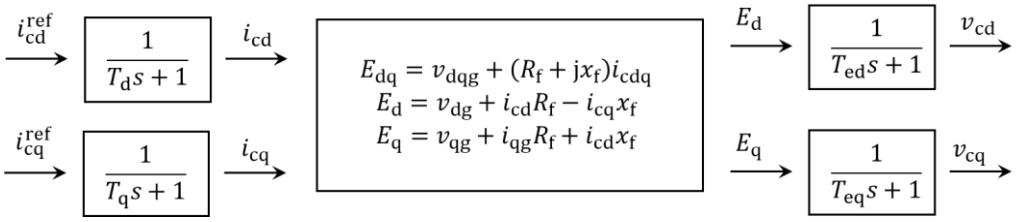

Figure B.9. The CIG model developed in [35]

The set of differential-algebraic equations, considering $x_f = L_f$ because the quantities are in pu system, are given by:

$$\frac{di_{cd}}{dt} = \frac{1}{T_d}\left(i_{cd}^{ref} - i_{cd}\right) \tag{B.28}$$

$$\frac{di_{cq}}{dt} = \frac{1}{T_q}\left(i_{cq}^{ref} - i_{cq}\right) \tag{B.29}$$

$$E_d = v_{gd} + R_f i_{cd} - i_{cq}L_f \tag{B.30}$$

$$E_q = v_{gq} + R_f i_{cq} + i_{cd}L_f \tag{B.31}$$

$$\frac{dv_{cd}}{dt} = \frac{1}{T_{ed}}\left(E_d - v_{cd}\right) \tag{B.32}$$

$$\frac{\mathrm{d}v_{\mathrm{cq}}}{\mathrm{d}t} = \frac{1}{T_{\mathrm{eq}}}\left(E_q - v_{\mathrm{cq}}\right) \tag{B.33}$$

Finally, the VS – Type V model is developed. The main difference from the DPC model is that VFF is not represented, and the AC filter is of type LCL. There are differential equations for modeling the LC part of the AC filter and algebraic equations for modeling the second inductance L of the AC filter. Also, the VFF terms are not implemented. The diagram related to CIG-GFM shown in Figure A.5 is used for this model. The current control loops used in this model are shown in Figure B.10. Taking into account the block diagram of this figure, the following equations are developed to model the current control loops.

$$\frac{\mathrm{d}xPI_{\mathrm{i}_{\mathrm{L_{fd}}}}}{\mathrm{d}t} = k_{\mathrm{i}}(i_{\mathrm{L_{fd}}}^{\mathrm{ref}} - i_{\mathrm{L_{fd}}}) \tag{B.34}$$

$$u_{\mathrm{Id}} = xPI_{\mathrm{i}_{\mathrm{L_{fd}}}} + k_{\mathrm{p}}(i_{\mathrm{L_{fd}}}^{\mathrm{ref}} - i_{\mathrm{L_{fd}}}) \tag{B.35}$$

$$v_{\mathrm{cd}} = u_{\mathrm{Id}} - \omega_{\mathrm{e}}^{\mathrm{pu}} L_{\mathrm{f}} i_{\mathrm{L_{fq}}} + v_{\mathrm{C_{fd}}} \tag{B.36}$$

$$\frac{\mathrm{d}xPI_{\mathrm{i}_{\mathrm{L_{fq}}}}}{\mathrm{d}t} = k_{\mathrm{i}}(i_{\mathrm{L_{fq}}}^{\mathrm{ref}} - i_{\mathrm{L_{fq}}}) \tag{B.37}$$

$$u_{\mathrm{Iq}} = xPI_{\mathrm{i}_{\mathrm{L_{fq}}}} + k_{\mathrm{pI_q}}(i_{\mathrm{L_{fq}}}^{\mathrm{ref}} - i_{\mathrm{L_{fq}}}) \tag{B.38}$$

$$v_{\mathrm{cq}} = u_{\mathrm{Iq}} + \omega_{\mathrm{e}}^{\mathrm{pu}} L_{\mathrm{f}} i_{\mathrm{L_{fd}}} + v_{\mathrm{C_{fq}}} \tag{B.39}$$

The AC filter LCL is defined by:

$$\frac{L_{\mathrm{f}}}{\omega_{\mathrm{b}}}\frac{\mathrm{d}i_{\mathrm{L_{fd}}}}{\mathrm{d}t} = v_{\mathrm{cd}} - v_{\mathrm{C_{fd}}} - R_{\mathrm{f}} i_{\mathrm{L_{fd}}} - \omega_{\mathrm{b}}^{\mathrm{pu}} L_{\mathrm{f}} i_{\mathrm{L_{fq}}} \tag{B.40}$$

$$\frac{L_{\mathrm{f}}}{\omega_{\mathrm{b}}}\frac{\mathrm{d}i_{\mathrm{L_{fq}}}}{\mathrm{d}t} = v_{\mathrm{cq}} - v_{\mathrm{C_{fq}}} - R_{\mathrm{f}} i_{\mathrm{L_{fq}}} - \omega_{\mathrm{b}}^{\mathrm{pu}} L_{\mathrm{f}} i_{\mathrm{L_{fd}}} \tag{B.41}$$

$$\frac{L_{\mathrm{c}}}{\omega_{\mathrm{b}}}\frac{\mathrm{d}i_{\mathrm{L_{cd}}}}{\mathrm{d}t} = v_{\mathrm{C_{fd}}} - v_{\mathrm{gd}} - R_{\mathrm{c}} i_{\mathrm{L_{cd}}} - \omega_{\mathrm{b}}^{\mathrm{pu}} L_{\mathrm{c}} i_{\mathrm{L_{cq}}} \tag{B.42}$$

$$\frac{L_{\mathrm{c}}}{\omega_{\mathrm{b}}}\frac{\mathrm{d}i_{\mathrm{L_{cq}}}}{\mathrm{d}t} = v_{\mathrm{C_{fq}}} - v_{\mathrm{gq}} - R_{\mathrm{c}} i_{\mathrm{L_{cq}}} + \omega_{\mathrm{b}}^{\mathrm{pu}} L_{\mathrm{c}} i_{\mathrm{L_{cd}}} \tag{B.43}$$

$$0 = v_{\mathrm{C_{fd}}} - v_{\mathrm{gd}} - R_{\mathrm{c}} i_{\mathrm{L_{cd}}} - \omega_{\mathrm{b}}^{\mathrm{pu}} L_{\mathrm{c}} i_{\mathrm{L_{cq}}} \tag{B.44}$$

$$0 = v_{\mathrm{C_{fq}}} - v_{\mathrm{gq}} - R_{\mathrm{c}} i_{\mathrm{L_{cq}}} + \omega_{\mathrm{b}}^{\mathrm{pu}} L_{\mathrm{c}} i_{\mathrm{L_{cd}}} \tag{B.45}$$

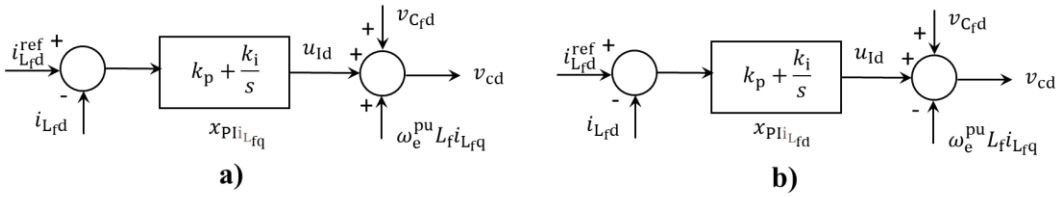

Figure B.10. Current control loops; a) current controller on the d-axis; b) current controller on the q-axis

B.3 CIG-GFM Model

The CIG-GFM model used in Chapter 5 is only used for the case of 100% of the CIG level. Droop-based active power controllers (see Figure B.11) and droop-based reactive power controllers (see Figure A.7) are used for outer loops. Voltage and current controllers are used for inner control loops. These are the same used in the CIG-GFM with the virtual synchronous generator model described in appendix A. it is also considered an AC filter LCL. As a result, the equations (A.25)-(A.47) are also considered in this model. It is included the DPQ and QPC-based models. Instead of using virtual synchronous generator control, droop control is used. The block diagram associated with the droop control is shown in Figure B.11 and its model in equations (B.46)-(B.49).

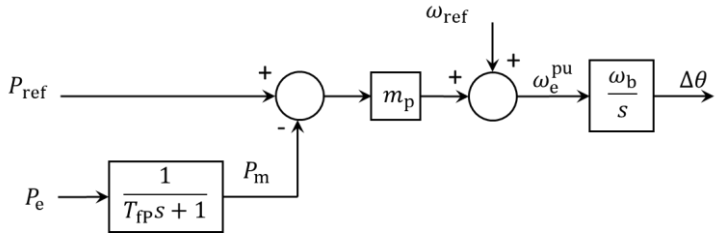

Figure B.11. Droop-based active power controller

$$\omega_\mathrm{e}^{\mathrm{pu}} = \omega^{\mathrm{ref}} + m_\mathrm{p}\left(P^{\mathrm{ref}} - P_\mathrm{m}\right) \tag{B.46}$$

$$\frac{\mathrm{d}\Delta\theta}{\mathrm{d}t} = \omega_\mathrm{b}\omega_\mathrm{e}^{\mathrm{pu}} \tag{B.47}$$

$$P_\mathrm{e} = v_{\mathrm{C_fd}} i_{\mathrm{L_cd}} + v_{\mathrm{C_fq}} i_{\mathrm{L_cq}} \tag{B.48}$$

$$\frac{\mathrm{d}P_\mathrm{m}}{\mathrm{d}t} = \frac{1}{T_{\mathrm{fP}}}\left(P_\mathrm{e} - P_\mathrm{m}\right) \tag{B.49}$$

B.4 Parameter of CIG Models

Table B.1 shows the control parameters related to CIG-GFM with droop control considering DPC and QPC approaches. The parameter used in each CIG-GFL model based on QPC are depicted in Table B.2. In red are marked the CIG models that do not consider the particular parameter, and in green are marked the CIG models that consider the particular parameter.

Table B.1. Control system parameters of CIG – GFM with droop control for DPC and QPC based models

Properties	Value
Inductance L_{f} of AC filter LCL	0.150
Resistance R_{f} of AC filter LCL	0.005
Inductance L_{c} of AC filter LCL	0.005
Resistance R_{c} of AC filter LCL	0.005
Capacitance C_{f} of AC filter LCL	0.066
Time constant of active power measurement T_{fP}	0.333
Droop coefficient m_{p}	0.05
Damping coefficient of virtual synchronous generator D	20.00
Inertia constant of virtual synchronous generator H	3.333
Proportional gain of the voltage controller $k_{\mathrm{pV_d}}, k_{\mathrm{pV_q}}$	0.520
Integral gain of the voltage controller $k_{\mathrm{iV_d}}, k_{\mathrm{iV_q}}$	1.160
Proportional gain of the current controller $k_{\mathrm{pI_d}}, k_{\mathrm{pI_q}}$	0.730
Integral gain of the current controller $k_{\mathrm{iI_d}}, k_{\mathrm{iI_q}}$	1.190
Time constant of reactive power measurement T_{fQ}	0.333

Table B.2. Control system parameters of CIG-GFL units considering QPC-based approach

Properties	Value	CS-Type I	CS-Type II	VS-Type I	VS-Type II	VS-Type III	VS-Type IV	VS-Type V	VS-Type VI
Inductance L_f of AC filter LC and LCL	0.34643	☒	☒	☑	☑	☑	☑	☑	☑
Resistance R_f of AC filter LC and LCL	0.03938	☒	☒	☑	☑	☑	☑	☑	☑
Inductance L_c of AC filter LCL	0.03	☒	☒	☒	☒	☒	☒	☑	☒
Resistance R_c of AC filter LCL	0.0012	☒	☒	☒	☒	☒	☒	☑	☒
Capacitance C_f of AC filter LCL	0.0326	☒	☒	☒	☒	☒	☒	☑	☒
Proportional gain of the current controller k_p	0.40	☒	☒	☑	☑	☒	☑	☑	☒
Integral gain of the current controller k_i	90	☒	☒	☑	☑	☒	☑	☑	☒
Time constant of first transfer function, T_d and T_q of current source controlled representation	0.01	☑	☑	☒	☒	☒	☒	☒	☒
Time constant of first transfer function, T_d and T_q of voltage sourceontrolled representation	0.005	☒	☒	☒	☒	☑	☒	☒	☑
Time constant of first transfer function, T_{ed} and T_{eq}	0.005	☒	☒	☒	☒	☑	☒	☒	☑
Proportional gain of PLL controller k_{pPLL}	101	☒	☑	☑	☑		☑	☑	☑
Integral gain of PLL controller k_{iPLL}	2562	☒	☑	☑	☑		☑	☑	☑
Time constant of voltage measure T_r $[s]$	0.05	☑	☑	☑	☑	☑	☑	☑	☑
Proportional gain of voltage controller k_{pV}	5.00	☑	☑	☑	☑	☑	☑	☑	☑
Integral gain of voltage controller k_{iV}	25	☑	☑	☑	☑	☑	☑	☑	☑
Proportional gain of the active power controller k_{pP}	0.4	☑	☑	☑	☑	☑	☑	☑	☑
Integral gain of the active power controller k_{iP}	40	☑	☑	☑	☑	☑	☑	☑	☑
Time constant of active power measure T_{rP}	0.05	☑	☑	☑	☑	☑	☑	☑	☑
Droop coefficient m_p	0.05	☑	☑	☑	☑	☑	☑	☑	☑

Annex C: Acronyms and Abreviations

CIG	:	Converter interfaced generation
CIGRE	:	Conseil International des Grands Réseaux Electriques
DPC	:	Dynamic phasor calculus
EMT	:	Electromagnetic transient
EMTP	:	Electromagnetic transient program
EPRI	:	The Electric Power Research Institute
GE	:	General Electric
PCC	:	Point of common coupling
PLL	:	Phase- locked loop
PWM	:	Pulse width modulation
QPC	:	Quasi-static phasor calculus
RoCoF	:	Rate of change of frequency
SCL	:	Short circuit level
SCR	:	Short circuit ratios
SRF	:	Synchronous reference frame
TSO	:	Transmission system operator
ISO	:	Independent System Operator
UFLSS	:	Under frequency load shedding schemes
VSC	:	Voltage source converter
WECC	:	Western Electricity Coordinating Counsil
GFL	:	Grid following
GFM	:	Grid forming
PMSG	:	Permanent magnet synchronous generator

Annex D: Detailed Analyses Related to Chapter 5

This appendix presents the main results obtained by applying the methodology described in Section 3.2 (see Figure 3.3). These results are used for the summary and comparisons shown in Chapter 5. Sensitivity analysis based on modal analysis, the H-infinity norm $\|\boldsymbol{G}\|_\infty$ plots and time-domain simulations are presented in the appendix. Consequently, the results described validate the statements of Chapter 5. The results are shown below, starting with Stage 2 of the methodology.

D.1 Sensitivity Analysis

D.1.1 Case Study 1: Impacts PLL and CIG Levels

The PLL bandwidths and the CIG levels vary to perform the sensitivity analysis of this case study. The PLL bandwidth is changed from 2 to 80 Hz, which are typical values. The CIG levels up to 100%. The H-infinity norm $\|\boldsymbol{G}\|_\infty$ is used to summarize the main results. This case study does not implement frequency control in the CIG units.

Figure D.1 shows the H-infinity norm $\|\boldsymbol{G}\|_\infty$ for different levels of CIG and PLL bandwidths. To highlight operating conditions where the system is unstable and improve the readability of the plots, Figure D.1 considers the symbol ∞ on the y-axis. As the PLL bandwidth increases and the CIG levels also increase, the system represented using the DPC approach becomes unstable. This can be seen due to the norm $\|\boldsymbol{G}\|_\infty$ constantly increase without boundaries. Significant changes appear when the CIG levels take values higher than 35%. In that case, the synchronous generators G1 and G3 are disconnected, implying a decrement in the system's inertia and the SCR. In this scenario, generator G2 gives frequency support, and CIG1 and CIG3 give voltage support.

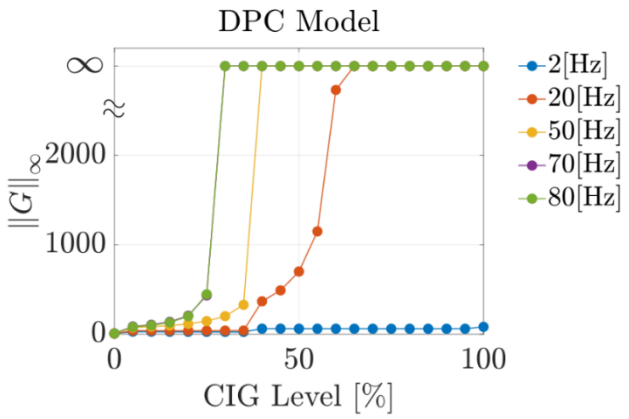

Figure D.1. $\|\boldsymbol{G}\|_\infty$ as a function of CIG penetration level and different PLL bandwidth frequencies in the DPC-based model

A comparison of the H-infinity norm $\|\boldsymbol{G}\|_\infty$ among the CIG models using DPC and QPC approaches is shown in Figure D.2. PLL bandwidths of 2 Hz and 20 Hz are considered because the results obtained from the DPC models indicate that the system is small signal stable and unstable, respectively. Therefore, it can be seen if the CIG models based on QPC can predict these conditions.

For a PLL bandwidth of 2 Hz, The infinity norm $\|\boldsymbol{G}\|_\infty$ in Figure D.2.a) shows that the system is

small-signal stable using all the CIG models. The DPC and VS-Type II models change more when the CIG levels are higher than 35%. In Figure D.2.b), as the PLL bandwidth increases, entailing a faster dynamic response, the QPC-based CIG models fail to predict the system stability for CIG levels above 70%. The VS-Type II suggests that the system is unstable for CIG levels above 70% of the considered CIG models. This means that both the VS-Type II and DPC-based models predict the test system's instability for a range of CIG levels and PLL bandwidth. On the other hand, for the rest of the CIG models, Figure D.2.b) reveals no significant variation in the $\|\boldsymbol{G}\|_\infty$ for different levels of CIG and PLL designs. This in turn means that these models cannot predict the system's stability as the DPC model when the PLL has a faster dynamic response. This causes the transient simulations based on the QPC to differ from those obtained through its counterpart based on DPC. Therefore, erroneous conclusions regarding power system stability may be drawn.

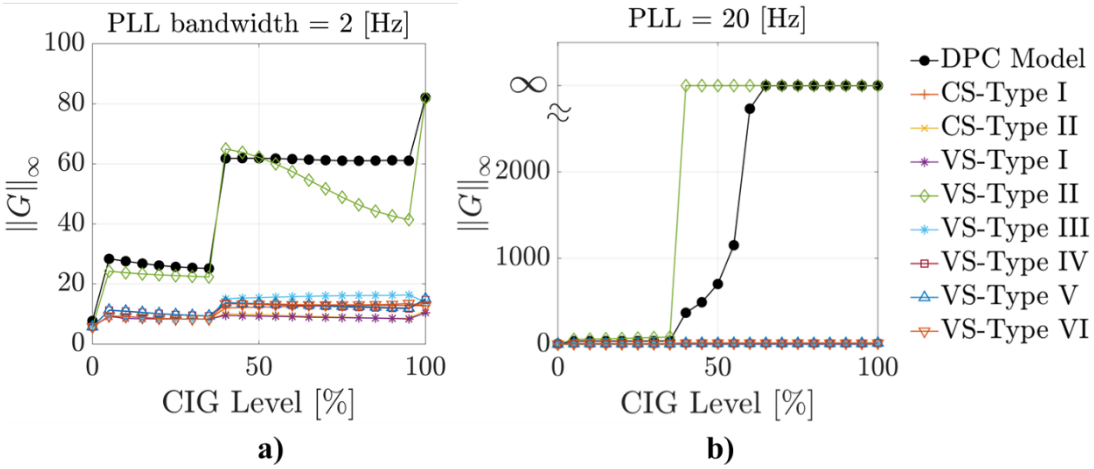

Figure D.2. $\|\boldsymbol{G}\|_\infty$ as a function of CIG penetration level and different PLL bandwidths; a) 2 Hz; b) 20 Hz

Modal analysis is performed to understand the root cause of the instability shown in the DPC and VS – Type II models. This allows for determining whether the VS-type II models can identify causes of instabilities in operating conditions similar to those studied in this section. The impact of different PLL bandwidths on the eigenvalues related to DPC and VS-type II models for 70% of CIG is shown in Figure D.3. This penetration level is where both models give similar results in terms of the infinity norm $\|\boldsymbol{G}\|_\infty$, and the rest of the CIG models suggest that the system is small signal stable. There are no relevant differences among them; hence they are not detailed here. On the left side of the segmented line in Figure D.3 are the modes with a damping coefficient greater than 5% because it is a typical value to consider that the oscillations are sufficiently damped [124].

For the system modeled using DPC, there is a critical mode in Figure D.3.a which is identified by $\mathrm{M1_{DPC}}$. This mode is of interest because it is on the right side of the complex plan, suggesting that the system is unstable. For a PLL bandwidth of 20 Hz, the mode $\mathrm{M1_{DPC}}$ has a damping coefficient ξ of -0.25% and an oscillation frequency of 35 Hz. The participation factor analysis reveals that the mode $\mathrm{M1_{DPC}}$ is mainly related to the dynamic interaction between the control systems of CIG1 and CIG3 units. It should be noted that state variables related to the PLL, current controller, AC filter, and VFF term have high participation factors. This is verified in Table D.1 where the participation factor with values higher than 0.3 is shown. Therefore, according to DPC-based models, fast dynamic interactions cause instability. The mode has an oscillation frequency above

5 Hz, which makes most of the CIG models based on QPC inaccurate.

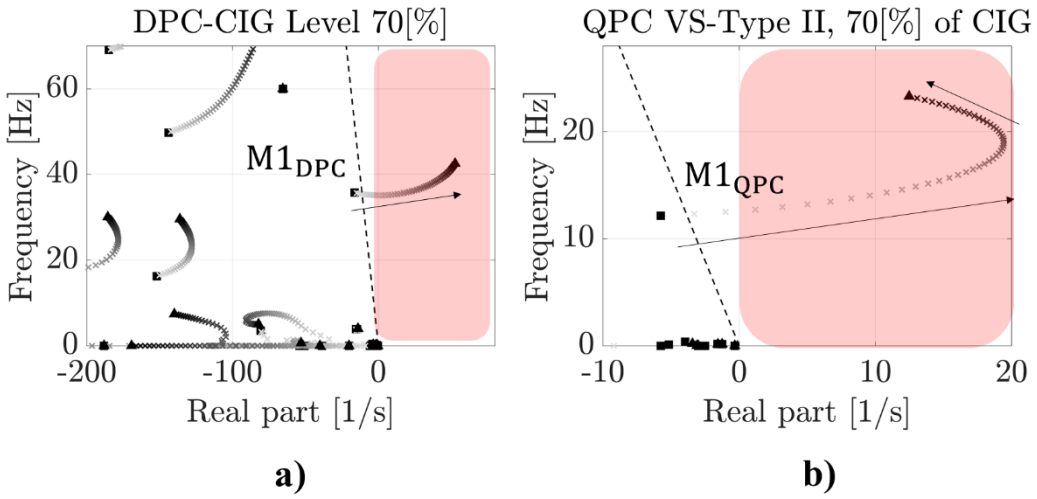

Figure D.3. Eigenvalue loci for PLL bandwidth between 2 Hz and 80 Hz for 70% of CIG levels; a) DPC – based model, b) VS-Type II model

Table D.1. Participation factors related to $M1_{DPC}$ for 70% of CIG and PLL bandwidth of 20 Hz

State Var.	PF
CIG1, i_{LfD}	0.398
CIG1, i_{LfQ}	0.761
G2, ψ_{qs}	0.255
G2, ψ_{2q}	0.236
CIG3, i_{LfD}	0.146
CIG3, i_{LfQ}	0.315
CIG1, θ_{PLL}	0.316
CIG3, θ_{PLL}	0.241
CIG1, $xPI_{i_{cq}}$	1.000
CIG1, $xPI_{i_{cd}}$	0.817
CIG3, $xPI_{i_{cq}}$	0.364
CIG3, $xPI_{i_{cd}}$	0.303
T1, i_{LQ}	0.101
T2, i_{LD}	0.132
T2, i_{LQ}	0.164
L9, i_{LQ}	0.102
CIG1, xq_{VFF}	0.902
CIG3, xq_{VFF}	0.341
CIG1, x_{mV}	0.944
CIG1, xd_{VFF}	0.929
CIG3, x_{mV}	0.341
CIG3, xd_{VFF}	0.342

In the case of the system modeled using QPC and CIG units represented by the VS-type II model, there is a critical mode in Figure D.3.b which is identified by $\mathrm{M1_{QPC}}$. For a PLL bandwidth of 20 Hz, the mode $\mathrm{M1_{QPC}}$ has a damping coefficient ξ of -12% and an oscillation frequency of 14 Hz. This model suggests that the system is not stable as the DPC-based model. The participation factor analysis shows that the mode $\mathrm{M1_{QPC}}$ is related to the state variables of the CIG1 control system, as shown in Table D.2. This model does not include the dynamic of the VFF term, the transmission network, and the decoupling terms. Although the DPC- and VS-type II models are not stable for the same CIG level and PLL, the dynamic behavior and interactions differ significantly. This means that QPC-based stability analysis and using the VS-type II model for CIG may not be used to determine the stability margin or propose solutions for stability improvements of power systems with high levels of CIG.

According to the above, fast dynamic responses of the PLL considerably impact the accuracy of transient simulation and dynamic interaction of CIG models based on QPC. If the DPC system is small signal stable, there are no significant differences with the QPC-based CIG models.

Table D.2. Participation factors related to $\mathrm{M1_{QPC}}$ for the model VS-Type 2 for 70% of CIG and PLL bandwidth of 20 Hz

State Var.	PF
CIG1, x_{mP}	0.240
CIG1, xPI_P	0.184
CIG1, θ_{PLL}	0.676
CIG1, $xPI_{i_{cd}}$	1.000
CIG1, x_{mV}	0.817
CIG1, $xPI_{i_{cq}}$	0.852
G2, ψ_{2q}	0.179
CIG3, θ_{PLL}	0.269
CIG3, $xPI_{i_{cd}}$	0.334
CIG3, x_{mV}	0.268
CIG3, $xPI_{i_{cq}}$	0.268
CIG1, xPI_{PLL}	0.177

D.1.2 Case Study 2: Impacts of SCR Levels

This study analyzes the impacts of SCR levels on the suitability of CIG models based on QPC by considering different CIG levels of 35%, 50%, 70%, and a PLL bandwidth of 20 Hz. The CIG units are operating in GFL mode without frequency control. The SCR is defined by [39]:

$$\mathrm{SCR} = \frac{S_{\mathrm{SCMVA}}}{P_{\mathrm{RMW}}} \tag{D.1}$$

Where S_{SCMVA} is the short–circuit MVA capacity at the bus in the existing network before connecting a CIG unit and P_{RMW} is the rated active power in MW of the new CIG unit. The value of the SCR levels depends on the synchronous generators connected to the systems. In the test system, the SCR is modified by changing the inductive reactance x_{14} from 0.05 to 1 in [pu] on a base of 100 [MVA]. This reactance is related to the transformer between bus B1 and B4. For a CIG level of 35%, the SCR at bus B1 ranges 1.6-0.45 [pu], and for the CIG levels of 50% and 70%, the

SCR at bus B1 ranges 1.2-0.4 [pu]. In the former, generators G2 and G3 are connected, and in the latter, only the synchronous generator G2 is connected.

Figure D.4 display the values of $\|\boldsymbol{G}\|_\infty$ for the range of SCR selected and CIG levels of 35% 50%, and 70% considered in this case study. In the DPC models, as the CIG levels increase and the SCR decrease, the values of $\|\boldsymbol{G}\|_\infty$ are not bounded, meaning that the systems become unstable. Based on the QPC approach, these stability issues are not seen accurately for the CIG models. For low SCR values, such as 1.0 and 50% of CIG, almost all the CIG models suggest small-signal stability, contrary to the results obtained from DPC models. In the scenario of a CIG level of 70%, the models VS-Type VI, VS-Type V, CS-Type I, and CS-Type II also suggest system instabilities for SCR lower than 0.8, as shown in Figure D.4c. These models are shown to be less accurate because, for a set of SCR, these models indicate that the system is small signal stable when the DPC model indicates the contrary. Significant differences in their values of $\|\boldsymbol{G}\|_\infty$. Similar to Case Study 1, the VS – Type II predicts the stability problems for some SCR, as the analysis using DPC shows.

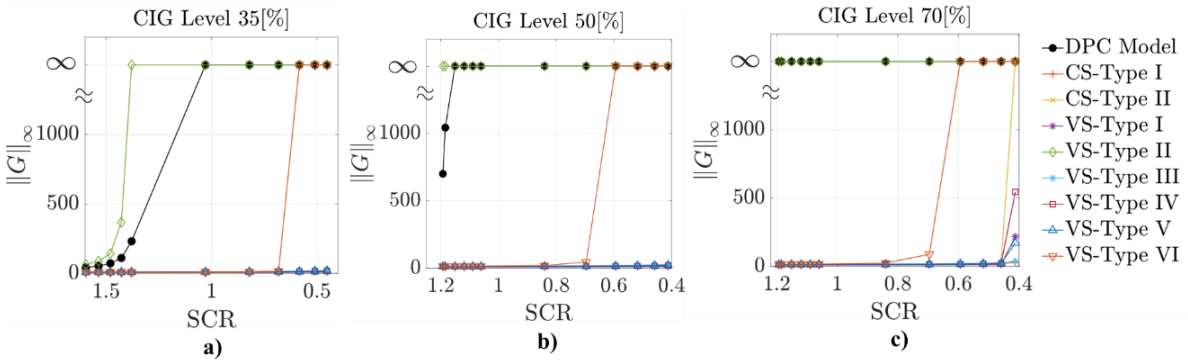

Figure D.4. $\|\boldsymbol{G}\|_\infty$ as a function of SCR; a) CIG Level 35%; b) CIG Level 50%; c) CIG Level 70%

Modal analysis is performed to understand the similarities and differences between the DPC and VS-Type II models. Figure D.5 shows the impact of varying the SCR in these models. The CIG levels of 50% and a PLL bandwidth of 20 Hz are selected. The impact of the different SCRs on the eigenvalues related to the mode of interest is shown in Figure D.5. Figure D.5.a shows the impact on the system model using DPC, and Figure D.5.b displays the impact on the system model using QPC with the CIG model VS-Type II. For the DPC model, the system becomes unstable for SCR=1.15. This is consistent with Figure D.4b, where the norm $\|\boldsymbol{G}\|_\infty$ tends to the infinity. The mode $M1_{DPC}$ causes stability issues. For SCR = 1.15, the mode $M1_{DPC}$ has a damping coefficient of -0.5% and an oscillation frequency of 36 Hz. Participation factor analysis reveals that this mode is mainly related to the CIG control systems and other fast dynamics components. The participation factors are shown in Figure D.3. From this table, it can be seen that state variables associated with the current controllers, PLL, the filter of VFF, Stator fluxes, AC filter, and currents on transformers are related to the mode $M1_{DPC}$. These complex dynamic interactions show that CIG units in different locations can interact to frequencies higher than those typical of electromechanical oscillations typical of synchronous oscillations.

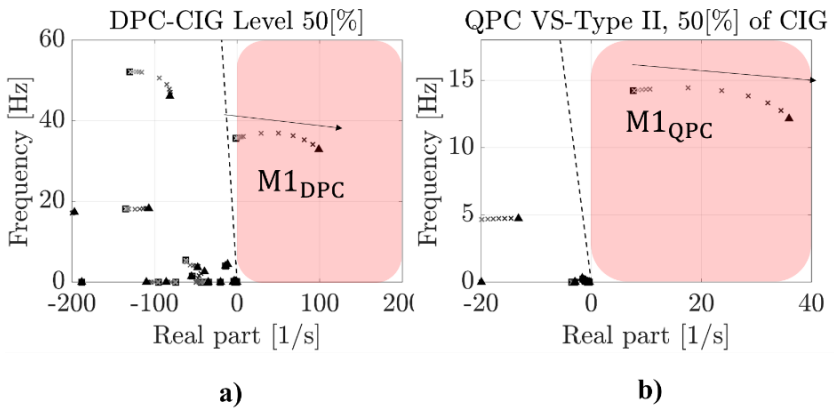

Figure D.5. Eigenvalue loci for SCR between 1.19 and 0.41 for 50% of CIG levels; a) DPC-based model, b) VS-Type II model

Table D. 3. Participation factors related to $M1_{DPC}$ for 50% of CIG and SCR of 20 Hz

State Var.	PF
CIG1, i_{LfD}	0.448
CIG1, i_{LfQ}	0.721
G2, ψ_{qs}	0.236
G2, ψ_{2q}	0.204
CIG3, i_{LfD}	0.146
CIG3, i_{LfQ}	0.274
CIG1, θ_{PLL}	0.280
CIG3, θ_{PLL}	0.170
CIG1, $xPI_{i_{cq}}$	1.000
CIG1, $xPI_{i_{cd}}$	0.774
CIG3, $xPI_{i_{cq}}$	0.339
CIG3, $xPI_{i_{cd}}$	0.265
T1, i_{LQ}	0.104
T2, i_{LD}	0.151
T2, i_{LQ}	0.117
CIG1, xq_{VFF}	0.922
CIG3, xq_{VFF}	0.324
CIG1, x_{mV}	0.904
CIG1, xd_{VFF}	0.891
CIG3, x_{mV}	0.302
CIG3, xd_{VFF}	0.303

Figure D.5.b displays the impacts of SCR on the system modeled using QPC with the CIG model VS-Type II. According to this model, it is suggested that the system is unstable for the selected values of SCR. This is due to the mode $M1_{QPC}$ which has negative damping coefficients. This behavior is consistent with the plot in Figure D.5.b, where the norm $\|\boldsymbol{G}\|_\infty$ tends to the infinity for the range of SCR used. For an SCR of 1.15, the damping coefficient is -8.5%, and 14 [Hz] oscillation frequency. The participation factor analysis reveals that the state variables related to this mode pertain mainly to the control systems of CIG1 and CIG3. Table D.4 shows the participation factor related to $M1_{QPC}$. Particular attention should be paid to the different state variables that participate in this mode which are not presented in the mode $M1_{DPC}$. In Table D.4 it can be seen that the control of active power $(x_{\mathrm{mP}}, xPI_{\mathrm{P}},)$, the measurement of voltage (x_{mV}) at buses where are connected have a significant impact on $M1_{QPC}$. Furthermore, the impact of PLL is higher than

the DPC models.

This model's assumption causes dynamic interactions not observed in the system model using DPC. VS-Type II can predict small signal stability for some conditions but can not determine stability margin or propose new control systems to improve power system stability. Finally, it should be noted that poorly damped modes with oscillation frequencies higher than 5 [Hz] may suggest that QPC-based models are unsuitable and less accurate for stability assessment.

Table D.4. Participation factors related to $\mathrm{M1_{QPC}}$ for the QPC VS-Type 2, 50% of CIG and SCR of 1.15

State Var.	PF
CIG1, x_{mP}	0.196
CIG1, xPI_P	0.152
CIG1, θ_{PLL}	0.696
CIG1, $xPI_{i_{cd}}$	1.000
CIG1, x_{mV}	0.825
CIG1, $xPI_{i_{cq}}$	0.926
G2, ψ_{2q}	0.146
CIG3, θ_{PLL}	0.273
CIG3, $xPI_{i_{cd}}$	0.330
CIG3, x_{mV}	0.271
CIG3, $xPI_{i_{cq}}$	0.297
CIG1, xPI_{PLL}	0.185

D.1.3 Case Study 3: Impacts of Current Control Loops

Previous sections have shown that, in the case of DPC models, the state variables related to the inner current control and the filter associated with VFF terms have high participation factors (see Table D.1 and Table D. 3). Thus, despite PLL, this control may impact the small-signal stability of the test system and then on the CIG models based on CIG. In this case study, it is performed sensitivity analysis varying the integral gain k_{i} associated with the current controller and the time constant $\tau_{v\mathrm{dq}}$ associated with the VFF terms. The sensitivity analysis considers a PLL bandwidth of 20 Hz. The term VFF and the current controller are not represented in the following CIG models CS-Type I, CS-Type II, VS-Type III, and VS-type VI. Therefore, these models are not relevant in this case study. However, these models are included in the figures below, but only for comparison.

The integral gain k_i of the current controller range from 5 to 200, and the time constant $\tau_{v\mathrm{dq}}$ associated with the VFF take values of 0.01, 0.001, and 0.0001. According to Table 5.3, in previous cases $\tau_{v\mathrm{dq}} = 0.001$ and $k_i = 90$. The selected values are generic and typical [74], [244]. These parameters are selected to perform the sensitivity analysis because the study of participation factors reveals a considerable impact on the accuracy of QPC-based models. The ranges of values are generic and typical from different research works in the literature, e.g. [74], [75], [180], [181], [244]–[246]. Given the above, the dynamic interactions related to the mode $\mathrm{M1_{DPC}}$ can be modified, and then the effect of k_{i} can be understood. Higher values cause a faster dynamic response of the current controllers.

The values of $\|\boldsymbol{G}\|_\infty$ for the range of integral gain k_{i} of the current controller selected and CIG levels of 35%, 50%, and 70%, and PLL bandwidths of 2 Hz, 20 Hz, and 50 Hz considered in this

case study are shown from Figure D.8 to Figure D.14. It can be seen that as the CIG levels increase, the model using DPC suggests that the system becomes unstable as the constant k_{i}, PLL bandwidths, and $\tau_{v_{\mathrm{tdq}}}$also increase. It is also revealed that it is possible to perform operation scenarios with high penetration levels by adequately tuning the control system. The rest of the CIG models based on QPC do not reveal the same region in which the system is small signal stable or unstable. Furthermore, for the range of the constant k_{i} when the system modeled using DPC indicates small-signal stability, there is no significant difference among the CIG models based on QPC. This means that transient simulations should give similar dynamic behavior. The exception is related to the model VS-Type II, in which it is seen that it becomes inaccurate for low values of the constant k_{i}. This in turn means that the model is more sensitive to the PLL than the dynamics related to the current controllers.

Furthermore, it should be mentioned that in the most common models of CIG used in stability assessments of power systems dominated by CIG, the VFF term is not represented. Therefore, the impact of VFF is described considering only the DPC models. The VFF terms are typically used to improve the dynamic performance and reject the current harmonic caused by the voltage [255]. Proper values of k_{i} and $\tau_{v_{\mathrm{tdq}}}$ can affect the small system stability, allowing the system's operation under high penetration levels of CIG. These system stability issues are not observable in the CIG models based on QPC. On the other hand, when the system represented using DPC is small signal stable, the CIG models based on QPC may give similar dynamic behavior. This is because the infinity norm $\|\boldsymbol{G}\|_\infty$ does not change significantly between the CIG models.

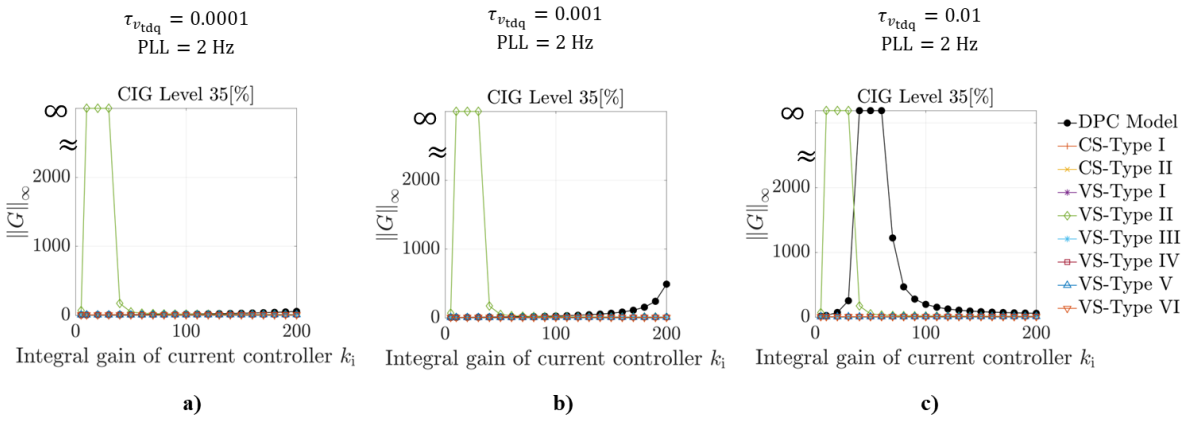

Figure D.6. $\|\boldsymbol{G}\|_\infty$ as a function of with the integral gain of the current controller k_{i} ranging from 5 to 200 for a CIG level of 35% and PLL bandwidth of 2 Hz; a) $\tau_{v_{\mathrm{tdq}}} = 0.0001$; b) $\tau_{v_{\mathrm{tdq}}} = 0.001$; c) $\tau_{v_{\mathrm{tdq}}} = 0.01$

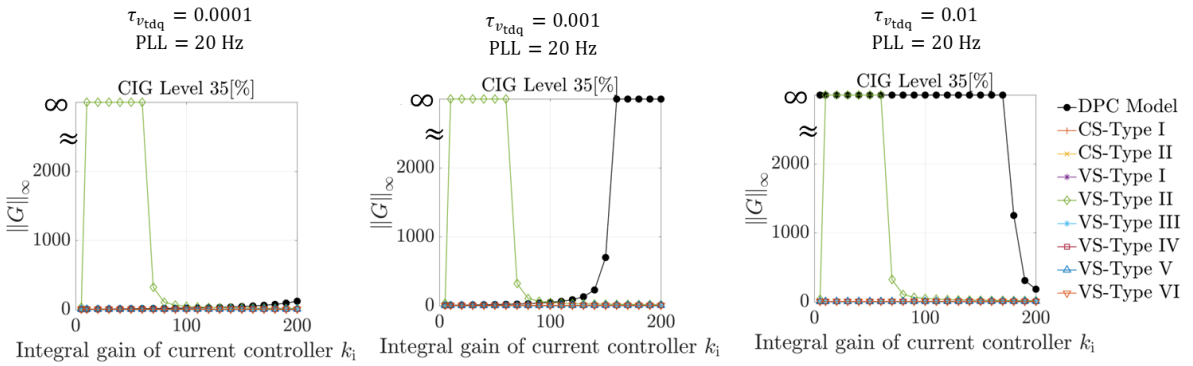

Figure D.7. $\|\boldsymbol{G}\|_\infty$ as a function of with the integral gain of the current controller k_i ranging from 5 to 200 for a CIG level of 35% and PLL bandwidth of 20 Hz; a) $\tau_{v_{\mathrm{tdq}}} = 0.0001$; b) $\tau_{v_{\mathrm{tdq}}} = 0.001$; c) $\tau_{v_{\mathrm{tdq}}} = 0.01$

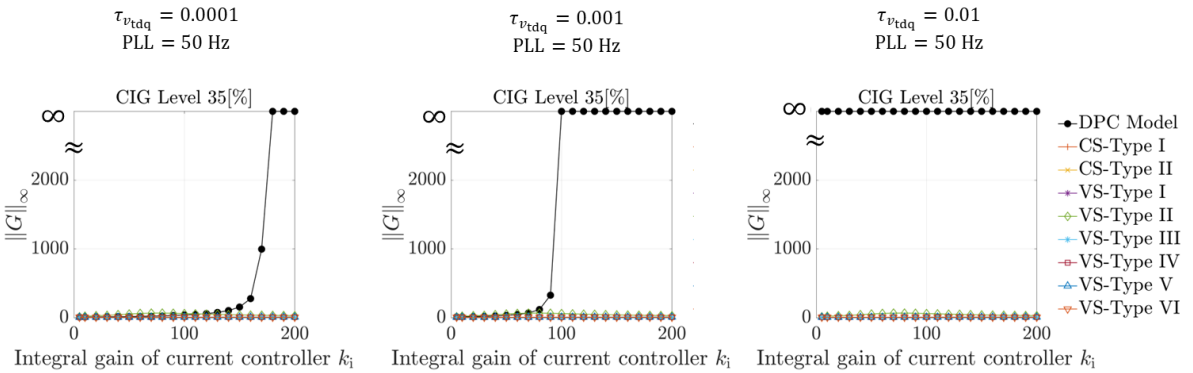

Figure D.8. $\|\boldsymbol{G}\|_\infty$ as a function of with the integral gain of the current controller k_i ranging from 5 to 200 for a CIG level of 35% and PLL bandwidth of 50 Hz; a) $\tau_{v_{\mathrm{tdq}}} = 0.0001$; b) $\tau_{v_{\mathrm{tdq}}} = 0.001$; c) $\tau_{v_{\mathrm{tdq}}} = 0.01$

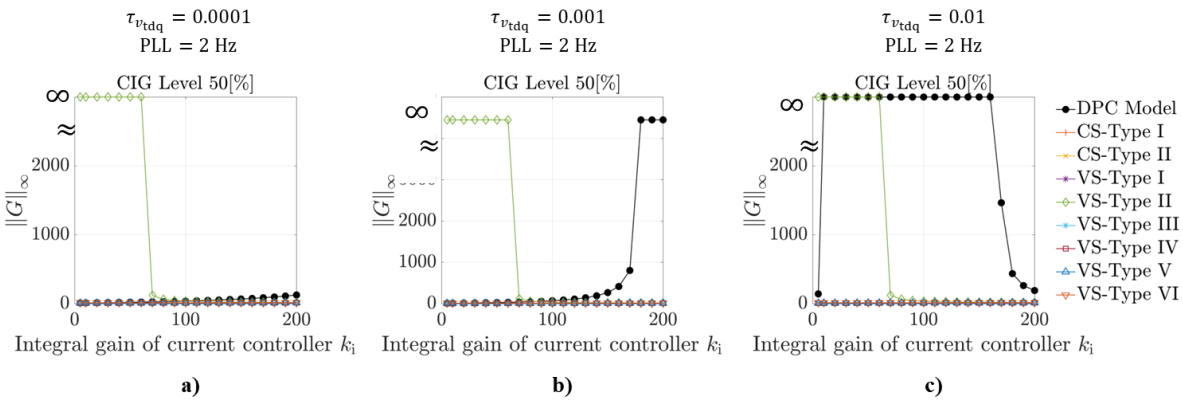

Figure D.9. $\|\boldsymbol{G}\|_\infty$ as a function of with the integral gain of the current controller k_i ranging from 5 to 200 for a CIG level of 50% and PLL bandwidth of 2 Hz; a) $\tau_{v_{\mathrm{tdq}}} = 0.0001$; b) $\tau_{v_{\mathrm{tdq}}} = 0.001$; c) $\tau_{v_{\mathrm{tdq}}} = 0.01$

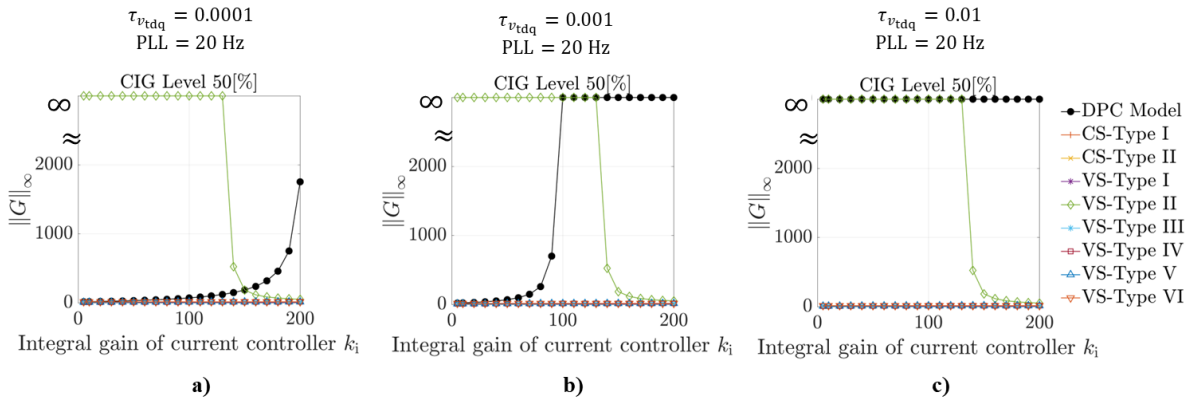

Figure D.10. $\|\boldsymbol{G}\|_\infty$ as a function of with the integral gain of the current controller k_i ranging from 5 to 200 for a CIG level of 50% and PLL bandwidth of 20 Hz; a) $\tau_{v_{\mathrm{tdq}}} = 0.0001$; b) $\tau_{v_{\mathrm{tdq}}} = 0.001$; c) $\tau_{v_{\mathrm{tdq}}} = 0.01$

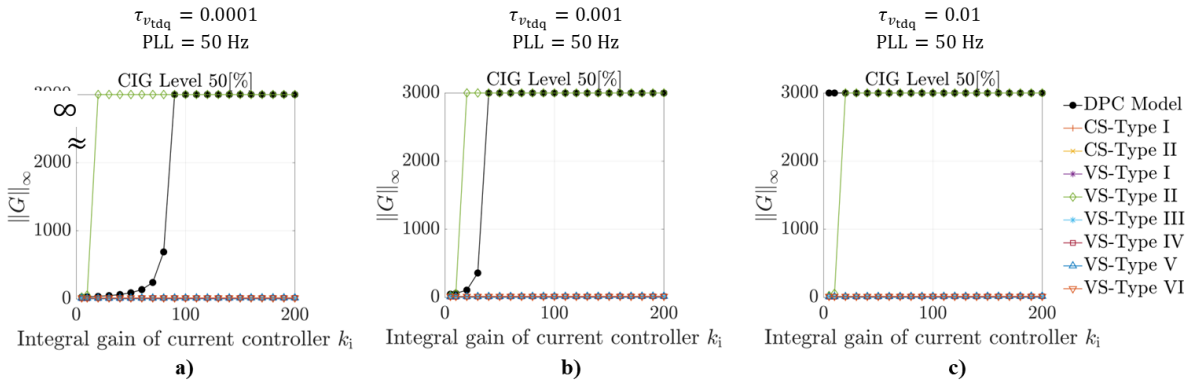

Figure D.11. $\|\boldsymbol{G}\|_\infty$ as a function of with the integral gain of the current controller k_i ranging from 5 to 200 for a CIG level of 50% and PLL bandwidth of 50 Hz; a) $\tau_{v_{\mathrm{tdq}}} = 0.0001$; b) $\tau_{v_{\mathrm{tdq}}} = 0.001$; c) $\tau_{v_{\mathrm{tdq}}} = 0.01$

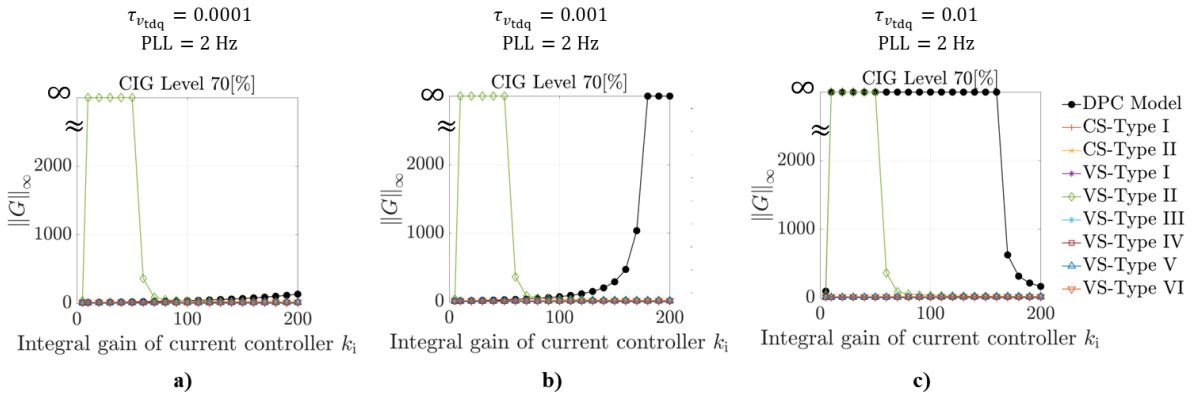

Figure D.12. $\|\boldsymbol{G}\|_\infty$ as a function of with the integral gain of the current controller k_i ranging from 5 to 200 for a CIG level of 70% and PLL bandwidth of 2 Hz; a) $\tau_{v_{\mathrm{tdq}}} = 0.0001$; b) $\tau_{v_{\mathrm{tdq}}} = 0.001$; c) $\tau_{v_{\mathrm{tdq}}} = 0.01$

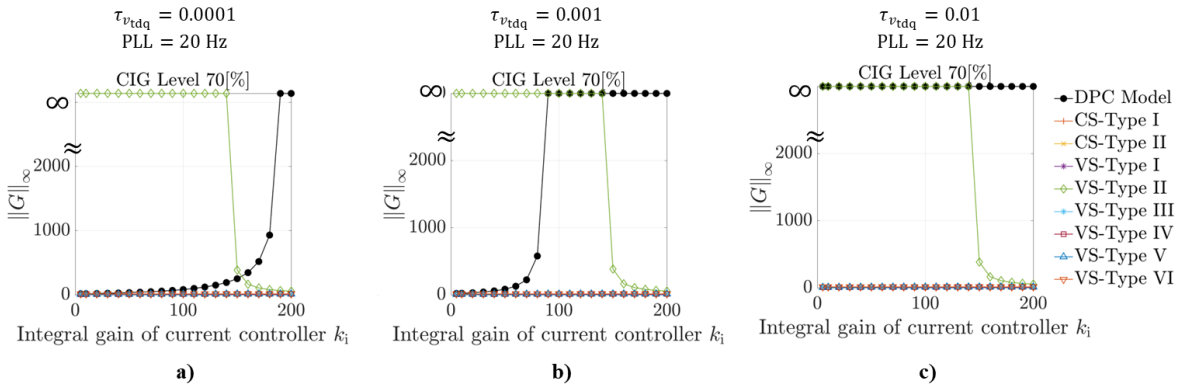

Figure D.13. $\|\boldsymbol{G}\|_\infty$ as a function of with the integral gain of the current controller k_i ranging from 5 to 200 for a CIG level of 70% and PLL bandwidth of 20 Hz; a) $\tau_{v_{\mathrm{tdq}}} = 0.0001$; b) $\tau_{v_{\mathrm{tdq}}} = 0.001$; c) $\tau_{v_{\mathrm{tdq}}} = 0.01$

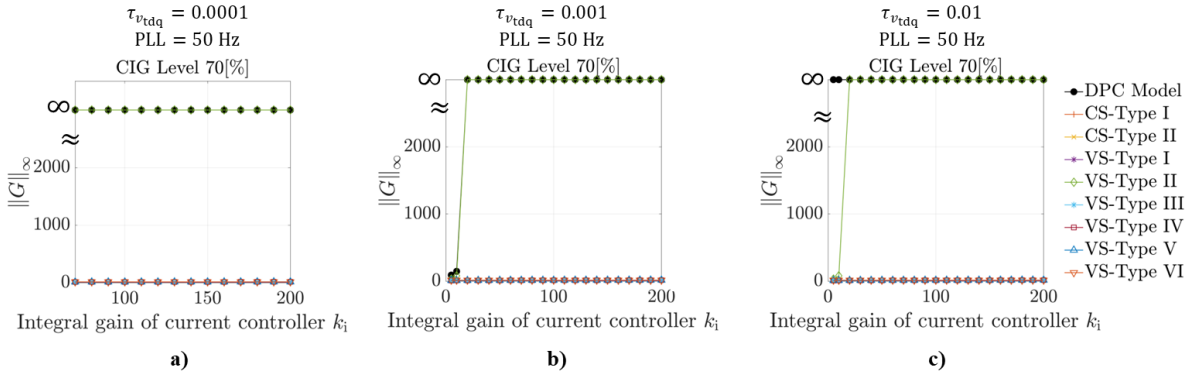

Figure D.14. $\|\boldsymbol{G}\|_\infty$ as a function of with the integral gain of the current controller k_i ranging from 5 to 200 for a CIG level of 70% and PLL bandwidth of 50 Hz; a) $\tau_{v_{\mathrm{tdq}}} = 0.0001$; b) $\tau_{v_{\mathrm{tdq}}} = 0.001$; c) $\tau_{v_{\mathrm{tdq}}} = 0.01$

Modal analysis is performed, and the eigenvalues loci for the system model using DPC is shown in Figure D.15. The effects of the k_i and $\tau_{v_{\mathrm{tdq}}}$ on the mode $\mathrm{M1}_{\mathrm{DPC}}$ can be seen in this figure. The mode $\mathrm{M1}_{\mathrm{DPC}}$ causes the system to become unstable. The participation factor analysis reveals that the state variables related to this mode are similar to Section D.1.2. The state variables are associated with the CIG control systems and other dynamic responses. Similar observations can be made for higher CIG levels. For these reasons, these results are not shown here.

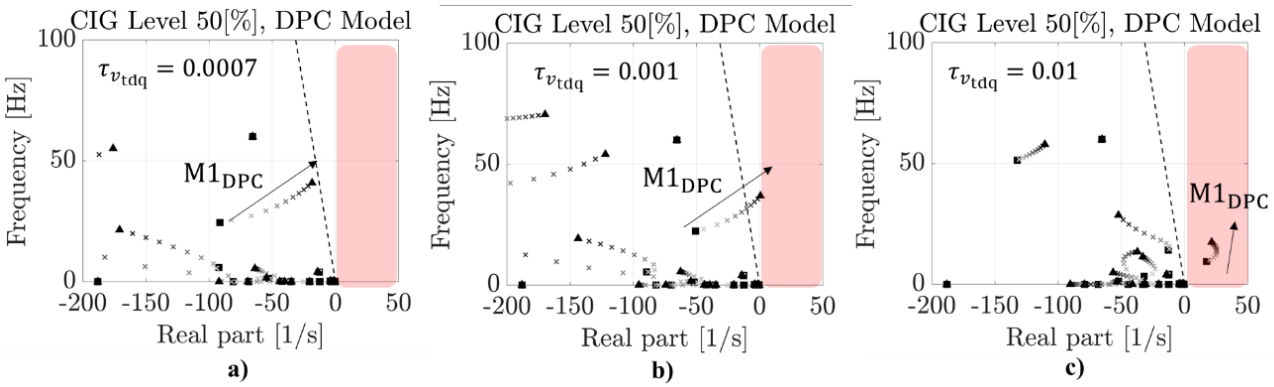

Figure D.15. Eigenvalue loci for k_i between 5 and 100 for 50% of CIG level and the system represented using DPC; a) $\tau_{v_{tdq}} = 0.0007$, b) $\tau_{v_{tdq}} = 0.001$; c) $\tau_{v_{tdq}} = 0.01$

It is generally believed that fast dynamics do not cause stability issues from a system perspective. This result shows that fast dynamics, such as inner control loops, affect the stability of CIG units and the power system. To observe such new stability issues, inner control loops and the transmission network need to be adequately represented by differential equations. Defining a level of CIG in a power system dominated by power electronics should be taken with caution. Re-tuning the control systems of CIG could improve dynamic performance. As a result, a higher level of CIG could be achieved.

D.2 Validation Through Dynamic Simulation

The relevant results obtained in the previous stage are verified in this methodology stage through time-domain simulations using DPC, QPC, and EMT models. A step decrease of 5% of the reference active power for the generator CIG1 connected at bus B1 is considered. This is a small perturbation because the analyses performed in Section D.1 are based on small-signal models. For each case study, operating conditions are selected to validate the results obtained, starting with Case Study 1.

First, time domain simulations are performed for 70% of the CIG level and PLL bandwidths of 2 Hz and 20 Hz to validate the results of Case Study 1. Figure D.16 and Figure D.17 show the dynamic response of the angular frequency estimated by the PLL at CIG1 and the active power at bus B1, respectively. When the PLL bandwidth is low, in this example, 2 Hz, there are no significant differences between the model based on DPQ and the CIG models based on QPC. This can be seen in D.16.a and Figure D.17.a. Figure D.16.c, and Figure D.17.c. show a zoom in. It is seen that there are minor differences, but these can not affect the results regarding system stability.

On the other hand, when the PLL bandwidth is 20 Hz, the errors using CIG models based on QPC are significant, as shown in Figure D.16.b, and Figure D.17.b. CIG models based on QPC cannot represent oscillation frequencies higher than 5 Hz. The VS-Type II also shows system instability, but the oscillation frequency and damping differ from the DPC simulation. This observation is consistent with the eigenvalue loci depicted in Figure D.3. The dynamic behaviors observed are consistent and expected because for low PLL bandwidths the $\|\boldsymbol{G}\|_\infty$ are always bounded and similar, as shown in Figure D.2.a. For a high PLL bandwidth the $\|\boldsymbol{G}\|_\infty$ There are significant differences between DPC and QPC approaches. The exception is the VS-Type II model, which can predict system instability but is still not accurate in dynamic performance. Figure D.18 verified

these results by comparing the DPC and EMT simulations. DPC models predict small-signal instability and oscillations frequencies. However, slight differences in terms of damping and due to high-frequency transients of power electronic switchings are seen.

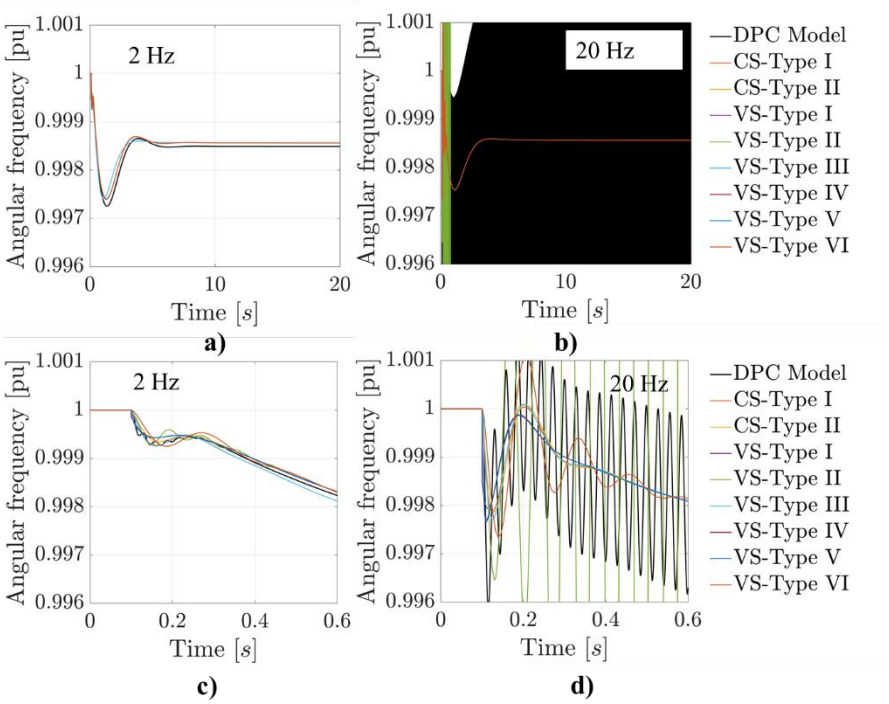

Figure D.16. Angular frequency ω_e of CIG1 for 70% of CIG; a) 2 Hz; b) 20 Hz; c) zoom 2 Hz; d) zoom 20 Hz

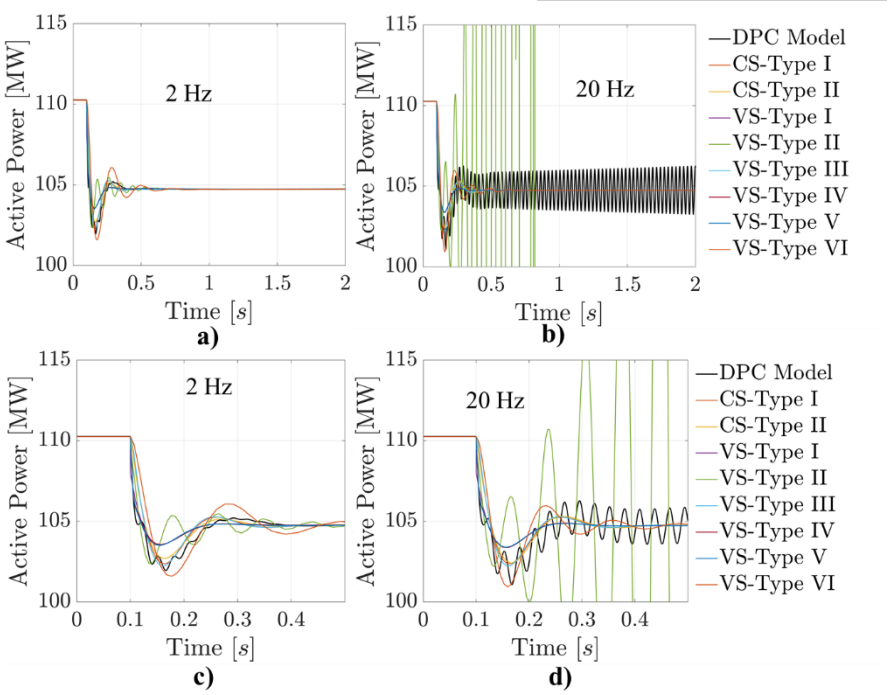

Figure D.17. Active power injected at bus B1 for 70% of CIG; a) 2 Hz; b) 20 Hz;c) zoom 2 Hz; d) zoom 20 Hz

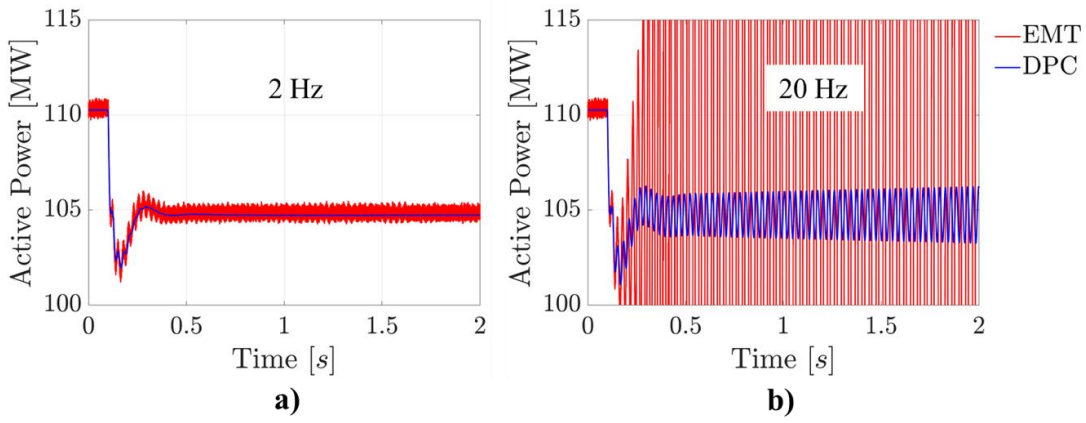

Figure D.18. Active power injected at bus B1 for 70% of CIG; a) 2 Hz; b) 20 Hz

Second, time domain simulations are performed to validate the results obtained from Case Study 2. PLL bandwidths of 20 Hz, CIG Level of 50%, and SCR of 1.2 and 1.15 are considered. Figure D.19 and Figure D.20 depict the dynamic response of the angular, estimated by the PLL at CIG1 and the active power at bus B1, respectively. As the SCR decreases, the errors of QPC models significantly increase. Unlike Case Study 1, the VS-Type II model is inaccurate for the selected SCR. This is clearly seen in Figure D.19a., Figure D.19b, Figure D.20.a, and Figure D.20.b. The results are consistent with the plot of $\|\boldsymbol{G}\|_\infty$ and eigenvalue loci depicted in Figure D.4 and Figure D.5, respectively. Similar observations made in Case Study 1 are retained in this case. Thus, they are not repeated here. Although it is not observed in the transient simulations performed, it should be noted that the PLL may suffer from instability issues when CIG are connected to a bus with low values of SCR. It is highly recommended to represent its dynamic properly. Consequently, CIG models based on QPC that do not represent PLL are not recommended [15], [34], [71], [134]. The previous statements can be verified and validated using EMT simulations are it is shown in Figure D.21.

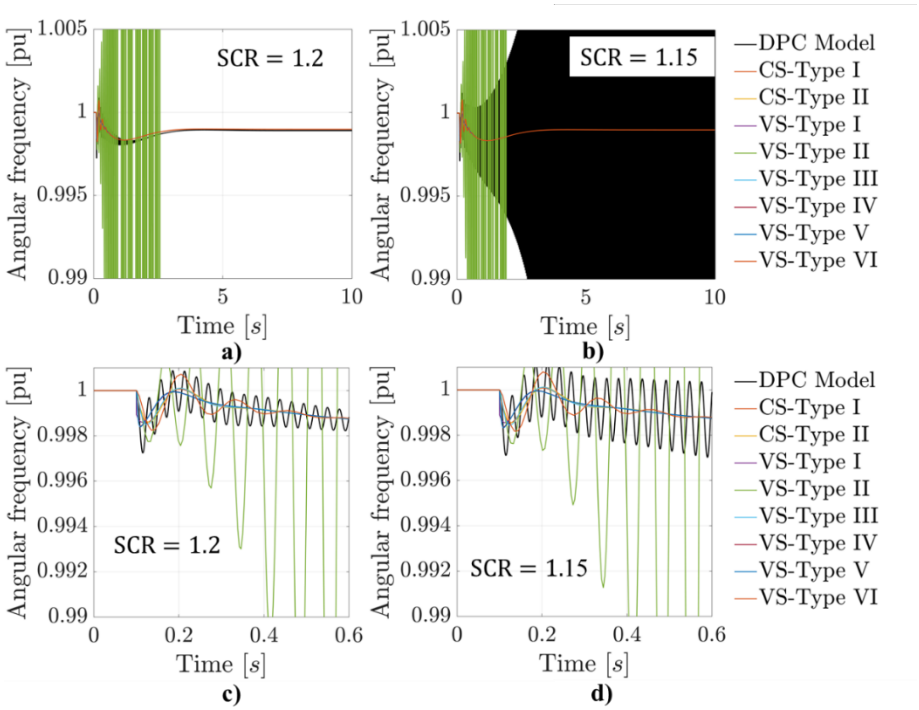

Figure D.19. Angular frequency ω_e of CIG1 for 50% CIG; a) SCR =1.2; b) SCR = 1.15; c) zoom out SCR = 1.2; d) SCR = 1.15

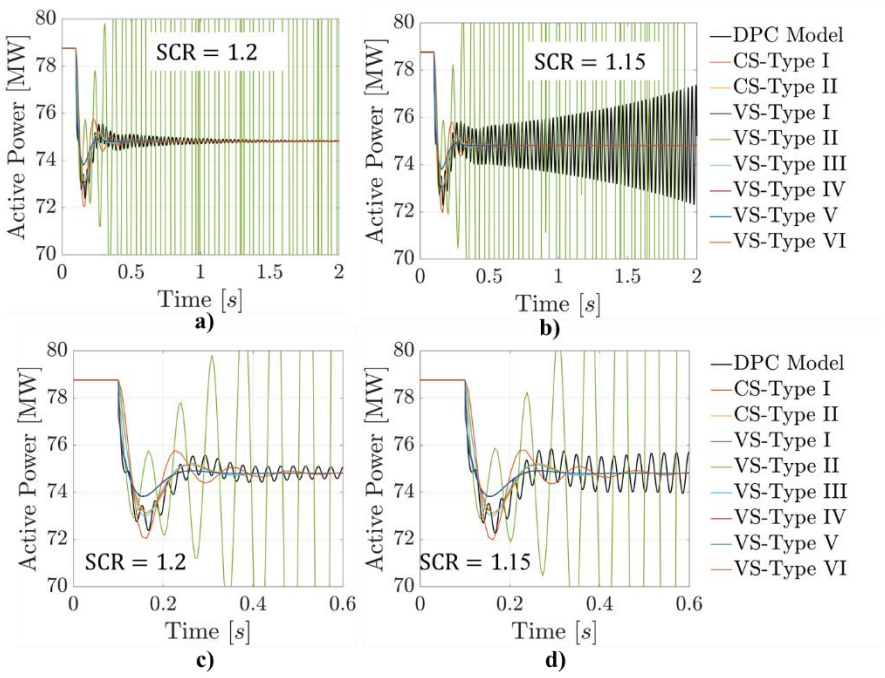

Figure D.20. Active power injected at bus B1 for 50% CIG; a) SCR =1.2; b) SCR = 1.15; c) zoom out SCR=1.2; d) SCR = 1.15

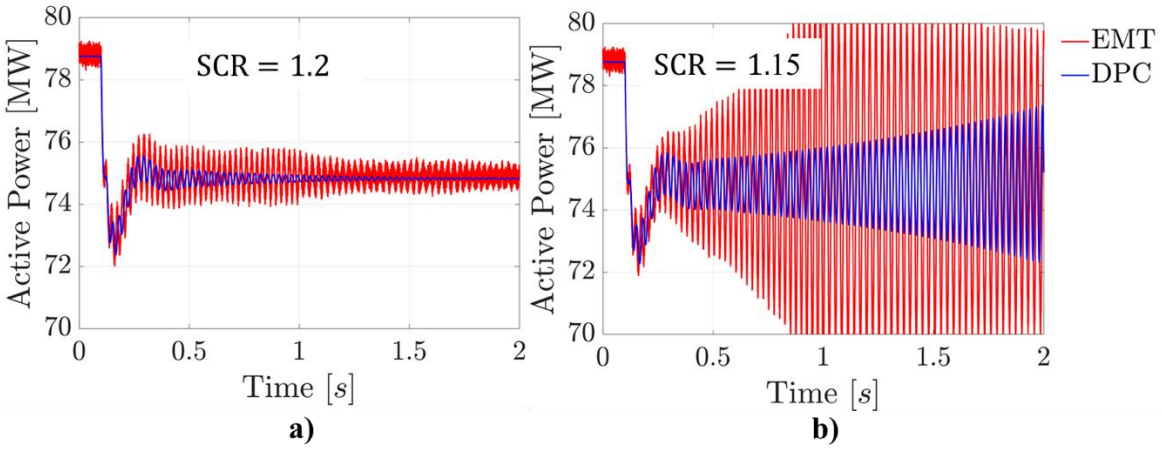

Figure D.21. Active power injected at bus B1 for 50% CIG; a) $SCR = 1.2$; b)$SCR = 1.15$

Third, for Case Study 3, time domain simulations are carried out for 50% of CIG level and PLL bandwidths of 20 Hz. The time constant $\tau_{v_{\mathrm{tdq}}}$ related to the VFF and the integral gain of the current controllers k_{i} are modified in CIG1 and CIG3. The integral gain k_{i} takes the values 50, 90, and 100. The time constant $\tau_{v_{\mathrm{tdq}}}$ take values of 0.0001, 0.001 and 0.01.

Figure D.22, Figure D.23, and Figure D.24 show the active power injected to B1 by the CIG1 unit considering the selected integral gain constant k_{i} and the time constant $\tau_{v_{\mathrm{tdq}}}$. As $\tau_{v_{\mathrm{tdq}}}$ decreases, the model based on DPC suggests good dynamic performance, and the QPC-based models give similar dynamic behavior. This behavior differs from the model VS-Type II, which is always unstable for selected control parameters. CIG models based on QPC can not predict system instability when $\tau_{v_{\mathrm{tdq}}}$ and k_{i} increases. This fact can be seen in Figure D.22.c, Figure D.23.c and Figure D.24.c. In such cases, the VS-Type II model predicts the stability of the power system. These observations are consistent with the eigenvalue loci and $\|\boldsymbol{G}\|_{\infty}$ plots are shown in Figure D.8 and Figure D.15, respectively. It should be noted that fast dynamic responses of CIG significantly impact the system stability. The tuning of inner control parameters can not be made using QPC models because these models cannot correctly represent the small signal stability. On the other hand, the modularity, flexibility, and fast responses of power electronics can allow good dynamic performance for high levels of CIG. The previous observations are maintained when DPC and EMT models are compared in Figure D.25, Figure D.26, and Figure D.27.

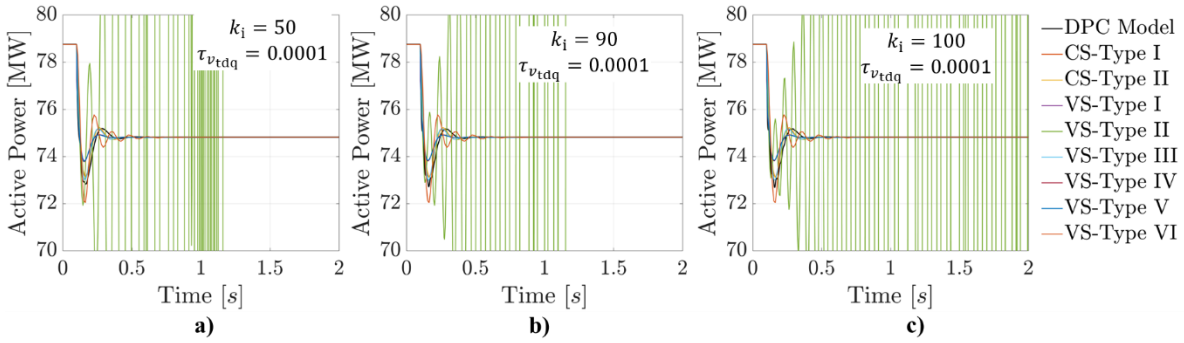

Figure D.22. Active power injected by CIG1 to B1 for 50% CIG and $\tau_{v_{tdq}} = 0.0001$; a) $k_i = 50$; b) $k_i = 90$; c) $k_i = 100$

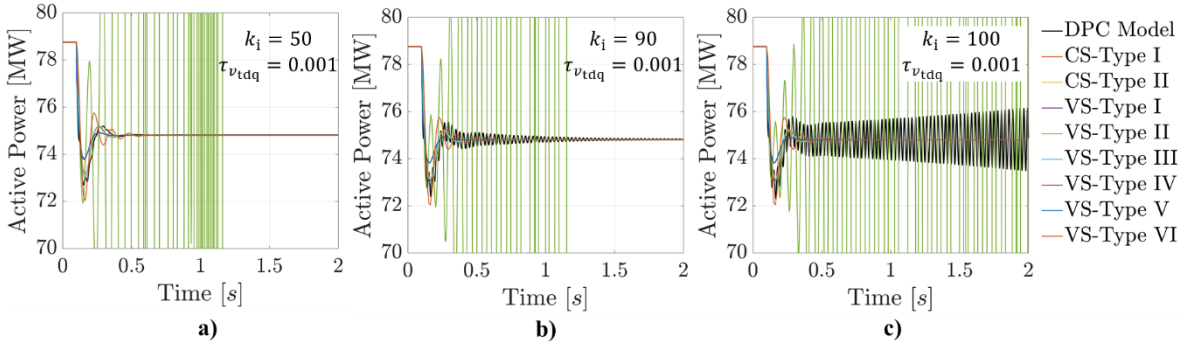

Figure D.23. Active power injected by CIG1 to B1 for 50% CIG and $\tau_{v_{tdq}} = 0.001$; a) $k_i = 50$; b) $k_i = 90$; c) $k_i = 100$

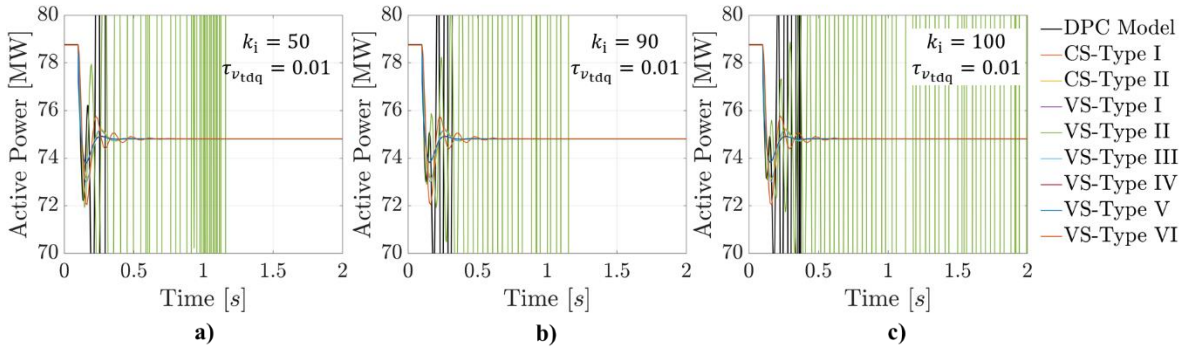

Figure D.24. Active power injected by CIG1 to B1 for 50% CIG and $\tau_{v_{tdq}} = 0.01$; a) $k_i = 50$; b) $k_i = 90$; c) $k_i = 100$

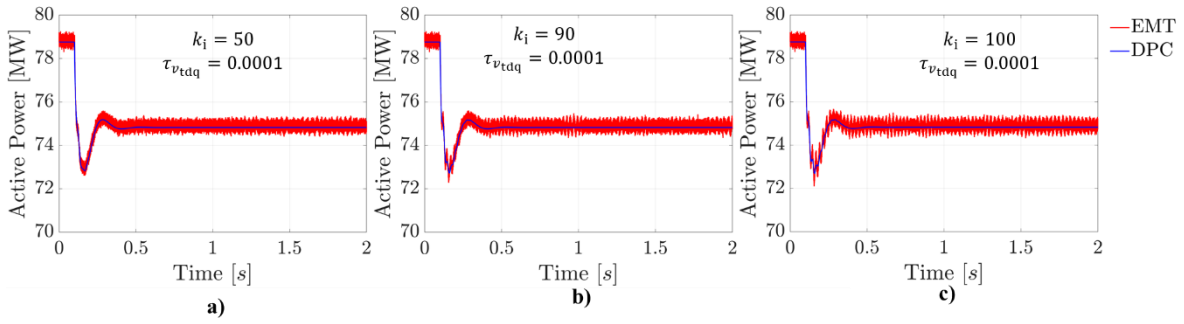

Figure D.25. Active power injected by CIG1 to B1 for 50% CIG and $\tau_{v_{tdq}} = 0.0001$; a) $k_i = 50$; b) $k_i = 90$; c) $k_i = 100$

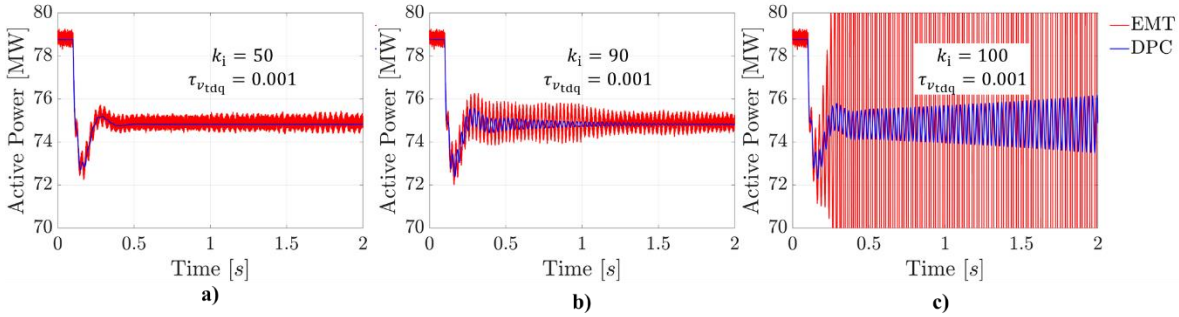

Figure D.26. Active power injected by CIG1 to B1 for 50% CIG and $\tau_{v_{tdq}} = 0.001$; a) $k_i = 50$; b) $k_i = 90$; c) $k_i = 100$

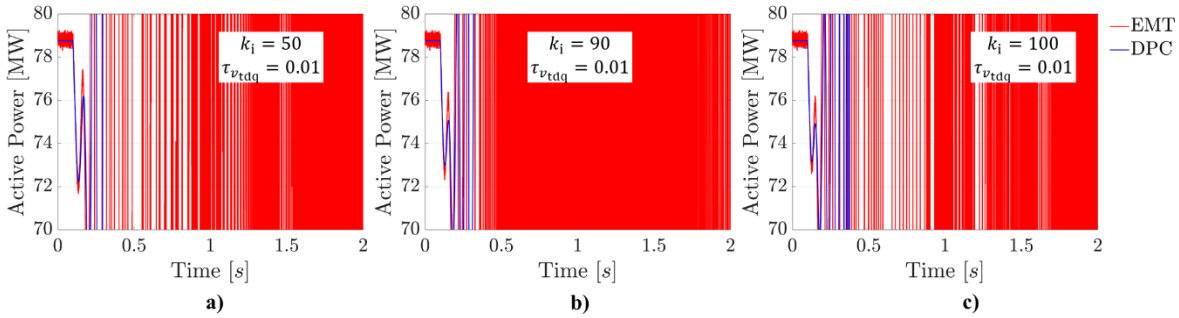

Figure D.27. Active power injected by CIG1 to B1 for 50% CIG and $\tau_{v_{tdq}} = 0.001$; a) $k_i = 50$; b) $k_i = 90$; c) $k_i = 100$

Annex E: Extended Abstract

Power system stability studies have traditionally focused on slow electromechanical phenomena typical of synchronous generators and their control systems. This enables the network and synchronous machine stators to be modeled using quasi-static phasor calculus (QPC). Thus, the associated fast transients are neglected and represented by algebraic equations. It is assumed that the transients decay rapidly and are irrelevant for stability assessments. However, as the penetration of converter interfaced generation (CIG) increases, the dynamic behavior of power systems is starting to depend on the fast and complex dynamics related to power electronics. Thus, relevant transients for stability studies may include the time scale of slow electromechanical and electromagnetic phenomena. Therefore, traditional assumptions made in QPC may lead to erroneous conclusions about system stability. Moreover, synchronous generator models are standard, well-known, and widely accepted in stability studies. There is a consensus on the appropriate level of detail. This consensus does not exist for CIG models. In this thesis, the validity range of stability assessments based on QPC models is identified, verified, and investigated. Dynamic phasor calculus (DPC) is considered the alternative. To accomplish the purpose of this thesis, a systematic methodology is proposed to compare QPC and DPC. It includes frequency response, modal, and sensitivity analyses. Additionally, common CIG models based on QPC are compared with DPC models to investigate and identify the appropriate level of detail required for stability analysis. Modal analyses are performed in these comparisons. The studies are performed in an IEEE test network considering CIG of up to 100% penetrations. The results show that the QPC is suitable for stability analysis when low bandwidths of converter controls are implemented. Also, for transients with oscillation frequencies lower than 5 Hz. In power systems where the CIG has to support the frequency, QPC models become highly inaccurate for predicting system stability. This is due to the complexity of dynamic interactions increasing. Relevant transient phenomena are the time scale of electromechanics and electromagnetic phenomena. For these systems, DPC is suitable and applicable to generic stability studies of power systems dominated by CIG.